INTERACTIONS OF THE RECEPTOR FOR ADVANCED GLYCATION END PRODUCTS (RAGE) WITH ADVANCED GLYCATION END PRODUCTS AND S100B

A Dissertation
Submitted to the Graduate Faculty
of the
North Dakota State University
of Agriculture and Applied Science

By

Venkata Shravan Kumar Indurthi

In Partial Fulfillment of the Requirements
for the Degree of
DOCTOR OF PHILOSOPHY

Major Department:
Pharmaceutical Sciences

October 2015

Fargo, North Dakota

North Dakota State University
Graduate School

Title

INTERACTIONS OF THE RECEPTOR FOR ADVANCED GLYCATION END PRODUCTS (RAGE) WITH ADVANCED GLYCATION END PRODUCTS (AGEs) AND S100B

By

Venkata Shravan Kumar Indurthi

The Supervisory Committee certifies that this ***disquisition*** complies with North Dakota State University's regulations and meets the accepted standards for the degree of

DOCTOR OF PHILOSOPHY

SUPERVISORY COMMITTEE:

Dr. Stefan Vetter
Chair

Dr. Stephen O'Rourke

Dr. Bin Guo

Dr. Christopher Colbert

Approved:

11/20/2015	Dr. Jagdish Singh
Date	Department Chair

ABSTRACT

RAGE is a multi-ligand pattern recognition receptor. RAGE can bind several damage associated molecular pattern proteins. RAGE- ligand interaction is pathophysiologically relevant to several major diseases including diabetes and certain cancers. RAGE inhibition has been reported to reduce morbidity in these disease states. However, to design better RAGE inhibitors it is necessary to understand the structural basis behind the RAGE-ligand interaction and currently this is not well understood. This thesis focuses on understanding the interaction of RAGE with two of its ligands; AGEs and S100B.

AGEs are highly heterogeneous and are formed as a result of non-enzymatic glycation. A panel of AGEs were characterized in terms of their side chain modifications, thermal stability, secondary structure, aggregation and surface charge. These glycation induced changes were then correlated to RAGE binding.

Building on these results the role of AGE-RAGE interaction in pancreatic cancer cell proliferation and migration was determined. Ribose modified BSA induced ROS formation, which then triggered NF-κB upregulation via RAGE induced ROS signaling. Ribose BSA increased pancreatic cell proliferation and migration. Anti-RAGE antibodies and RAGE inhibitors prevented AGE induced cellular effects. The role of ribose modified BSA was also determined in macrophage activation and pro-inflammatory cytokine release. Rapid internalization was observed of the ribose-BSA and confocal imaging revealed the internalization of the AGE compound into the lysosomes which lead to the ROS production, NF-κB activation and pro-inflammatory cytokine release in a RAGE independent signaling mechanism.

Finally, the role of tryptophan residues of the V domain in domain stability and S100B binding was determined. We have generated single, double and triple tryptophan mutants of the

V domain by site directed mutagenesis. The effect of Trp residues in the domain stability could not elucidated as no change was observed in the secondary structure of the mutants when compared to the wild type suggesting the plasticity of the V-domain. The fluorescence emission and life time properties of each Trp residue was determined. Our binding assays of the Trp → Ala mutants indicate tighter binding of the S100B to the mutants. The S100-RAGE peptide structures suggest multi modal interaction of S100B-RAGE interaction.

ACKNOWLEDGEMENTS

I am bereft of all words to describe the contribution of my advisor, mentor and guru Dr. Stefan Vetter. I joined the Ph.D. program at 21, I needed a guru to be the guiding light in my scientific endeavors and I am grateful to Dr. Vetter for accepting me into his lab and being the guiding light. The role he has played in my growth as a scientist is indescribable. He will always be an inspiration. I consider myself extremely fortunate to have been advised by Dr. Vetter and I am proud to be his first student. His contribution extends way beyond honing my scientific skills and has been instrumental in the overall growth of me as an individual. In the same breath, I would also like to express my deepest gratitude to Dr. Estelle Leclerc for all her contributions.

To be successful it is very important to have a strong family. I am extremely fortunate to have a very supporting family. I would like to acknowledge my family; my parents, my grandparents, my sister and my brother-in-law for the unconditional support. My cousin Abhishek has been my pillar of strength during my graduate studies and would like to thank him for all his support.

The last year of my graduate studies have been the toughest and the most frustrating. I cannot thank my lab mate Priyanka enough for bearing with me through this phase and making sure that I had a smile on my face every single day. My special thanks to Jean; the nicest person I have ever met and Clyde. Thank you for making me feel a part of your family and making sure I did not miss home.

I have made some fabulous friendships during my graduate studies in the college of health professions, these are the people who believed in me and always motivated me to take that extra step. I would like to express my sincere gratitude to Dana, Sara, Lori and Kelly for all their support and making me feel at home here at North Dakota State University. They have an immense contribution in making me a better person. I would like to acknowledge my friends Rhishi, Mayura, Anil, Prajakta and Gaurav for taking care of me and being there for me whenever I needed.

I would like to express my heartfelt gratitude to my advisory committee, Prof. Guo, Prof. O'Rourke, and Prof. Colbert for your valuable suggestions and expert advice. Their input was instrumental in shaping me as a scientist and honing my critical reasoning skills.

Finally, I would like to express my sincere gratitude to ND-EPSCoR and the graduate school for the doctoral dissertation assistantship, I am grateful to the financial support provided to me through this assistantship.

DEDICATION

Dedicated to my parents

Krishnaveni and Ramesh Kumar Indurthi

And my sister,

Swetha Mula

TABLE OF CONTENTS

LIST OF TABLES

LIST OF FIGURES

LIST OF ABBREVIATIONS

RAGE..Receptor for Advanced Glycation End Products

AGE ....Advanced Glycation End Products

TAGE..Toxic Advanced Glycation End Products

sRAGE ....Secretory Form of Receptor for Advanced Glycation End Products

DNRAGE...Dominant Negative Receptor for Advanced Glycation End Products

NF-κB ....Nuclear Factor Kappa-Light-Chain-Enhancer of Activated B Cells

CNS..Central Nervous System

DAMPS...Damaged Associated Molecular Patterns

EAE..Experimentally Induced Autoimmune Enphalomyelitis

DTH ....Delayed Type Hypersentivity

HbA1C ....Glycated Hemoglobin

BSA..Bovine Serum Albumin

DF-BSA ....Defatted Bovine Serum Albumin

Glc..Glucose

Ace ....Acetoin

GA..Glyoxalic Acid

Dia..Diacetyl

Gly..Glyceraldehyde

Gla..Glycolaldehyde

MG ....Methyl Glyoxal

Rib..Ribose

CML...Carboxymethyl Lysine

L ....Low Modified

H..High Modified

vH..Very High Modified

ELISA ....Enzyme Linked Immunosorbent Assay

DSC...Differential Scanning Calorimetry

CD ....Circular Dichroism

PBS ....Phosphate Buffered Saline

HPLC ....High Performance Liquid Chromatography

DLS ....Dynamic Light Scattering

ITC ....Isothermal Calorimetry

SDS ....Sodium Dodecyl Sulphate

PAGE ....Polyacrylamide Gel Electrophoresis

CRD ....Carbohydrate Recognition Domain

°C ....Degree Centigrade

T_m ....Thermal Transition Mid-Point

ΔH ....Change in Enthalpy

ΔS..Change in Entropy

K_d ....Dissociation Constant

ROS...Reactive Oxygen Species

NO...Nitric Oxide

Cy5.5...Cyanine 5.5

NAC ....N-Acetyl Cysteine

TNF ....Tumor Necrosis Factor

IL...Interleukin

TGF ....Tumor Growth Factor

IFN ....Interferon

TLR ....Toll like Receptor

PCR ....Polymerase Chain Reaction

Q-RT-PCR ....Quantitative Real Time PCR

SiRNA ....Small Interfering RNA

GFP ....Green Fluorescent Protein

iNOS ....Inducible Isoform of Nitric Oxide Synthase

RPL4 ....Ribosomal Protein L4

LPS ....Lipopolysaccharide

DCF ....Dichlorofluorescein

E.F ....Endotoxin Free

Trp ....Tryptophan

NMR ....Nuclear Magnetic Resonance

FITC ....Fluorescein Isothicyanate

NMR ....Nuclear Magnetic Resonance

APS ....Advanced Photon Source

CHAPTER 1: INTRODUCTION

Receptor for advanced glycation end products

The Receptor for Advanced Glycation End Products (RAGE) is a multi-ligand cell surface receptor of the immunoglobulin super family and was first characterized as the receptor for the Advanced Glycation End Products (AGEs)[1-3]. The RAGE gene is localized on chromosome 6 near the HLA locus in humans and mice and is located in the vicinity of MHC III complex [4]. RAGE is composed of three immunoglobulin-like regions extracellularly: one "V-type" or "Variable-type" and two "C-type" or "Constant-type" domains, a short 21- amino acid residue transmembrane and 43- amino acid residue cytoplasmic tail [1-3]. The 320-amino acid residue extracellular domain is crucial for ligand binding and the cytoplasmic tail is critical for intracellular signaling. Alternative splicing of mRNA of RAGE leads to additional RAGE isoforms including N-truncated forms and C-truncated forms [4-6]. RAGE isoforms can be loosely classified into three major isoforms; full-length RAGE, secretory RAGE (sRAGE) and dominant negative RAGE (DNRAGE)[7] (Figure 1.1). Full length RAGE is the most well studied isoform and contains all the domains for ligand binding and signaling. The soluble form of RAGE or secretory RAGE or sRAGE contains the V domain and the C1 and C2 domains but lacks the transmembrane region and the cytoplasmic tail. Due to the absence of the transmembrane and the cytoplasmic tail sRAGE is released into the extracellular space, where it can interact with the RAGE ligands prior to full length RAGE. As a result, sRAGE can antagonize full length RAGE signaling *in vitro* and *in vivo* [8]. sRAGE can be derived from mRNA splicing as described earlier and can also be derived from the full length RAGE by protein cleavage[9]. The DNRAGE consists of all the extracellular domains and the transmembrane region however, it lacks the cytoplasmic tail. This is the least understood of the RAGE isoforms. Presumably, like sRAGE, DNRAGE competes with the full length RAGE for ligands and functions as a decoy receptor due to the lack of the cytoplasmic tail. Majority of our understanding of the DNRAGE has evolved from transfection studies, the over expression of DNRAGE resulted in the decrease of full length RAGE activation [10-12]. The expression of DNRAGE has been described in the brain and is similar to the expression levels of full length RAGE [13]. Various other splice variants of RAGE have also been identified. For example, N truncated form of RAGE lacks the N-terminal signal sequence and the first V-like extracellular domain (Figure 1.1). This is incapable of binding to ligands such as the AGEs [14, 15].

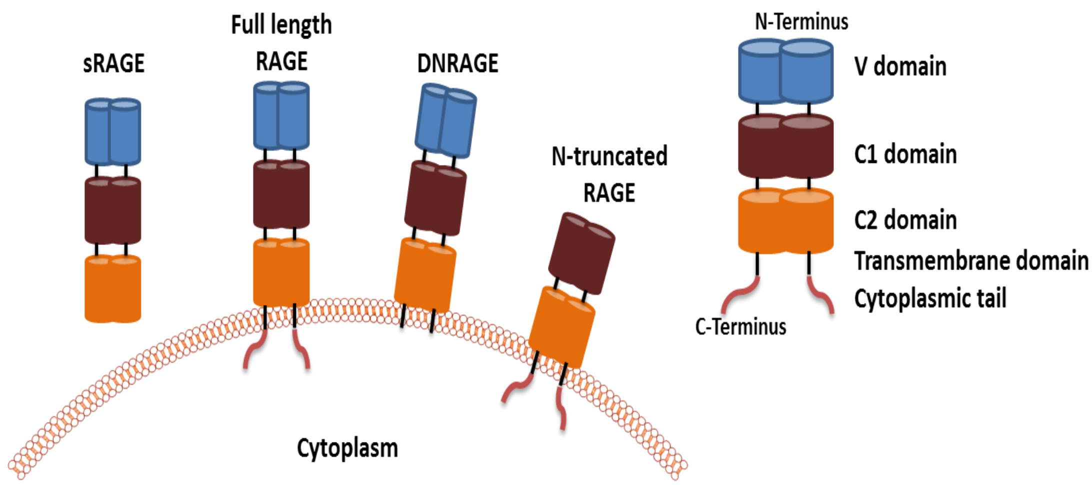

Figure 1.1. Isoforms of the RAGE receptor.

Initially, RAGE was discovered as a receptor of AGEs, however, various other ligands including the calcium binding S100/calgranulins that accumulate extracellularly at the sites of chronic inflammation [15, 16] and the proinflammatory DNA binding HMGB1(amphoterin) which is released from necrotic cells [17-20] have also been identified to bind to RAGE. Studies on the structural basis of RAGE-ligand interaction revealed that the receptor recognizes specific three dimensional structures such as fibrils and β-sheets, rather than any specific amino acid sequence [21, 22]. In Alzheimer's disease RAGE binds amyloid β-peptide [11, 12] and in systemic amyloidosis

RAGE binds to amyloid A [23]. Besides these ligands RAGE interacts with surface molecules such prions [24] and leukocyte integrins[25]. Hence, RAGE can be characterized as a multi ligand receptor as it binds to a broad range of unrelated ligands that accumulate in tissues during inflammation, host response, aging and chronic degenerative diseases. Therefore, RAGE is considered as a pattern recognition receptor (PRR) and more specifically it recognizes damaged associated molecular patterns (PAMPs).

RAGE-mediated NF- κB signaling

RAGE-ligand interactions result in activation of proinflammatory signaling pathways. RAGE can trigger intra-cellular signaling by both NF-κB dependent and NF-κB independent pathways. Classically, RAGE triggered pro-inflammatory signaling has been described by the activation of NF-κB [26]. RAGE-mediated NF-κB activation has been reported to have a prolonged time course suggesting that RAGE can inhibit endogenous auto-regulatory feedback inhibition loops [26] . NF-κB activation can upregulate RAGE expression, further activating NF-κB and ensuring the amplification and maintenance of the signal [27].

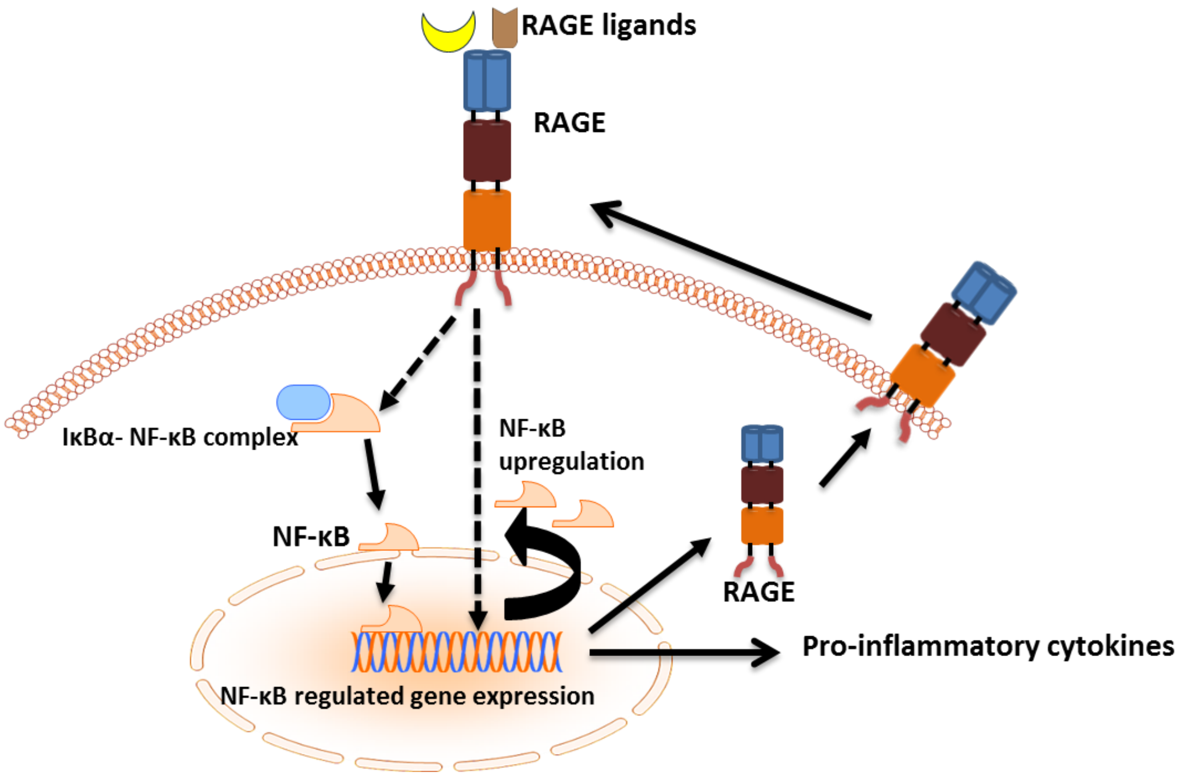

Figure 1.2. RAGE dependent NF-κB signaling.
The initial step of RAGE mediated NF-κB activation is the degradation of IκBα- NF-κB complex (Solid arrow). The activated NF-κB translocates into the nucleus and binds to specific DNA sequence. This triggers the expression of pro-inflammatory cytokines, and also the upregulation of RAGE. RAGE activation can also trigger the upregulation of NF-κB (Dashed arrow). This is critical to inhibit the negative feedback mechanisms triggered by IκBα production.

RAGE induced activation of NF-κB has been reported to activate various cellular signaling cascades [28]. Table 1.1 summarizes the different cellular signaling cascades triggered by NF- κB. The diverse RAGE signaling is the result of its multi-ligand nature. RAGE signaling is also dependent on the cell type.

Table 1.1. RAGE induced signaling pathways.

Cell Type	Signaling Cascade	Ligand	Reference
Osteoblasts	ERK1/2	AGEs	[29]
Myoblasts	ERK1/2	S100B	[30]
Tubular epithelial myofibroblasts	ERK1/2	AGEs	[31]
Smooth muscle cells	ERK1/2	AGEs	[32]
Monocytes	ERK 1/2	AGEs/S100B	[33]
Monocytes (Acute monocytic leukemia)	p38 and p44/p42	AGEs	[34]
Myoblasts	p38	HMGB1	[35]
C6 glioma cells	p44/p42, p38 and SAP/JNK	HMGB1	[36]
Neuroblastoma cells	JAK/STAT	HMGB1	[37]
Kidney fibroblasts	JAK/STAT	AGEs	[38]

RAGE expression and physiological function

RAGE expression depends on the cell type and developmental stage and the expression can be both constitutive and induced [17, 39]. RAGE is constitutively expressed during embryonic development and the expression is down regulated in adult life with the exceptions of lung, skin and thyroid [40 41]. RAGE expression is expressed at very low levels under physiological conditions in most of the cells including endothelial cells, smooth muscle cells, monocytes/macrophages, neuronal cells and fibroblasts; however, RAGE expression is induced in these cells either on ligand binding or on the activation of transcription factors regulating the transcription of RAGE in disease states (reviewed in[28]). Transcription of RAGE is under the control of various transcription factors including NF-κB, AP-2, SP-1 and NF-IL6 [27].

Physiological role of RAGE in development is poorly understood. RAGE knock out mice studies reveal that the RAGE is not essential to life and its deletion does not have any lethal effects [42]. RAGE deletion lead to hyper activity and increased sensitivity to auditory stimulus when compared to wild type mice, however, no change was observed in spatial memory or anxiety when compared to the wild type [42]. Studies have indicated the role of RAGE in neurite growth and differentiation. RAGE-HMGB1 or/and RAGE-S100B interactions have been reported to play an important role in the promotion of neurite outgrowth and neuronal differentiation. HMGB-1 on binding to RAGE regulates cell survival and cell migration[17, 37, 43]. The calcium binding S100B is expressed and released by astrocytes into the CNS. The released S100B binds to RAGE in the CNS and contributes to neuronal survival and neurite outgrowth by the activation of Cdc42/Rac-dependent signaling triggered by Ras/MAPK dependent NF-κB nuclear translocation[44]. RAGE knockout studies also confirm the role of RAGE in neurite outgrowth[37]. RAGE also plays important role in pathophysiological processes in the lung including modulation of cell spreading, adhesion to ECM components, proliferation, and migration [45].

RAGE and disease

RAGE plays an important role in the pathophysiology of various diseases. The role of RAGE has been implicated in inflammatory conditions [46, 47], diabetic complications [48, 49], neurogenerative diseases [50, 51], vascular disease [52, 53], and multiple cancers [54]. As described earlier, RAGE binds to a wide range of ligands and can trigger diverse signaling in various disease states. Most of the RAGE ligands can be characterized as damaged associated molecular patterns (DAMPs) which elicit a pro-inflammatory response. The role of RAGE has been described in innate immunity at both the early and late stages [25, 55, 56]. The blockage of RAGE by anti-RAGE antibody or by soluble RAGE (sRAGE) in cells resulted in the suppression of experimentally induced autoimmune enphalomyelitis (EAE) in mice [56]. In addition, the role of RAGE was also established in delayed-type hypersensitivity (DTH) mice model by treating the mice with sRAGE [15]. Due to the ability of RAGE to sustain cellular activation, it has the potential to function as a master switch to convert a transient pro-inflammatory response, evoked by an inflammatory stimulus into sustained cellular dysfunction [22, 26]. RAGE biology and signaling depends on the ligands which accumulate and interact with RAGE, the signaling also depends on the cell type. The role of RAGE is most well described in diabetes and its complications. Over expression of RAGE in diabetic mice lead to increase in diabetic nephropathy and neuropathy, and a decrease was observed in the RAGE-/- mice. Treatment with sRAGE and anti-RAGE antibodies also decreased diabetic neuropathy and nephropathy [57-59]. Activation of RAGE and AGE-RAGE interaction has also been described in chronic vascular dysfunction in diabetic vasculopathy and atherosclerosis [60]. In diabetic complications, in addition to the long known role of AGE-RAGE interaction [61], the role of other RAGE ligands have also been recently recognized to contribute to its pathology. Increased serum levels of S100A8/A9 in type 1 diabetic patients provided the first evidence [62], increased levels of S100A12 were observed in type 2 diabetes [63] and increased HMGB1levels were associated with the coronary heart disease in type 2 diabetes [64]. The role of HMGB1 has been described in the endothelial dysfunction in diabetes [65]. This suggests the complex RAGE signaling in diabetic complications. In Alzheimer's disease RAGE plays an important role in the transportation of pathophysiologically relevant concentrations of amyloid-β peptide into the CNS [66]. Treatment of transgenic rodent models with sRAGE or anti-RAGE antibodies suppressed RAGE associated abnormalities [67, 68] and reduced the amyloid-β peptide transport across the blood-brain barrier[66]. RAGE blocker, FPS-ZM1 also effectively controlled the progression of Aβ-mediated brain disorder and may have the potential to be a disease-modifying agent for Alzheimer's disease [69].

RAGE also plays an important role in the disease progression of multiple cancers. The role of AGE-RAGE interaction in cancer cell growth was first described in renal carcinoma cells[70]. The role of RAGE and its ligands including AGEs, HMGB1 and S100 proteins have been implicated in multiple cancers such as colon cancer [71], prostate cancer [72], oral squamous carcinoma [73], breast cancer [74], hepatocellular carcinoma[75], gastric cancer[76], pancreatic cancer [77] and others [54]. Molecular mechanism concerning the activation and function of RAGE during malignant progression and neoplastic transformation is scarce, however various in vitro studies and in vivo reports in mouse xenograft models support a direct link of RAGE activation with survival, proliferation, migration and invasion of tumor cells[78 79]. Therapeutic inhibition of RAGE by using anti-RAGE antibodies have been reported to inhibit RAGE mediated cancer progression in in vivo mice xenograft models. For example, anti-RAGE antibodies reduced growth of RAGE overexpressing tumors in the mice xenograft model of melanoma [80 81]. Interestingly treatment with anti-RAGE antibody also significantly enhanced the efficacy of dacarbazine resulting in reducing the growth rate in RAGE overexpressing tumors cells [80]. Recently, a RAGE antagonistic peptide was designed and used to block RAGE-S100P interaction in pancreatic cancer and a reduction in tumor growth was observed [81]. These results suggest RAGE as an important therapeutic target in the treatment of various cancers.

RAGE inhibition is an important strategy for the treatment due to its role in various disease states. However, due to the multi ligand nature of RAGE and its complex signaling it is highly difficult to design and develop RAGE inhibitors. The structural basis behind the RAGE-ligand interaction is still not clearly understood. RAGE has three extracellular domains and the ligands can bind to any of the three domains. Even though we know on which domain of RAGE some of the ligands bind, the exact binding regions on the receptor is not known.

The overall goal of my Ph.D. is to obtain a better understanding of the role of the interaction of RAGE-ligand interaction which would provide the basis for the development of efficient RAGE inhibitors. More specifically, the interaction of RAGE with AGE compounds and S100B is addressed in this thesis.

The first three chapters of the thesis focus on AGE compounds and the fourth chapter on S100B. The first chapter focuses on understanding the glycation induced biochemical and biophysical changes on serum albumin and their interaction with RAGE. The second chapter studies the role of AGE-RAGE interaction in pancreatic cancer cell proliferation. The inflammatory role of AGE compounds, more specifically the role of AGE compounds in macrophage activation is described in chapter in three. The final chapter focuses on understanding the structural basis of RAGE-S100B interaction. The role of tryptophan residues in the V domain of RAGE has been determined in domain stability and S100B binding.

CHAPTER 2: GLYCATION, ADVANCED GLYCATION END PRODUCTS (AGES) AND THEIR INTERACTION WITH RECEPTOR FOR ADVANCED GLYCATION END PRODUCTS (RAGE)

Introduction

Non-Enzymatic glycation and AGE compound formation

The non-enzymatic glycation reaction (Maillard reaction) between nucleophilic groups in biomolecules and reactive carbonyl groups leads to complex modification of proteins and other biomolecules [82] (Figure 2.1). Among the physiologically occurring reactive glycation reagents are the reducing carbohydrates, in particular glucose and ribose and their phosphorylated derivatives, but also short chain aldehydes (oxo- and hydroxy aldehydes) such as glyceraldehyde, methyglyoxal and glycolaldehyde, which are formed as intermediates during metabolic reactions and lipid peroxidation [83]. The initial step of protein glycation (Schiff base formation) is reversible but can slowly proceed to the formation of more stable Amadori products and through subsequent rearrangements, elimination, fragmentation and oxidation reactions to chemically stable products. These so called advanced glycation end products (AGE) are highly diverse and introduce novel side chain modifications including chromophores, fluorophores and intra- and intermolecular crosslinks into proteins [84]. A single glycation reagent can lead to multiple chemically distinct modifications at different amino acid side chains within a single protein molecule [85]. Glycation occurs most frequently at the N-terminal amino group and the side chains of arginine and lysine residues. Glycation may also occur on cysteine, histidine, and tryptophan side chains [86]. The covalent chemical modification of serum proteins is likely to alter their normal physiological function. At least two dozen AGE modification have been identified in biological samples. When multiple glycation reagents are present very complex and heterogeneous mixtures result (Figure 2.2).

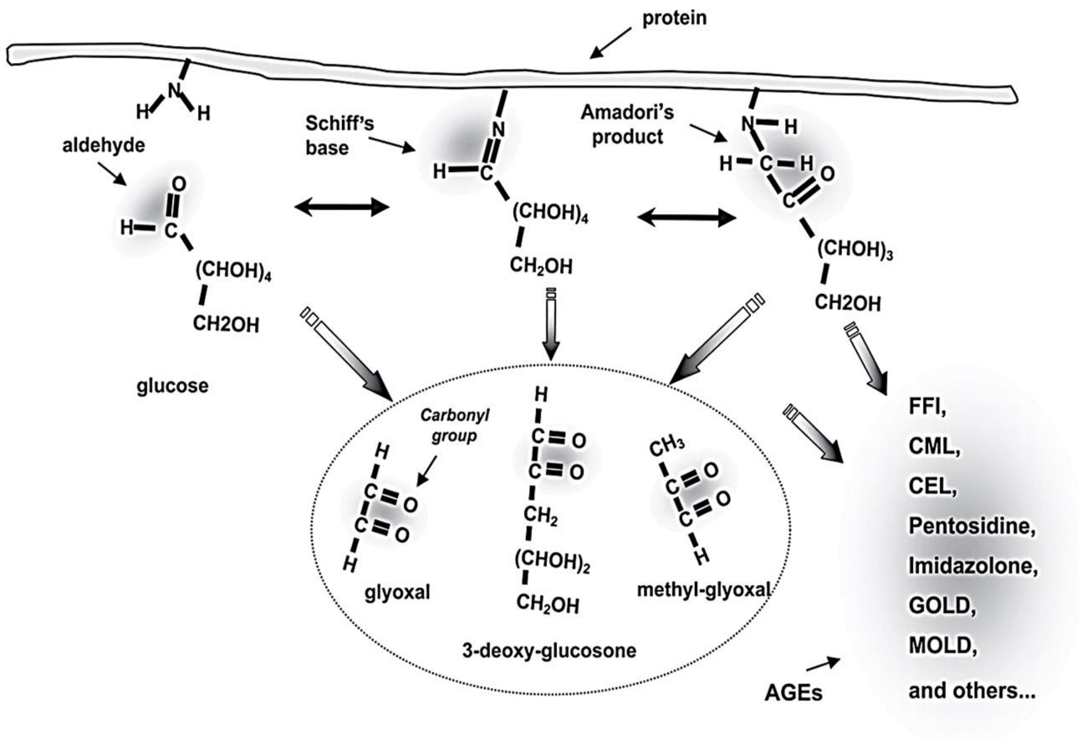

Figure 2.1. Possible mechanism for the formation of AGE compounds.
(The Figure is reproduced from [87]).

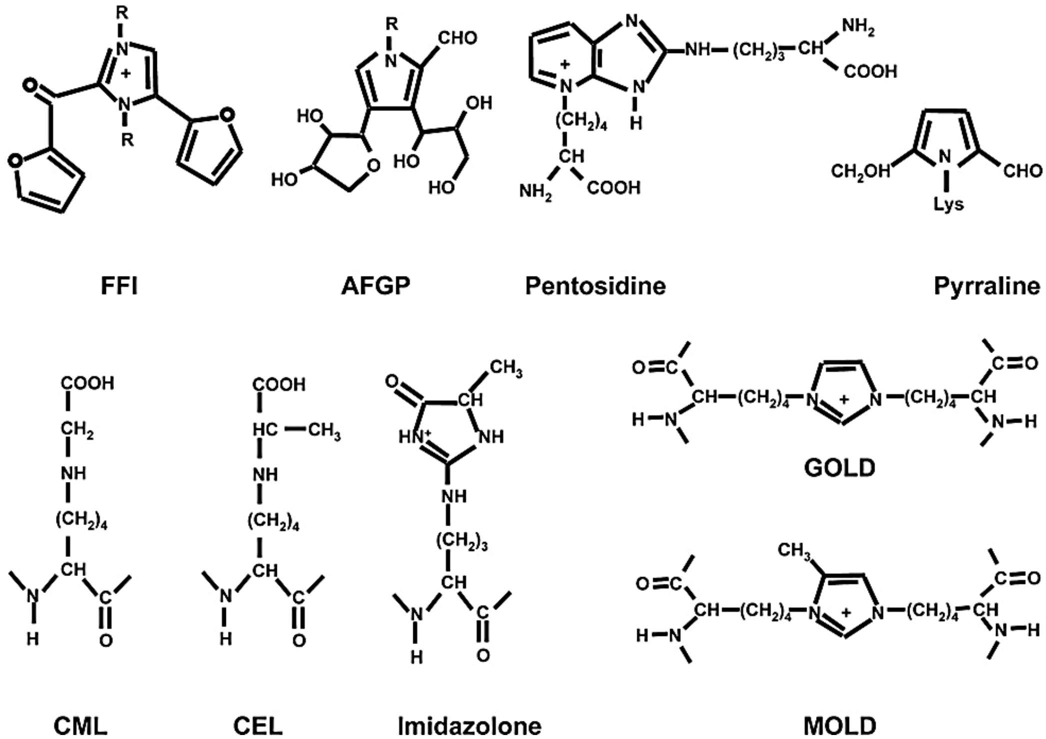

Figure 2.2. The chemical structures of common AGE modifications.
(The Figure 2.2 is reproduced from [87]. FFI: 2-(2-furoyl)-4(5)-furanyl-1H-imidazole; AFGP: 1-alkyl-2-formyl-3,4-diglycosyl pyrrole; CML: N-ε-carboxy-methyl-lysine; CEL: N-ε-carboxy-ethyl-lysine; GOLD: glyoxal-lysine dimer; MOLD: methyl-glyoxal-lysine dimer).

AGE compounds and disease

Increased glycation of serum proteins is well documented in diabetic patients [88-90], but also be found in patients with other conditions such as cardio-vascular disease [88-90], arthritis [91, 92], kidney failure [93], or liver cirrhosis [94]. Advanced glycation end products have been also been observed in various tissues under pathological conditions such as atherosclerotic plaques [95], sites of inflammation or neurodegeneration [96] and cancer tumors [97]. They also accumulate in proteins with long half-life such as collagen of the skin and cartilage [98] or crystalline in the eye-lens [99]. It has been hypothesized that diabetic complications are causatively linked to the formation of advanced glycation end products [100]. For example, diabetic patients show increased concentrations of glycated and AGE-modified hemoglobin (HbA1c) compared to normoglycemic individuals. HbA1c levels are clinically used as reliable reporter on long-term blood glucose levels [101] and are positively correlated with diabetic complications such as microvascular damage, nephropathy and retinopathy [102-105]. In fact, Soluble AGE compounds in the circulation and extracellular fluids have been demonstrated to be useful as prognostic and diagnostic biomarkers for diabetes related complications [106]. It is important to note that protein glycation in diabetic patients is not limited to modification by glucose but also involves other reactive aldehydic intermediates (described earlier), which are chemically much more reactive than glucose and are rapidly bound by proteins [107, 108]. Metabolic intermediates such as glyoxal, methylglyoxal and 3-deoxyglucosone are formed as metabolic by-products and are formed at an accelerated rate in diabetic patients [109-111]. They accumulate at elevated rates in tissues under oxidative stress, at sites of inflammation, or under conditions involving reduced renal function [109, 112-114].

An important question is whether AGE compounds are causatively involved in disease development and progression, or whether AGE compounds are simply by-products of metabolic reactions without significant biological activity. There seems to be a consensus that AGE compounds are biologically active and promote various cellular processes including inflammation [115], tumor growth [116] and neurodegeneration [51]. However, considering the large number of possible AGE modifications in many different proteins it becomes important to investigate whether all AGE modifications are equally significant form a pathophysiological standpoint. It might be that certain glycation reactions yield AGE compounds with toxic properties (sometimes called TAGE, toxic-AGE), while other may be benign [117]. The present research focuses on soluble AGE compounds that may exert their biological activities through activation of AGE-specific cell surface receptors.

AGE-specific cell surface receptors

We chose serum albumin as a model protein for glycation because serum albumin undergoes significant glycation in diabetic patients, has been studied as a substrate for glycation [118, 119] and because AGE-BSA is frequently used in biomedical research studies as a representative example for AGE compounds. Bovine and human serum albumins are highly homologous and both forms of protein are expected to respond identically to glycation.

AGE products in the circulation or extracellular space can interact with two types of cell surface receptors [120]. Clearance and scavenger receptors are predominantly involved in AGE capture, removal and degradation [121]. This group of receptors includes type I (SR-AI) and type II (SCARA2) macrophage scavenger receptors [122], CD-36 [123], FEEL-1 and -2 [124], scavenger receptor proteins SR-BI and SR-BII [125] and the lectin-like oxidized low-density lipoprotein receptor 1 (Lox-1) [126]. The other type of AGE-receptors initiates specific cellular signaling events in response to AGE exposure. The receptor for advanced glycation endproducts (RAGE) is the best characterized AGE-signaling receptor and generally considered to be the medically most relevant AGE receptor [127]. The cellular signaling pathways activated by AGE binding to RAGE have been studied in various cell types and generally lead to the formation of oxidative stress and reactive oxygen species that can promote AGE formation, activation of the Nf-κB transcription factor, induction of pro-inflammatory gene expression and release of inflammatory cytokines and chemokines [128, 129].

The other cell surface receptor with AGE signaling potential is the "AGE-receptor complex" and consists of three proteins AGE-R1 (OST-48), AGE-R2 (80-K-H) and AGE-R3. AGE-R3 is also known as galectin-3 (LGALS3) and is responsible for AGE binding 130. AGE binding to galectin-3 is less well studied, but there are several reports that suggest that the AGE-receptor complex and galectin-3 are indeed involved in diabetes related complications and mediate biological effects of AGE in the eye 131, vascular endothelium 132, kidney 133 and liver 134.

All AGE binding receptors are pattern recognition receptors and recognize any molecule that displays a particular molecular signature. The molecular pattern in AGE compounds that is recognized by RAGE or galectin-3 is currently not known. However, it would be important to distinguish AGE compounds that activate RAGE from those that are not able to initiate RAGE signaling. This would allow to develop diagnostic tests for AGE compounds with detrimental health effects and to design novel drugs that could specifically target the AGE-RAGE axis in important pathologies.

Serum albumin, drug binding and glycation

Serum albumin is the major drug binding protein in plasma and greatly influences the pharmacokinetics of drugs that bind to it. Consequently, changes in the capacity of serum albumin to bind drug molecules can have profound effects on the free drug concentration and can consequently affect both toxicity and therapeutic efficacy. The binding of many drug molecules to whole plasma, isolated plasma proteins and in particular serum albumin has been studied in great detail [135-137]. Biophysical studies investigating drug binding to serum albumin use both the human and the closely related bovine protein as a valid substitute [138, 139]. These studies have identified two major drug binding sites (Sudlow I and II) and at least four additional secondary drug binding sites in serum albumin [140-142]. Surprisingly little is known about the effects of chemical modification by glycation of serum albumin on its drug binding properties.

Diabetic patients have notoriously elevated levels of glycated blood proteins. In this patient group levels of albumin glycation average ~ 25% of total serum albumin and can exceed glycation levels of 40 or 50% in individual cases [88-90]. These patients often show additional co-morbidities and receive multiple medications with different plasma protein binding properties. Therefore, a better understanding of albumin glycation and its effects on drug binding is clinically relevant in patients with increased glycation of serum proteins.

The binding of many drug molecules to whole plasma, isolated plasma proteins and in particular serum albumin has been studied in great detail [137, 143, 144]. Biophysical studies investigating drug binding to serum albumin use both the human and the closely related bovine protein as a valid substitute [139]. These studies have identified two major drug binding sites (Sudlow I and II) and at least four additional secondary drug binding sites in serum albumin [140 145].

The binding of several drug molecules to glycated serum albumin has been investigated [146-148 149], but no consensus mechanism that would allow prediction of changes in binding affinity for particular drugs has emerged yet. Our studies combine structural and thermodynamic experiments to gain a better understanding of the relationship between glycation induced structural changes in albumin and its drug binding properties.

We chose diclofenac as a representative example of small acid drug molecules with high plasma protein binding. Diclofenac (Figure 2.3) binds to two sites on serum albumin with $K_a = 10^5$ to 10^4 M^{-1} affinities, depending on the methodology used to measure binding affinities and the composition of the buffer system used in the experiments [150-153]. Diclofenac can interact via ionic and hydrophobic interactions with drug binding sites on proteins [154, 155]. Samples modified with low concentrations of glycation reagents were used for the diclofenac binding study as the glycation conditions are very close to physiological conditions.

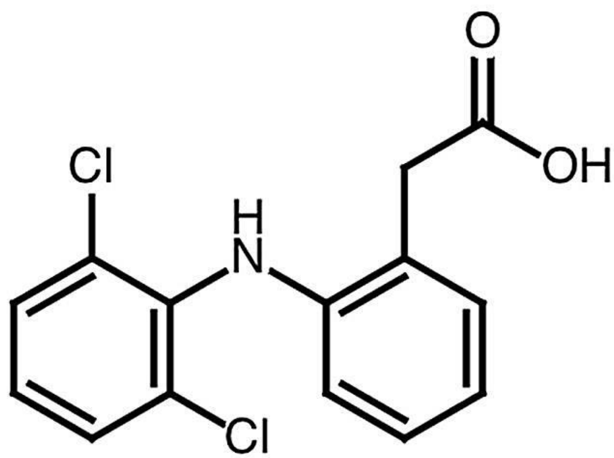

Figure 2.3. Chemical structure of the non-steroidal anti-inflammatory drug diclofenac.

Problems associated with AGE compound research

A fundamental problem in AGE related research is the complexity and heterogenicity of AGE samples, which make the analytical characterization very difficult. Biomedical researchers use AGE-compounds derived under a variety of conditions, modified with different glycation reagents and generated with very high concentrations of glycation reagent, which lead to complete modification of reactive amino acids and likely to denaturation of the protein. For example, AGE-compounds have been generated using highly reactive aldehydes, such as methylglyoxal and glyceraldehyde at 100 mM, or glucose and ribose at 1 M concentration [156, 157]. Whether the resulting AGE compounds are good models of physiological relevant AGE has not been shown and results from different studies are difficult to compare when AGE compounds have not been characterized.

With this in mind, a panel of AGE-modified serum albumin samples was generated under conditions that used lower concentrations of glycation reagents than commonly reported in AGE related studies. These compounds are referred to as “moderately glycated”. To achieve moderate glycation, near physiological concentrations of glycation reagents were used. For example, we used a low glucose concentration of 20 mM, a concentration that can be observed in diabetic patients. Indeed, blood glucose concentrations as high as 100 mM have been reported in certain diabetic patients [158]. The true physiological concentrations of many of the reactive aldehydes are difficult to estimate because of their high reactivity [159]. Also, blood concentrations of glycation reagents are not reflective of localized concentration within tissues or individual cells, which can be much higher. The reagent concentrations used by us for the glycation reactions (mostly 1 and 5 mM) were significantly lower than the reagent concentrations used in many previously published studies.

The goal of this study was to determine how each of these different glycation reagents affected the physical and chemical properties of the protein, and to correlate these changes in the protein to 1) RAGE interaction and cancer cell proliferation 2) to diclofenac binding.

This study was initiated to characterize glycation induced biophysical and biochemical changes in serum albumin and to correlate these changes to the degree of glycation in general and the different glycation reagents in particular. The direct binding of the panel of AGE modified serum albumin samples to two known AGE receptor proteins: the receptor for advanced glycation endproducts (RAGE) and galectin-3 (AGE receptor complex protein 3) was measured *in vitro*. Finally, the role of AGE-compounds derived from different glycation reagents in cancer cell proliferation was determined in a melanoma cell line called WM115. We finally investigate with spectroscopic and calorimetric methods, how glycation of serum albumin modifies its interactions with diclofenac.

Materials and Methods

Reagents were of molecular biology or ACS purity grade and purchased through Fischer Scientific or VWR. Bovine serum albumin (BSA), fraction V, was purchased from Amresco.

Antibodies were purchased from R&D Systems. An assay kit for the quantitative determination of fructosamine modified serum proteins was purchased from Diazyme (Poway, CA). Molecular biology reagents and enzymes were purchased from New England Biolabs (Ipswich, MA), OriGene (Rockville, MD) and Fermentas (ThermoFisher). Chromatography media for protein purification were purchased from GE Healthcare. Reagents and media for cell culture were from Life Technologies Cooperation (Invitrogen).

Preparation of glycated serum albumin

BSA (fraction V, was purchased from Amresco) was glycated following the procedure published by Schmitt et al. [160-162]. The protein was dissolved 500 mM sodium phosphate buffer, 1mM EDTA and 1mM sodium azide, pH 8 at a final concentration of 20-40 mg/ml. Glycation agents were added to the final concentrations indicated in Table 2.1and sterile filtered using a 0.2 micron syringe filter. The solutions were sealed in sterile (autoclaved) glass vials and incubated at 37 °C for 21 days. The CML modified serum albumin was generated following the procedure described by Ahmed et al. [163]. The Schiff base was formed using 2.3mM and 23mM in the low and high modified CML samples respectively and 55mM of sodium cyanoborohydride was used to reduce the Schiff base formed between lysine and glyoxylic acid. The samples were incubated at 37 °C for 24 hrs. After the incubation periods the samples were dialyzed twice against 200 volumes of PBS (8mM KH_2PO_4, 42mM Na_2HPO_4 and 150mM NaCl) at 4 °C. Protein concentration of the samples were measured by Pierce-BCA protein assay calibrated with commercial BSA standards. The samples were then aliquoted into 1.5 mL freezing tubes and were stored at -80°C. A single batch of bovine serum albumin (biotechnology grade) was used for all glycation experiments. As an additional control for non-glycated BSA, we used ethanol precipitated BSA (fraction V), which showed a single Tm in thermal unfolding studies, typical for non-fatty acid containing albumin (DF-BSA). Both BSA preparations were purchased from Amresco, USA. BSA incubated at 37 °C for 21 days was used as the third control.

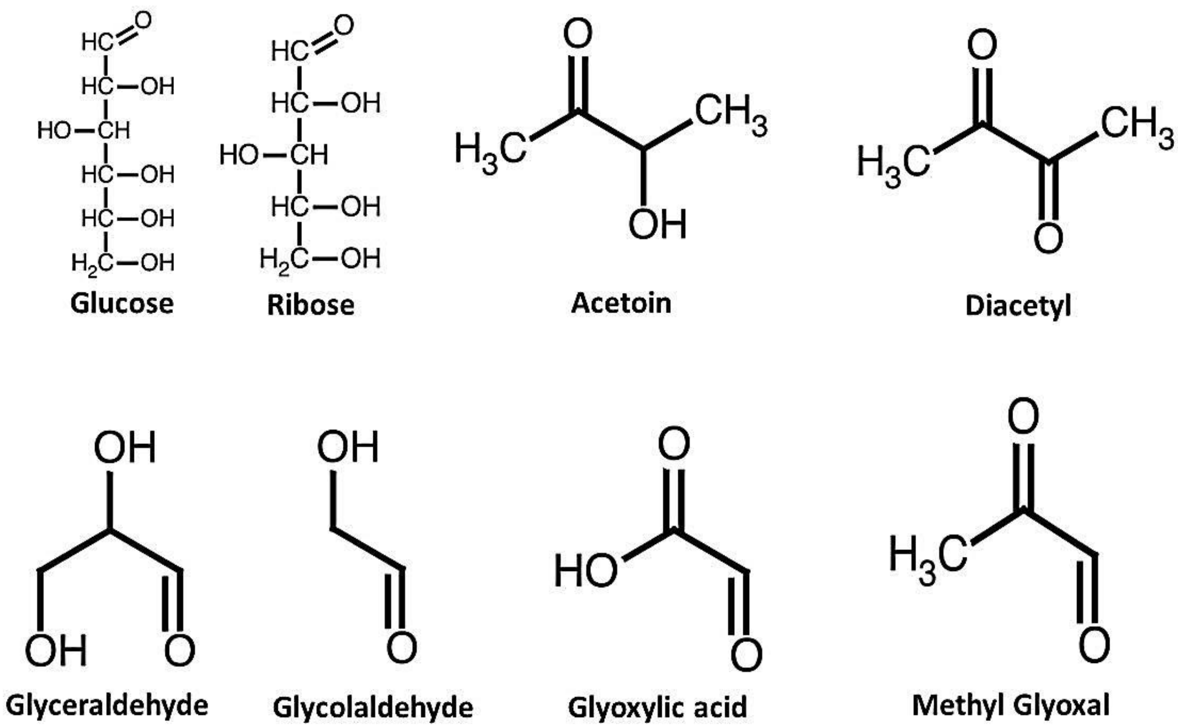

Figure 2.4. Chemical structures of the glycation reagents used to modify bovine serum albumin for this study.
Rib: ribose; Glc glucose; Dia diacetyl (2, 3-butanedione); Ace acetoin (3-hydroxybutanone); Gla glycolaldehyde (2-hydroxyacetaldehyde); Gly glyceraldehyde (2, 3-dihydroxypropanal); GA glyoxylic acid (oxoethanoic acid); MG methylglyoxal (2-oxopropanal).

Table 2.1. Concentrations of the different glycation reagents used.

Sample Name	Glycation Reagent	Concentration (mM)
BSA-fresh	none	n/a
Glc-L BSA	glucose	20
Glc-H BSA	glucose	200
Glc-vH BSA	glucose	500
GA-L BSA	glyoxylic acid	1
GA-H BSA	glyoxylic acid	10
Ace-L BSA	acetoin	1
Ace-H BSA	acetoin	5
Dia-L BSA	diacetyl	1
Dia-H BSA	diacetyl	5
Gly-L BSA	glyceraldehyde	1
Gly-H BSA	glyceraldehyde	5
Gla-L BSA	glycolaldehyde	1
Gla-H BSA	glycolaldehyde	5
MG-L BSA	methylglyoxal	1
MG-H BSA	methylglyoxal	5
Rib-L BSA	ribose	20
Rib-H BSA	ribose	200
Rib-vH BSA	ribose	500
CML-L BSA	glyoxylic acid $NaBH_3CN$	2.3 55
CML-H BSA	glyoxylic acid $NaBH_3CN$	23 55

UV/Vis and fluorescence spectroscopy

UV/Vis spectra were recorded on an Agilent 8543 diode array spectrophotometer using a quartz cuvette with a path length of 10 mm. The protein samples were normalized based on their concentrations determined by the BCA assay. The glycated serum samples were diluted in the PBS (8mM KH_2PO_4, 42mM Na_2HPO_4 and 150mM NaCl) buffer. Fluorescence emission spectra were recorded on a Horiba Jobin Yvon FluoroMax-4P spectrofluorometer. A quartz cuvette with

600 µL volume and a reduced pathlength of 5 mm was used for all fluorescence experiments and the slit size of 3nm was used for the excitation and emission filters.

Amino acid analysis

Amino acid analyses were performed by the Molecular Structure Facility at the University of California, Davis. Proteins were hydrolyzed in liquid phase with 6 N HCl/1% phenol at 110 °C for 24 hrs. Samples were analyzed on a Hitachi L8800 amino acid analyzer using a sodium citrate buffer system and post-column ninhydrin modification. Norleucin was used as internal standard.

Lysine side chain modification

Modified lysine side chain modifications were determined using fluorescamine (Acros Organics), which forms a highly fluorescent reaction product with amino groups [164, 165]. Commercial BSA standards (Pierce Thermo Scientific) (0-1000 mg/ml in PBS) were used to obtain the standard curve. The assay was performed in a 96 well plate. 50 µl of 10.8 mM of fluorescamine dissolved in acetone was added to each well and 150 µl of the standard/sample were added. The samples were incubated for a minute and the fluorescence was measured using a SpectroMaxM5 plate reader from Molecular Devices with an excitation wavelength set to 390 nm and emission recorded at 490 nm.

Arginine side chain modification

Arginine side chain modifications were monitored by determining free arginine side chains with 9,10-phenanthrenequinone (PAQ) [166] which forms a strongly fluorescent compound [167]. The fluorescence was measured in a SpectroMax M5 plate reader (Molecular Devices) using a 96 well plate. Briefly, 50 µl protein sample (1 mg/ml) was mixed with 25 µl of 2 M NaOH and 150 µl of 9,10-phenanthrenequinone (150 µM in EtOH). The mixture was incubated at 60 °C for

3 h. 100 µl of the mixture was then mixed with 100 µl of 1.2 N hydrochloric acid and incubated at room temperature in the dark for fluorophore formation for 1 h. Fluorescence of modified arginine side chains was measured with an excitation wavelength of 312 nm and an emission wavelength 395nm.

Fructosamine content estimation

Fructosamine content was determined using the "Glycated Serum Protein Assay" kit from Diazyme, Poway, California. This assay uses Diazyme's specific fructosaminase™, a microorganism originated amadoriase. In the first step the AGE modified protein is digested with proteinase K into low molecular weight glycated peptides. In the second, fructosaminase degrades the Amadori products catalytically and generates glucosone and hydrogen peroxide. The hydrogen peroxide is quantified colorimetrically by a Trinder end-point reaction by measuring the absorbance at 546nm. Briefly, 200uL of reagent 1 was added in a 96 well plate, 10ul of the AGE compound (1mg/mL final concentration), calibrator or control was added and the blank absorbance was recorded at 546nm. Five different dilutions of the calibrator were used. The plate was then incubated at 37 °C for 5 min. 50ul of reagent 2 was added and the increase in absorbance was recorded at 546nm after incubation at 37 °C for 5 min. The calibration curve was plotted using the calibrator absorbance values and the fructosamine content was obtained for the AGE samples.

Carboxymethyl lysine estimation

The carboxymethyl lysine (CML) content in the AGE samples was estimated by ELISA using an anti-CML antibody (R&D Systems, IgG2B MAB 3247) and an alkaline phosphatase labeled secondary antibody. 100 µL of 100 µg/mL protein was used for the assay. The samples were coated on a high binding capacity ELISA plate overnight at room temperature. The samples were then blocked with 3% BSA at 37 ºC for 2 hours. The anti-CML antibody was added for one hour and then washed with PBS/0.05% tween for 5 times. The secondary antibody was added for an hour and then washed with PBS/0.05% tween for 5 times. The alkaline phosphatase substrate p-nitrophenol phosphate (1mg/mL) was added and was incubated at 37 ºC. The absorbance was measured in an ELX800 multiwell plate reader (BioTek, Winooski, VT) with a 405 nm filter at different time points.

Carbonyl content estimation

The carbonyl content of glycated serum albumin was measured using the 2,4-dinitrophenylhydrazine method [168]. Briefly, 0.2 mL of 4 to 5 mg/ml protein were mixed with 0.8 mL of 0.1% dinitrophenylhydrazine in 2.5 M hydrochloric acid and incubated at room temperature for 1.5 hours. Then, 1 mL of 20 % trichloroacetic acid was used to precipitate the protein followed by centrifugation. The pellet was resuspended and washed with 10 % trichloroacetic acid. The pellet was then washed twice with ethyl acetate: ethanol (1: 1). The final pellet was resuspended in 0.5 mL of 6 M guanidium chloride and the absorbance was measure at 370 nm. To calculate the carbonyl content of the AGE modified proteins an extinction coefficient of 22 mM^{-1} cm^{-1} for dinitrophenylhydrazone was used.

Differential scanning calorimetry

Thermal stability of glycated BSA was monitored by differential scanning calorimetry (DSC) using a Nano DSC (TA Instruments, New Castle, DE) with 0.3 ml micro-volume cell. The protein was diluted in PBS to a final concentration of 70 µM. The samples were degassed for 10 minutes at 4 °C. The sample was loaded into the sample cell and PBS was loaded into the reference cell. Temperature scans were carried out from 10 ºC to 100 ºC at a heating rate of 1 ºC/min under 3 atm. PBS was loaded into both the sample and reference cell to obtain the baseline. DSC curves were analyzed using the Nano Analyze Software v2.1.9 provided by the instrument manufacturer. Baseline curve was subtracted and two state scaled model was used to obtain the Tm and enthalpy of unfolding.

For the diclofenac binding studies, the final concentrations of protein and diclofenac were 45 µM and 1 mM, respectively. The protein was premixed with the drug in PBS and was incubated for 2 min at room temperature and 300 µl of this mixture was loaded into the sample cell. These concentrations were chosen based on the observed signal strength (changes in heat capacity) and to allow >90 % saturation of diclofenac binding sites on most of the glycated forms of serum albumin. All samples were degassed thoroughly under vacuum for 10 minutes at 4°C. A scan rate of 1ºC/min was used and the scans were carried out from 10°C to 95°C. The Tm and enthalpy of unfolding ΔH of the protein were estimated using the Nano Analyze Software v2.3.6 provided by the instrument manufacturer as described before.

Circular dichroism spectroscopy

Circular dichroism spectra were recorded on a Jasco J815 spectropolarimeter equipped with a PFD-425S Peltier cell holder. A constant concentration of 1.3 µM (300 µl) protein in PBS was used for all measurements. The samples were scanned from 200 nm to 350 nm and multiple (3 scans) scans were averaged. The scans were carried out at 20 °C with an integration time of 1 sec and a scanning rate of 50 nm/min. Temperature scans were carried between 10 °C to 90 °C with a scan rate of 1 °C/min and the wavelength was set to 222 nm to observe the change in alpha helical content. A cuvette of 2 mm path length was used for the CD scans. CD-spectra were deconvoluted after baseline correction(PBS was used to record the baseline) using spectral data ranging from 200 to 260 nm using the CD-pro software package/ Dichroweb software [169, 170 171] using the CONTIN algorithm.

For the drug binding experiments, the protein and drug were premixed to achieve final concentrations of 45 µM and 1 mM, respectively (premixed in PBS as described earlier). This protein—drug ratio was identical to the conditions used in DSC experiments. The samples were scanned from 200 nm to 280 nm in a quartz cuvette of 1 mm path length with an integration time of 1 sec and a scanning rate of 50nm/min and multiple CD scans were averaged. The temperature was kept constant at 20°C. Spectra were deconvoluted using spectral data ranging from 200 to 260 nm using the Dichroweb software using the CONTIN algorithm as described earlier.

Aggregation and surface charge analysis by HPLC

A BioLogic DuoFlow F10 chemically inert HPLC system (Biorad) was used for chromatographic analysis. Size exclusion separations of the AGE samples were carried out using a Zorbax GF-250, 4.6 x250 mm gel filtration column with 4 µm particles and 150 Å pore diameter (Agilent Technologies), 50 µL of 1.5 mg/mL protein samples were injected using a 50 uL static loop. The isocratic phase consisted of 50 mM potassium phosphate, 150 mM sodium chloride, pH 7.4 and the flow rate was set at 300 µl/min. Protein elution was detected by 280 nm UV absorbance at 1 second intervals. The peaks in the elution profile were integrated and all samples were measured in triplicates.

Anion-exchange chromatography using a UNO-Q1 anion-exchange column (Biorad) was utilized to analyze differences in the surface charge of glycated serum albumin. A binary buffer system was used to generate a linear salt gradient. Buffer A contained 20 mM Tris pH 8.2, buffer B contained 20 mM Tris, 1 M NaCl, pH 8.2. 50 µL of 1.5 mg/mL protein was used. All samples were analyzed three times.

Dynamic light scattering (DLS) and fluorescence spectrometry

Dynamic light scattering was used to determine the average particle size and size distribution of all protein samples using a Zetasizer Nano-ZS 90 (Malvern, UK) dynamic light scattering instrument. The protein concentration was 10 mg/ml for all samples in 50mM phosphate, 150mM NaCl, pH 7.4 (PBS) and samples were filtered through a 0.2 micron syringe filter. Data were recorded for two independent experiments and analyzed for hydrodynamic particle diameter and sample polydispersity using the software provided by the instrument manufacturer.

Isothermal calorimetry (ITC)

Isothermal titration calorimetry measurements were performed using a Nano ITC instrument (TA Instruments, USA). A microcell with a volume of 190 µL was used to study the binding of diclofenac to glycated BSA. All solutions were prepared in PBS and degassed using a dedicated, stirred vacuum station for 10 minutes at 4°C. The protein concentration was 110 µM while the concentration of the titrated drug was 5 mM. Concentrations were chosen based on the observed binding affinities for each sample from preliminary experiments to achieve binding saturation for optimal analysis of binding titration curves. The drug was titrated into the protein solution in 25 injections of 2 µl using the 50 µl auto-pipette with a constant stir rate of 400 rpm. Each injection had a duration of 2 sec with an interval of 400 sec. The heats of the dilutions of the drug were determined by titrating 5mM drug into PBS. After subtracting the heats of dilutions data were analyzed using the Nano analyze software® v2.3.6 provided by the instrument manufacturer. We used a model assuming a set of identical, independent binding sites to obtain the thermodynamic parameters.

Recombinant RAGE-VC1 expression and purification

The plasmid pET15b_RAGE-VC1 encoded RAGE residues 23-243 with an additional N-terminal 6xHis-tag. The protein was expressed in Shuffle T7 Express cells NEB C3029 cells (New England Biolabs). The plasmid (1 µL) was inserted into electro-competent Shuffle T7 Express cells (100 µL) by electroporation at 1600V. The cells were expanded in L.B. media containing the selection antibiotic ampicillin. The cells were grown in 400mL media in 2L culture flasks at 37 °C with continuous shaking at 220 rpm. The cells were induced with 100mM IPTG after they have reached an OD_{600} of 0.6. After induction the temperature was reduced to 27 °C, the cells were grown overnight and harvested by centrifugation at 4000rpm. The cells from 4 liter culture were suspended in a buffer containing 50mM Tris, 20mM Imidazole, 300mM NaCl, pH-8.0 and frozen at -20 °C.

For purification, the cells expressing RAGE-VC1 were thawed on ice and sonicated with a power of 15 with the sonicator (Misonix XL-2000). The cell debris was separated by centrifugation at 12000 rpm at 4 °C and the supernatant was collected. The protein was purified from the supernatant by a two-step process. First, using a pre-packed HisTrap HP column (GE Healthcare) the His-tagged RAGE VC1 was purified. The bound RAGE-VC1 was eluted using 50mM Tris, 200mM Imidazole, 300mM NaCl, pH-8.0. Protein elution was detected by 280 nm UV absorbance at 1 second intervals. The eluted protein was collected and diluted (1:1) using 10mM Na-acetate buffer, pH 5.5. We then used the pre packed HiTrap SP FF column (GE healthcare 17-5054-01) which contains the cation sulfopropyl to separate out the DNA bound to the protein. The bound protein was eluted from the column using a linear gradient of NaCl from 0M to 1M in the 10mM Na-acatate buffer, pH 5.5. The eluted protein was collected, concentrated by ultra-filtration using regenerated cellulose 10 Kda MWCO membrane

(Millipore), aliquoted and stored at -80 °C. The purity of the protein was estimated by sodium dodecyl sulfate polyacrylamide gel electrophoresis (SDS-PAGE) and showed a single band of the expected molecular weight when stained with colloidal Coomassie Blue (Figure 2.5). 11.3 mg of RAGE VC1 was obtained from 4 liters culture. The protein could be concentrated up to 10 mg/mL in the presence of 800mM NaCl.

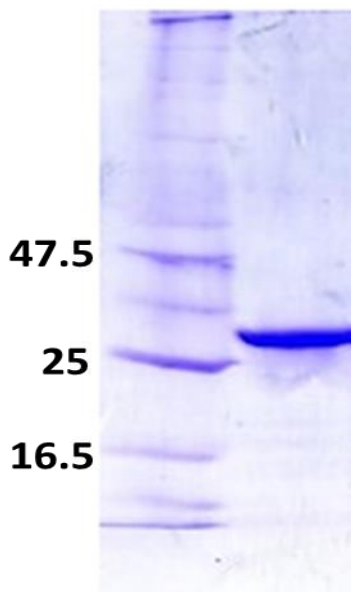

Figure 2.5. SDS-PAGE of purified RAGE VC1 domain.

Galectin-3 CRD expression and purification

The carbohydrate recognition domain (CRD) residues 112-250 of galectin-3 was cloned into the pEX-N-His PrecisionShuttle bacterial expression vector from OriGene. The protein was expressed in BL21 (DE3) cells. The conditions used for the expression of galectin-3 were exactly similar to the RAGE-VC1 expression.

The expressed protein was purified by a single step metal chelate affinity chromatography using a HisTrap HP column (GE Healthcare) and 200 mM imidazole for elution as described earlier. The protein was dialyzed twice against 200 volumes of 10mM Tris, pH 7.5, concentrated and characterized by UV/VIS spectroscopy and SDS-PAGE. Only a single band of the expected molecular weight was detected after Coomassie Blue staining of the gel (Figure 2.6). We obtain about 12.5 mg of the gal3-CRD from 4 liters culture. However, the protein could be concentrated to more than 1.3 mg/mL.

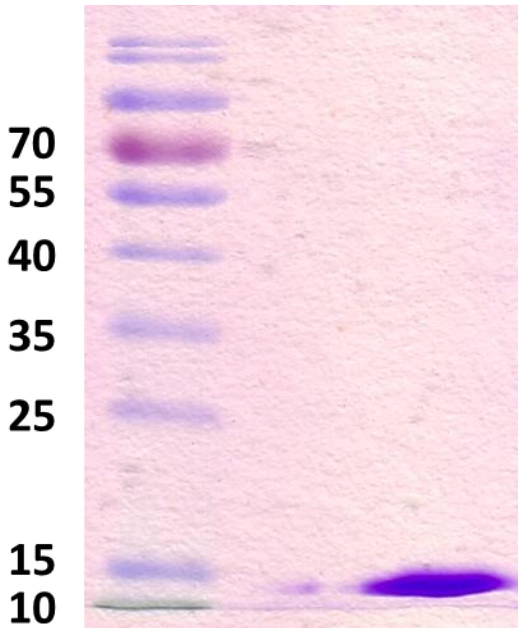

Figure 2.6. SDS-PAGE of purified RAGE Gal-3 CRD domain.

Pull-down of glycated BSA by RAGE-VC1 and galectin-3 CRD

Binding between glycated BSA and its potential receptor proteins was determined by affinity pull down assay. The AGE-BSA samples and AGE-receptors were mixed in solution and the complex was pulled down using an affinity resin binding to the 6His-tag attached to RAGE-VC1 and galectin-3, respectively. The assay was carried out in a micro-spin column, 50 µL Ni^{2+} charged Profinity IMAC resin (Biorad) was loaded on to the column. The resin was equilibrated using 50mM Tris, pH 7.4. Equal molar amounts of AGE-BSA and His6xs-RAGE-VC1or 6xHis-galectin-3, respectively, (25 µM 50mM Tris, pH 7.4) were mixed and allowed to incubate for 10 min on ice. The samples (100uL final volume) were then loaded onto a micro-column of and allowed to bind to the resin for 5 min. The resin column was washed up to 10 times with 10 column volumes of 50 mM Tris at pH 7.4. Flow through fractions were collected. After the final wash, proteins retained on the solid resin and in wash fractions were analyzed by SDS-PAGE. The samples were boiled in a reducing buffer with 4% BME before loading on the gel.

Interaction of Rib-vH BSA with RAGE-VC1 or Galectin-3 by fluorescence polarization

Fluorescence polarization was measured on a FluoroMax® (Horiba Jvon Yvon) spectrofluorometer equipped with a Glan-Thompson polarizing prism. A quartz cuvette with reduced path length of 5 mm was used for all experiments. The internal fluorescence of rib-vH BSA was used for this assay. An excitation wavelength of 350nm and an emission of 500nm were used. The slit size of the excitation and emission filters was set to 4nm. The proteins were dialyzed against 200 volumes of 50mM Tris, pH 7.4 overnight at 4 °C. 600 µl of 1 µM solution of AGE product in 50mM Tris, pH 7.4 was titrated by incremental addition of RAGE-VC1 or galectin-3. The polarization values were measured after each addition with an equilibration time of 2 min at room temperature, the increase in sample volume at the end point of the titration was less than 3%. The fluorescence polarization values were plotted against RAGE-VC1/galectin-3 concentration and the binding affinities (dissociation constants K_d) were calculated by fitting the data obtained to a modified quadratic equation (Eq 1) using kaleidograph software (synergy software). This equation was described by Anderson et al. (1988) [172] for a 'one-binding-site model'.

$$F=F_o+(\Delta F_{max}/[P_o])*\ [([P_o]+[C]+K_d)-[([P_o]+[C]+K_d)^2-(4*[C]*[P_o])]^{1/2}]/2 \qquad (2.1)$$

ΔF_{max}= is the total change in polarization

F_o = is the initial polarization value

P_o= is the total concentration of RAGE/galectin-3

C= is the concentration of the AGE compound after every addition

Cellular proliferation assay

We used the human melanoma cell line WM-115, stably transfected with RAGE in our assay. The cells were maintained in Opti-MEM (Invitrogen) supplemented with 4 % FBS in the presence of penicillin, streptomycin and 1mg/ml G418 at 37 °C and 5 % CO_2. For cell proliferation assays, the cells were detached with 0.25 % trypsin and seeded ($4x10^4$ cells per well) in 24 well plates in Opti-MEM supplemented with 4 % FBS, penicillin, streptomycin and G418. After 24 h incubation, the different preparations of glycated BSA were added to the wells at a final concentration of 230µg/ml and the plates were incubated for another 24 h. Alamar Blue (resazurin) was then added to the wells ($1/10^{th}$ the total volume of the well) and the plates were further incubated for 3-4 h at 37 °C. The reduced form of Alamar Blue was detected by fluorescence spectroscopy (excitation: 540 nm; emission: 590 nm) using a Spectramax M5 plate reader. Wells containing only cell culture medium, but no cells, were used for fluorescence background correction. Three proliferation experiments were performed using four wells for each experimental condition.

Results and Discussions

UV/Vis spectroscopy

We assessed the effect of eight glycation reagents (Figures 2.3 and 2.4) on the modification of lysine and arginine side chains in serum albumin (Table 2.2). Glycation of BSA with glucose and ribose were performed at three different concentrations. The lowest concentration of 20 mM was chosen based on pathophysiologically relevant blood glucose concentration observed in patients with uncontrolled diabetes. The highest concentration of 500 mM is frequently described in the literature for the in-vitro preparation of AGE-modified proteins for glycation related studies. We included these high concentrations of modifying ribose and glucose into our study to allow comparison to literature data. The concentrations of the other glycation reagents were chosen to be 1-5 mM to account for their increased chemical reactivity. These concentrations exceed concentrations observed in the blood; however, the true concentration of these reactive carbonyl compounds in specific tissues or inside individual cells under pathological conditions is uncertain [159]. Methylglyoxal, glyoxylic acid, glyceraldehyde and glycolaldehyde are metabolic intermediates; acetoin and diacetyl are products of liver metabolism [173]. Acetoin and diacetyl are also formed during fermentation and found in many foods [174], or intentionally added as flavoring agents to impose a butter-like aroma. Diacetyl has been linked to obliterative brochiolitis in workers exposed to the compound [175].

Visual inspection and high-speed centrifugation of AGE-modified BSA samples at the end of the 21 days glycation period and after dialysis did not indicate any significant formation of protein precipitation in any of the glycated samples. This shows that BSA can undergo prolonged glycation without significant loss of solubility (10–40 mg/ml).

The “Maillard” reaction is also known as “browning reaction” because it leads to compounds that absorb in the visible region of the spectrum, resulting in a brown coloration of the products. We recorded the UV/VIS spectra of all glycated serum albumin samples to distinguish glycation reagents that do result in colored advanced glycation end products from those that do not generate chromophores absorbing light in the near UV and visible region. Characteristic spectroscopic features of advanced glycation end products formed by specific reagents may be useful to identify specific AGE compounds. UV/VIS absorbance traces are nearly identical for nonmodified BSA and CML- and glyoxylic acid modified BSA, indicating that no new chromophores with absorbances above 250 nm have been introduced into the protein structures.

BSA modified with lower concentrations of most glycation reagent also remained colorless to the eye, except for samples modified with ribose or diacetyl, which appear light yellow in color. The Figure 2.8 shows the UV/VIS absorbance spectra of BSA modified with low concentrations of modifying reagents. Spectral traces for Glc-L and Ace-L are nearly superimposable with non-modified BSA-fresh. Modifications in samples MG-L BSA, Glc-L BSA, or Gla-L BSA do not change absorbance in the visible region (>380 nm), but indicated the formation of novel chromophores which absorb in the region between 260-370 nm.

Diacetyl glycated BSA (Dia-L BSA) clearly showed a novel chromophore with a well-developed absorbance maximum at 327 nm. In contrast, ribose modified samples (Rib-L BSA) also showed strong absorbance between 300-370 nm, but the absorbance profile is broad and featureless, without clear peaks or troughs between 300 to 500 nm. We also noticed variations in the region around 280 nm, which, in non-modified proteins, is caused by UV absorbance by phenylalanine, tyrosine and tryptophan residues. Decreased molar absorbance in the 280 nm region may indicate modification of tryptophan residues, while increases in molar absorbance indicate formation of novel chromophores absorbing in this region of the spectrum. Figure 2.7 shows the UV/VIS absorbance profiles of AGE-BSA produced with high concentrations of glycation reagents. The spectral properties or Rib-H and Rib-vH BSA showed broad absorbances between 300-500 nm, with a clear shoulder or second peak around 302 nm. Diacetyl (Dia-H BSA), glycoaldehyde (Gla-H BSA) and methylglyoxal (MG-H BSA) modified BSA show similar absorbance between 300-400 nm, possibly indicating formation of identical or similar chromophores. These latter samples can be distinguished spectroscopically form samples modified with glucose (Glc-H BSA, Glc-vH BSA) or glyceraldehyde (Gly-H BSA). Acetoin glycated serum albumin contains only minimal quantities of novel chromophores absorbing above 300 nm.

Our data demonstrate that there are significant differences in the extent of UV/Vis absorbance caused by individual glycation reagents. However, UV/Vis absorbance spectra of glycated protein samples provide only very limited information about the extent and the nature of the glycation modification.

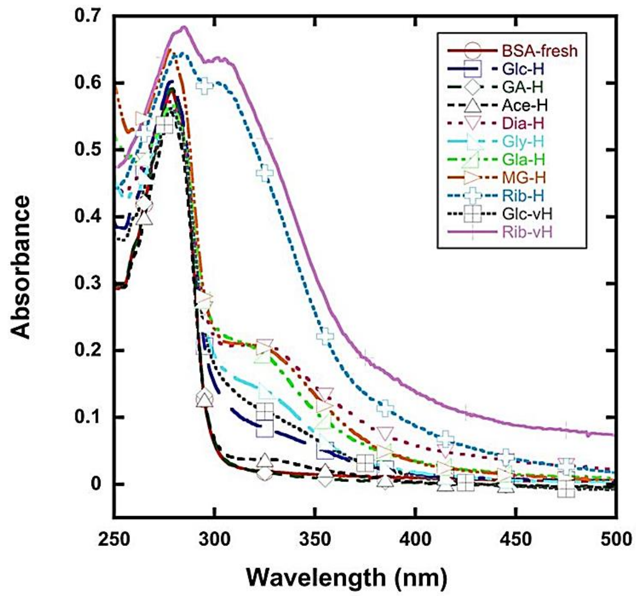

Figure 2.7. UV absorbance spectra of BSA glycated with high concentrations of glycation reagents.
Increased concentration of glycation reagent leads to formation of novel chromophores in in most samples, except for acetoin and glyoxylic acid.

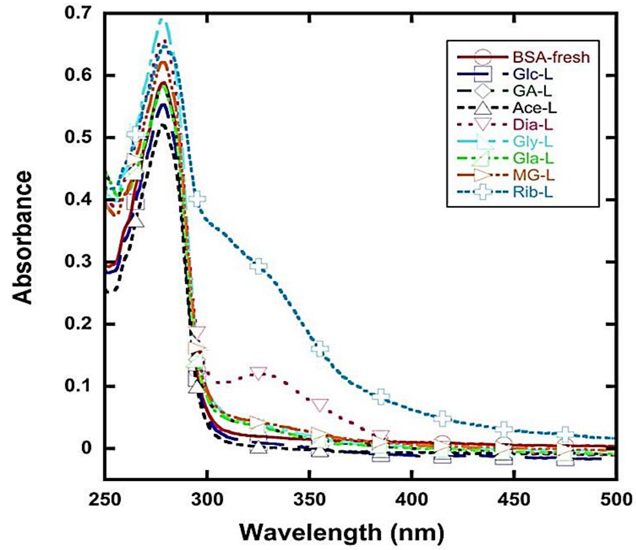

Figure 2.8. UV absorbance spectra of BSA glycated with low concentrations of glycation reagent.
Diacetyl and ribose modified samples are clearly distinguishable from the other samples by their increased absorbance between 300 and 350 nm.

Fluorescence spectroscopy

The fluorescence properties of the AGE-BSA samples were investigated. Many AGE compounds are fluorescent and their fluorescence is often used as a measure for AGE content in tissues such as skin [176], cartilage [177] and the eye lens [178].

We expected that the different glycation reagents lead to the formation of chromophores with distinguishable fluorescence properties. Fluorescence spectra were collected at 285 nm, 340 nm, 375 nm, 400 nm, 475nm and 525 nm excitation wavelengths. The emission scans of the 340 nm excitation wavelength are shown in Figure 2.9. Proteins that had not undergone a browning reaction showed fluorescence emission spectra nearly identical the non-modified BSA. The emission spectra of CML and glyoxylic acid modified BSA could be attributed solely to the fluorescence of the tryptophan residues. This observation is expected, since UV/VIS absorbance is a prerequisite for fluorescence.

Protein modification with acetoin (Ace-H BSA), diacetyl (Dia-H) and CML modification did not result in significant formation of fluorophores in the protein. All other glycation reagents did generate novel fluorophores. At the chosen excitation wavelength of 340 nm we observed fluorescence emission maxima between 391 nm (Gly-H BSA) and 432 nm (Dia-H BSA). The fluorescence intensities varied greatly between samples. The strongest fluorescence was observed for the ribose modified sample (Rib-vH BSA), which was over three-fold stronger than the fluorescence emitted from glucose modified albumin (Glc-vH BSA). Glyceraldehyde and glycolaldehyde modification also led to formation of strong fluorophores, whereas the fluorescence intensity of methylglyoxal modified BSA (MG-H BSA, 5 mM methylglyoxal) was comparable to the highly glucose modified sample (Glc-vH BSA, 500 mM glucose). However, the peaks of the emissions were clearly separated by 27 nm (Em_{max} MG-H: 399 nm, Em_{max} Glc-vH: 426 nm).

The samples were excited at 285 nm to determine the effect of glycation on Trp fluorescence. We do not see a huge shift in the fluorescence maxima of the AGE samples except in the methyl glycoxal (MG-H) and the ribose (rib-H, rib-vH) modified samples. In the rib-vH BSA the emission maxima was at 426nm, this suggests the modification Trp residues in the ribose modified samples. In the MG-H BSA sample two distinct peaks were observed which had their emission maxima at 332nm and 378nm respectively. This suggests the formation of a novel fluorophore. We also observe a drop in the emission intensities. We suspect this could be the result of an environmental change in the environment surrounding the Trp residues due to unfolding of the protein due to glycation. Trp fluorescence is highly dependent on the surrounding environment (This aspect is described in detail in chapter 5).

When the samples were excited at 375nm an emission maxima was observed at around 445nm in the rib-vH BSA sample. The MG, Gly and Gal modified samples also showed an emission maxima at around 445 nm however, the intensity was much lesser when compared to the Rib-vH BSA sample.

The spectroscopic characterization demonstrates that the reaction products of serum albumin glycation depend on the glycation reagent used. Depending on the chemical structure and reactivity of the glycation reagent, novel chromophores and fluorophores are formed. For example, while glucose and ribose are chemically closely related, they differ greatly in their ability to glycate proteins as reflected by chromophore and fluorophore formation. In addition, the spectral features of glycated albumins demonstrate the chromophores / fluorophores introduced by glucose, ribose and the other reactive aldehydes are chemically not identical. It appears that refined fluorescence spectroscopic methods may be suitable to distinguish between glycation end products derived from different glycation reagents. This would be valuable for the analysis of AGE compounds and may offer the possibility to identify the glycation reagent responsible for glycation under physiological conditions.

Glycation in general primarily involves the modification of lysine and arginine residues. It has been reported that the modification of arginine residues by compounds such as methylglyoxal leads to formation of hydroimidazolones, tetrahydropyrimidine and argpyrimidine. Crosslinkage between modified arginine and lysine side chains leads to pentosidine [179]. Of these compounds, only argpyrimidine and pentosidine are fluorescent [180]. Argpyrimidine shows high absorbance between 320 and 335 nm and a fluorescence emission maximum around 400 nm [178]. Pentosidine also absorbs between 325 and 335 nm, but has an emission maximum at 375–385 nm [178]. Analysis of the fluorescence emission spectra suggests that pentosidine and argpyrimidine have been formed, but also indicate that additional fluorophores are present. These fluorophores produce maximum emission at 435 nm when excited at 365 nm, which has been previously reported for AGE-proteins [160]. The changes in fluorescence emission profiles with changes of the excitation wavelengths indicate that multiple fluorophores with overlapping absorbance and emission spectra exist in the samples. Despite the fact that the fluorescence properties of AGE modified protein have been investigated for almost two decades, very few of the fluorescent compounds present in AGE proteins have been identified unambiguously.

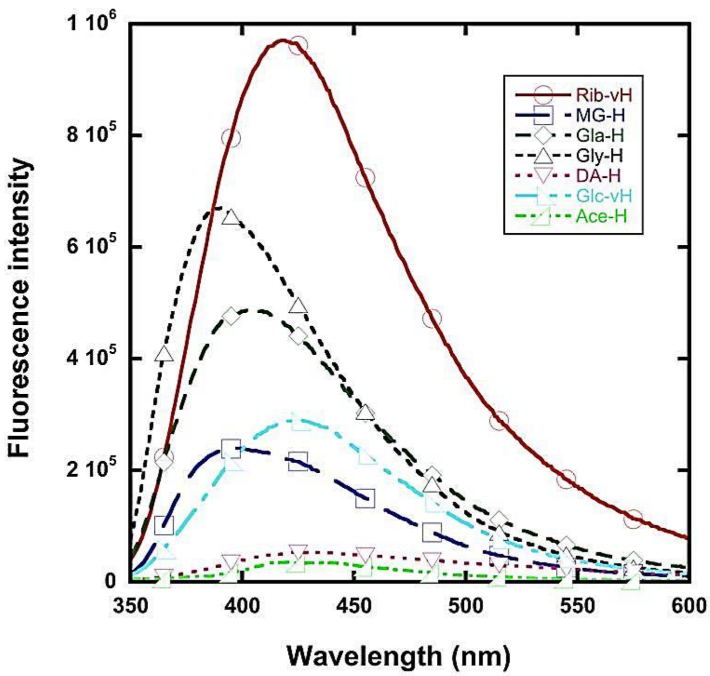

Figure 2.9. Fluorescence emission spectra of glycated BSA at an excitation wavelength of 340 nm.
Ribose, glyceraldehyde and glycolaldehyde glycation leads to strongly fluorescent compounds. Gycation with methylglyoxal and even high concentration of glucose (500 mM) leads to moderate fluorescence. No significant fluorescence was observed in acetoin and glyoxylic acid modified samples.

Amino acid side chain glycation

The degree of amino acid modification was assessed with several complimentary methods. Standard amino acid analysis uses strong acidic conditions for amide bond hydrolysis. These conditions are likely to destroy many glycation and advanced glycation endproducts. Therefore, amino acid analysis can only determine a subset of amino acid modifications that are acid resistant, such as CML, argpyrimidine and other advanced glycation endproducts. We performed amino acid analysis on only the BSA samples derivatized with glucose (200 mM), glyoxylic acid (10 mM), methylglyoxal (5 mM) and CML (23 mM) concentrations of modifiers and on non-modified, aged BSA. BSA contains 59 lysine residues and 23 arginine residues. It was found that approximately 15% of arginine residues were modified in the methylglyoxal modified sample and approximately 15% of lysine residues in the CML-H preparations. The lysine and arginine contents detected for glyoxylic acid and glucose modified samples were found to be N95% (Table 2.2). To get a more precise assessment, the modification of arginine and lysine side chains was assessed using the 9,10-phenanthrenequinone and fluorescamine assays, respectively. The mild conditions of these assays, when compared to standard amino acid analysis, allowed us to determine hydrolysis sensitive glycation-modifications in the samples. We also measured the formation of the early glycation product fructosamine and the advanced glycation end product carboxymethyl lysine (CML) as described earlier.

As expected, for a given glycation reagent, the extent of side chain modification increased with increasing reagent concentration. However, a substantial portion of arginine and lysine residues remained un-modified even at high reagent concentrations. This demonstrates that glycation does not proceed to completion and suggests that modification of amino acids may occur preferentially on the protein surface or specific glycation “hot-spots”. A similar conclusion has been drawn by Barnaby et al. after they studied albumin glycation by mass-spectrometry [85, 181, 182].

Table 2.2 summarizes the amino acid modifications in the all the different glycated samples. There are profound differences between the glycation reagents in terms of overall reactivity, as well as in their selectivity for either lysine or arginine modification. For example, glucose is a relatively unreactive glycation reagent when compared to ribose, or any of the other compounds tested. The differences in reactivity between glucose and ribose arise from the higher stability of the closed ring form (hemiacetal) for glucose, when compared to ribose [183]. Interestingly, the reactivity of ribose towards lysine side chains allows for almost complete modification of lysine (96 %), whereas arginine side chains are only moderately modified (15 %). High percentage of modified lysine residues were also observed in the rib-L BSA sample (48.7%). 58.7% and 24.4% of the lysine and arginine residues were found to be modified in the glc-vH BSA sample respectively. Fructosamine was only detected in glucose modified albumin. The glc-vH BSA sample has a fructosamine content of 27 mol/mol of protein. Fructosamine was not observed in any other sample. Fructosamine modification seems to be the dominant lysine side chain modification in glucose modified samples, which is in agreement with previously reported findings[184]. The carboxymethyl lysine was found in ribose glycated albumin but not in glucose glycated albumin. These differences in composition between glucose and ribose glycated proteins may have implications for their biological activities.

Methylglyoxal, glyceraldehyde, glycoaldehyde and diacetyl showed similar reactivities towards arginine and lysine and lead to substantial modification (>40%) at 5 mM reagent concentration. We detected CML only in glyceraldehyde and glycoaldehyde modified samples, but not in methylglyoxal or diacetyl modified samples (5%). The reactivity of glyoxylic acid is generally minimal; hence we do not observe substantial modification of lysine and arginine residues (> 5%). The initial formation of the Schiff-base between the protein and the glyoxylic acid is nearly completely reversible in the absence of an additional reducing reagent and the high oxidation state of the carboxyl group prevents Amadori rearrangement. However, in the presence of sodium cyanoborohydride as reducing reagent (used in the CML modified BSA), the formation of CML on lysine residues occurs, while arginine residues remain unaltered. 18% and 32% of the lysine residues were modified in the CML-L and CML-H BSA samples respectively.

Acetoin, which is chemically related to diacetyl by reduction of one of the keto groups, is significantly less reactive when compared to diacetyl or the other reactive aldehydes. Arginine residues appear not to be modified by acetoin and the modification of lysine residues by this reagent is only modest.

Finally, we measured the carbonyl content using the dinitrophenylhydrazine method, which involves exposure of the protein to strong acidic conditions, which, as mentioned above, can lead to destruction of glycation and AGE-products. The CML samples did not contain detectable carbonyl groups. Glc-BSA and rib-BSA samples did contain detectable levels of carbonyl groups and the carbonyl content increased with the concentration of glucose and ribose. Higher carbonyl content was observed in the rib-BSA samples. The glc-vH BSA sample had a carbonyl content of 0.71 mol/mol and the rib-vH BSA had a carbonyl content of 1.90 mol/mol.

High carbonyl content was also observes in the Dia-H, Gly-H, Gla-H and the MG-H BSA samples. In general, the detected carbonyl content was approximately one carbonyl group per BSA molecule (Table 1.2). Carbonyl content was minimal in GA-BSA samples.

Our observations regarding amino acid side chain modification by glycation are consistent with previous reports in the literature and underline that AGE formation depends qualitatively and quantitatively on the glycation reagent. It also underscores that AGE compounds formed at low or moderate concentrations of glycation reagent are only partially glycated, leaving a substantial percentage of arginine and lysine side chain unmodified.

Table 2.2. Summary of amino acid side chain modifications, CML, fructosamine and carbonyl content. n.d., none detected.

Sample Name	**Lysine Modified %**	**Arginine Modified %**	**Content CML mol/mol**	**Content Fructosamine mol/mol**	**Content Carbonyl mol/mol**
BSA-fresh	0 ± 0	0 ± 0	n.d.	n.d.	0.02 ± 0.01
Glc-L BSA	8.2 ± 3.5	3.7 ± 1.2	n.d.	1.8 ± 0.5	0.15 ± 0.02
Glc-H BSA	22.0 ± 2.6	14.0 ± 3.1	n.d.	21.8 ± 1.5	0.71 ± 0.04
Glc-vH BSA	58.7 ± 2.3	24.4 ± 2.5	n.d.	27.0 ± 4.7	1.04 ± 0.06
GA-L BSA	5.0 ± 2.0	3.7 ± 1.5	n.d.	n.d.	0.10 ± 0.02
GA-H BSA	10.0 ± 3.0	4.3 ± 1.5	n.d.	n.d.	0.10 ± 0.01
Ace-L BSA	10.7 ± 3.1	5.0 ± 1.0	n.d.	n.d.	0.15 ± 0.03
Ace-H BSA	17.0 ± 4.3	6.6 ± 1.5	n.d.	n.d.	0.42 ± 0.03
Dia-L BSA	13.0 ± 2.0	11.0 ± 2.6	n.d.	n.d.	0.36 ± 0.04
Dia-H BSA	40.2 ± 5.5	38.3 ± 1.5	n.d.	n.d.	1.20 ± 0.08
Gly-L BSA	19.7 ± 2.5	9.0 ± 2.6	n.d.	n.d.	0.29 ± 0.02
Gly-H BSA	42.0 ± 1.7	38.3 ± 2.2	5.9 ± 0.1	n.d.	1.18 ± 0.03
Gla-L BSA	19.3 ± 3.1	12.3 ± 2.5	n.d.	n.d.	0.38 ± 0.03
Gla-H BSA	45.3 ± 4.2	40.3 ± 2.1	5.7 ± 0.2	n.d.	1.38 ± 0.03
MG-L BSA	19.5 ± 2.2	13.0 ± 2.0	n.d.	n.d.	0.35 ± 0.03
MG-H BSA	44.7 ± 2.5	39.3 ± 6.0	n.d.	n.d.	1.30 ± 0.03
Rib-L BSA	48.7 ± 0.8	12.3 ± 2.1	7.5 ± 0.3	n.d.	0.72 ± 0.03
Rib-H BSA	89.5 ± 0.5	13.7 ± 2.3	10.3 ± 1.2	n.d.	1.78 ± 0.04
Rib-vH BSA	96.0 ± 0.7	15.0 ± 2.6	13.8 ± 0.7	n.d.	1.90 ± 0.04
CML-L BSA	18.0 ± 9.0	8 ± 2.0	18.1 ± 1.2	n.d.	0.02 ± 0.01
CML-H BSA	32.0 ± 9.0	10.0 ± 4.0	31.5 ± 1.6	n.d.	0.02 ± 0.01

Changes in secondary structure resulting from glycation and AGE formation

Extensive modification of lysine and arginine residues in proteins can be expected to disturb the secondary and tertiary structure of the protein. We used circular dichroism (CD) spectrometry for secondary structure analysis and Figure 2.10 shows the CD-traces of selected glycated BSA samples at 20ºC. Table 2.3 summarizes the results of CD based secondary structure deconvolution. Native BSA has a high degree of α-helical secondary structure (63%) and very little β-sheet content (5%). These values are very similar to values reported in the literature (67% helix, 10% turn, 23% unordered) [185]. We observed that glycation indeed altered the secondary structure of the protein. There was a general decline in α-helical content as result of glycation and the content of β-sheet increases, for example, 4-fold from 5 % to 20 % for BSA modified with glyceraldehyde (Gly-H BSA) or ribose (Rib-vH BSA). However, the structure of the protein does not collapse into a random coil state. It rather seems to approach a molten globule state, in which residual secondary and tertiary structure is retained by the protein. Plotting the change in α-helical and β-sheet secondary structure as a function of the extent of lysine residue modification revealed an approximately linear correlation (Figure 2.11).

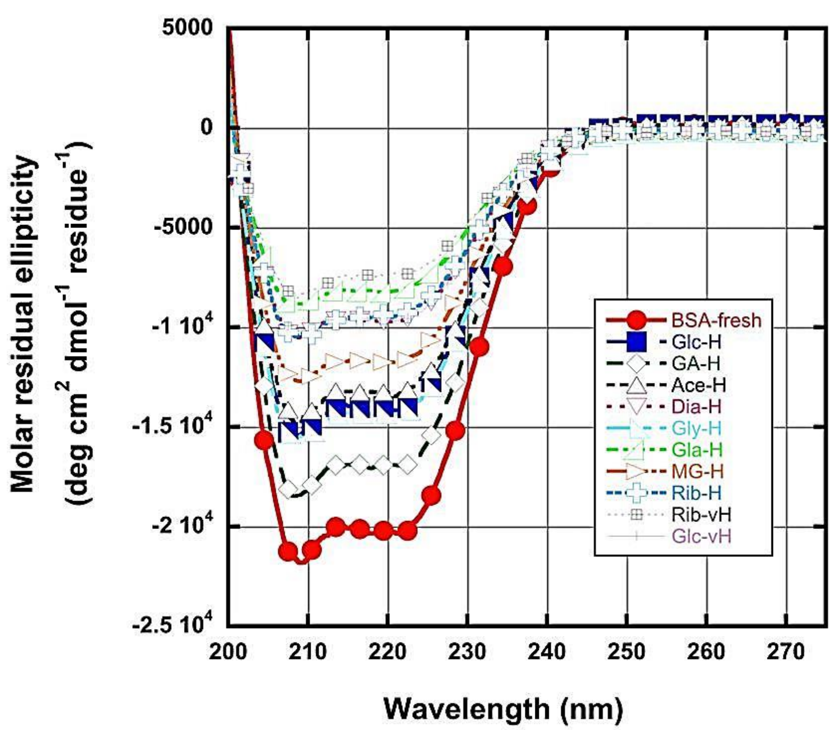

Figure 2.10. Circular dichroism spectral data of selected glycated BSA samples demonstrate the gradual loss in secondary structure, and particularly in α-helical content upon glycation. Fresh BSA is shown in red and demonstrates highest α-helical content.

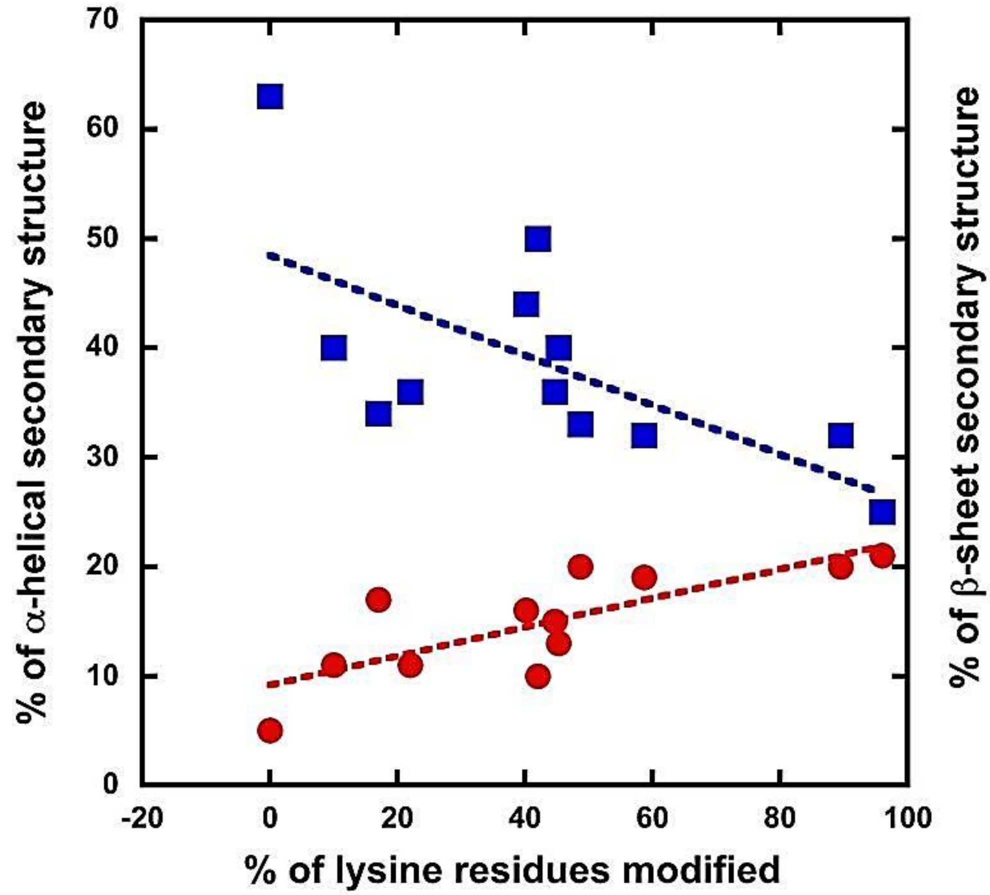

Figure 2.11. Blotting the extent of lysine side chain modification in glycated samples against the relative content of α-helical and β-sheet secondary structure in the corresponding samples reveals a linear correlation.

The red dots show the increase in β-sheet relative to increased lysine modifications. The blue squares show the decrease in α-helical content as function of lysine modification. The sample at the out left represents non-modified BSA, the sample at the outer most right corresponds BSA glycated with 500mM ribose.

Table 2.3. Analysis of secondary structure distribution in glycated BSA samples based on the deconvolution of circular dichroism (CD) spectra.

Sample	Temperature (^{0}C)	Alpha Helices (%)	Beta Sheets (%)	Turns (%)	Unordered (%)
BSA-fresh	20	63	5	12	20
Glc-L BSA	20	43	10	22	25
Glc-H BSA	20	36	11	24	29
Glc-vH BSA	20	32	19	10	39
GA-L BSA	20	40	13	19	28
GA-H BSA	20	40	11	23	26
Ace-L BA	20	41	15	16	28
Ace-H BSA	20	34	17	17	32
Dia-L-BSA	20	44	16	9	31
Dia-H BSA	20	33	20	10	37
Gly-L BSA	20	50	10	11	29
Gly-H-BSA	20	40	13	11	36
Gla-L BSA	20	48	9	11	32
Gla-H BSA	20	30	20	10	40
MG-L BSA	20	46	14	14	26
MG-H BSA	20	36	15	11	38
Rib-L BSA	20	33	20	9	38
Rib-H BSA	20	32	20	9	39
Rib-vH BSA	20	25	21	9	45

Glycation induced protein oligomerization

Glycation of BSA also did not result in the formation of large protein aggregates that would form visible precipitates or cause significant UV/VIS scattering. However, glycation has been reported to lead to protein cross-linkage and induce the formation of amyloid-like aggregates in some cases [157, 186]. In order to determine the effect of glycation on protein oligomerization and cross linking, the extent of non-monomeric protein was estimated by high-performance size exclusion chromatography. Monomeric and non-monomeric protein could be clearly distinguished from each other. However, the non-monomeric content could not be separated sufficiently to distinguish between dimers, trimers and higher order oligomers. Therefore, only a single value for "non-monomeric" proteins reported in Figure 2.12. Freshly dissolved BSA showed consistently a low level (6.1 ± 0.4%) of non-monomeric material. Glycation with 20 mM glucose had no effect on oligomerization and even glycation with 500 mM glucose only led to a minimal increase in protein oligomers to 7.6 ± 0.4 %. In contrast to glucose, ribose caused very significant oligomerization of BSA molecules, resulting in 23.3 % non-monomeric material at 20 mM ribose and 38.4 % at 500 mM ribose. Glycolaldehyde also showed high oligomerization potential, resulting in 11.5 % of non-monomeric material at 1 mM and 28.8 % at 5 mM glycoaldehyde in the glycation reaction. Significant oligomerization was also observed in samples glycated with 5 mM of methylglyoxal (11.5 %) and glyceraldehyde (10.7 %). It is important to note that these oligomeric proteins are still highly soluble and probably consist of cross-linked dimers, trimers and tetramers. These data demonstrate that ribose and glycolaldehyde have significant potential to cause inter-protein cross linkage of albumin, whereas glucose does not effectively drive cross-linkage of the same protein.

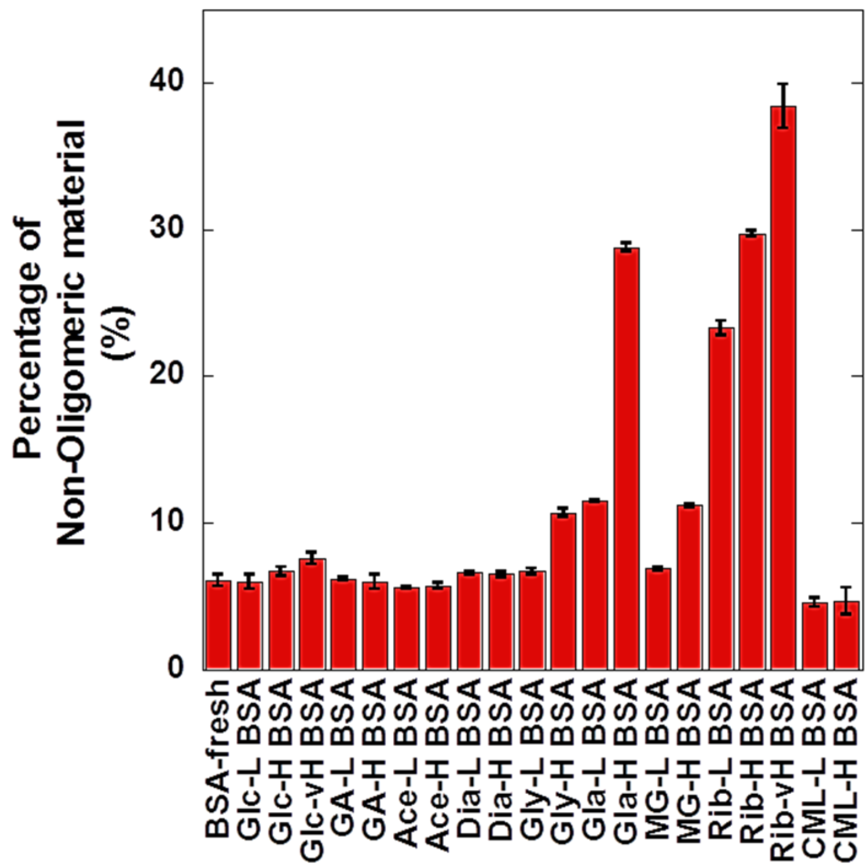

Figure 2.12. Percentage of non-monomeric content in glycated BSA samples.
Highest percentage of non-monomeric content was observed in the rib-vH BSA sample.

Effect of glycation on surface charge

Glycation occurs preferentially on lysine and arginine residues and eliminates the positive charge located at these side chain groups. To gain insight into the changes in surface charge changes upon glycation with various agents, high performance ion exchange chromatography was used and the retention of the glycated protein on the charged chromatographic matrix during elution with a linear salt gradient was analyzed. The peak shape of the eluted material provides information about sample heterogenicity. Sharp, symmetric peaks indicate little heterogenicity, while broad and non-symmetric peaks indicate increased heterogenicity in sample composition. The elution profiles for selected AGE-modified samples are shown in Figure 2.13. We noticed significant peak asymmetry for all samples. The elution profile of non-modified BSA indicated that some heterogenicity existed in the sample. The natural glycosylation and some oligomerization caused the heterogenicity observed in non-glycated BSA can be speculated. For all glycated samples increased retention on the chromatography matrix was observed, indicating a decrease in positive surface charge. As expected, the samples showing the highest degree of lysine and arginine side chain modification show the greatest change in surface charge. Glycation generally increases sample heterogenicity, most prominently for glycolaldehyde and ribose. Reagents that showed little glycation reactivity, such as acetoin and glyoxylic acid, showed only minimal effects. BSA glycated with 500 mM glucose showed a decrease in positive surface charge and relatively little sample heterogenicity. Isoelectric focusing was also used to estimate that the isoelectric point of BSA modified with 500 mM ribose is approximately 1 pH unit lower than the isoelectric point of non-glycated BSA.

The reduction in isoelectric point of glycated proteins may affect protein - protein and protein - lipid membrane interactions. However, to significantly change the surface charge of BSA, many residues have to be modified by glycation. It thus appears more likely that the glycation of specific residues on the protein surface will affect protein function, for example by changing an α-helical segment into a β-sheet or by disrupting hydrogen bonding networks involving lysine and arginine residues.

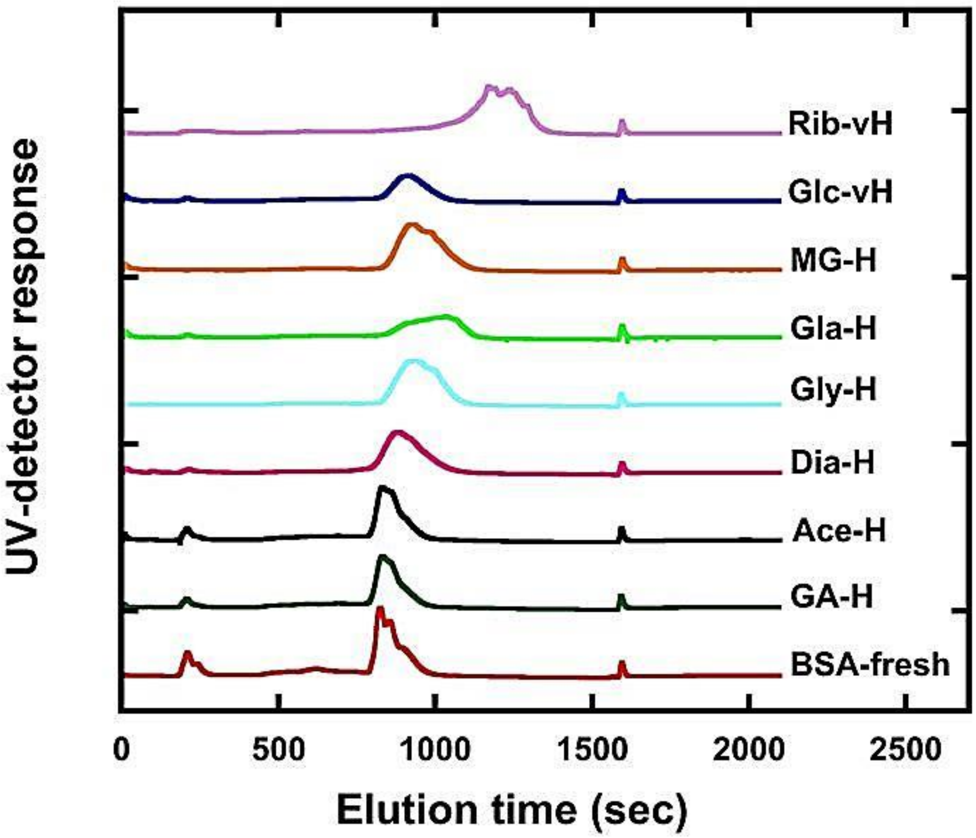

Figure 2.13. HPLC elution traces of glycated BSA during anion exchange chromatography. The lowest trace corresponds to non-modified BSA. A peak elution peak shift to the right (later elution times) indicates increased retention on the column due to decreased positive surface charge of the molecules. Broadening and asymmetry in the peaks demonstrates sample heterogenicity as result of glycation. The small peak at 160 sec is related to gradient switching.

Effect of glycation on thermal unfolding

Since we confirmed that glycation altered the secondary structure and reduced the positive surface charge of serum albumin, we hypothesized that glycation would also influence the thermal stability and unfolding of the proteins. Circular dichroism (CD) spectrometry and differential scanning calorimetry (DSC) was used to characterize the thermal unfolding of glycated BSA.

The change in α-helical secondary structure content in glycated BSA samples as a function of increasing temperature was measured. The molar ellipticity at 223 nm is a good indicator of α-helical content in protein samples and was continuously recorded between 20 ºC and 90 ºC (Figure 2.14). Unmodified BSA showed a gradual decrease in mean molar residual ellipticity up to about 60 ºC, corresponding to a reduction of α-helical structure from 63% to 54 %. At that temperature a transition occurred and accelerated protein unfolding set in, reducing the α-helical content to 38 % at 80 ºC. All glycated samples showed a lower α-helical content than non-modified BSA over the entire temperature range. Despite the reduced α-helical content, an unfolding transition could be observed for most samples, except for samples modified with 200 mM and 500 mM ribose (Rib-H-BSA, Rib-vH-BSA). The lack of an unfolding transition suggests that the protein either forms a highly heterogeneous population of partially unfolded structures or a folding state that approximates a molten globule. In both cases, the protein has access to many unfolding intermediates, which are energetically similar and thus lead to "slow melting", rather than a sharp and defined unfolding event.

To gain more detailed insights in the structural transitions during heating the CD-spectra was recorded at 20 ºC, 50 ºC, 60 ºC, 70 ºC and 80 ºC and determined the relative secondary structure composition at each temperature. Unmodified BSA showed a high α-helical content of 63%, low β-sheet content (5%), 12% turns and 20% unordered structures at 20 ºC, as previously reported in the literature [185]. Elevating the temperature to 80 ºC reduced the α-helical content to 38% and increased the β-sheet content to 12%.

All glycated samples showed significantly decreased α-helical and increased β-sheet structure at all temperatures when compared to non-modified BSA. There are significant similarities between the glycation reagents in terms of their effect on secondary structure. For example, samples modified with 1 mM of glycation reagent generally retain between 40 -50% α-helices and 9 - 16 % β-sheet structures at 20 ºC. At 80 ºC the differences between glycated samples are more pronounced. Glyceraldehyde (Gly-L) modified BSA shows only 15 % β-sheet, whereas the methylglyoxal (MG-L) samples possess 24% β-sheet. Higher concentration of modifying reagent exaggerates the loss of α-helices, leaving only 30 – 40% α-helices, and 13-20 % β-sheet at 20 ºC.

As seen with our other analytical methods, ribose caused the most pronounced change in the secondary structure. BSA modified with 20 mM ribose (Rib-L BSA) had an α-helical content of only 33%, and BSA modified with 500 mM ribose (Rib-vH BSA) showed the least α-helical content of all samples with 25%. Ribose modification also showed a high β-sheet content (21%).

The general effect of glycation on the secondary structure of BSA can be summarized as decreasing the α-helical content and increasing the β-sheet. Our results are in agreement with previous studies, which describe that glycation causes the disruption of α-helical conformation [187]. Also, the effect of glycation seems to induce secondary structure changes similar to the changes observed during thermal unfolding of non-modified BSA. Interestingly, thermal unfolding of BSA has been reported to lead to formation of aggregates and amyloid like structures [185, 186]. As pointed out above, we observed a significant degree of non-monomeric material in ribose and glycolaldehyde modified samples. Therefore, we have β-sheet enriched soluble oligomers in these samples, which may be similar to soluble oligomers reported for the prion protein or amyloid-beta peptide [188]. This could be significant, because the hypothesis has been put forward that the neuronal toxicity of misfolded prion protein and amyloid beta peptide is associated with soluble oligomers, rather than insoluble aggregates, deposits or plaques [189, 190].

Next thermal unfolding of glycated BSA by differential scanning Calorimetry was investigated. DSC provides thermodynamic parameters of the unfolding process, in particular the transition midpoint (Tm) and enthalpy ΔH and entropy ΔS of the unfolding process.

Non modified BSA showed two thermal transition peaks, as previously reported [191]. The first partially unfolding transition is reversible, whereas the second transition is irreversible, but does not lead to complete unfolding of the ordered structure [192]. The midpoint temperature of the thermal melting curve (T_m) and the associated change in enthalpy of the unfolding process (ΔH_{Tm}) were determined using a two state model (Table 2.4). The T_{m1} of the unmodified BSA was found to be 62.3 ± 0.1°C and T_{m2} was 79.3 ± 0.2 °C. These values are higher than the ones reported previously [191, 193], but can be explained by the differences in the buffer systems.

The majority of samples showed two thermal transition peaks similar to unmodified BSA. The shapes of the thermograms were broadened for most samples, indicating increased heterogenicity in the protein population (Figure 2.15). However, only a single transition could be discerned for samples modified with glucose (Glc-vH), ribose (Rib-L), diaceteyl (Dia-H), glyceraldehyde (Gly-H), glycolaldehyde (Gla-H) and methylglyoxal (MG-H) (Table 1.4). Thermograms obtained for highly ribose modified samples could not be analyzed.

The determined transition temperatures T_m and changes in enthalpy ΔH for the folding transition were shifted to higher temperatures and lower enthalpies for most samples (Table 2.4). This indicates increased conformational heterogenicity as result of glycation, reduced thermal stability and a decrease in ordered structure in the protein. As observed with the other analytical methods, higher concentrations of modifying reagents and higher levels of side chain modification lead to reduced thermal stability. However, one has to keep in mind that the thermal unfolding of BSA and its glycated derivatives does not lead to complete structure dissolution, but rather to a β-sheet rich molten globule state. Our CD analysis has shown that this molten globule state is structurally different for different glycation modification.

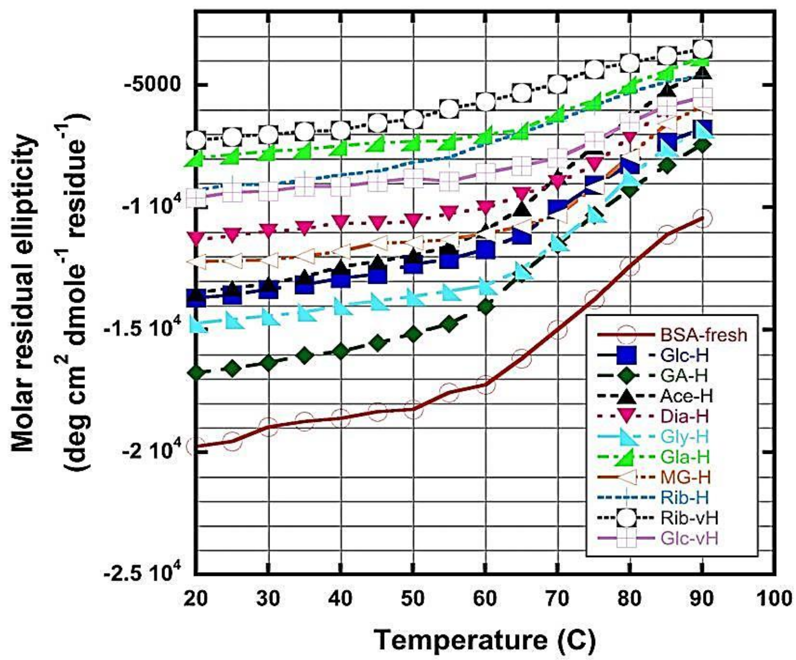

Figure 2.14. Thermal unfolding of glycated BSA samples followed by circular dichroism. Changes in the molar residual ellipticity at 223 nm was followed as a function of temperature and are indicative of the relative decrease in α-helical content in the samples.

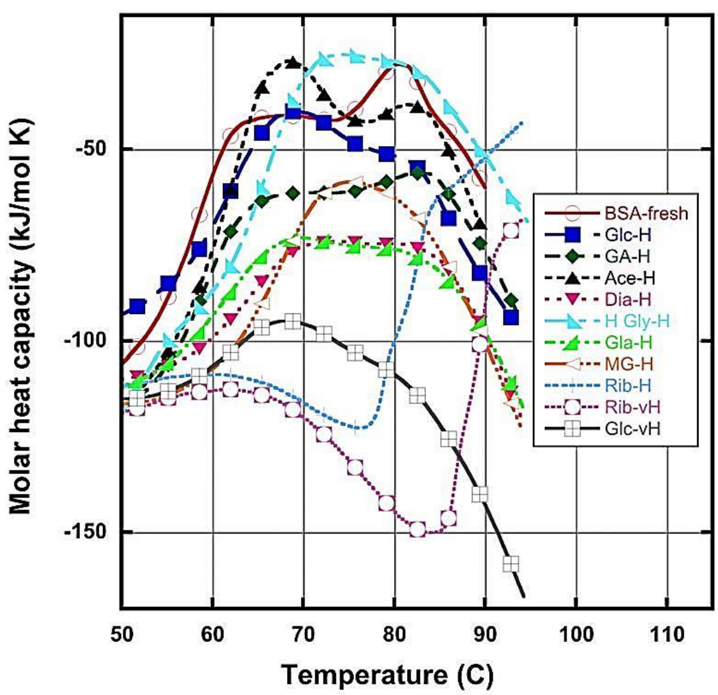

Figure 2.15. Differential scanning calorimetry thermograms for selected glycated samples. The trace for non-modified BSA is shown in red. Glycation greatly influences thermal unfolding behavior of the samples. Samples glycated by ribose do not show defined, DSC detectable thermal unfolding.

Table 2.4. Differential scanning calorimerty derived thermal transition mid temperatures (T_m) and the associated enthalpies (ΔH) and entropies (ΔS) of thermal unfolding of AGE-BSA samples.
These parameters could not be calculated for rib-H BSA and 500mM rib BSA samples as they did not show any defined peak.

Sample	**T_{m1} (^{0}C)**	**ΔH_{Tm1} (kJ/mol)**	**ΔS_{m1} (kJ/mol * K)**	**T_{m2} ^{0}C)**	**ΔH_{Tm2} (kJ/mol)**	**ΔS_{m2}**
BSA-fresh	62.3 ± 0.1	492 ± 4	1.47 ± 0.02	79.3 ± 0.2	838 ± 12	2.38 ± 0.05
Glc-L BSA	64.1 ± 0.2	382 ± 7	1.13 ± 0.03	84.2 ± 0.3	860 ± 8	2.40 ± 0.03
Glc-H BSA	66.4 ± 0.1	403 ± 8	1.19 ± 0.03	81.8 ± 0.3	612 ± 7	1.72 ± 0.02
Glc-vH BSA	65.4 ± 0.2	418 ± 3	1.23 ± 0.01	-	-	
GA-L BSA	63.0 ± 0.1	460 ± 8	1.37 ± 0.03	82 ± 0.4	630 ± 6	1.77 ± 0.02
GA-H BSA	65.0 ± 0.3	410 ± 6	1.21 ± 0.03	84.3 ± 0.2	872 ± 7	2.44 ± 0.03
Ace-L BSA	63.5 ± 0.2	420 ± 11	1.25 ± 0.05	80.1 ± 0.2	848 ± 6	2.40 ± 0.02
Ace-H BSA	65.5 ± 0.2	442 ± 8	1.30 ± 0.03	82.3 ± 0.1	797 ± 7	2.24 ± 0.03
Dia-L BSA	65.9 ± 0.1	418 ± 4	1.23 ± 0.02	82.5 ± 0.1	767 ± 5	2.16 ± 0.02
Dia -H BSA	74.3 ± 0.3	295 ± 7	0.85 ± 0.03	-	-	
Gly-L BSA	66.0 ± 0.1	436 ± 8	1.28 ± 0.03	82.2 ± 0.1	850 ± 2	2.39 ± 0.02
Gly-H BSA	74.2 ± 0.1	320 ± 1	0.92 ± 0.01	-	-	
Gla-L BSA	64.1 ± 0.1	414 ± 2	1.23 ± 0.01	82.8 ± 0.2	746 ± 6	2.10 ± 0.02
Gla-H BSA	74.2 ± 0.2	300 ± 4	0.86 ± 0.02	-	-	
MG-L BSA	66.3 ± 0.1	420 ± 2	1.23 ± 0.01	82.6 ± 0.4	856 ± 3	2.41 ± 0.01
MG-H BSA	75.1 ± 0.1	287 ± 7	0.82 ± 0.03	-	-	
Rib-L BSA	72.2 ± 0.1	349 ± 3	1.01 ± 0.01	-	-	
Rib-H BSA	-	-		-	-	
Rib-vH BSA	-	-		-	-	

Binding of glycated BSA to the AGE-receptor proteins: RAGE and Galectin-3

It has long been proposed that glycated and AGE modified proteins exert biological effects on target tissues by interaction with specific cell-surface AGE receptor proteins [130, 194-196]. Therefore, the *in-vitro* binding of our panel of AGE-modified protein samples to two known AGE receptors: RAGE and galectin-3 was studied. RAGE is an immunoglobulin-like multi-ligand and pattern recognition receptor [197], which not only binds AGE compounds, but also S100 proteins [198], amyloid peptides [199], amphoterin [17], and double stranded DNA [200]. Galectin-3 is a component of the AGE-receptor complex and member of the lectin protein family with affinity for β-galactosides [201], but galectin-3 also has high binding affinity for AGE [202].

Initially, pull-down assays between glycated BSA samples and immobilized RAGE-VC1 domain and galectin-3, respectively were performed. These binding experiments indicated that most glycated BSA samples did not bind to either galectin-3 or RAGE with high affinity. However, the ribose modified samples did bind tightly to both RAGE and galectin-3, respectively. Our pull down assay involves intensive washing of the isolated protein-protein complex and weak binding will not be detected. To estimate the sensitivity of our pull-down experiments, S100B was used as a positive control protein. S100B binding to RAGE has been well characterized by us [203, 204] and is in the low to sub-micromolar range. S100B binding to RAGE could be detected in our experimental set-up, suggesting that the binding affinity of ribose modified BSA is in a similar range, whereas the binding affinity of our other glyacted samples is likely to be lower (K_d > 50 μM).

To further define the binding of RAGE and galectin-3 to AGE-modified proteins in a more quantitative manner, a fluorescence polarization based assay was developed. The intrinsic fluorescence of our AGE modified protein samples was used, which allowed us to avoid any additional reporter label or immobilization of the proteins. The interaction of the two protein components directly and label free in solution was measured. The binding affinities for the protein-protein interactions in solution could also be calculated by this polarization assay. Typical titration binding curves of AGE-BSA to RAGE-VC1 are shown in Figure 2.16. We estimate that we are able to detect binding affinities lower than 50 μM in our experimental set-up.

The results of the polarization assays are in agreement with those of the pull down assay. Binding to RAGE was observed only with the rib-H BSA and 500mM rib BSA (Table 2.5). The binding experiments with galectin-3 confirmed binding of all ribose modified samples bound more tightly to galectin-3 than to RAGE. None of the other glycated samples showed binding affinity below $K_d < \sim 50$ μM to either RAGE or galectin-3 *in vitro*. This includes glucose modified modified BSA, which is frequently used in glycation related research studies. However, there is an ongoing controversy about which type of AGE compounds can bind to RAGE. For example, several authors have reported independently, that CML-modified BSA does not interact with RAGE in cell based assays [205-208]. Whereas others report CML-modified proteins to be bind to RAGE and to activate cellular signaling [209, 210]. There is general agreement in the literature that ribose glycated proteins do bind to RAGE. Discrepancies between *in-vitro* and *in-vivo* binding studies may be explained by the intrinsic differences between the experimental systems. The spatial arrangement of AGE-receptors on the cell surface, and possibly the recruitment of co-receptors, can significantly influence ligand binding.

Our studies are the first to measure the binding of a panel of moderately glycated BSA to RAGE and galectin-3 *in vitro* in solution with monomeric RAGE-VC1 and galectin-3. Under these conditions, only ribose derived AGE compounds bound with high affinity to either RAGE or galectin-3.

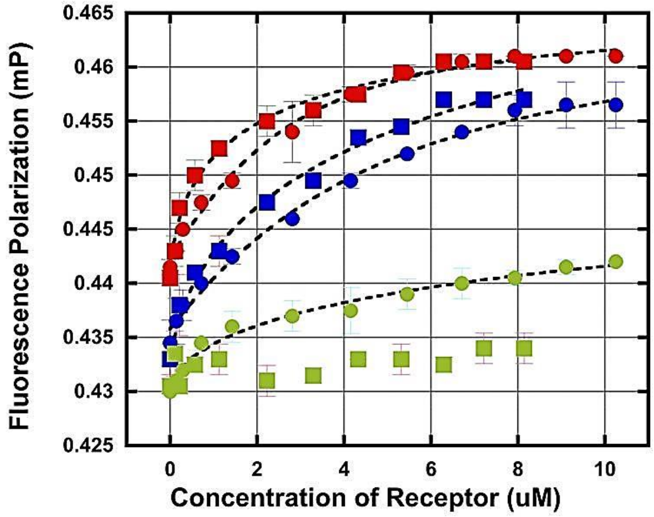

Figure 2.16. Binding curves of ribose modified BSA to RAGE-VC1 (solid squares) and galectin3 (solid dots).
Binding of BSA modified with 20 mM ribose (Rib-L) is shown in green, samples modified with 200 mM ribose (Rib-H) are shown in blue and samples modified with 500 mM ribose (Rib-vH) are shown in blue. The intrinsic fluorescence of ribose glycated BSA was used to follow changes in fluorescence polarization upon binding to RAGE or galectin-3.

Table 2.5. Binding affinities between AGE-BSA samples and RAGE and galectin-3, respectively.
Binding affinities were calculated based on data from fluorescence polarization titrations. The K_d values shown as >50 µM indicate that these compounds do not bind with affinities below 50 µM to either RAGE or galectin-3.

Sample	**K_d AGE-RAGE (µM)**	**K_d AGE-galectin (µM)**
Dia-H BSA	> 50	> 50
Gly-H BSA	> 50	> 50
Gla-H BSA	> 50	> 50
MG-H BSA	> 50	> 50
Rib-L BSA	> 50	17.0 ± 0.4
Rib-H BSA	9.1 ± 0.3	2.4 ± 0.6
Rib-vH BSA	2.0 ± 0.8	0.9 ± 0.1
Glc-vH BSA	> 50	> 50

Effects of glycated BSA on cell proliferation

Our binding assays indicated that most of our AGE samples did not bind tightly to RAGE. However, lack of tight binding *in vitro* does not preclude biological activity in more complex biological assays.

Therefore, the effects of AGE on cellular proliferation in a model system using the WM115 primary human melanoma cell line was studied. RAGE overexpression in melanoma tumors has been previously reported [211]. The WM115 cell line naturally expresses galectin-3 and was further modified to stably express RAGE. Our research group has characterized this cell line in detail and demonstrated that RAGE overexpression increases cell motility and tumor growth in a mouse model [212]. We therefore believe that our cell based model is suitable to test whether different AGE preparations affect cellular behavior.

Twelve of our AGE–modified BSA samples was studied for their cell mediated effects. Figure 2.17 summarizes the results of our proliferation assay and indicates that most glycated samples increased cellular proliferation when compared to non-modified BSA. Glyoxylic acid modified BSA (GA-H-BSA) had no significant effect on cell proliferation. GA-H-BSA was also the least glycated sample in our panel based on lysine and arginine modification (Table 2.2). All other glycated BSA samples increased proliferation to varying degrees. Ribose modification was most effective in enhancing proliferation, whereas AGE-BSA derived from equal concentrations of glucose were much less effective. In fact, AGE-BSA derived from 20 mM ribose (Rib-L-BSA) increased cell proliferation more effectively than AGE-BSA obtained by glycation with 500 mM glucose. Comparing the three ribose modified protein samples showed enhanced proliferation with increased degree of glycation. The observed increase in cellular proliferation was correlated with the biophysical characterized properties of the samples. A linear correlation was observed between enhancement of cell proliferation and extend of lysine modification (R = 0.92) (Figure 1.18), as well as with β-sheet content (R = 0.83) (Figure 2.18) and the percentage of non-monomeric material (R = 0.79) (Figure 2.18). There was no correlation with the degree of arginine modification (R = 0.39). However, the extent of amino acid side chain modification of glycated BSA alone is not sufficient to predict efficacy as proliferation enhancer in our system. For example, acetoin modified (Ace-H-BSA) and glyceraldehyde modified (Gly-H-BSA) samples showed similar proliferation activity, but varied greatly in the extent of lysine and arginine modification (Table 2.2) and spectroscopic properties. This demonstrates that not only the extent of modification, but also the chemical nature of the glycation reagent and the structure of newly formed side chain modifications is important for the biological activity of glycation and AGE compounds.

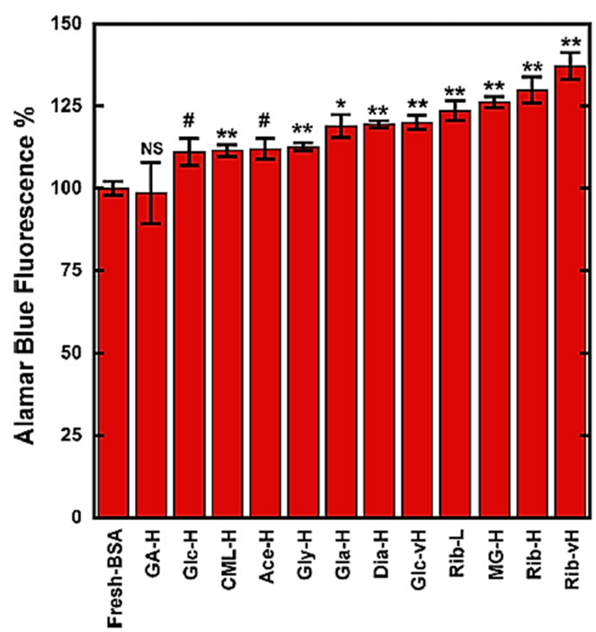

Figure 2.17. Cellular proliferation was assessed by measuring the fluorescence of reduced resazurin (Alamar blue).
The measured proliferation signal is proportional to the number of cells and their metabolic activity. All samples tested increased proliferation when compared to non-modified BSA. Methylglyoxal and ribose modified samples were the most effective proliferation enhancers. **$p < 0.001$;*$p < 0.01$; #$p < 0.05$, NS not significant. The assay was performed three times independently, a representative example is shown in which each sample was analyzed in four independent assay plate wells.

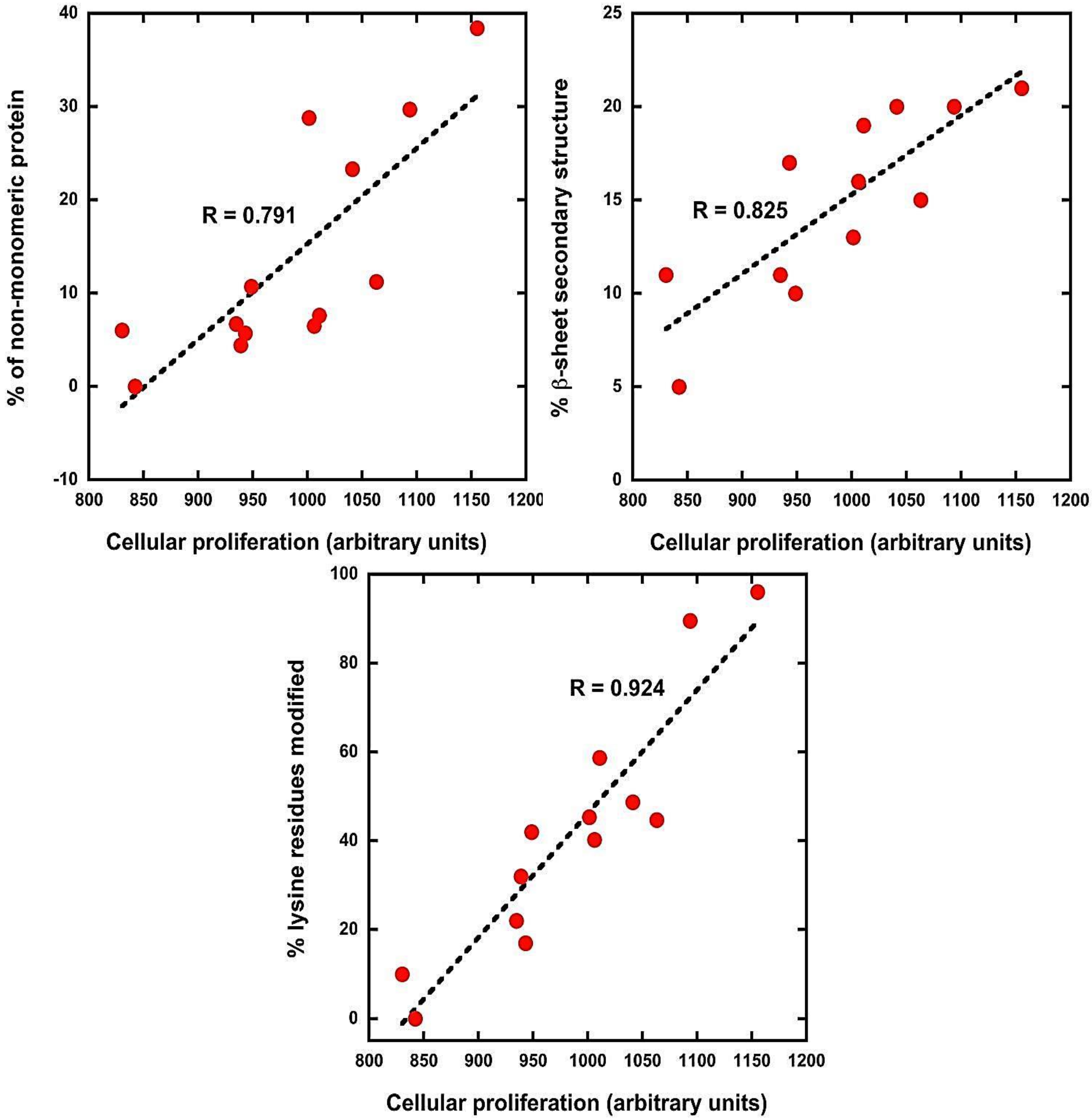

Figure 2.18. The cellular proliferation enhancement by AGE-modified BSA samples could be correlated with biophysical properties such as the extent of lysine side chain modification (top), b-sheet secondary structure content (middle) and the degree of non-monomeric in the sample (bottom).

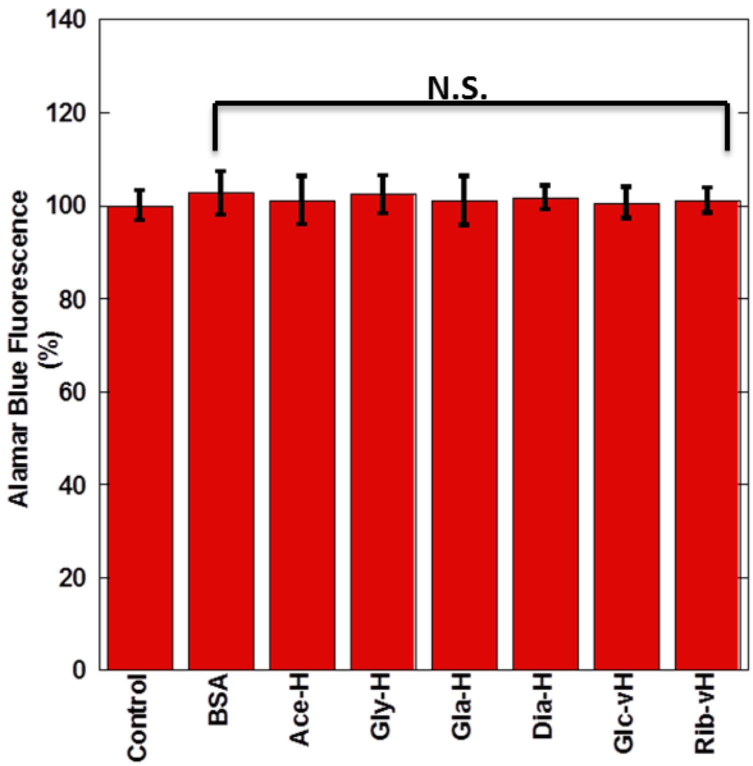

Figure 2.19. AGE induced cellular proliferation of the WM115 mock transfected cells These cells do not over express RAGE.

Thermodynamic characterization of diclofenac binding to glycated-BSA by isothermal titration calorimetry (ITC)

The interaction and the thermodynamic characteristics between diclofenac and glycated BSA was measured by Isothermal titration calorimetry. The low glycated samples were used for the study as the glycation conditions are very close to physiological conditions. The changes in Gibbs free energy ΔG and of the entropic parameter ΔS were calculated based on experimentally determined changes of the enthalpy ΔH and the affinity constant K_a. The stoichiometry of the drug – albumin interaction was derived directly from the fitting of experimental data. The parameters for the complete thermodynamic description of the interaction between diclofenac and glycated forms of BSA are summarized in table 2.6. Two experimental ITC traces and the fitting of the data are shown in Figure 2.20.

To fit the data several models were explored to fit the titration curves and found that all data could be fitted well using a model assuming a set of identical, independent binding sites. More complex models accounting for multiple binding sites with different affinities or cooperativity did not yield better fits [213]. Our experiments showed that the addition of diclofenac to glycated, as well as to native BSA, resulted in an exothermic interaction with well-developed heat peaks (Figure 2.21). For non-glycated, defatted BSA, both, the enthalpic DH and entropic components -TΔS were negative and contributed positively to the negative Gibbs energy ΔG. For non-defatted BSA the entropic component -TΔS was close to zero and the binding was almost exclusively driven by the change in ΔH. Surprisingly, the diclofenac binding properties for the CML-L-BSA modified samples were very similar to the properties of the non-modified protein. The diclofenac binding to CML-L-BSA was driven by the negative change in ΔH of -22 kJ mol^{-1} K^{-1} and only a small contribution of -TΔS of -1.77 kJ mol^{-1}. For all other glycated BSA samples the entropic components –TΔS were opposing the enthalpic ΔH components contributions by +4 to +45 kJ mol^{-1} K^{-1}.

Figure 2.20 shows the relative magnitude of ΔG, ΔH and –TΔS for diclofenac binding to glycated BSA. The Gibbs free energy ΔG changes only little, while values for ΔH and -TΔS increase with glycation. The interpretation of these data on the molecular level is not unambiguous, but could be interpreted to indicate that increased ΔH contributions from hydrophobic interactions are off-set by entropic factors, possibly resulting from reduced flexibility in the protein after drug binding.

The binding affinity for diclofenac to non-glycated BSA was determined to be K_a $2.4x10^4$ M^{-1} (K_d = 42 μM) which is in agreement with literature values [150, 152, 153]. In general, glycation of albumin resulted in reduced binding affinities for diclofenac. The extent by which the binding of the drug to the protein was weakened depended on the glycation reagent and was reduced maximally by six-fold from K_a 2.4x10^4 M^{-1} to K_a 4x10^3 M^{-1} (K_d 42 to 250 μM) for modifications with ribose, glycolaldehyde and diacetyl. For the other glycation reagents the decrease in binding affinity was less pronounced.

The data also suggest that glycation not only modulated binding affinity, but also altered the number of apparent diclofenac binding sites (Table 2.6). Non-glycated BSA possess two diclofenac binding sites and glycation with the majority of the tested reagents (Ace, Dia Gly, Gla, MG) reduced the number of binding sites by about 25% to a nominal number of 1.5 binding sites. A much more pronounced loss of binding sites was detected for ribose modified BSA (Rib-L-BSA), where almost two thirds of the drug binding capacity was lost and only 0.8 nominal binding sites remained. Interestingly, the opposite effect was seen for glycation with glucose (Glc-L-BSA), which increased the number of diclofenac binding sites to 2.7 and with CML-modified albumin (CML-L-BSA), with a 75% increase in binding capacity to 3.5 binding sites.

Our ITC experiments demonstrated that the nature of the glycation reagents determined the binding properties for diclofenac. Glycation decreased binding affinity for all samples analyzed but could either increase or decrease the number of drug binding sites, depending of the glycation reagent used. This leads to situations in which decreased binding affinity can be compensated by increased binding stoichiometry, thus not altering the binding capacity significantly. It can also have the opposite effect in which the drug binding capacity is reduced because of lower binding affinity and concomitant loss of binding sites. We estimated the diclofenac binding capacity of glycated serum albumin samples using:

$$K_d * n * [Alb] = \frac{[Alb - DCF]}{[DCF]} \tag{2.2}$$

Figure 2.22 shows the ratio between albumin bound diclofenac (Alb-DCF) and unbound, free diclofenac (DCF). An invariant serum albumin concentration [Alb] of 600 mM (4g/dL) based on the physiological albumin concentration and a concentration for diclofenac below 10 mM based on therapeutic peak serum concentrations [214, 215] was assumed. This analysis showed that the diclofenac binding capacity dropped significantly upon glycation for some glycation reagents. Correspondingly, the free drug concentration increased from 3% for non-glycated BSA and CML-L-BSA (Glc-L-BSA) to ~10% for glucose modified BSA and 50% for ribose modified BSA (Rib-L-BSA).

Table 2.6. Thermodynamic parameters for the interaction between glycated serum albumin and diclofenac determined by ITC.

Sample	**K_a (M^{-1})**	**n**	**ΔH (kJ mol^{-1})**	**ΔG (kJ mol^{-1})**	**-TΔS (kJ mol^{-1}K^{-1})**
DF-BSA	(24.9 ± 4.5) x 10^3	2.04 ± 0.16	-18.9 ± 0.4	-25.05 ± 0.46	-6.14 ± 0.83
BSA	(24.2 ± 2.8) x 10^3	2.07 ± 0.03	-24.3 ± 0.2	-25.00 ± 0.29	-0.72 ± 0.47
Glc-L BSA	(6.0 ± 0.5) x 10^3	2.69 ± 0.18	-25.5 ± 2.0	-21.53 ± 0.24	3.97 ± 1.71
Ace-L BSA	(12.3 ± 0.9) x 10^3	1.61 ± 0.11	-28.9 ± 0.4	-23.32 ± 0.19	5.54 ± 0.23
Dia-L BSA	(4.4 ± 0.1) x 10^3	1.47 ± 0.01	-49.3 ± 1.0	-20.80 ± 0.04	28.54 ± 0.96
Gly-L BSA	(5.6 ± 0.4) x 10^3	1.46 ± 0.01	-43.1 ± 0.8	-21.37 ± 0.17	21.72 ± 0.92
Gla-L BSA	(3.8 ± 0.7) x 10^3	1.55 ± 0.01	-54.6 ± 5.9	-20.38 ± 0.45	34.24 ± 6.34
MG-L BSA	(7.0± 1.3) x 10^3	1.57 ± 0.05	-34.8 ± 3.6	-21.93 ± 0.46	12.89 ± 4.11
Rib-L BSA	(4.7 ± 0.3) x 10^3	0.76 ± 0.16	-65.9 ± 7.6	-20.94 ± 0.15	44.91 ± 7.41
CML-L BSA	(14.6 ± 2.4) x 10^3	3.48 ± 0.23	-22.0 ± 2.1	-23.73 ± 0.41	-1.77 ± 2.53

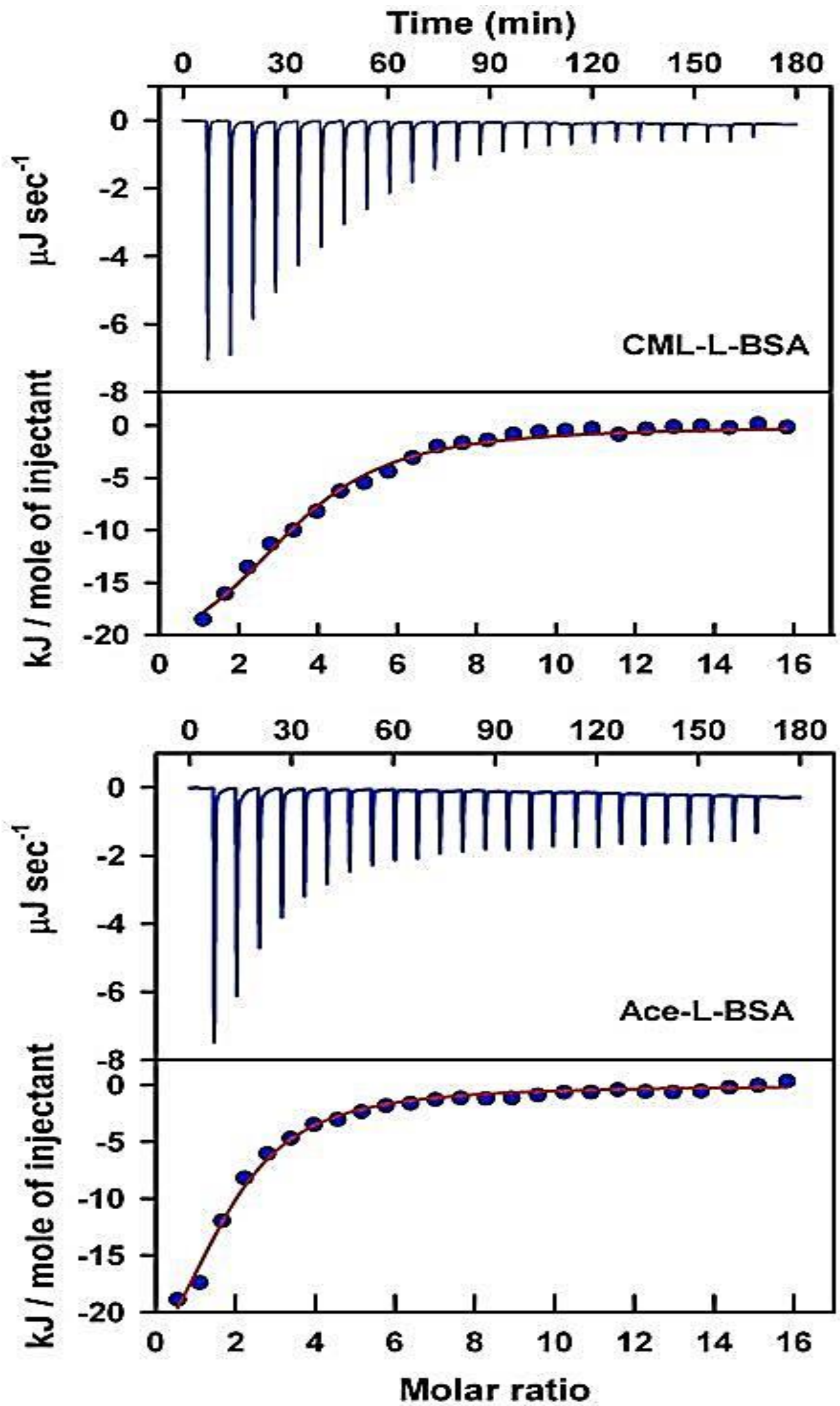

Figure 2.20. Representative ITC titrations profiles and corresponding fits two glycated forms of BSA.

The top panels show the raw heats measured during each injection of diclofenac into a solution of CML-L-BSA and Ace-L-BSA respectively. The lower panels show fit (red line) of the experimental data (blue dots) using a model for multiple independent binding sites.

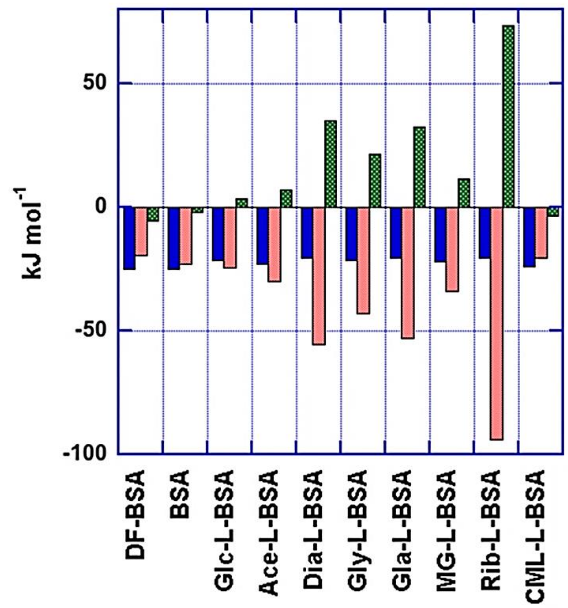

Figure 2.21. Contribution of ΔH (red shaded bars) and –TΔS (green shaded bars) to the change in free Gibbs energy ΔG (blue solid bars).

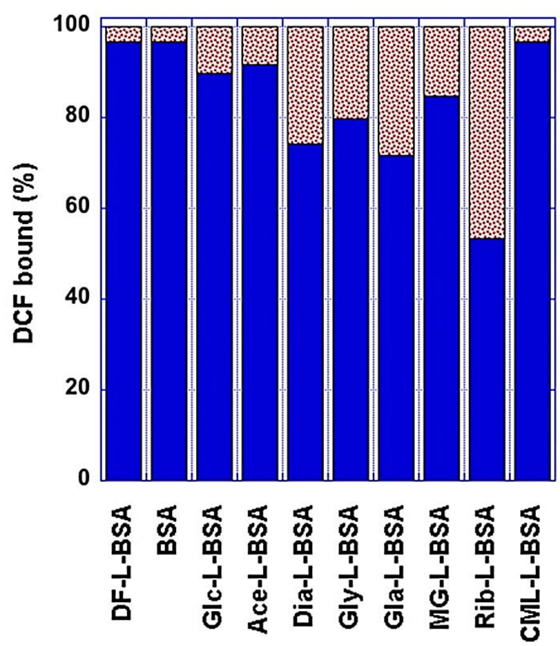

Figure 2.22. The relative distribution in % between diclofenac (DCF) protein bound to different forms of glycated bovine serum albumin (solid blue) and non-bound, free diclofenac (shaded red).

Estimations are based on binding affinities and stoichiometries determined in this study, and assumed concentration of 0.6 mM serum albumin in serum and a total DCF concentration below 10 mM. Non-glycated BSA has high DCF binding capacity, leaving only 3% unbound. Glycation generally reduces DCF binding capacity.

Binding of diclofenac to glycated BSA stabilizes the protein

Our ITC data we shown that the number of diclofenac binding sites and the binding affinity was altered by glycation and we wanted to obtain additional insight in the mechanism of diclofenac binding to glycated BSA. Differential scanning calorimetry (DSC) was used to investigate the consequences of diclofenac binding on the stability of glycated BSA against thermal unfolding. DSC provides information about the thermal properties of molecules and can directly measure enthalpies associated with thermal transitions [216, 217]. Complete thermodynamic characterization of protein unfolding requires that the process is reversible. If a thermal transition is irreversible, then the midpoints of the thermal transition(s) Tm and the overall shape of the thermogram are of interest.

The thermal unfolding of BSA occurs in multiple transitions in a temperature range between 50 °C to above 90 °C and significant changes in heat capacity (Cp). The thermal unfolding of serum albumin is irreversible, thus limiting the thermal analysis to the unfolding of the protein only. The thermal stability of BSA is also known to be sensitive to the presence of bound fatty acids and the buffer composition [193, 218]. Near physiological phosphate buffered saline (PBS) was used for all experiments. The protein concentration in all DSC experiments was 45 mM and a 22-fold molar excess of diclofenac (1 mM) ensured high occupancy of diclofenac binding site on glycated based on the binding affinities determined by ITC.

Non-defatted BSA shows two transition peaks in the DSC profile, whereas defatted BSA shows only a single transition peak [191, 219]. A first transition occurs at Tm 62.8 ºC, followed by a second transition at Tm 80.9 ºC (Table 2.7 and Figure 2.23). The estimated enthalpies of unfolding associated with these transitions are 380 and 824 kJ mol^{-1} K^{-1}. In the presence of diclofenac a very significant a significant stabilization of the protein against heat induced unfolding was observed and the first Tm_1 increased by almost 13 ºC from 62.8 to 75.7 ºC, and the second Tm_2 by almost 3 ºC to 83.7ºC. The associated enthalpies also increase dramatically to 622 kJ mol^{-1} K^{-1} and 1672 kJ mol^{-1} K^{-1}. The increase in Tm clearly and the increased enthalpy changes ΔH showed that diclofenac bound to BSA and increased the energy necessary to disrupt non-covalent, intra-molecular interactions to unfold the drug-BSA complex.

Our DSC data for the unfolding of defatted BSA (DF-BSA, Tm of 61.8 ºC and ΔH of 451 kJ mol^{-1} K^{-1}) and for the diclofenac-DF-BSA complex (Tm 76.1ºC, ΔH to 701 kJ mol^{-1} K^{-1}) confirmed previously reported data by Sharma et al. [153].

The increases in thermal stability upon diclofenac binding were similarly impressive for the glycated samples. Increases in Tm_1 between 10 ºC and 15 ºCare observed, except for ribose modified BSA, which shows only a marginal increase in thermal stability upon drug binding by 3.8 ºC. Table 2.7 summarizes the calculated Tm and ΔH values for all samples analyzed and Figure 2.23 shows DSC thermograms for glycated BSA in the presence and absence of diclofenac. Comparing the thermograms clearly shows the shift of the unfolding transition to higher temperatures. Additional peaks and shoulders in thermograms also indicate changes in unfolding mechanism between samples and upon diclofenac binding. This is indicative of different binding modes of diclofenac to the differentially glycated serum albumin samples.

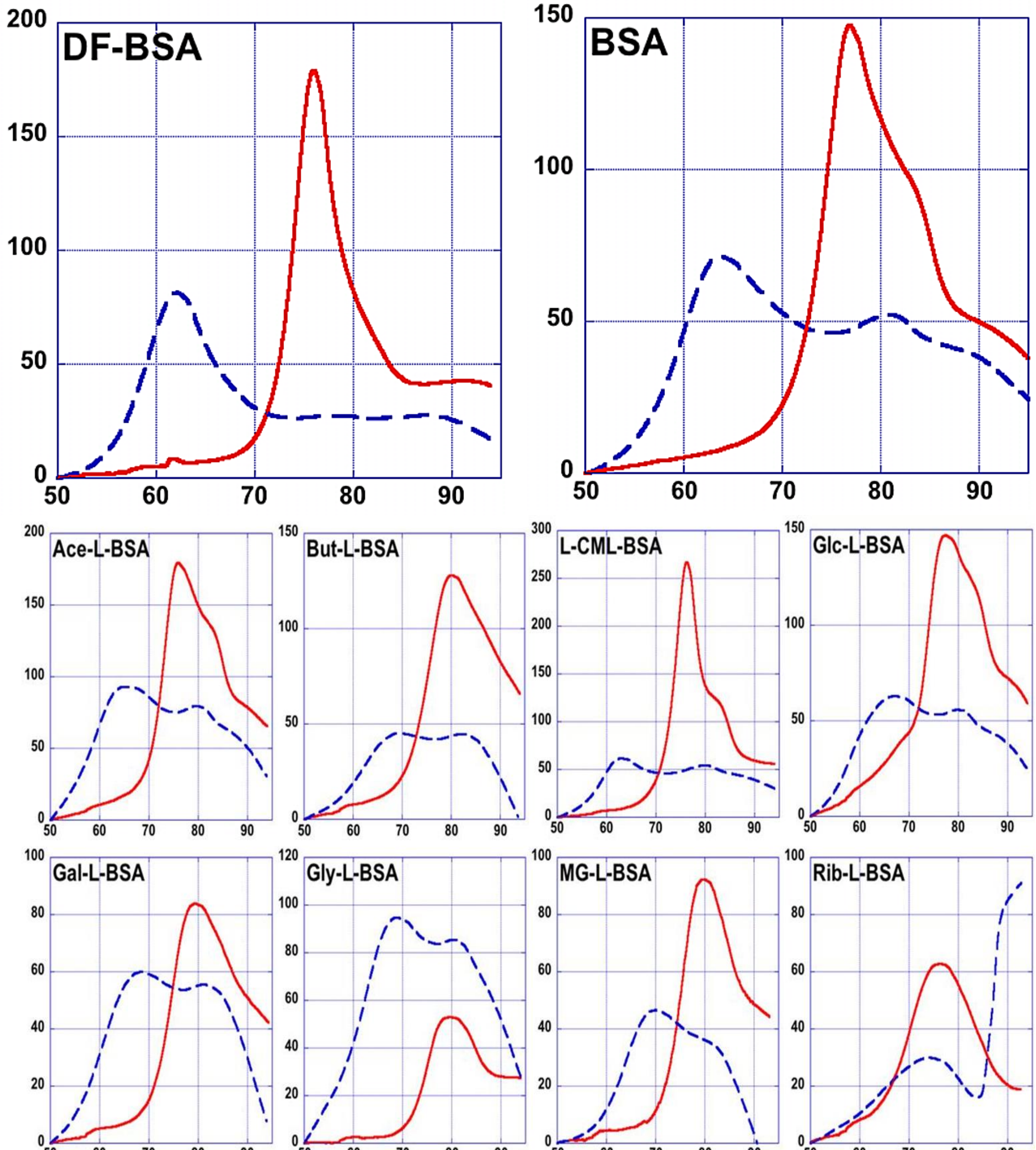

Figure 2.23. DSC traces of glycated BSA in absence (dashed blue lines) and the presence of diclofenac (solid red lines). Binding of diclofenac to all samples caused a significant shift of the thermal transition midpoint Tm to higher temperatures.

Table 2.7. Thermal stability and unfolding characteristics of glycated serum albumin in the absence and presence of diclofenac (DCF) as determined by DSC.
Diclofenac binding to albumin leads to a significant increase in thermal stability for all samples analyzed. Thermal transition midpoint temperatures T_m increased by 10 - 15 °C and DH values for the unfolding process increased as well. Compare to Figure 3 for differences in thermogram profile.

Sample	**DCF**	**T_{m1} (°C)**	**Δ H_1 (kJ mol^{-1} K^{-1})**	**T_{m2} (°C)**	**Δ H_2 (kJ mol^{-1} K^{-1})**
DF-BSA	1 mM	76.1 ± 0.1	701 ± 2	-	-
DF-BSA	--	61.8 ± 1.0	452 ± 5	-	-
BSA	1 mM	75.7 ± 0.3	623 ± 14	83.7 ± 0.1	1672 ± 28
BSA	--	62.8 ± 0.2	379 ± 2	80.9 ± 0.8	825 ± 13
Glc-L BSA	1 mM	74.0 ± 0.5	573 ± 29	84.1 ± 0.2	1155 ± 75
Glc-L BSA	--	64.1 ± 0.2	382 ± 7	84.2 ± 0.3	860 ± 8
Ace-L BSA	1 mM	75.0 ± 0.4	682 ± 38	84.0 ± 0.1	1216 ± 43
Ace-L BSA	--	63.5 ± 0.2	420 ± 11	80.1 ± 0.2	848 ± 6
But-L BSA	1 mM	79.3 ± 0.3	399 ± 25	-	-
But-L BSA	--	65.9 ± 0.1	418 ± 4	82.5 ± 0.1	767 ± 5
Gly-L BSA	1 mM	79.2 ± 0.1	433 ± 1	-	-
Gly-L BSA	--	66.0 ± 0.1	436 ± 8	82.2 ± 0.1	850 ± 2
Gal-L BSA	1 mM	79.0 ± 0.1	383 ± 2	-	-
Gal-L BSA	--	64.1 ± 0.1	414 ± 2	82.8 ± 0.2	746 ± 6
MG-L BSA	1 mM	79.0 ± 0.3	431 ± 8	-	-
MG-L BSA	--	66.3 ± 0.1	420 ± 2	82.6 ± 0.4	856 ± 3
Rib-L BSA	1 mM	76.0 ± 0.4	296 ± 4	-	-
Rib-L BSA	--	72.2 ± 0.1	349 ± 3	-	-
CML-L BSA	1 mM	75.8 ± 0.1	698 ± 12	83.6 ± 0.1	1196 ± 7
CML-L BSA	--	62.9 ± 0.4	514 ± 13	79.8 ± 0.2	759 ± 22

Effect of diclofenac binding on secondary structure

The structural characteristics of diclofenac binding to glycated BSA was determined by circular dichroism spectrometry. The effect of different glycation reagents on the secondary structure of serum albumin was described earlier and we observe that glycation affects the secondary structure of serum albumin by breaking α-helices and increasing the β-sheet content and the number of poorly ordered residues[118, 187]. This process leads to partial loss of native structure of the protein, but does cause extensive unfolding. We expanded this study and investigated if the binding of diclofenac to glycated BSA would further alter the secondary structure composition.

We found that binding of diclofenac to non-glycated serum albumin caused only minor alterations in secondary structure compositions, that were not statistically significant in the student t-test ($p>0.05$) (Figure 2.24). This result was expected and demonstrated that the natively folded serum albumin does not alter its secondary structure upon drug binding to an extent that can be detected by CD. Surprisingly, we found similar structural stability for the glycated forms of serum albumin. Statistical analysis of the secondary structure composition for glycated serum albumin samples in the presence and absence of a 22-fold molar excess of diclofenac did not indicate any significant changes in secondary structure. There was only one exception in which diclofenac binding had a significantly ($p = 0.008$) effect on secondary structure. The ribose glycated sample did show a reduction of poorly ordered residues from 37.6 to 34.0 % upon diclofenac binding. Based on 583 amino acid residues in mature BSA, we calculated that approximately 20 residues changed from a disordered conformation and adopted an α-helical (~9 residues), β-sheet (~6 residues) or turn conformation (~5 residues).

Our CD-data showed that while glycation altered the secondary structure of serum albumin for all glycated forms, the binding of diclofenac did not further affect the secondary structure compositions to a significant level. A notable except was the ribose modified BSA sample. The ribose glycation did disturb the native secondary structure the most, showed the least thermal stabilization in DSC experiments and had retained the lowest diclofenac binding cap

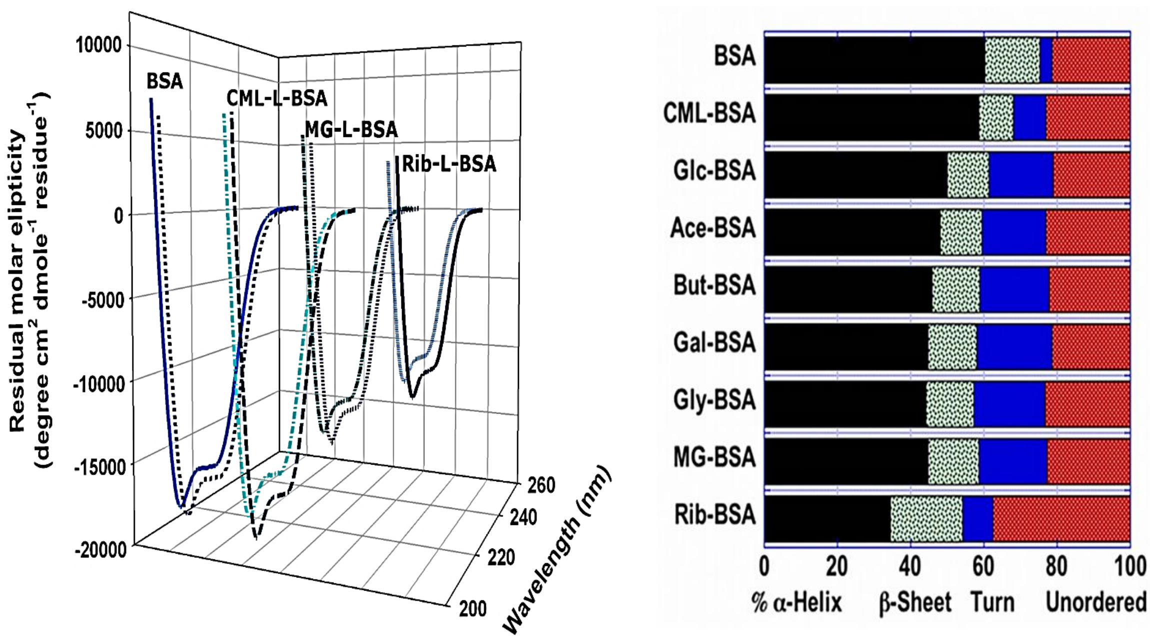

Figure 2.24. Circular dichroism (CD) analysis of glycated serum albumin samples for secondary structure composition and changes in secondary structure composition in the presence a saturating excess of diclofenac.
Binding of diclofenac did not significantly change the secondary structure of albumin. Top: representative CD traces of BSA, CML-L-BSA, MG-L-BSA and Rib-L-BSA in the absence (solid lines) and presence (dashed lines) of diclofenac. Bottom: Distribution of secondary structure elements in glycated samples of serum albumin. Glycation reduces a-helical (black) content and increases the content of residues in b-sheet (green), turn (blue) and unordered conformation.

Dynamic light scattering studies

Here we expended these studies using dynamic light scattering as an analytical method that provides insights into particle size and size distribution within a particle population. Literature data report a hydrodynamic diameter for non-glycated bovine serum albumin between 3.3 – 4.3 nm depending on pH and buffer composition [221, 222]. We measured a Z-average radius of 4.4 nm for non-glycated BSA under our experimental conditions. The majority of glycation reagents did only cause minimal increases in average particle size, indicating that intermolecular cross linkage between protein chains was not extensive. The only exception was found in samples modified with ribose. In these samples the average particle radius doubled suggesting that multiple albumin chains had been cross-linked. Minor cross-linkage was detected based in increased particle size (5.05 - 5.25 nm) for glycation with diacetyl and glcolaldehyde, respectively. Our data from DLS experiments are in excellent agreement with previous results from analytical size exclusion chromatography.

Table 2.8. Dynamic light scattering was used to characterize protein aggregation and to determine the Z-average size and polydispersity of the samples.

Sample Name	**Z-Average Radius (nm)**	**Polydispersity Index**
BSA	4.41± 0.01	0.28 ± 0.01
Glc-L-BSA	4.51 ± 0.01	0.21 ± 0.01
Glc-H BSA	9.18±0.11	0.17±0.000
Glc-vH BSA	10.83±0.33	0.30±0.01
Ace-L BSA	4.65 ± 0.01	0.29 ± 0.01
Ace-H BSA	9.91±0.08	0.33±0.002
Dia-L BSA	5.06 ± 0.01	0.35 ± 0.01
Dia-H BSA	9.91±0.19	0.29±0.004
Gly-L BSA	4.67 ± 0.07	0.25 ± 0.01
Gly-H BSA	10.22±0.16	0.26±0.003
Gla-L BSA	5.25 ± 0.19	0.29 ± 0.01
Gla-H BSA	16.18±0.33	0.22±0.001
MG-L BSA	4.75 ± 0.03	0.28 ± 0.01
MG-H BSA	9.54±0.16	0.22±0.001
Rib-L BSA	8.64 ± 0.03	0.37 ± 0.01
Rib-H BSA	19.83±0.82	0.24±0.004
Rib-vH BSA	19.19±0.08	0.24±0.001
CML-LBSA	4.22 ± 0.03	0.25 ± 0.01
CML-H BSA	9.19±0.22	0.30±0.02

Conclusions

Protein glycation and AGE formation are physiologically relevant processes and excessive AGE formation has been clearly correlated with severe health problems as described earlier. Consequently, there is much interest in assessing the effects of AGE products at the molecular and cellular levels. In vitro produced AGE products are very frequently synthesized under conditions that lead to levels of excessive modification and are unlikely to occur under (patho) physiological conditions. Also, different investigators employ various reagents to produce AGE proteins, further complicating interpretation and comparisons between studies.

It was our goal to produce serum albumin with moderate modification levels similar to physiological conditions and to analytically characterize its properties. We therefore used low modifier concentrations and equally important limited the time of modification to three weeks, which is the half-life of serum albumin.

Glycation and subsequent formation of intermediate and advanced glycation end products was qualitatively and quantitatively characterized. Chemical reactivity and concentration of the glycation reagent determined the extent of side chain modification. For example, glucose was a relatively poor glycation reagent when compared to ribose or reactive aldehydes such as methylglyoxal or glyceraldehyde. This may have implications for the hypothesis that the elevated AGE levels observed in diabetic patients are directly derived from increased blood glucose. Chemically distinct side chain modifications are introduced into glycated albumin depending on the glycation reagent. This was demonstrated by the differences in absorbance and fluorescence spectroscopic properties between the different glycation products produced in the study. Spectroscopic analysis techniques may become useful in characterizing biological AGE compounds and deducing the glycation reagent involved in AGE formation. We confirmed by circular dichroism spectrometry that glycation of BSA, which is a largely α-helical protein, led to the breakage of α-helices and increased formation of β-sheet secondary structures. At the same time, glycation destabilized the overall protein fold and increased flexibility of the protein. However, even high levels of glycation did not unfold BSA completely, but rather led to the formation of a heterogeneous population of molten globule like conformations. The fact that BSA remains soluble even in a highly glycated state may not be a general feature of glycation. Few reports in the literature suggest that high levels of glycation induced protein aggregation [223, 224]. This suggests that the highly glycated AGE compounds can exist in a soluble form and bind to AGE signaling receptors such as RAGE and galectin-3 to trigger signaling. *In vitro* binding studies between AGE-BSA and RAGE or galectin-3 revealed that binding of most compounds to the AGE-receptors is weaker than our detection limit (K_d ~ 50 µM). However, ribose glycated protein bound tightly to RAGE (2.0 µM), as well as to galectin-3 (2.0 µM). Interestingly, the binding affinity (K_d) increased with the extent of glycation, which suggests a qualitative difference between the samples. It may be possible that higher glycation generates more potential binding sites for RAGE or galectin-3 in the protein surface, or that oligomerization clusters more binding epitopes. In both scenarios, avidity effectively increases the apparent macroscopic binding affinity.

The biological activity of our glycated samples was determined in a cell based proliferation assay. The observed increase in cell proliferation could be correlated with the extent of lysine residue modification, β-sheet content and oligomerization state of the glycated protein. However, other factors, most probably the chemical structure of the formed AGE modifications on the protein surface are important too. The observation that AGE compounds exert biological activity at concentrations (3.5 µM) well below their *in-vitro* determined binding affinities (K_d > 50µM) may be explained by multiple hypotheses. It is conceivable that RAGE or galectin-3 receptors form larger clusters on the cell surface, thus effectively increasing binding affinity by avidity. In fact, RAGE has been shown to form dimers in the plasma membrane [225].

Alternatively, RAGE or galectin-3 may associate with additional co-receptors on the cell surface, which could increase binding affinity for glycated proteins.

Building upon our studies on the structural changes in albumin upon glycation we finally investigated the role of glycation in drug binding of serum albumin. We hypothesized that glycation of serum albumin affects drug binding in a manner that is specific to individual glycation reagents.

Our investigation shows that glycation does significantly alter the thermodynamics and the mechanism of diclofenac binding to serum albumin. Glycation reduces the binding affinity by up to six-fold, alters the number of diclofenac binding sites from 2 to between 0.8 to 3.5 binding sites per albumin molecules, depending on the nature of the glycation. The relative enthalpic and entropic contributions of the protein—drug interaction are greatly altered, while the differences in Gibbs free energy changes ΔG remained relatively small (~ 5 kJ mol^{-1}) between samples.

The data demonstrate that increased serum protein glycation reduces the diclofenac binding capacity to an extent that could be pharmacologically relevant in patients with high levels of serum albumin glycation. The modification of drug binding properties also depends on the chemical nature of the glycation reagent and thus on the physiological source of the reactive carbonyl compound causing glycation.

In summary, our study demonstrates significant differences between different glycation reagents in their ability to alter the biophysical properties of serum albumin and to generate biologically active AGE-compounds. It also underlines the importance of choosing the most appropriate glycation reagent when AGE compounds are being prepared for biological studies.

Our findings should accelerate our understanding of the biological role of AGE compounds in disease development and progression.

CHAPTER 3: THE ROLE OF AGE COMPOUNDS AND THEIR INTERACTION WITH RAGE IN PANCREATIC CANCER CELL PROLIFERATION AND MIGRATION

Introduction

Pancreatic cancer

Pancreatic adenocarcinoma is one of the most devastating malignant diseases and is responsible for more than 227,000 deaths each year in the world [226]. It is the fourth leading cause of cancer related deaths in the US with an estimated 34,000 deaths every year [227]. Pancreatic cancer is characterized by very poor prognosis due to the absence of specific early symptoms [228, 229]. Consequently, the median survival rate is about 5-6 months in conventional therapies and the 5-year overall survival rate is less than 5% [228]. The etiology of pancreatic cancer is poorly understood and the disease is characterized by high metastatic rates. The low survival rates are primarily due to the fact that the pancreatic cancer tumors exhibit very few symptoms and progress very rapidly and when detected are at an advanced stage and only 10% being operable [230]. Hence, the early detection and diagnosis of the disease is essential to improve outcomes. However, the lack of prognostic markers hampers the early detection of the disease. Pancreatic cancer is also genetically complex which adds to the difficulty in treating the disease. Several key genes including the KRAS, TP53, SMAD4 and CDKN2A are mutated which in turn effect signaling pathways such as KRAS signaling, apoptosis and hedgehog signaling[231, 232] hence making the treatment of the disease difficult. Presently, the most effective therapy for the treatment of pancreatic cancer is by palliative chemotherapy of FOLFIRINOX (folinic acid, 5-fluorouracil, irinotecan and oxaliplatin) and gemcitabine/nab-paclitaxel [233]. However, to ensure the best treatment for patients and to reduce the mortality it is important to further identify new targets and treatment strategies. We focus on the role of the receptor for advanced glycation end products (RAGE) as a target in the treatment of pancreatic cancer.

RAGE and its ligands in pancreatic cancer

As described earlier RAGE is a member of the Ig protein super family and is a pro-inflammatory receptor. RAGE and its ligands, which are secreted from the cancer cells and leukocytes, such as high-mobility group box 1 (HMGB1) and S100 proteins facilitate the maintenance of a chronic inflammatory state which leads to the development and progression of several cancers and also promotes metastases [36, 234]. The role of RAGE in tumor growth and metastasis has been described in pancreatic cancer [81, 235, 236]. RAGE has been described to be permissive for the early pancreatic neoplasia which leads to pancreatic cancer [237]. The role of RAGE-HMGB1 interaction in sustaining autophagy and limiting pancreatic cancer cell apoptosis during chemotherapy and oxidative stress has been described in vivo and in vitro [235, 236]. Recently, the role of RAGE in enhancing neutrophil extracellular traps (NETs) formation in autophagy mediated pathways has been described in pancreatic cancer [238]. The other ligand of RAGE which is well studied in pancreatic cancer is S100P. S100P promotes pancreatic cancer growth, survival and invasion and is a novel therapeutic target for pancreatic cancer [239, 240]. S100P-RAGE interaction has been described to be essential in the S100P mediated effects in pancreatic cancer. Inhibition of S100P-RAGE prevented S100P induced pancreatic cancer growth [81]. All these studies establish RAGE as an important target for the treatment of pancreatic cancer. However, RAGE signaling is highly complex the role of other RAGE ligands such as the AGE compounds has not been studied in pancreatic cancer. The role of AGE-RAGE interaction in pancreatic cancer cell survival, proliferation and migration has not been reported. As described in chapter1, AGEs are highly heterogeneous in nature and the structural basis behind the toxic AGE compounds is not understood currently. This study was undertaken to elucidate the role of AGE compounds in pancreatic cancer cell proliferation and migration and to identify the role of AGE-RAGE interaction in the AGE mediated cellular effects. Targeting the AGE-RAGE axis is an effective strategy to prevent AGE mediated cellular effects. Several approaches have been used to inhibit RAGE-ligand interaction like truncated form of the receptor (sRAGE) [36], RAGE blocking antibodies [241], ligand derived peptides [81, 242] and several other chemical inhibitors have also been described to have RAGE inhibiting effects [243 69]. The ultimate goal of the study was to pharmacologically inhibit AGE-RAGE interaction to prevent AGE mediated effects in pancreatic cancer.

Pancreatic cancer and glycation

Glycation and AGE compounds formation is not very well understood in the context of tumor biology and cancer disease progression. In malignant tumors there is a shift in metabolism away from oxidative phosphorylation to aerobic glycolysis [244]. This results in increased glucose uptake into the tumor. This effect is called Warburg effect and is a hallmark of cancer [245]. This increased glucose flux coupled with hypoxic conditions in the tumor can lead to significant increase in glycation and the formation of AGE compounds. The formation of AGE compounds and the presence of certain AGE compounds such as CML and argpyrimidine have been identified in cancer tissues such as adenocarcinomas of the colon and leiomyosarcomas, squamous cell carcinomas of the larynx and adenocarcinomas of the breast [97]. The mitogenic effect and migratory potential of AGE compounds have also been demonstrated in breast [246], lung [247] and oral [248] cancer cell lines. The role of glucose modified AGE compounds has been described to stimulate the growth of human pancreatic cancer cells by promoting DNA synthesis [249]. The AGE compounds are highly heterogeneous in nature and our knowledge on the AGE compounds formed in tumors and their effects in tumor growth is limited. It is not clear if only certain AGE compounds play an important role in the tumor progression while the others are benign. Reports suggest that glyceraldehyde derived AGE compounds and methyl glyoxal derived AGE compounds play a role in increased tumor cell proliferation and migration [246, 247] while the AGE compounds derived from glucose were reported to be benign [247]. However, there is no consensus on the toxic AGE compounds (TAGE) and it is unclear if there is a certain modification or a structural feature of the AGE compounds responsible for their activity. We previously characterized an entire panel of AGE compounds (Chapter 2) and this study was initiated to correlate the glycation induced structural changes in this AGE compounds to their activity, more specifically their mitogenic and proliferative effect in pancreatic cancer cell lines. The AGE compounds trigger signaling through several surface receptors such as RAGE and AGE receptor complex, as described in chapter 2. RAGE is the most well studied signaling receptor for the AGE compounds.

Pancreatic cancer patients are frequently characterized by hyperglycemia [250, 251]. About 85% of the patients diagnosed with pancreatic cancer are found to have impaired glucose tolerance or frank diabetes [250, 251]. Reports also suggest the onset of diabetes 2-3 years preceding the diagnosis of pancreatic cancer (T3cDM) [252]. A recent report suggests the role of glucose mediated hypoxia to promote cell proliferation and migration in pancreatic cancer [253]. These increased hypoxic conditions could cause the accelerated formation of AGE-compound generation and accumulation at the tumor site. However, the role of AGE-compound accumulation has not been described in pancreatic cancer and requires further investigation.

We hypothesized that AGE-RAGE interaction triggers cellular signaling which leads cancer cell proliferation and migration.

Glycation induced changes in the protein leading to their toxicity were elucidated more specifically, the role of glycation induced protein oligomerization will be studied. The significance of AGE-RAGE interaction, the signaling pathways and role of RAGE inhibition in pancreatic cancer cell proliferation were determined. Three pancreatic cancer cells with differential RAGE expression were selected for the study; PANC-1, MIA PaCa-2 and BxPC-3 cells. PANC-1 and MIA Paca-2 have a high RAGE expression when compared to BxPC-3 cells [254]. The PANC-1 and MIA PaCa-2 cells contain a KRAS mutation at the 12 Asp and 12 Cys respectively whereas the BxPC-3 cells do not have the KRAS mutation [255].

Materials and Methods

Reagents were of molecular biology or ACS purity grade and purchased through Fischer Scientific or VWR. Bovine serum albumin (BSA), fraction V, was purchased from Amresco. Antibodies for western blotting were purchased from Cell Signaling Technologies. Molecular biology reagents and enzymes were purchased from New England Biolabs, Life Technologies, OriGene and Fermentas. Chromatography media for protein purification were purchased from GE Healthcare. Reagents and media for cell culture were from ATCC.

AGE compound preparation

Described in chapter 2.

Isolation of Rib-vH BSA oligomers and formation of BSA oligomers

The Rib-vH BSA oligomers were separated by size exclusion chromatography using a HiPrep 16/60 Sephacryl S-100 HR column (GE Healthcare) with a bed volume of 120 mL. The column was equilibrated with phosphate buffered saline with a flow rate of 300 uL/min. Rib-vH BSA was diluted to a concentration of 3 mg/mL and 2 mL of this was loaded on to the column with a flow rate of 300 µL/min. 10 mL fractions were collected throughout the run and the elution was observed by the UV detector trace.

BSA oligomers were generated by carboxyl-to-amine cross linking using water soluble cross linker, EDC (1-ethyl-3-(3-dimethylaminopropyl) carbodiimide hydrochloride) and N-hydroxysuccinimide (NHS) to form an amide bonds. Briefly, 1 mL of 1 mg/mL solution of BSA was prepared in 100 mM MES and 100 mM NaCl, pH 6.0. Final concentrations of 20mM EDC and 5mM NHS were added to the protein. The reaction was carried out at RT for 2 hours. The reaction was quenched by adding 100 mM ethanolamine solution (Solution prepared in D.I water) for 30 min. The protein solution was then dialyzed against 1000 volumes of PBS, pH 7.4 at 4 °C. The oligomers were separated by size exclusion chromatography using a HiPrep 16/60 Sephacryl S-100 HR column (GE Healthcare) with a bed volume of 120 mL.

Cell lines used in the study

The role of glycation and AGE compounds in pancreatic cancer cell proliferation was elucidated in two human pancreatic cancer cell lines. Pancreatic cancer cell lines PANC-1, MIA PaCa-2 and BxPC-3 were purchased from ATCC. PANC-1 cells were cultured in DMEM media with 10% FBS and MIA PaCa-2 cells in DMEM media with 10% FBS and 2.5% horse serum. BxPC-3 cells were cultured in the RPMI-1640 medium containing 10%FBS. The DMEM media, FBS and horse serum were obtained from ATCC. The cells were maintained in a sterile incubator at 37 °C with 5% CO_2.

Cell proliferation by alamar blue assay

To determine the mitogenic effect of Rib-vH BSA we measured cell proliferation by a fluorogenic oxidation-reduction indicator "Resazurin". The non-fluorescent resazurin undergoes reduction in the reducing environment of the cells to form resorufin which exhibits absorption/emission maxima at around 575 nm and 585 nm respectively. Briefly, 5000 cells were seeded in a cell culture 96 well plate and allowed to adhere overnight at 37 °C. The media was then replaced with fresh DMEM media with reduced serum of 2%. The cells were then treated with Rib-vH BSA (1mg/ml) for 24 hours at 37 °C. After the required time period, 10% of the total well volume was added with resazurin (0.1 mg/mL in D.I water and sterile filtered) and the plate was incubated at 37 °C the emission maxima was measured at 585 nm using the SpectraMax M5® plate reader. For RAGE inhibition 25 µg/mL of anti-RAGE antibody (2A11) or 10 µM of RAGE inhibiting peptide (RAP) were used.

Cell proliferation by Ki-67 staining

Rib-vH BSA induced cellular proliferation was also determined using the Ki-67 staining. 10,000 cells were seeded in an ibidi 60µ dish ™. The cells were incubated at 37 °C overnight. The media was then replaced with fresh DMEM media with reduced serum of 2%. The cells were then treated with Rib-vH BSA (1mg/ml) for 24 hrs at 37 °C. The media was aspirated and the cells were washed with PBS twice. The cells were then fixed with 100% methanol at -20 °C for 10 minutes. The cells were then washed with PBS and blocked with 5% BSA in PBS containing 0.1% triton X-100. Anti Ki-67 (ab15580) was diluted (1:100 dilution) in 2% BSA in PBS containing 0.1% Triton™ X-100. The cells were incubated with the antibody at 4 °C overnight and washed with PBS after the incubation. 1:200 dilution of the Alexa Fluor® 647 conjugated anti-rabbit secondary antibody (Jackson Labs: 711-605-152) was added and incubated for 1 hour at RT. The cells were washed with PBS and then imaged using the Zeiss AxioObserver Z1, fully motorized inverted scope with LSM700 laser scanning head attachment.

Colony formation assay

50,000 cells per well were seeded in a 6 well cell culture plate and were incubated at 37 °C till they reached about 60% confluency. The cells were then treated with Rib-vH BSA to a final concentration of 1 mg/mL and then incubated at 37 °C for 48 hrs. After the incubation the cells were scrapped out using a sterile cell scrapper, resuspended in fresh media and counted using the haemocytometer. 1000 cells were seeded per well in a new 6 well cell culture plate. The cells were incubated at 37 °C for 10 days. The cells were grown in DMEM media containing 10% FBS without any Rib-vH BSA treatment. After the incubation the media was aspirated, cells were washed twice with ice cold PBS and fixed with ice cold methanol: acetone (1:1) for 10 minutes on ice. The fixed cells were then washed twice with PBS and stained with crystal violet solution for 10 minutes at RT. The wells were then washed with running tap water and air dried. The wells were imaged and the colonies formed were counted using ImageJ software.

Cell migration assay

To determine the AGE induced migration of pancreatic cancer cells 8.0 µM cell inserts were used (translucent, greiner bio-one). Briefly, the cells were scrapped using a sterile cell scrapper from a 75 cm^2 flask once the cells were 80% confluent. The cells were resuspended in serum free media and counted using a haemocytometer. 50,000 cells in serum free DMEM media were seeded in to each cell insert the cells were then treated with 1 mg/mL of rib-vH BSA. The cell insert was then placed in a 24 well plate. The well contained media with 10% FBS as the chemoattractant. The cells were allowed to migrate for 24 hours at 37 °C. Equal number of cells were also seeded in the well containing DMEM media with 10% FBS without the insert as a control. After 24 hours the non-migrated cells in the cell insert were removed with a sterile cell swab. Resazurin was added in the well (10% of the total well volume) containing the DMEM media with 10% FBS and the insert was placed back into the well and incubated at 37 °C for 24 hours. The percentage of cells migrated were determined by measuring the fluorescence as described above.

Reactive oxygen species (ROS) formation

AGE induced ROS formation was determined by a cell-permeable non-fluorescent ROS probe 2, 7-dichlorodihydrofluorescein diacetate. This compound is de-esterified intracellularly and on oxidation by ROS turns in to 2, 7- dichlorofluorescein which is highly fluorescent. 25,000 cells per well were seeded in a 96 well plate and incubated at 37 °C overnight. The media was aspirated and the cells were washed twice with PBS and were loaded with 5 µM per well of 2, 7 Dichlorofluorescein diacetate and incubated at 37 °C for 30 minutes. The cells were then treated with the AGE compound (1 mg/mL) at 37 °C. Fluorescence emission was measured at 535 nm with an excitation wavelength of 500 nm using the SpectraMax M5 plate reader.

Super oxide generation

Dihydroethidium was used to determine the super oxide generation. 25,000 cells/well were seeded in a 96 well plate and incubated at 37 °C overnight. The cells were loaded with 10 µM dihydroethidium and were incubated at 37 °C for 30 minutes. The loaded cells were treated with 1mg/mL of Rib-vH BSA at 37 °C. The oxyethidium fluorescence was monitored with an excitation wavelength of 500 nm and an emission maximum of 590 nm at different time points to determine the super oxide production. The cells treated with 1mg/mL of BSA and the untreated cells were used as the controls.

Nitric oxide generation

The effect of AGE compounds on nitric oxide production was evaluated by Griess reaction. Griess reaction measures the formation of the nitric oxide by measuring the nitrite ion which is a stable breakdown product of nitric oxide. 25,000 cells per well were seeded in a 96 well plate and were incubated at 37 °C overnight for the cells to adhere. The media was then aspirated and replenished with serum free media. The cells were then treated with 1 mg/mL AGE compound and incubated at 37 °C for 24 hours. from each well 50 µl of the cell supernatant was collected and transferred to a fresh 96 well plate, 50 µL of Sulfanilamide solution also called as solution 1(10 mg/mL solution in 5% phosphoric acid) was added in each well and incubated at RT in dark for 10 minutes and finally 50 µl of N-1-napthylethylenediamine dihydrochloride (NED) (1mg/mL of NED in D.I. water) solution was added and incubated in dark for 10 minutes at RT. The absorbance of the Azo compound formed was measured at 570 nm. Serial dilutions of sodium nitrite were made and the nitrite content was determined and a calibration curve was obtained. The exact nitrate content of the cells was measured using this standard curve.

NF-κB activity assay

Rib-vH BSA induced NFκB activity was determined by transient transfection of NFκB cis-reporting plasmid (Stratagene #219077) into the pancreatic cancer cell lines. Briefly, 100,000 cells/well were seeded in a 6 well plate and were incubated at 37 °C overnight. The NFκB reporter plasmid was transfected using Lipofectamine® 2000. For each well 2.5 µg of the plasmid was mixed with 8 µL of Lipofectamine® 2000 in 200 µL of serum free DMEM medium and was incubated for 30 minutes at RT. Before transfecting the cells, the media was aspirated and was replaced with serum free DMEM. The transfected cells were incubated at 37 °C overnight. After incubation the media was aspirated and was replaced with DMEM media containing 2% serum and the cells were treated with 1mg/mL Rib-vH BSA for 24 hours at 37 °C. After 24 hours the cells were washed twice with sterile PBS, pH 7.4 and then 400 µL of the supplied 1X cell lysis buffer was added in each well and incubated for 15 minutes at RT. 5 µL of this cell lysate was added to 100 µL of luciferase substrate and the luminescence was measured using a Berthhold tube luminometer. To determine the role of ROS induced NFκB activation 500 µM of N-acetyl cysteine was used. The role of RAGE in Rib-vH BSA induced NFκB activity was elucidated by 25 µg/mL of anti-RAGE and 1 µM of FPS-ZM1 which is a small molecule inhibitor of RAGE.

Fluorescent labelling of Rib-vH BSA

The cysteine residues of the rib-vH BSA were fluorescently labelled by a malemide derivative of a near infra-red cyanine dye called Cy5.5. It has an excitation wavelength of 675 nm and an emission maximum at 695 nm. Cy5.5_malemide was dissolved in methanol aliquoted and dried by vacuum centrifugation and stored at -80 °C. Rib-vH BSA was diluted in PBS to a final concentration of 10 mg/mL and was then mixed with 2 molar excess of Cy5.5 and incubated for 30 minutes at RT by stirring. The free dye was removed by dialyzing the protein against 500 volumes of PBS. The presence of free dye was visualized by running the labelled protein on a SDS-PAGE gel. Absorbance was measured at 280 nm and 675 nm and the moles of dye bound to the mole of protein were determined.

AGE uptake assay

The kinetics of rib-vH BSA uptake was determined by measuring the fluorescence of Cy5.5 of the rib-vH BSA_Cy5.5 at different time points. Briefly, 50,000 cells per well were seeded in a cell culture 24 well plate and incubated at 37 °C overnight for the cells to adhere. 50 ug/mL of the labelled rib-vH BSA was added to each well and incubated at 37 °C. The cells were lysed using TBS with 0.1% triton X-100 at different time points. For 0 hour time point the cells were lysed immediately as soon as the compound was added. Fluorescence of the cell lysate was measured in a 40 µL quartz cuvette with an excitation of 675 nm and an emission of 691 nm with a slit settings of 5 nm on the Horiba Jvon spectrofluorimeter. The exact protein content taken up was determined by a calibration curve of the labelled rib-vH BSA.

Western blot analysis for kinase activity

Rib-vH BSA induced kinase activation was estimated by western blot analysis. Briefly, 30 µg of total cell protein was loaded on a 12% SDS-PAGE gel and run at 150 V. The bands were transferred on to a nitrocellulose membrane at 250 mA for 1 hour. The blot was then blocked using 5% milk powder in TBS-T. SAPK/JNK (CST: 9358S), AKT (CST: 4685S), ERK1/2 (CST: 4695S), P38 (ab7952) and P53 (CST: 2527S) primary antibody dilution (1:1000 dilution) was made in 2% milk powder in TBS-T. The blot was incubated with the respective primary antibody overnight at 4 °C. The blots were washed with TBS-T for 5 times (2 minutes each) and the HRP conjugated secondary antibody was added (Jackson: 711-035-152, 1:10000 dilution). The blot was incubated for 2 hrs at RT then washed and developed on the X-ray film using the ECL substrate. The blot was then washed and stripped using 1.5% glycine, pH 2.2 with 1% Tween 20 at 80 °C for 20 minutes. The blot was washed several times with TBS-T and blocked with 5% milk powder at RT for 2 hours. Then the phosphorylated SAPK/JNK (CST: 4668S), phosphorylated AKT (CST: 4060S), phosphorylated p38 (ab45381), phosphorylated p53 (CST: 9281P), phosphorylated ERK1/2 (CST: 9101S) antibodies were added respectively (1:1000 dilution) and incubated overnight at 4 °C. The HRP conjugated secondary antibody was added and incubated for 2 hrs at RT. After developing the blot was washed and stripped as described above and the blot was then incubated with actin antibody (sc-1616) at 4 °C overnight and was then incubated with HRP conjugated secondary antibody and developed.

RNA extraction and cDNA synthesis

The whole cell RNA was extracted from the PANC-1 and MIA PaCa-2 cells using the Ambion's Protein and RNA Isolation System, PARIS™ (Life Technologies). Briefly, 50000 cells were seeded in each well of a 6 well plate. The cells were allowed to adhere and reach a confluency of 60% by incubating at 37 °C for 24 hours. After the cells reached the required confluency, the cells were stimulated with 1 mg/mL of Rib-vH BSA. The cells were then incubated at 37 °C. Cells were harvested at 24 hrs after stimulation and the RNA was extracted. The concentration of the RNA was measured by UV absorbance at 260 nm and the ratio of the absorbance at 260 nm/280 nm was calculated to estimate the purity of RNA. The RNA was immediately reverse transcribed using the Moloney Murine Leukemia Virus (M-MuLV) Reverse Transcriptase (NEB labs) using an oligo dT primer.

Quantitative real time PCR (q RT-PCR)

The expression of AGE-receptors (Table 2.1) in the PANC-1 and Mia PaCa-2 cells was determined by real time PCR using Eva green (Solis BioDyne) according to manufacturer's protocol. 1 ng of cDNA was used in each PCR reaction (20 µL) and 250nM of forward and reverse primers were used and reaction was amplified for 40 cycles.

Glycation of collagen

To determine the effect of different glycation agents on the glycation of extracellular matrix (ECM) collagen was used as a model for ECM glycation. Sterile rat tail collagen was dissolved in 70% ethanol and 50 µg of collagen in 70% ethanol was added in each well of a 96 well plate and were allowed to air dry under the sterile hood overnight for the ethanol to evaporate. The coated collagen was then washed with sterile glycation buffer twice and 600 µL the glycation agent was added in each well. The plate was sealed with tape and the incubated at

37 °C for 10 days to allow the collagen to glycate. After glycation, the glycation agent was aspirated and the collagen was washed 5 times with sterile PBS. Cells were seeded on the glycated collagen coated plates or the plates were sealed and stored at 4 °C.

Effect of collagen glycation on cell adhesion

The effect of collagen glycation on cellular adhesion was determined crystal violet staining. The sterile glycated collagen plates were seeded with 5000 cells per well and were then incubated at 37 °C for 12 hours. After 12 hours the media was aspirated and the un-adhered cells were removed by washing with sterile PBS twice. The adherent cells were then fixed with methanol: acetic acid (3:1) for 5 minutes at RT. The fixative was aspirated and the cells were washed with sterile PBS thrice. The cells were then stained with crystal violet solution for 15 minutes at RT. The excessive stain was washed away with tap water. 50 µL of methanol added in each well to dissolve the crystal violet from the stained cells. Absorbance of the dissolved crystal violet was measured at 545 nm.

Results and Discussions

Rib-vH BSA uptake in pancreatic cancer cell lines

The AGE compound uptake has not been studied and described in any cancer cells. It is not clear if the AGE compounds are taken up by the cancer cells or if they trigger signaling simply by binding to cell surface receptors. The Rib-vH BSA uptake was measured using the Cy 5.5 labelled Rib-vH BSA in the PANC-1 and MIA PaCa-2 cell lines. The uptake of the Rib-vH BSA was followed by measuring the fluorescence from the cell lysate obtained after treatment at different periods of time. Rib-vH BSA uptake was observed in the PANC-1 cells and the uptake was time dependent. We observe a significant uptake of Rib-vH BSA after 3 hours of incubation and a continuous increase was observed till 24 hours. The exact amount of protein internalized per well was determined using a standard curve. The uptake kinetics is shown in Figure 3.1. After 6 hours we observe an internalization of 4.15±0.02 µg per well and 7.4±0.01 µg per well after 10 hours. Internalization of 22.23±0.13 µg of the 25 µg added was observed after 24 hours of treatment. The internalization behavior of the PANC-1 cells was different from the RAW 264.7 cells (Figure 4.1). The Rib-vH BSA uptake by the macrophages is described in chapter 4.The uptake in macrophages was extremely rapid in the initial time points of the treatment, 5 µg, 8 µg and 14 µg of the AGE compound was taken up within 30 minutes, 1 hour and 6 hours respectively after incubation. No internalization was observed in the MIA PaCa-2 cells even after 24 hours of incubation. The role of multiple receptors in AGE compound uptake has been described (Chapter 2). However, the role a specific receptor primarily responsible for AGE compound uptake in pancreatic cancer cells has not been described. We suspect these differences could be due to the differences in the expression of AGE receptors. The macrophages express various scavenging receptors which could play a role in AGE uptake (Chapter 4). Our qPCR results of the PANC-1 and MIA PaCa-2 cells suggest differential expression of the AGE receptors in these two cell lines more specifically higher expression (4.32±2.29 Ct units) of CD36 which is a class B scavenger receptor was observed in the PANC-1 cells when compared to the MIA PaCa-2 cells. The Ct values are shown in table 3.1 are normalized to actin expression in each cell line. Further investigation is required in this direction to identify the receptors responsible for AGE compounds.

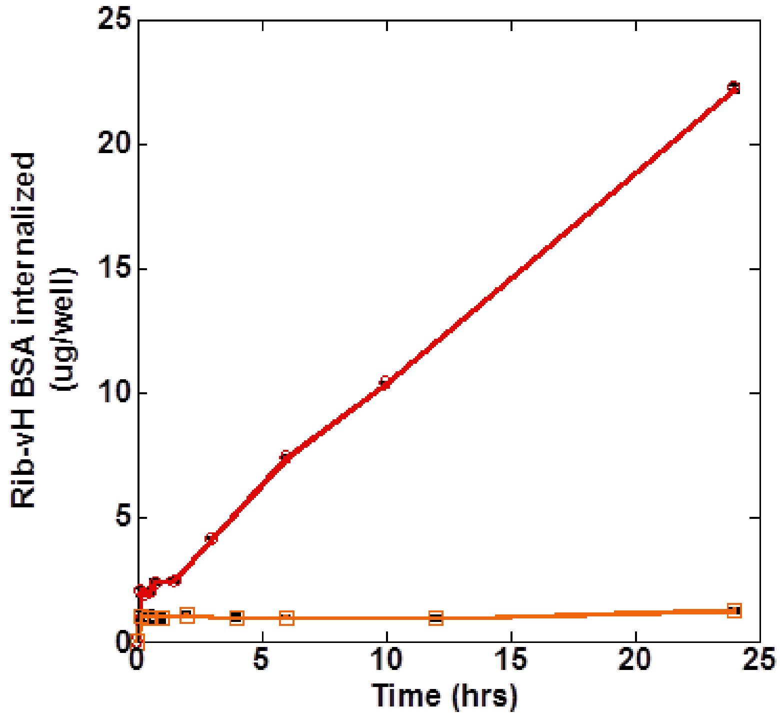

Figure 3.1. Rib-vH BSA_Cy 5.5 uptake kinetics by PANC-1 (Red) and MIA PaCa-2 (Orange) cells. (Representation of 2 independent experiments n=6 for each experiment).

Table 3.1. Expression of AGE receptors in PANC-1 and MIA PaCa-2 cells at the RNA level. The Ct values were normalized to actin expression. (Lower the Ct value higher the expression).

Gene (Gene ID)	**Primers (5'→3')**	**ΔCt PANC-1**	**ΔCt MIA PaCa-2**
CD36 (NM_001001548)	Forward: CTTTGGCTTAATGAGACTGGGAC Reverse: GCAACAAACATCACCACACCA	8.09±0.18	12.4±2.47
STAB1 (NM_0151436)	Forward: CCGGGAAATCCTTACCACAGC Reverse: ACCTTCGTGTTTGTTGGGTCC	13.11±0.14	11.19±0.12
STAB2 (NM_017564)	Forward: GTGCCCGGATGGTTACACC Reverse: CTTCCTACAAATATGGCGGCAT	20.42±0.98	16.80±1.80

Table 3.1. Expression of AGE receptors in PANC-1 and MIA PaCa-2 cells at the RNA level (continued).

Gene (Gene ID)	**Primers (5'→3')**	**ΔCt PANC-1**	**ΔCt MIA PaCa-2**
SCARB1 (NM_001082959)	Forward: ACTTCTGGCATTCCGATCAGT Reverse: ACGAAGCGATAGGTGGGGAT	6.64±0.60	6.08±0.78
SCARB2 (NM_005506)	Forward: AGATGGAGATTCTTTTCACCCAC Reverse: CAGGAACTTTATACCGAAAGGCA	6.85±0.70	6.04±0.42
MSR1 (NM_002445)	Forward: CCAGGTCCAATAGGTCCTCC Reverse: CTGGCCTTCCGGCATATCC	21.08±0.52	16.79±3.71
MARCO (NM_006770)	Forward: CAGCGGGTAGACAACTTCACT Reverse: TTGCTCCATCTCGTCCCATAG	22.11±0.05	15.87±4.13
DDOST (NM_005216)	Forward: GAGACTCATTCGCTTTTCTTCCG Reverse: CTCCAAAATCTTCTACCGAAGGG	4.02±0.11	3.49±0.24
PRKCSH (NM_002743)	Forward: TCAGGTCAACGATGACTATTGC Reverse: CCCGGTTGGAGGGGATATACA	No Ct	No Ct
OLR1 (NM_002543)	Forward: CAACGAGGAGCTGTTTATGC Reverse: GTGCCAATGATCACCTTGTT	12.98±0.77	9.74±3.14
RAGE (NM_001136.3)	Forward: TTTCTGGGCTCTCATGTTTG Reverse: CACAAGATGACCCCAATGA	11.79±0.16	9.20±2.18
Gal-3 (NM_002306)	Forward: CCCGATGATTGTACTGCAAC Reverse: CTGGGGAAGGGAAGAAAGAC	6.66±1.10	6.20±0.42

The uptake of Rib-vH BSA was also determined by fluorescence microscopy. PANC-1 cells were treated with Rib-vH BSA tagged with Cy5.5 and the images were taken after 3 hours of Rib-vH BSA treatment. We observe internalization of the Rib-vH BSA as indicated by our kinetic data. This confirms the internalization of the Rib-vH BSA in the PANC-1 cells. The internalization of the Rib-vH BSA was also determined in the BxPC-3 cells which do not have the KRAS mutation. Internalization was also observe in the BxPC-3 cells as well (Figure 3.2).

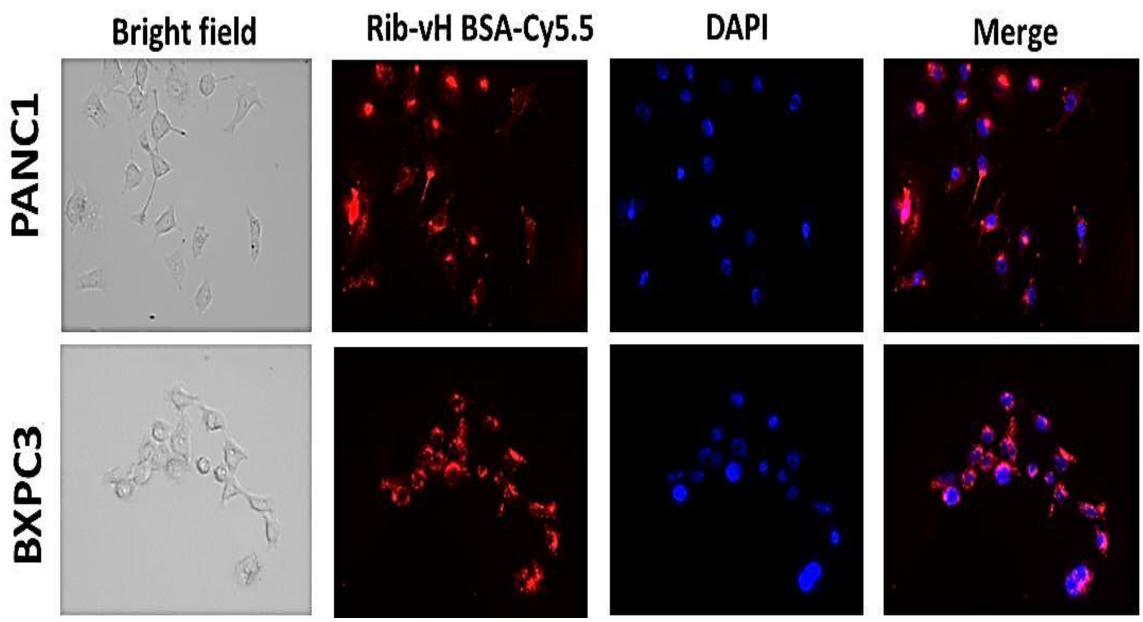

Figure 3.2. Internalization of Rib-vH BSA_Cy5.5 by fluorescence microscopy.

Rib-vH BSA induced oxidative stress

There is evidence that AGE compounds on their interaction with RAGE generate oxidative stress which subsequently elicits vascular inflammation in the context of diabetic complications [50, 256-259] . Inflammation and oxidative stress have been described as a contributing factor in the pathogenesis of pancreatic malignancy[260, 261]. However, the role of AGE compounds and AGE-RAGE axis in oxidative stress in pancreatic cancer etiology is unknown. Rib-vH BSA induced oxidative stress in PANC-1 cells was measured using the 2, 7-dichlorofluorescein diacetate. On treatment with 1mg/mL of Rib-vH BSA after 24 hours we observed a significant increase in ROS production. Rib-vH BSA induced ROS production with respect to control untreated cells is shown in Figure 3.3. We observe a 1.48±0.09 fold increase in ROS production on Rib-vH BSA treatment after 24 hours. On the addition of 500 µM N-acetyl cysteine (NAC), which is a quencher of ROS, the Rib-vH BSA induced ROS produced was back to baseline levels. The role of RAGE in AGE induced ROS production was determined by treating the cells with 1µM of a small inhibitor of RAGE called FPS-ZM1 and 25 µg/mL of an anti-RAGE antibody 2A11. When the cells were co-treated with Rib-vH BSA and FPS-ZM1 the ROS production was back to baseline levels (1.09±0.04 fold). Similar results were also obtained when the cells were co-treated with 2A11 antibody (0.99±0.03 fold). This clearly indicates that AGE induced ROS production is RAGE dependent.

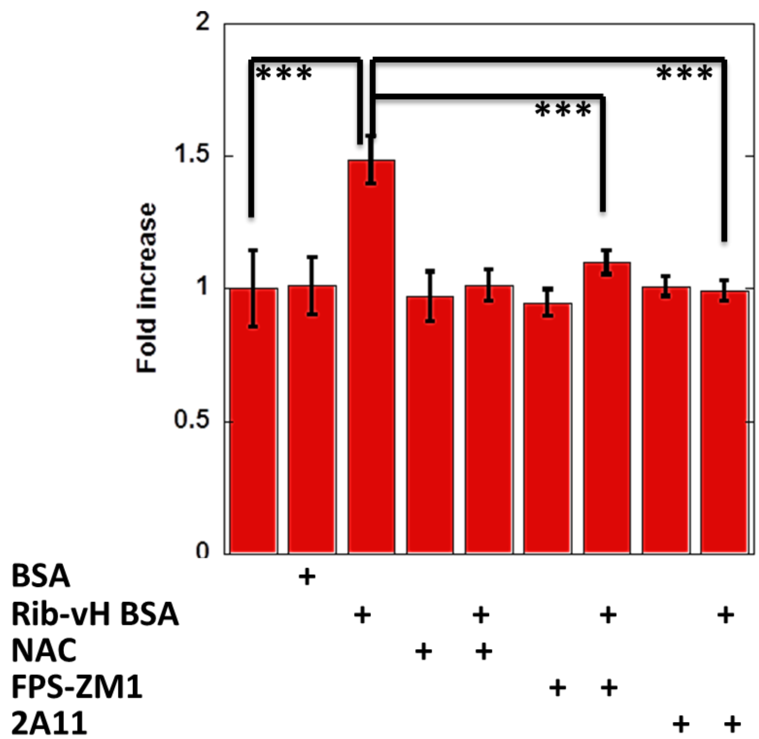

Figure 3.3. Rib-vH BSA induced ROS production in PANC-1 cells.
The first column represents the non-treated control. (Representation of 2 independent experiments n=6 for each experiment. *** P<0.0005).

Rib-vH BSA induced ROS production was also observed in the MIA PaCa-2 cell line (Figure 3.4). On Rib-vH BSA treatment a 1.96±0.11 fold increase in the ROS production was observed after 24 hours of incubation. On the treatment with FPS-ZM1 a decrease in the ROS to 1.45±0.05 fold was observed. Rib-vH BSA induced ROS production was also inhibited by the treatment with the anti-RAGE antibody 2A11 (0.988±0.07 fold).

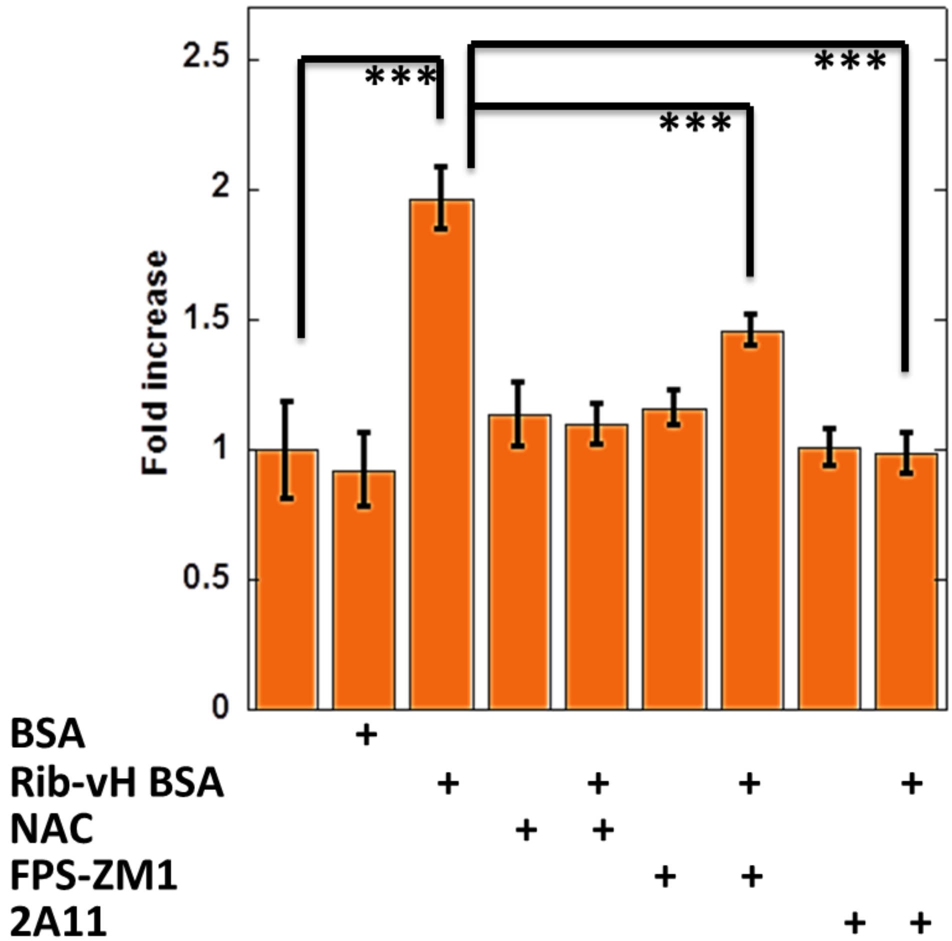

Figure 3.4. Rib-vH BSA induced ROS production in MIA PaCa-2 cells.
The first column represents the non-treated control. RAGE inhibition inhibited Rib-vH BSA induced ROS production. (Representation of 2 independent experiments n=6 for each experiment. *** P<0.0005).

Increased oxidative stress in pancreatic cancer has been implicated in the pathogenesis of pancreatic cancer [260]. There is evidence to support the notion that ROS activates various signaling pathways mediated by NF-κB and kinases such as Janus kinase/signal transducer and activator of transcription (JAK/STAT) and p38 mitogen-activated protein kinases (MAPK) [262-265], which in-turn leads to decreased cell apoptosis and cytokine release [235, 260].

Rib-vH BSA induced generation of super oxide

Super oxide production has been described in various cancer cells (Reviewed in [266]). Recent reports emphasize the role super oxide generation in pancreatic cancer cell growth specifically in the K-ras mutated pancreatic cancer cells [267, 268]. Recently a study reported the role of super oxide and nitric oxide in increased invasiveness in pancreatic ductal adenocarcinoma patients[269]. AGE induced super oxide generation has been described in various vascular complications of diabetes [270-272]. The role of AGE compounds in the induction of super oxide in cancer cells has not been described in the literature. This study was initiated to determine the role of Rib-vH BSA in super oxide generation in pancreatic cancer cells.

The super oxide produced on Rib-vH BSA treatment was determined by using a fluorescent probe dihydroethidium. Super oxide oxidizes the dihydroethidium to form a red fluorescent compound called oxyethidium[273]. On treatment with Rib-vH BSA we observe a significant increase in the super oxide production in the PANC-1 cells. Figure 3.5 visualizes the increase in the superoxide production in the PANC-1 cells as a function of time. Rapid increase in the Rib-vH BSA induced super oxide production was observed as indicated by the oxyethidium fluorescence. Increase in fluorescence was observed after 30 minutes of Rib-vH BSA treatment and the Rib-vH BSA induced super oxide production was observed even 24 hours after the Rib-vH BSA treatment. Similar results were also observed in the MIA PaCa-2 cells. On Rib-vH BSA treatment significant super oxide production was observed (Figure 3.6). Super oxide production was observed after 30 minutes of treatment and continued till 24 hours of the treatment.

Taken together, these results suggest that the AGE compounds increase super oxide production in pancreatic cancer cells and contribute to the oxidative stress in these cells.

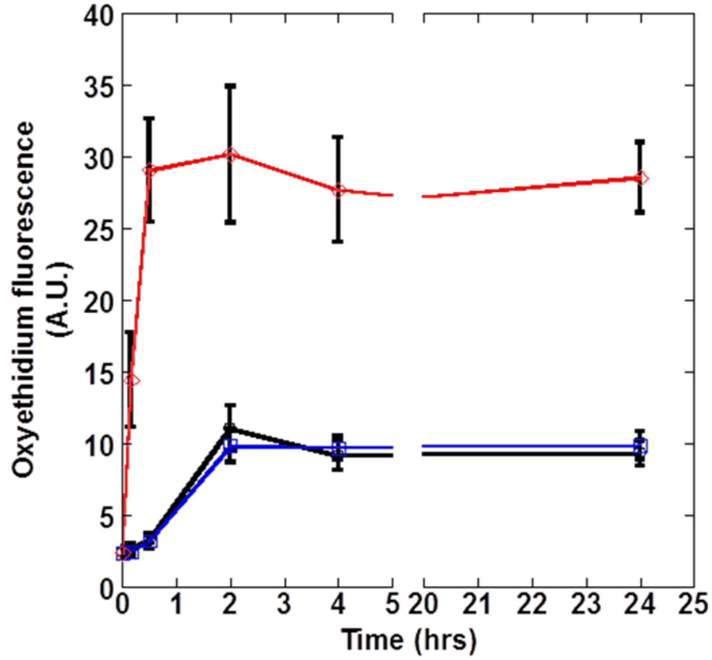

Figure 3.5. Rib-vH BSA induced superoxide production in PANC-1 cells.
Black: Control, Blue: BSA and Red: Rib-vH BSA (Representation of 2 independent experiments n=6 for each experiment).

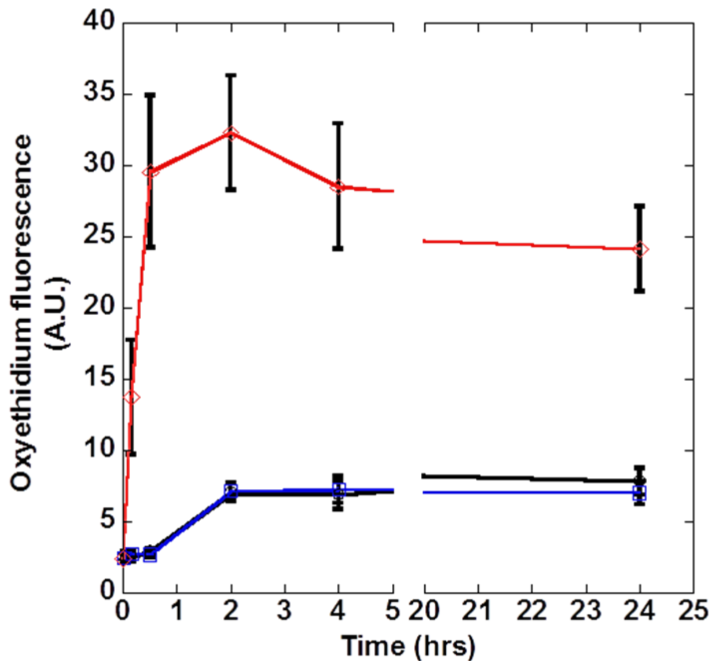

Figure 3.6. Rib-vH BSA induced superoxide production in MIA PaCa-2 cells.
Black: Control, Blue: BSA and Red: Rib-vH BSA (Representation of 2 independent experiments n=6 for each experiment).

Rib-vH BSA induced nitric oxide generation

AGE compounds have been described to induce nitric oxide production has been described in various vascular complications in diabetes [87, 274, 275]. Rib-vH BSA induced nitric oxide release in macrophages has been also been described (See chapter 4). In pancreatic cancer the role of nitric oxide is contradictory not well understood. Both, a tumorigenic and anti-tumorigenic activity of nitric oxide has been described [276, 277]. The role of AGE compounds in the nitric oxide release in pancreatic tumors has not been described and this study was initiated to determine the role of AGE compounds in nitric oxide production in pancreatic cancer cells.

Nitric oxide generation was measured using the Greiss reaction as described earlier. In the PANC-1 cells on treatment with Rib-vH BSA no detectable amounts of nitric oxide was observed even after 24 hours of treatment. Similar results were also observed in the MIA PaCa-2 cells (Figure 3.7). These results suggest that Rib-vH BSA does not lead to nitric oxide production in the pancreatic cancer cells.

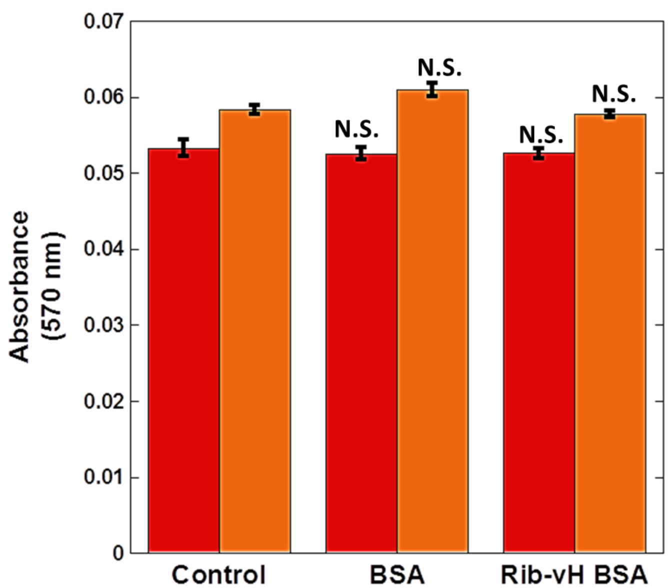

Figure 3.7. Rib-vH BSA induced nitric oxide production in PANC-1(Red) MIA PaCa-2 (Orange) cells.
(Representation of 2 independent experiments n=6 for each experiment. N.S.: No significant difference when compared to the control).

NF-κB activation

Various aspects of the immune and inflammatory response genes are under the control of a dimeric transcription factor called NF-κB. It is hypothesized that the activation of NF-κB is responsible for tumor pathogenesis [26]. It is believed that NF-κB provides a direct link between cancer development and progression and inflammation and immunity [278]. As described earlier NF-κB can be activated by oxidative stress. AGE-RAGE interaction has been described to trigger the NF-κB activity in diabetes associated with lacrimal gland and ocular surface dysfunctions by the activation of inflammatory signaling pathways [279, 280]. Evidence in the literature also suggests the role of RAGE in triggering NF-κB activity by interacting with its ligands such as HMGB1 and S100 proteins in certain cancers [281, 282]. However, no direct evidence on the role of AGE compounds in the ROS mediated NF-κB activity in pancreatic cancer cells has been published till date. On Rib-vH BSA treatment, a 1.6±0.11 fold increase was observed in the NF-κB activity after 24 hours (Figure 3.9). To elucidate the role of ROS in the AGE induced NF-κB activity we treated the cells with 500 μM of N-acetyl cysteine (NAC) which is a potent quencher of ROS. On the treatment with NAC, we observe a decrease in the NF-κB activity to 1.49±0.06 fold when compared to the control. This suggests a role of the AGE induced ROS produced in NF-κB activation. In the MIA PaCa-2 cells no increase was observed in the NF-κB activity on Rib-vH BSA treatment (Figure 3.8). This suggests that in the MIA PaCa-2 cells the Rib-vH BSA does not activate NF-κB signaling.

The role of AGE-RAGE interaction in NF-κB activity was determined using specific anti-RAGE antibody (2A11) and a small molecule inhibitor of RAGE (FPS-ZM1). On the treatment with 2A11 we observe a decrease in the basal NF-κB activity to 0.67±0.07 fold. This suggests the role of RAGE in basal NF-κB activity in the PANC-1 cells. We suspect this basal

NF-κB activity could also be the result of the presence of other RAGE ligands such as S100P and HMGB1. HMGB1 and S100P are released from the pancreatic cancer cells and have been reported to increase the NF-κB activity [235, 283]. When the cells were co-treated with Rib-vH BSA and 2A11 no increase was observed in the NF-κB activity (0.067±0.07 fold). This further emphasizes the role of RAGE in the Rib-vH BSA mediated effects. FPS-ZM1 treatment also reduces the basal NF-κB activity in the PANC-1 cells in a concentration dependent manner. When the cells were treated with 10 μM of FPS-ZM1 the NF-κB activity decreased to 0.12±0.01 fold and no increase was observed when the cells were co-treated with FPS-ZM1 and Rib-vH BSA. Taken together we conclude that the Rib-vH BSA induced NF-κB activity in PANC-1 cells in a RAGE dependent manner and the ROS generated by AGE-RAGE interaction is also responsible for the activating the NF-κB.

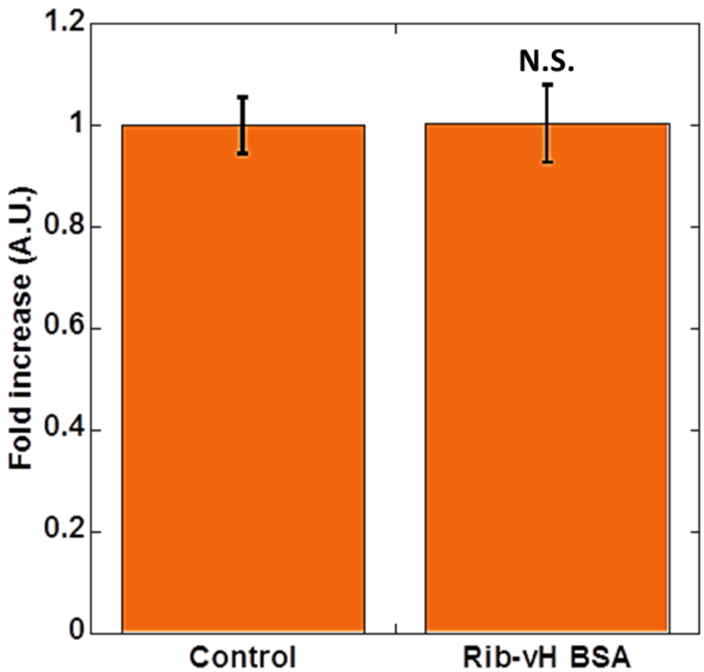

Figure 3.8. NFκB activity in MIA PaCa-2 cells.
(Representation of 2 independent experiments n=6 for each experiment. N.S.: No significant difference when compared to the control).

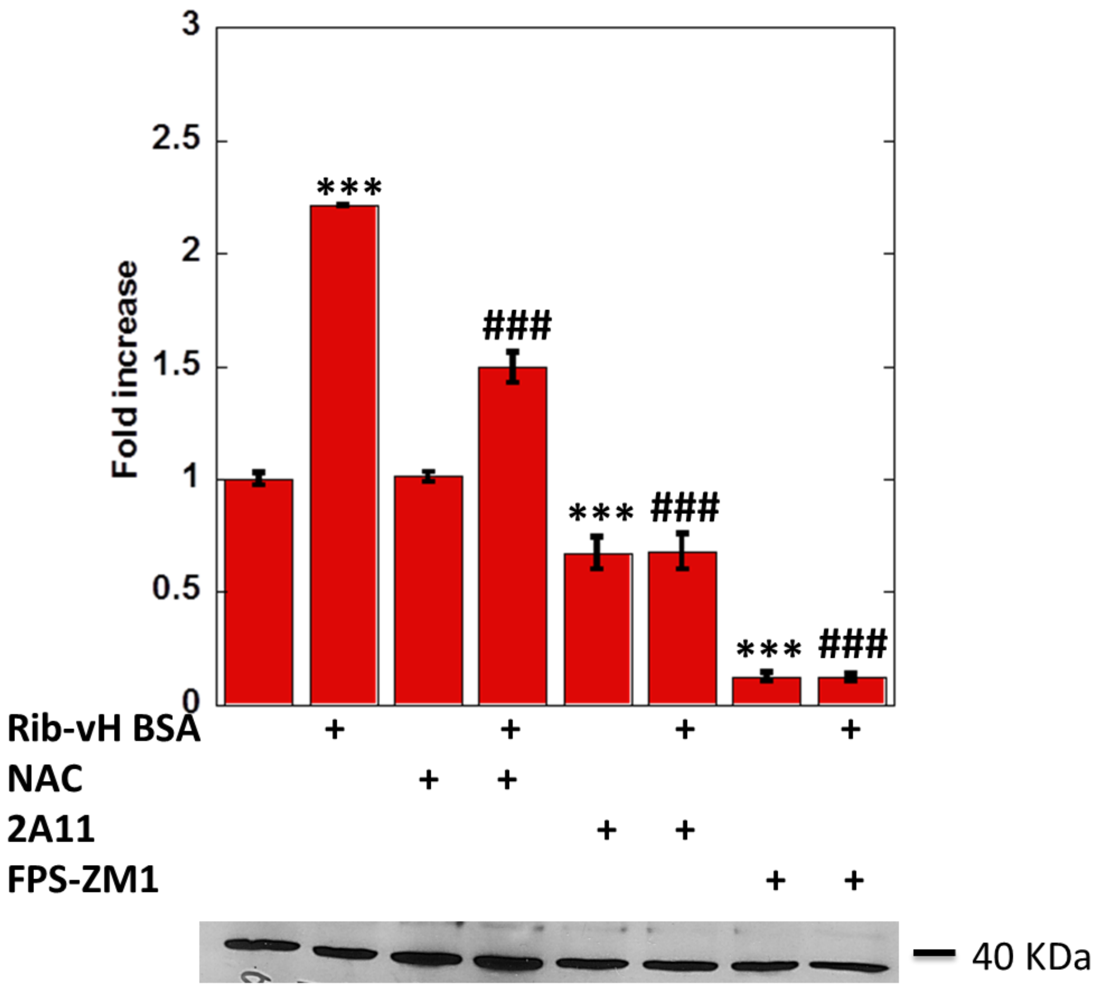

Figure 3.9. Rib-vH BSA induced NFκB activity in PANC-1 cells.
RAGE inhibition prevented the Rib-vH BSA induced NFκB activity. (Representation of 2 independent experiments n=6 for each experiment. *** P<0.0005 when compared to the control, ###P<0.0005 when compared to the RAGE induced sample).

AGE compounds induced cell proliferation in PANC-1 cells

Cancer progression is a complex process and it involves several different cellular processes such as cell proliferation, migration, angiogenesis, invasion and metastasis [284]. In this study we determine the role of Rib-vH BSA in pancreatic cancer cell proliferation and migration. A mitogenic effect of AGE compounds has been described in the context of diabetic complications. AGE induced cell proliferation was first described in the murine kidney mesenglial cells [285] and murine macrophages [286]. The role of AGE compounds in the migration of vascular smooth muscle cells contributing to diabetic vascular complications has been described [287]. The role of AGE-RAGE interaction has been implicated in the neo-intimal hyperplasia of balloon-injured arteries, thus playing a role in cardiovascular disease [288]. The effect of AGE-RAGE has been reported to promote cancer cell proliferation in certain cancerous cell lines such as melanoma [241], myeloid leukemia [289] and breast cancer cell lines[290]. The role of metformin, which is an inhibitor of glycation has also been described in the prevention of AGE induced cell growth in MCF7 cells (Breast cancer cell line) [290]. Recently, the anti-inflammatory role of a DNA aptamer raised against AGE compounds has been described in melanoma[291]. However, the role of AGE compounds in cancer progression is not well understood and the research is still in its infancy. The role of AGE compounds in pancreatic cancer cell proliferation has been indicated [249]. However, the molecular mechanisms of AGE induced cell proliferation is currently unknown. AGE biology is very complex owing to the heterogeneous nature of AGE compounds. As described in chapter 2, AGE compounds can be either toxic or benign to the body and it is not clear on what differentiates the toxic AGE compounds from the benign structurally.

AGE dependent cellular proliferation was determined by treating the PANC-1 cells with the characterized panel of AGE compounds (Table 2.1). The cell proliferation was determined by measuring the alamar blue fluorescence. The AGE induced cell proliferation could be correlated to the multimeric content of the AGE compounds. Figure 3.10 indicates the effect AGE compounds on cancer cell proliferation and the multimeric content of the different AGE compounds is represented on the Y-axis. The most significant effect was observed when the cells were treated with Rib-vH BSA which has a non-monomeric content of about 38.4 ± 1.5 %. On treatment with 1 mg/mL of Rib-vH BSA a 1.67±0.057 fold increase was observed when compared to the control cells (Figure 3.11).

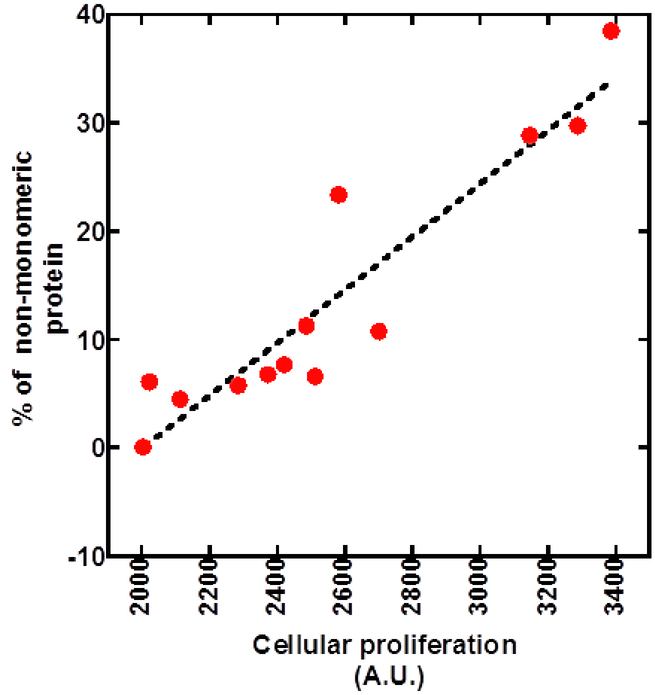

Figure 3.10. AGE compound induced cellular proliferation correlated to the percentage of the non-monomeric content of the different AGE compounds.
R=0.94 for the linear correlation (Representation of 2 independent experiments and n=6 in each experiment).

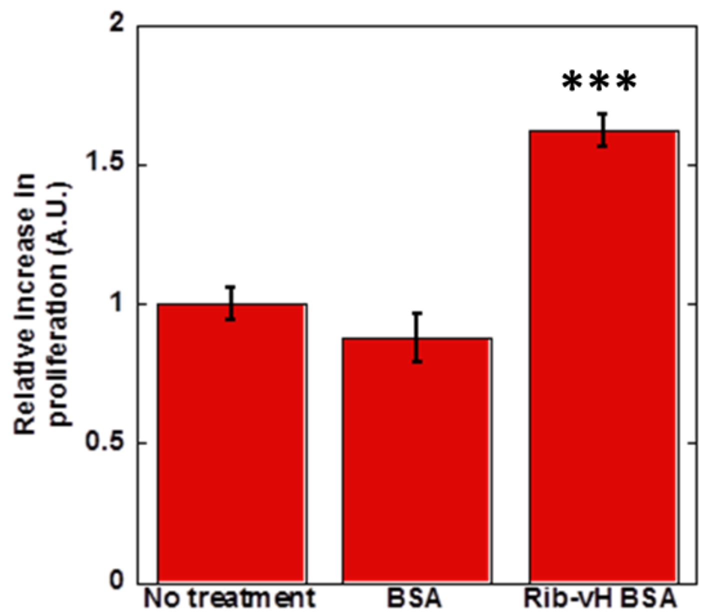

Figure 3.11. Rib-vH BSA induced AGE compound induced cellular proliferation. (Representation of 2 independent experiments and n=6 in each experiment, ***P<0.0005).

The role of RAGE in the AGE mediated mitogenic effects were determined by treating the cells with 25 ug/mL of anti-RAGE antibody (2A11) and also with 10μM of a RAGE inhibiting peptide (RAP). On treatment with RAGE inhibitors we observe the inhibition of Rib-vH BSA induced cellular proliferation (Figure 3.12). This emphasizes the role of RAGE in the AGE induced cellular proliferation. However, there are certain limitations of the alamar blue assay. The alamar blue is a redox indicator and hence it is not a direct cell counting technique and it is highly likely that the fluorescence signal can be affected by both changes in cell number and cell metabolism. To confirm the mitogenic effect of Rib-vH BSA we performed Ki-67 staining. Ki-67 is a well-established marker of cellular proliferation. It is absent during resting phase (G(0)) and present during all active phases of the cell cycle (G(1), G (2) and mitosis)[292]. Ki-67 staining was performed in the non-treated and treated samples. After staining the overall fluorescence was quantified in each image. The analysis was performed with 10 independent images and in the Rib-vH BSA treated cells 8.22±2.37 fold increase in the Ki-67 fluorescence was observed (Figure 3.13). Figure 3.13 represents the Ki-67 staining of the control and the Rib-vH BSA quantified using Imaris software and the Ki-67 fluorescence was normalized with the DAPI treated sample. This confirms that the Rib-vH BSA treatment induced a mitogenic effect in the PANC-1 cells as indicated by the alamar blue assay.

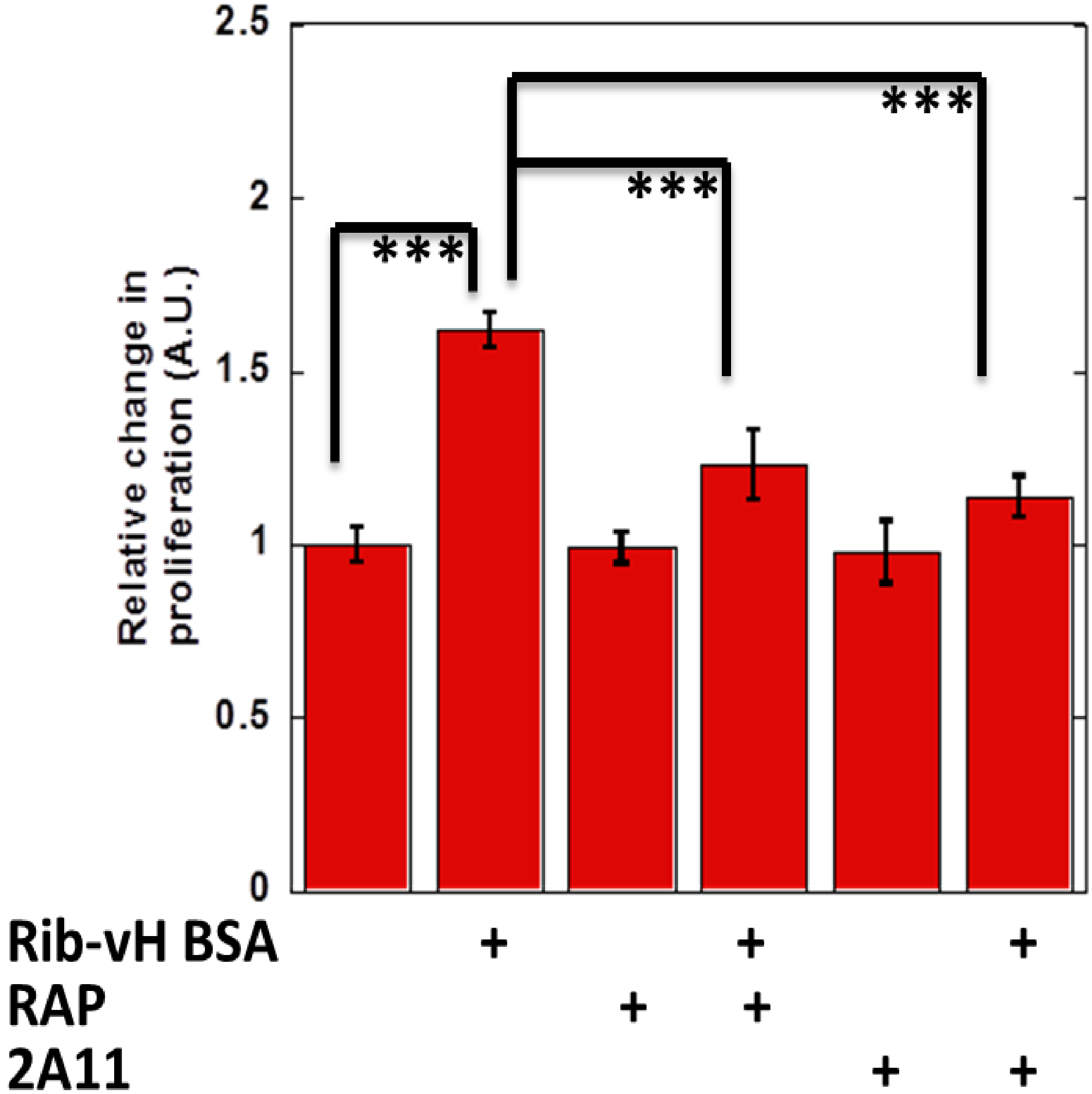

Figure 3.12. Rib-vH BSA induced cellular proliferation was prevented by using RAGE inhibitors RAP and 2A11 antibody.
(Representation of 2 independent experiments and n=6 in each experiment, ***P<0.0005).

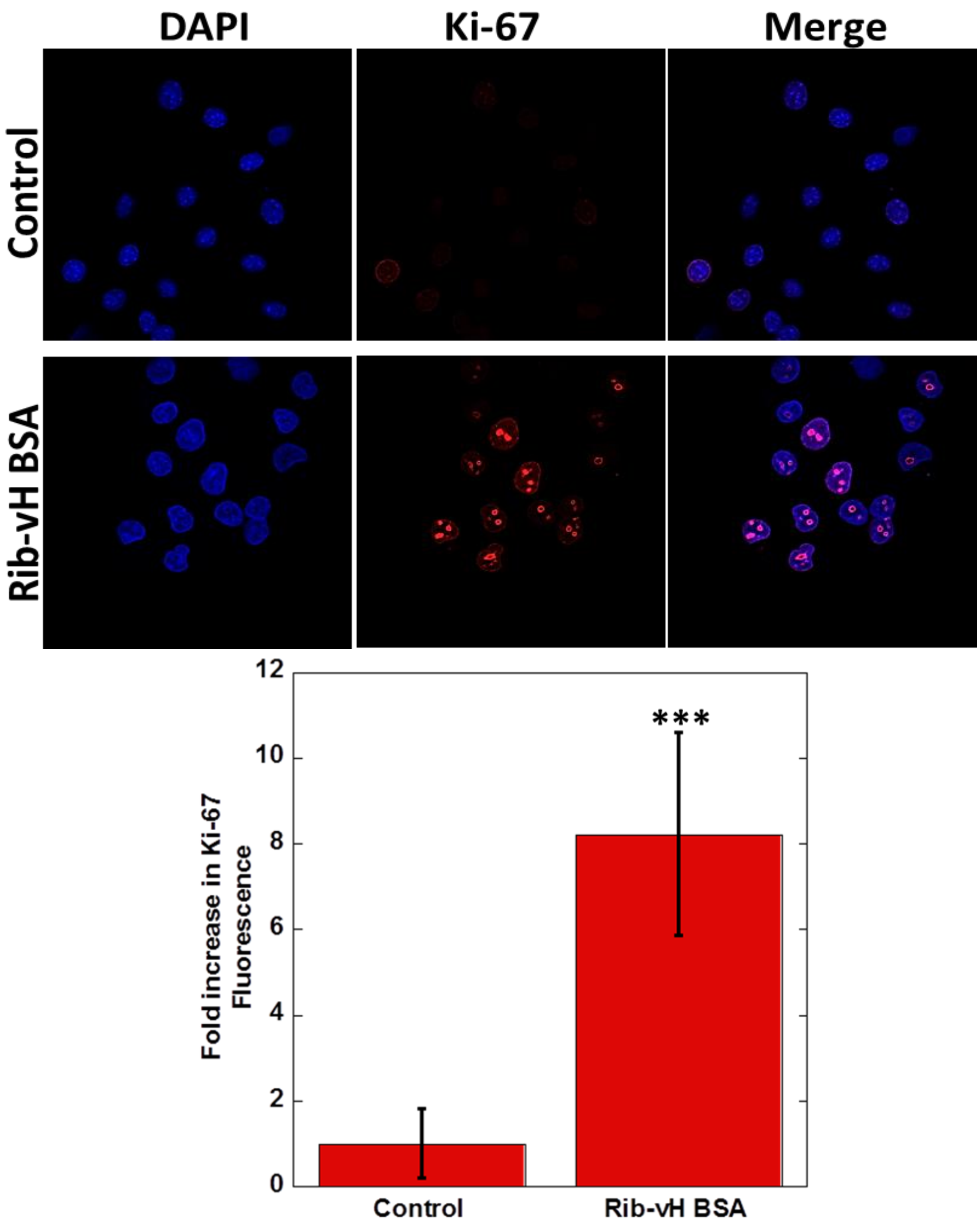

Figure 3.13. Rib-vH BSA induced cellular proliferation determined by Ki-67 staining. The Ki-67 fluorescence was normalized with the DAPI fluorescence in each image and then quantified. (Representation of 2 independent experiments and n=5 in each experiment, ***P<0.0005).

As described earlier the AGE compound induced cellular proliferation could be correlated to the non-monomeric content of the AGE compounds. Few reports in the literature suggest the role of ribosylation of serum albumin in the formation of protein oligomers which leads to protein aggregation [223, 224]. As described in chapter 2, we observe significant oligomerization in the Rib-vH BSA sample but no aggregation was observed as lower concentrations of ribose were used. This study was initiated to decipher the role of Rib-vH BSA induced oligomers in the mitogenic effect observed in PANC-1 cells.

The Rib-vH BSA oligomers were separated by size exclusion chromatography as described earlier. Figure 2.14 shows the elution profile of the Rib-vH BSA. Different fractions were collected and then run on the SDS-PAGE and the fraction with the oligomeric content was used. The oligomers were concentrated and concentration was determined by the BCA assay and then sterile filtered. The PANC-1 cells were treated with the sterile Rib-vH BSA oligomers. As a negative control, BSA was cross linked using the EDC_NHS chemistry and then the oligomers were separated, collected, concentrated and sterile filtered (Figure 3.15).

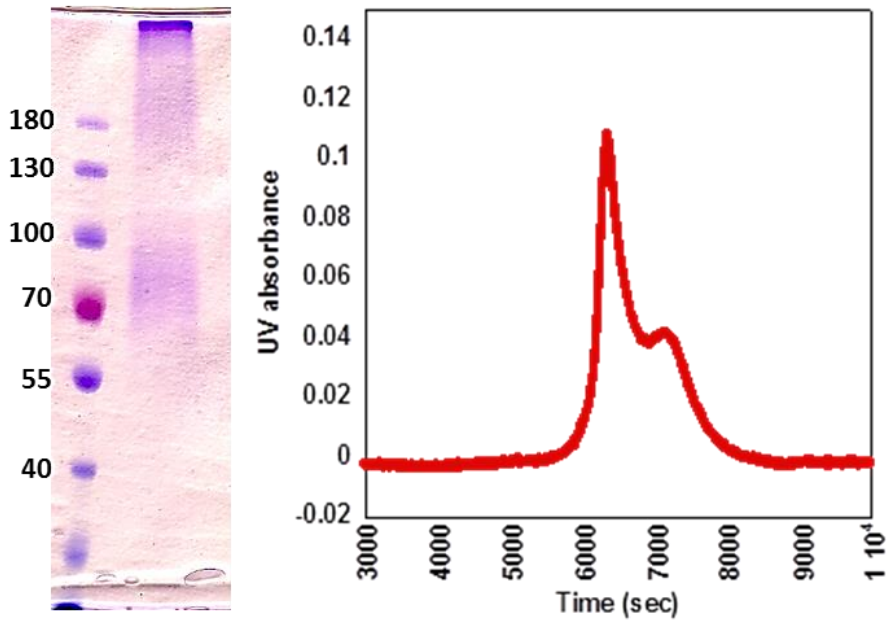

Figure 3.14. Coomaisse blue stained Rib-vH BSA on SDS-PAGE gel (left). Separation of Rib-vH BSA oligomers by size exclusion chromatography (Right).

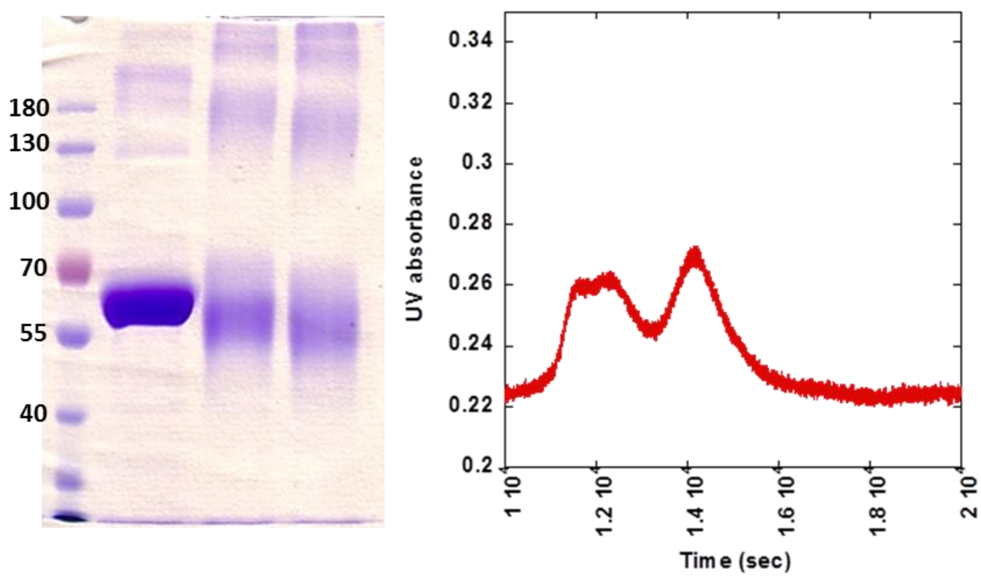

Figure 3.15. EDC-NHS crosslinking of BSA (Left); Separation of the BSA oligomers by size-exclusion chromatography (Right).
Lane 1: Ladder, Lane 2: BSA at 0 hours of cross linking, Lane 3: BSA after 3 hours of cross linking and Lane 4: BSA after 5 hours of cross linking.

The cells were treated with a final concentration of 65 µg/mL of the oligomers and equal concentration of the monomers and the unseparated Rib-vH BSA. On treatment with the purified oligomers we observe at significant increase (P<0.005) in the PANC-1 cellular proliferation (Figure 3.16). No increase in proliferation was observed when the cells were treated with equal amount of the Rib-vH BSA monomers. The treatment with 65µg/mL of unseparated Rib-vH BSA also did not induce any cellular proliferation. This suggests that the active AGE compounds necessary for cellular proliferation are present in the oligomeric content if the Rib-vH BSA and ribose induced cross linking plays a very important role in Rib-vH BSA mediated cellular effects. The isolated BSA oligomers did not induce any effect on cellular proliferation (Figure 3.16)

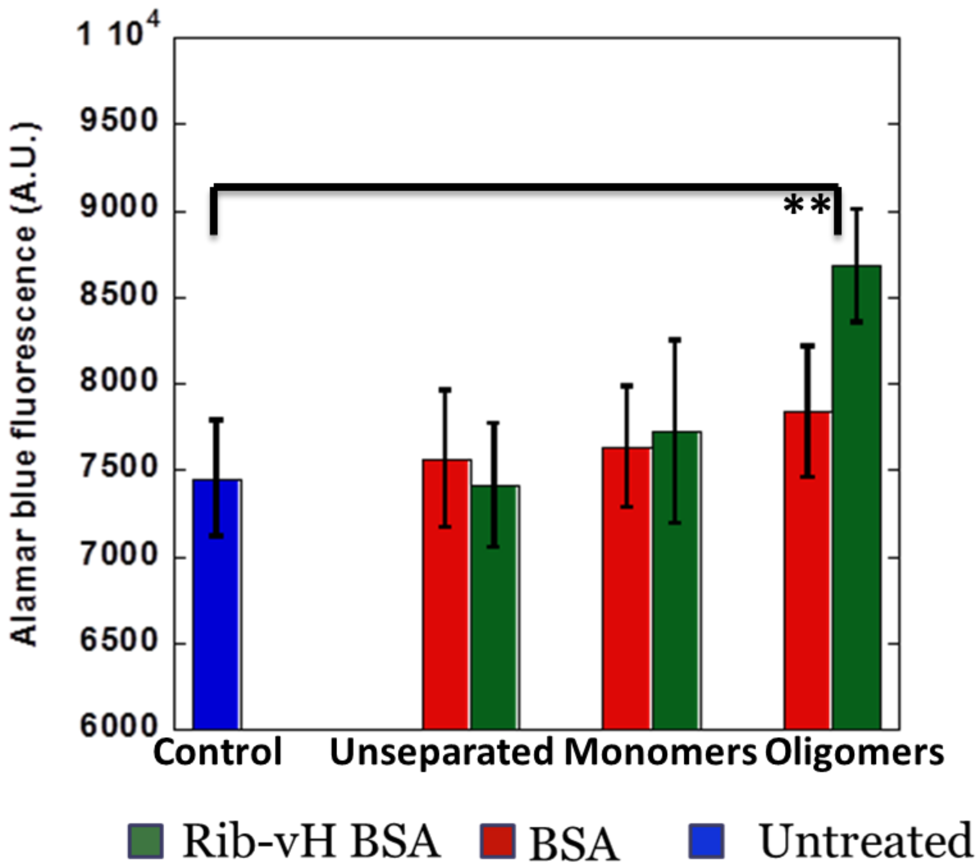

Figure 3.16. PANC-1cellular proliferation by Rib-vH BSA oligomers. (Representation of 2 independent experiments and n=6 in each experiment, **P<0.005).

To further elucidate the role of Rib-vH BSA in pancreatic cancer progression, the role of Rib-vH BSA in reproductive viability of the PANC-1 cells was determined by clonal formation assay. On crystal violet staining we observe a significant increase in the clone formation in the Rib-vH BSA treated cells when compared to the control (Figure 3.17). However, no significant differences were observed in the size of the clones between treated and non-treated samples. This suggests that Rib-vH BSA increased the clonal formation ability of the PANC-1 cells and this would contribute to the tumor growth and progression.

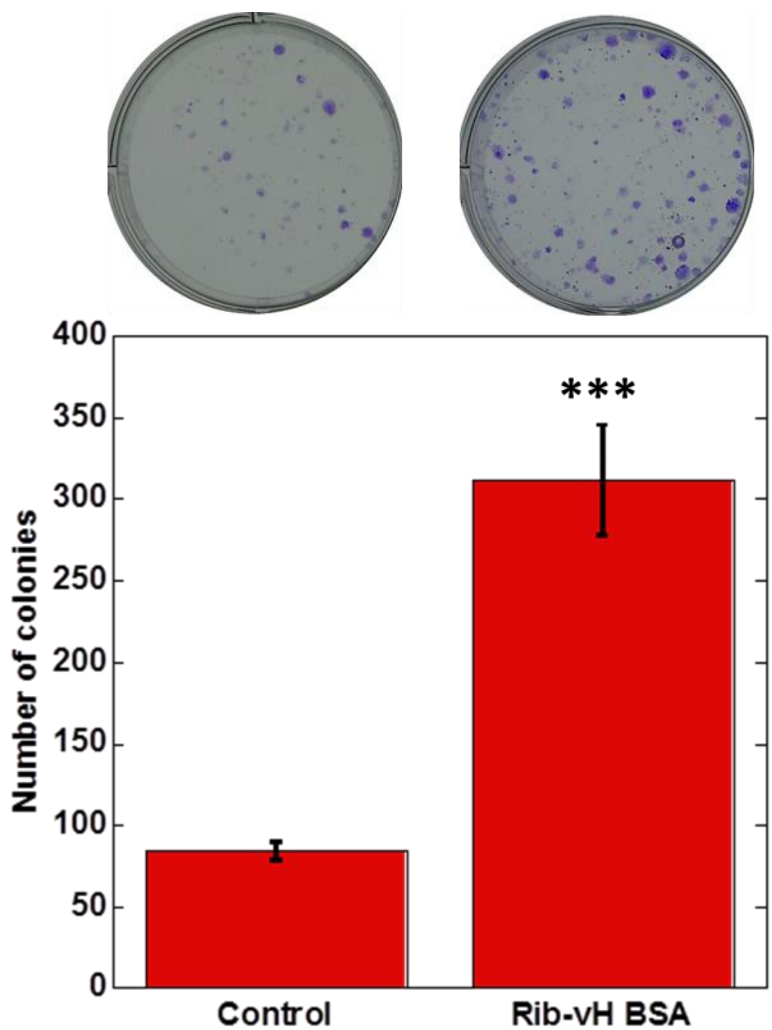

Figure 3.17. Rib-vH BSA induced colony formation in PANC-1 cells.
(Representation of 2 independent experiments and n=6 in each experiment, ***P<0.0005).

AGE compounds induced cell proliferation in MIA Paca-2 and BxPC-3 cells

Effect of further elucidate the role of mitogenic effect of AGE compounds in pancreatic cancer, we determine their role in other pancreatic cancer cell lines BxPC-3 and Mia PaCa-2. In BxPC-3 cells, on treatment with the panel of AGE compounds we observe a relationship between the mitogenic effect and the oligomeric content of the AGE compounds as observed in the PANC-1 cells (Figure 3.18). The most significant effect was observed with the Rib-vH BSA sample where a 1.34±0.04 fold increase was observed (Figure 3.19). The role of RAGE in the Rib-vH BSA mediated cell proliferation was determined using the 2A11 and RAP. Both the 2A11 and RAP inhibited the Rib-vH BSA induced cellular proliferation emphasizing the importance of RAGE interaction in Rib-vH BSA mediated effects (Figure 3.20). The treatment of BxPC-3 cells with isolated Rib-vH BSA oligomers also induced a significant increase in the cell proliferation, no increase in cellular proliferation was observed when the cells were treated with Rib-vH BSA monomers and unseparated Rib-vH BSA (Figure 3.21). This further emphasizes the importance of ribose induced cross linking in the Rib-vH BSA induced mitogenic effect of pancreatic cancer.

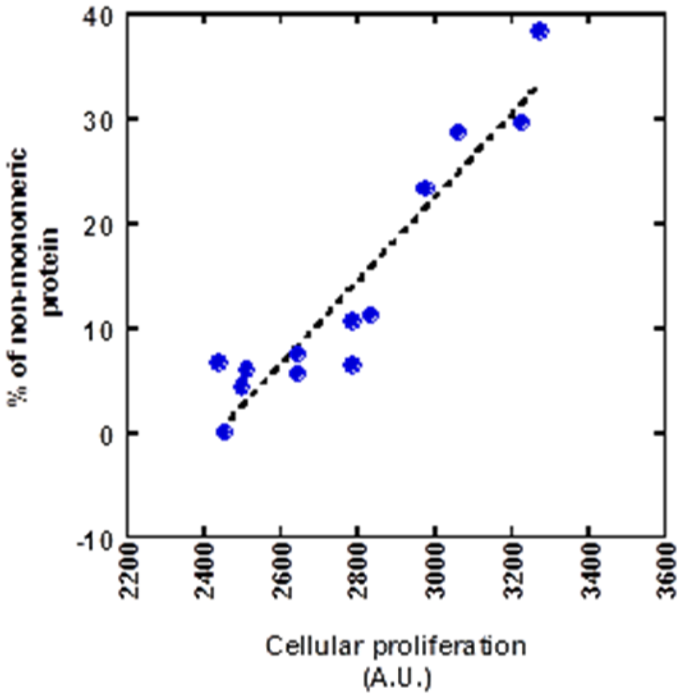

Figure 3.18. AGE compound induced cellular proliferation in BxPC-3 cells correlated to the percentage of the non-monomeric content of the different AGE compounds.
R=0.92 for the linear correlation (Representation of 2 independent experiments and n=6 in each experiment).

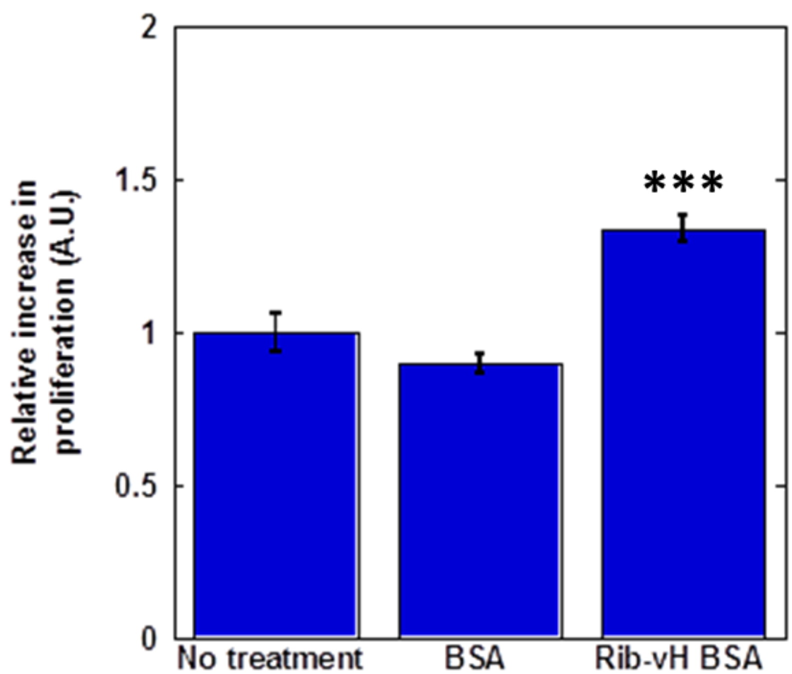

Figure 3.19. Rib-vH BSA induced AGE compound induced cellular proliferation.
(Representation of 2 independent experiments and n=6 in each experiment, ***P<0.0005).

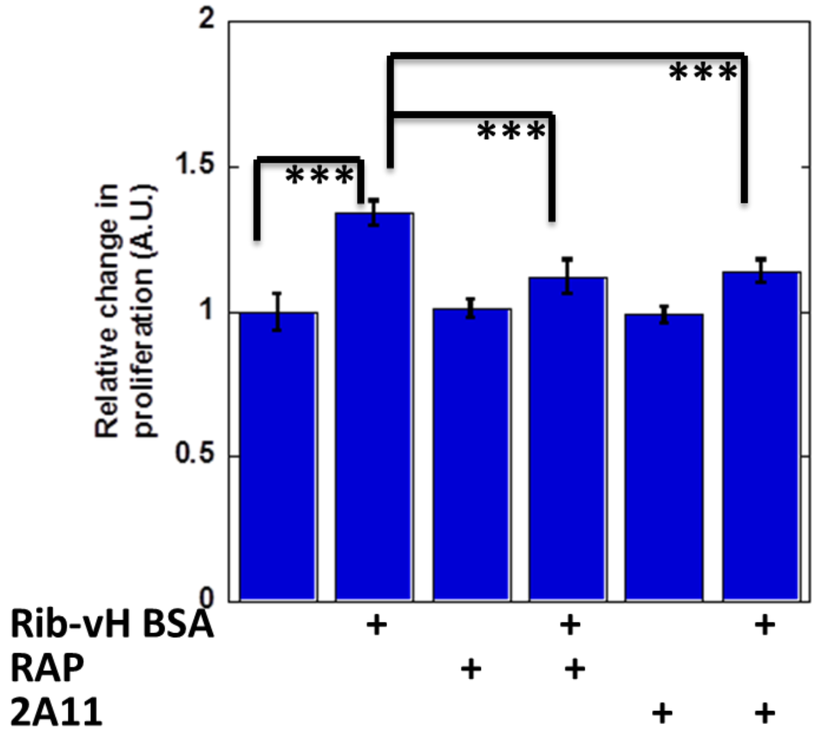

Figure 3.20. Rib-vH BSA induced cellular proliferation was prevented by using RAGE inhibitors RAP and 2A11 antibody.
(Representation of 2 independent experiments and n=6 in each experiment, ***P<0.0005).

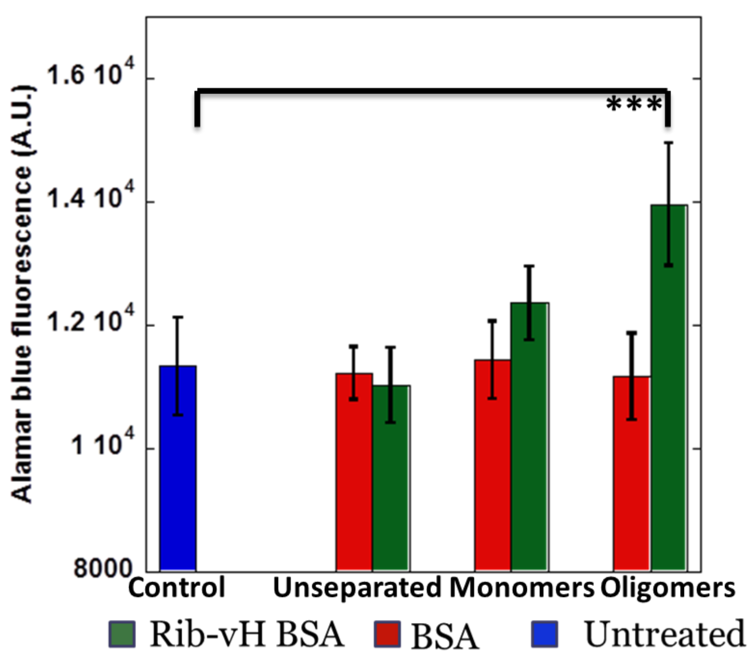

Figure 3.21. BxPC-3cellular proliferation by Rib-vH BSA oligomers.
(Representation of 2 independent experiments and n=6 in each experiment, **P<0.0005).

Similar results were observed in the MIA PaCa-2 cells. Figure 3.22 indicates the AGE induced cell proliferation and a linear correlation was observed with the oligomeric content of the AGE compounds. RAGE inhibition with the 2A11 anti-RAGE antibody also inhibited the Rib-vH BSA induced cell proliferation (Figure 3.24). Similar to the other cell lines the treatment with Rib-vH BSA oligomers also induced cell proliferation (Figure 3.25).

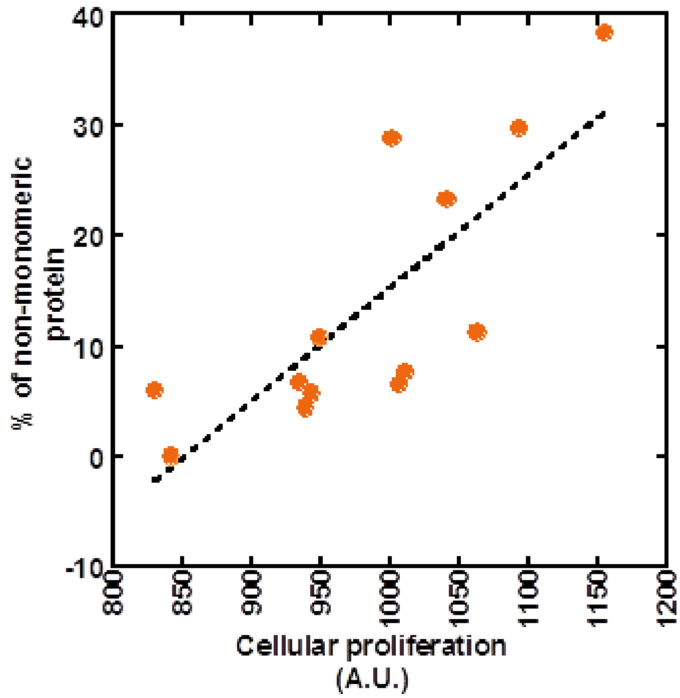

Figure 3.22. AGE compound induced cellular proliferation in MIA PaCa-2 cells correlated to the percentage of the non-monomeric content of the different AGE compounds.
R=0.74 for the linear correlation (Representation of 2 independent experiments and n=6 in each experiment).

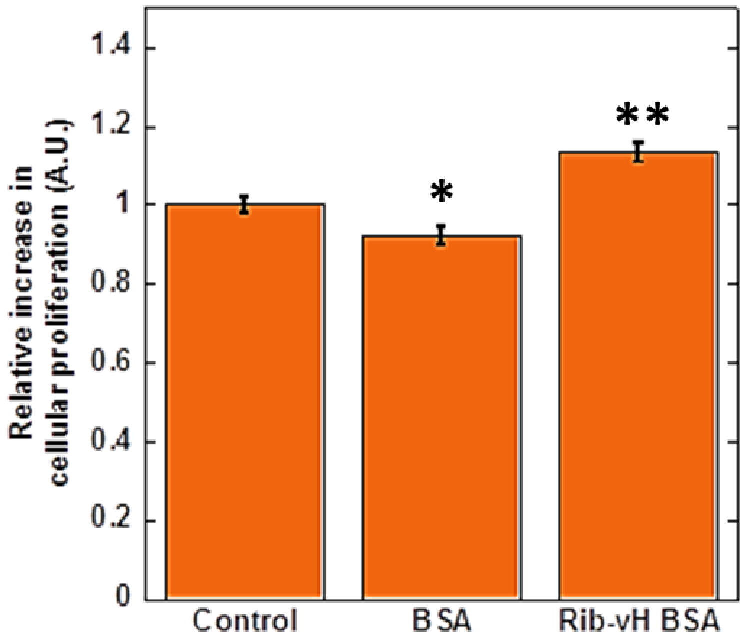

Figure 3.23. Rib-vH BSA induced AGE compound induced cellular proliferation.
(Representation of 2 independent experiments and n=6 in each experiment, *P<0.001; **P<0.005).

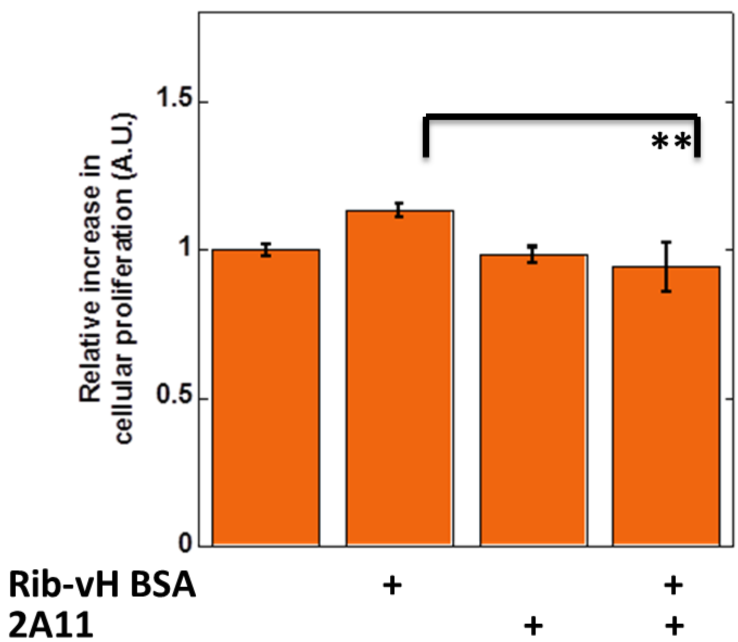

Figure 3.24. Rib-vH BSA induced cellular proliferation was prevented by using anti-RAGE 2A11 antibody.
(Representation of 2 independent experiments and n=6 in each experiment, **P<0.005).

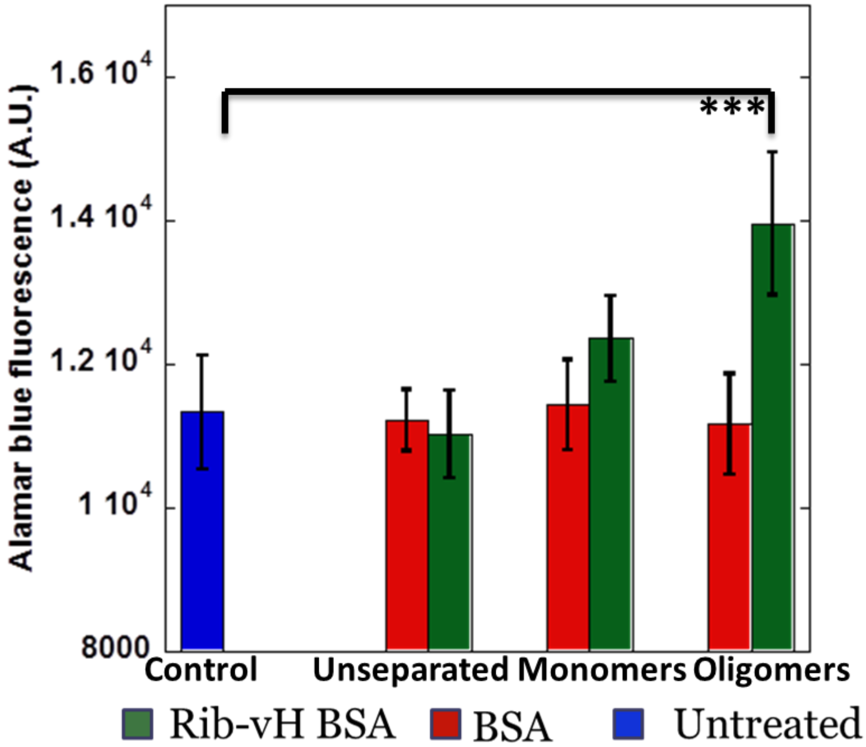

Figure 3.25. MIA PaCa-2cellular proliferation by Rib-vH BSA oligomers. (Representation of 2 independent experiments and n=6 in each experiment, ***P<0.0005).

Similar to the PANC-1 cells, increase in clonal formation was also observed in the MIA Paca-2 cells. No increase was observed in the size of the colonies between the treated and non-treated samples (Figure 3.26).

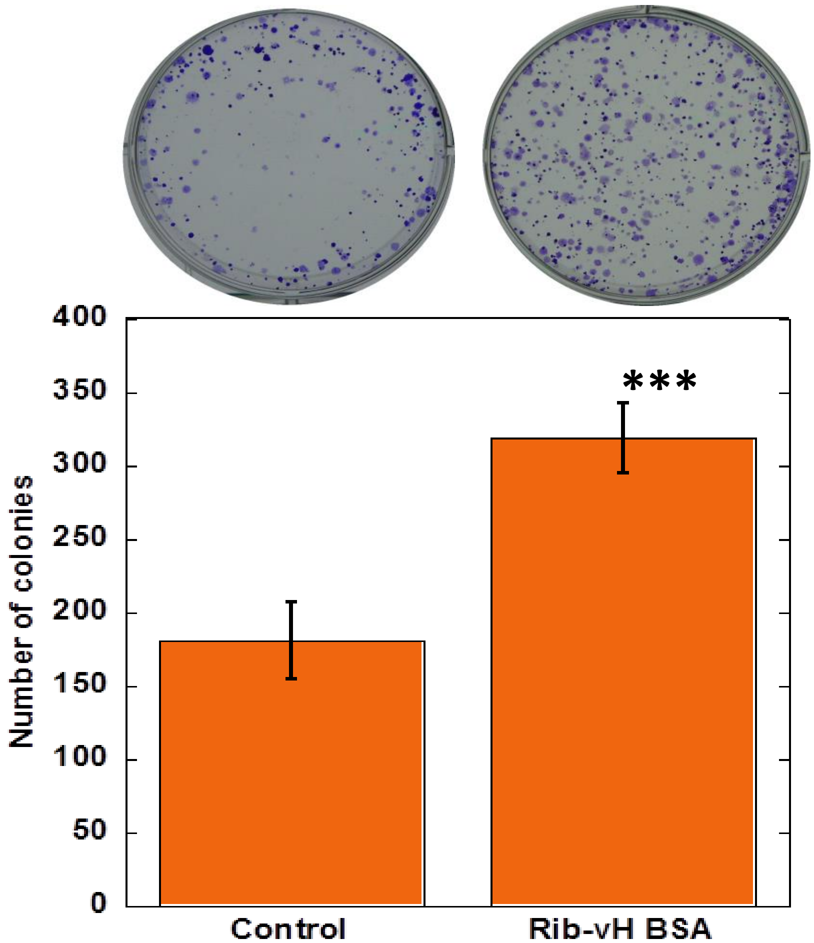

Figure 3.26. Rib-vH BSA induced colony formation in MIA PaCa-2 cells. (Representation of 2 independent experiments and n=6 in each experiment, ***P<0.0005).

Taken together these results suggest the role of AGE compounds in pancreatic cancer cell proliferation. More specifically, the importance of the AGE compound oligomers in the cell proliferation has been shown. Our results also emphasize the role of RAGE inhibition in the prevention of the AGE mediated cellular effects.

Rib-vH BSA induced cell migration

Cancer cell migration is hallmark of cancer progression. More specifically; it is the initial stage of cancer metastasis. Pancreatic cancer patients are characterized by very high metastatic rates and the mean survival rate of the patients with metastatic pancreatic tumor is about 3 to 6 months [293]. Certain AGE compounds have been demonstrated to induce cell migration and invasion. For example, MG BSA AGE compounds have been described to increase cell proliferation, migration and invasion in breast cancer cell line MDA-MB-231 [246], glyceraldehyde derived AGE compounds have been reported to interact with RAGE to induce migration in human oral cancer cells [248]. AGE induced cell migration has not been described in pancreatic cancer. We used Rib-vH BSA to determine the AGE induced cell migration in the pancreatic cancer cells. The Boyden chamber assay was used to determine Rib-vH BSA induced cell migration. The most significant effect was observed in the PANC-1 cells. On Rib-vH BSA treatment for 24 hours 42.3±2.8% of the cells migrated through the chamber and only 22.9±0.58% of cells migrated in the untreated control (Figure 3.27).

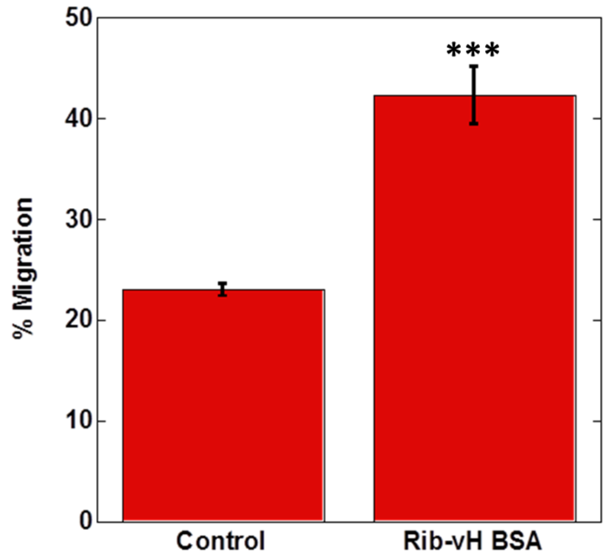

Figure 3.27. Rib-vH BSA induced PANC-1 cell migration.
(Representation of 2 independent experiments and n=6 in each experiment, ***P<0.0005).

Increase in migration was also observed in the MIA PaCa-2 and BxPC-3 cells on Rib-vH BSA treatment. In the MIA PaCa-2 cells 20.11±0.99% of cells migrated on Rib-vH BSA treatment whereas only 11.7±0.5% (Figure 3.28) of cells migrated in the control samples and 26.0±2.0% of the BxPC-3 cells migrated on Rib-vH BSA treatment when compared to the

16.0±2.4% (Figure 3.29) migrated cells in the untreated sample. These results demonstrate the role of Rib-vH BSA in increased cellular migration in pancreatic cancer cells.

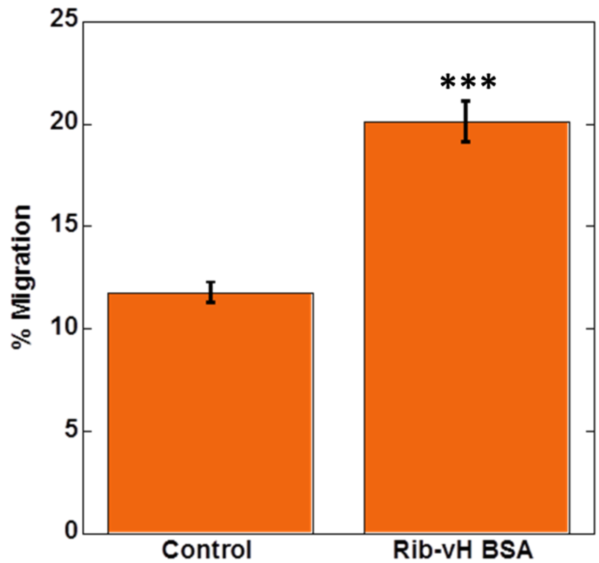

Figure 3.28. Rib-vH BSA induced MIA PaCa-2 cell migration.
(Representation of 2 independent experiments and n=6 in each experiment, ***P<0.0005).

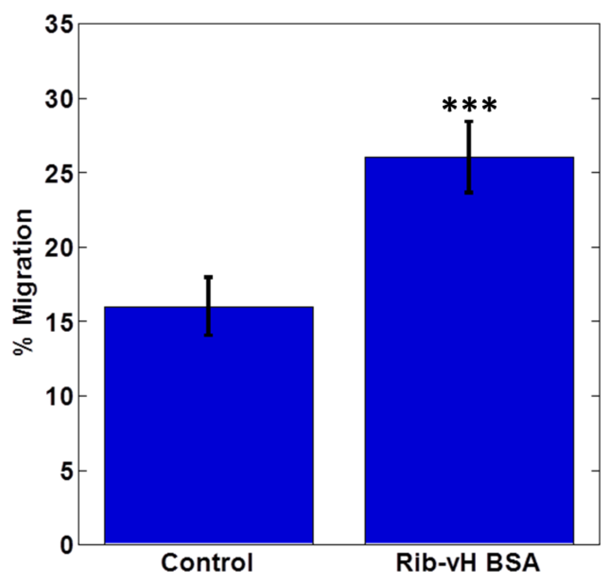

Figure 3.29. Rib-vH BSA induced BxPC-3 cell migration.
(Representation of 2 independent experiments and n=6 in each experiment, ***P<0.0005).

Rib-vH BSA induced kinase signaling

To obtain better insights into the AGE signaling pathways responsible of the AGE mediated cellular effects in pancreatic cancer, the role of Rib-vH BSA in the activation of kinase signaling was determined in the PANC-1 cells. Rib-vH BSA induced phosphorylation of ERK1/2, p38, p53, AKT and SAPK/JNK was elucidated.

ERK1/2 phosphorylation has been described to sustain pancreatic cancer progression [294] and chemoresistance [295]. The role of RAGE induced phosphorylation has been of ERK1/2 has been elucidated in cancers such as breast cancer [296]. The role of RAGE induced ERK1/2 phosphorylation is not described in pancreatic cancer. On Rib-vH BSA treatment no increase was observed in the ERK1/2 phosphorylation (Figure 3.30). This suggests that Rib-vH BSA does not trigger ERK signaling pathways. We then evaluated the phosphorylation of AKT, p53, p38 and JNK which have all been reported to enhance pancreatic tumor cell survival and disease progression [297-300]. No increase was also observed in the phosphorylation of AKT, p38 and JNK (Figure 3.30). Total p53 could not be detected under our conditions. Hence, the role of Rib-vH BSA triggered kinase signaling could not be evaluated and requires further evaluation.

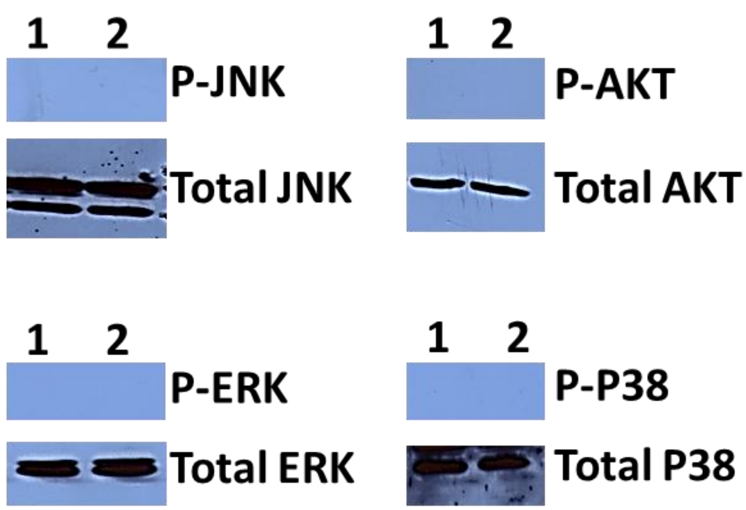

Figure 3.30. Western blots of the kinases.
1: Control, 2: Rib-vH BSA treated after 24 hours.

Role of extracellular matrix glycation in pancreatic cell adhesion

The extracellular matrix plays a very important role in carcinogenesis. Cancer progression is affected by abnormal ECM as it promotes cellular migration and metastasis.

Abnormal ECM facilitates angiogenesis and inflammation by deregulating the stromal cell behavior, which leads to the generation of a tumorigenic microenvironment [301]. Glycation of ECM leads to significant anomalies in the ECM structure[302]. Glycation induced cross-linking of ECM proteins such as collagen they stiffen the ECM[98]. The ECM proteins are characterized by very long half-life [303, 304], hence are susceptible to very significant levels of glycation. Glycation of collagen has been hypothesized to play an important role in various diabetic related vascular diseases [305-309]. Glycation of collagen was reported to reduce cancer cell adhesion in lung carcinoma cells[310]. However, the role of ECM glycation has not been well understood in cancer. ECM glycation has not been described in pancreatic cancer. Collagen was glycated with five different glycation reagents to determine the effect of ECM glycation on cell adhesion in pancreatic cancer cells. On glycation, a decrease in the cell adhesion was observed in the PANC-1 and BxPC-3 cells (Figure 3.31 and 3.32). We observe an approximately 33% decrease in cellular adhesion. These results are in agreement with literature reports in the lung carcinoma cells where a decrease was observed in the cellular adhesion [310]. However, no change in the adhesion properties were observed with the MIA PaCa-2 cells on glycated collagen (Figure 3.33), a decrease in the adhesion was observed in the non-glycated collagen when compared to the non-coated controls. This suggests that the MIA PaCa-2 cells do not adhere properly in the presence of collagen as strongly as other pancreatic cancer cells.

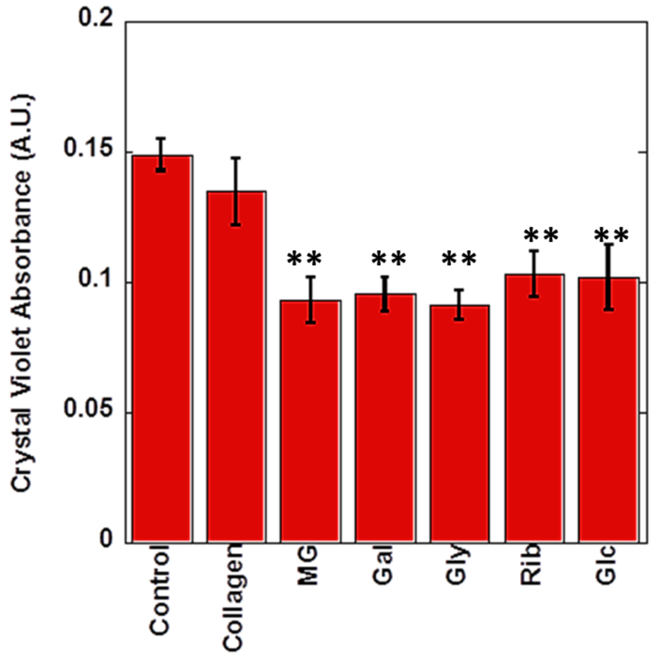

Figure 3.31. Effect of collagen glycation on PANC-1 cell adhesion.
(Representation of 2 independent experiments and n=6 in each experiment, **P<0.005).

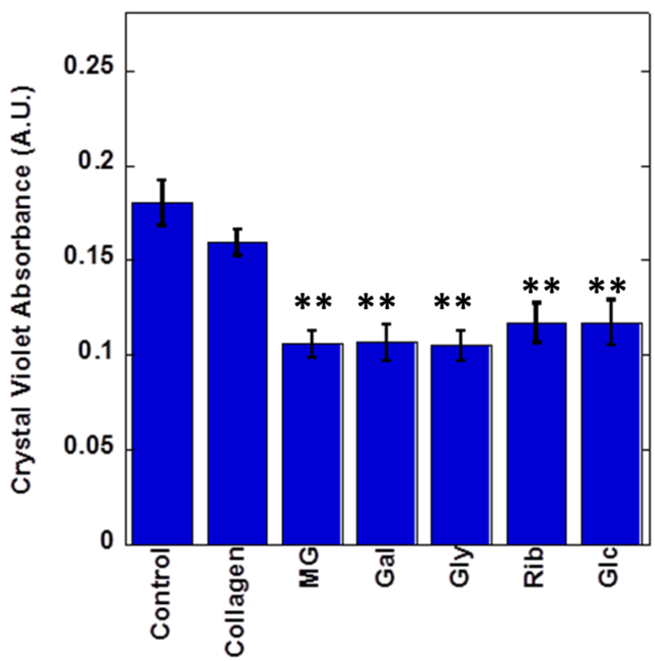

Figure 3.32. Effect of collagen glycation on BxPC-3 cell adhesion.
(Representation of 2 independent experiments and n=6 in each experiment, **P<0.005).

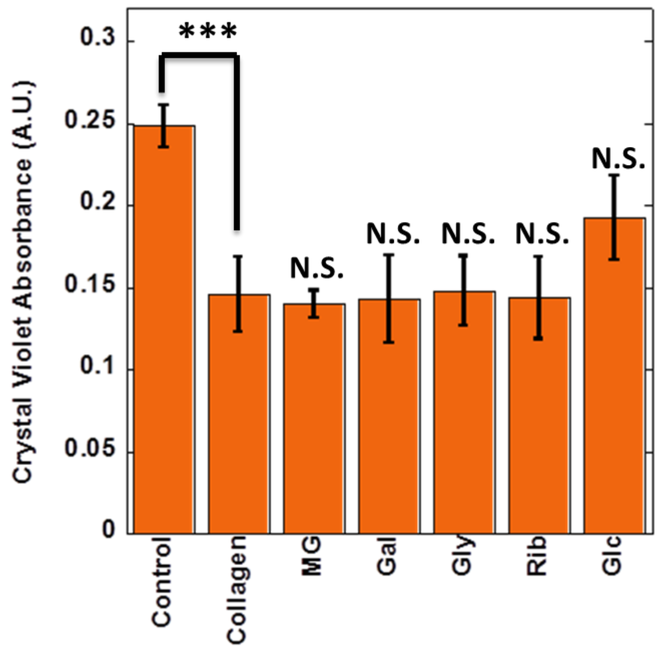

Figure 3.33. Effect of collagen glycation on MIA PaCa-2 cell adhesion.
(Representation of 2 independent experiments and n=6 in each experiment, ***P<0.0005, N.S.: Non Significant when compared to non-treated collagen).

Conclusions

The goal of this study was to understand the AGE compounds and the role of AGE-RAGE interaction in pancreatic cancer cell proliferation and migration leading to tumor growth and progression. It is not clear if the AGE compounds play a role in pancreatic cancer tumor growth. AGE compound research is highly complex due to the heterogeneous nature of the AGE compounds as described in chapter 2 the reason for the toxicity of AGE compounds is still unclear. Ribose modified BSA was used as the model AGE compound to study the AGE induced cellular effects in pancreatic cancer cell lines. Two pancreatic cancer cell lines with high RAGE expression; PANC-1 and MIA PaCa-2 were selected to understand the role of AGE compounds. Interestingly, we observe different cellular effects and diverse AGE induced cellular signaling in these two cell lines (summarized in Figures 3.34 and 3.35).

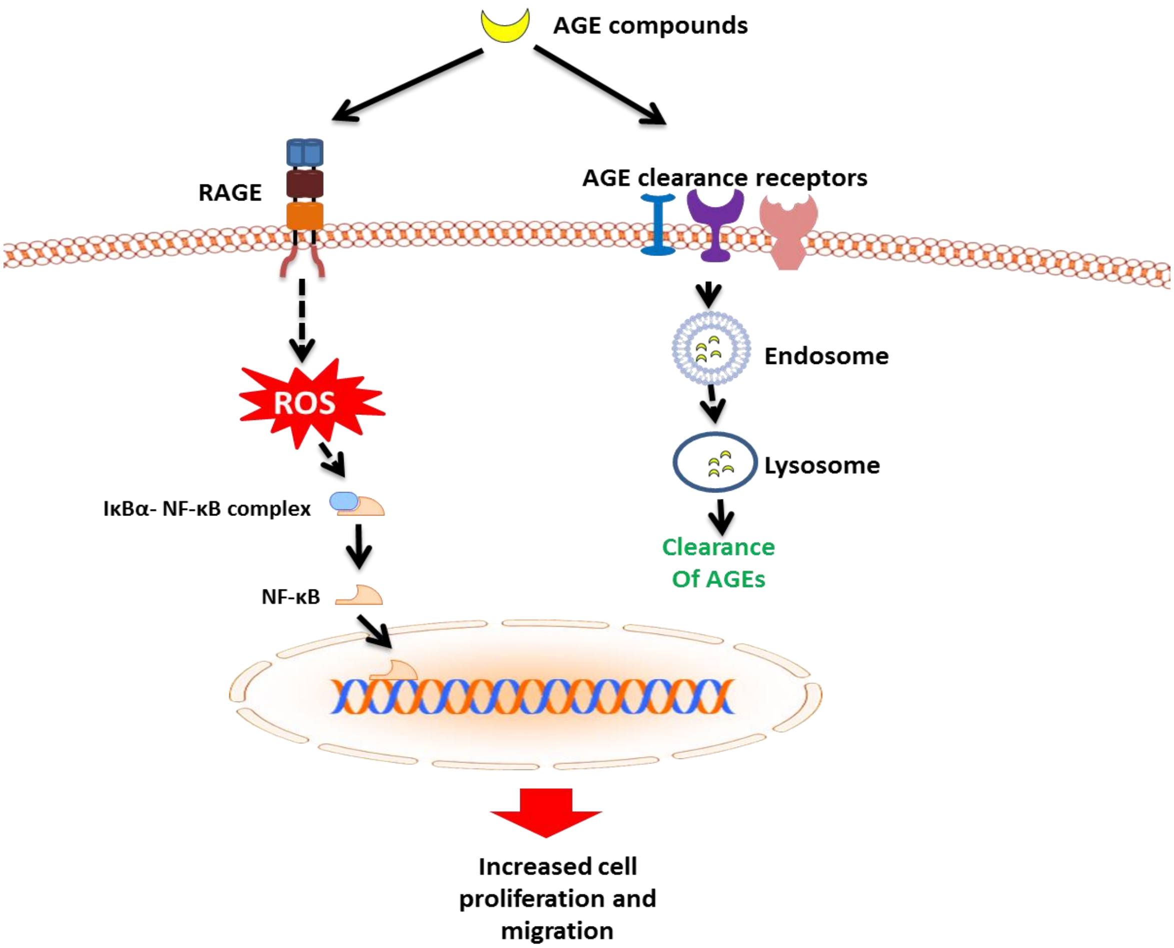

Figure 3.34. AGE-RAGE signaling in PANC-1 cells.
AGE-RAGE interaction triggers ROS formation which can in-turn trigger NF-κB activation. NF-κB is translocated into the nucleus where it binds to specific DNA sequence to trigger various cellular events such as cell proliferation and migration. AGE compounds are cleared by the AGE clearance receptors such as the scavenging receptors. AGE compounds are internalized and degraded by the endosomes and lysosomes respectively.

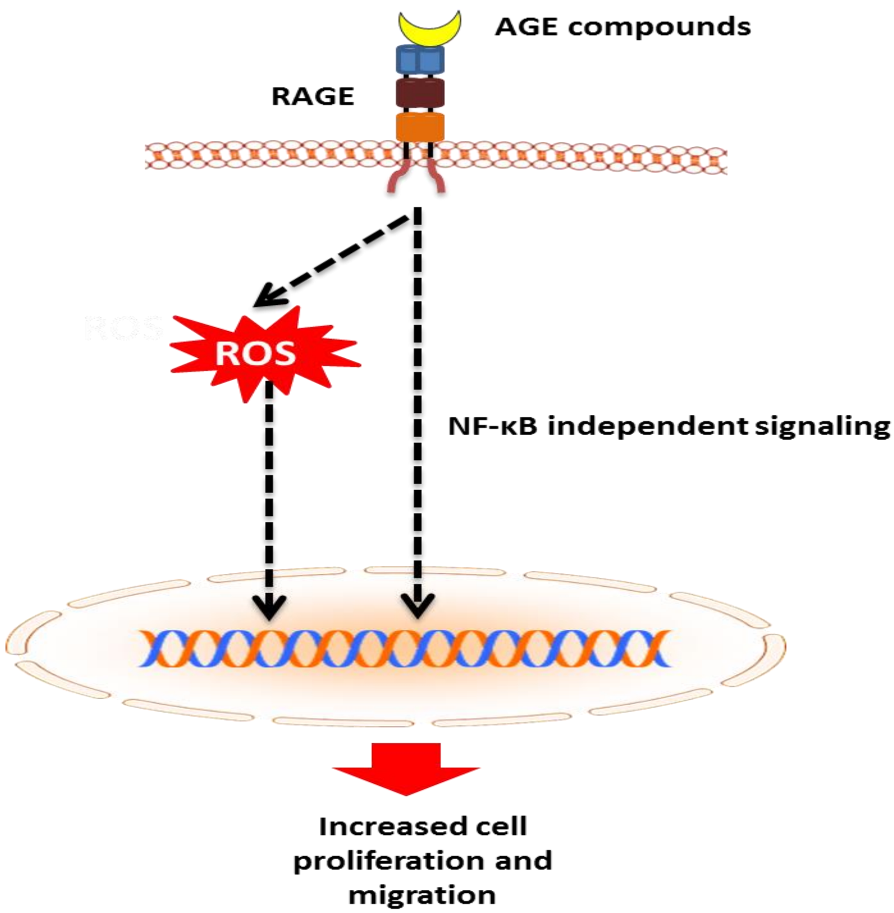

Figure 3.35. AGE-RAGE signaling in MIA PaCa-2 cells.
AGE-RAGE interaction triggers ROS formation. No activation of NF-κB was observed on AGE treatment. Increased cell proliferation and migration was observed via NF-κB independent signaling. No AGE compound internalization was observed in these cells.

Rapid Rib-vH BSA uptake was observed in PANC-1 cells and no uptake was observed in the MIA PaCa-2. Rib-vH BSA uptake lead to the increase in oxidative stress and super oxide production in PANC-1 cells which was RAGE dependent. RAGE dependent Rib-vH BSA induced oxidative stress and super oxide production was also observed in the MIA PaCa-2 cells. The ROS triggered NFκB activity in PANC-1 cells which was also inhibited by RAGE inhibitors. On the contrary, no increase in NFκB activity was observed in the MIA PaCa-2 cells on treatment.

The entire panel of AGE compounds (described in chapter 2) was used to describe the mitogenic role of AGE compounds. Both in the PANC-1 and the MIA PaCa-2 cells we observe a correlation in the mitogenic effect of the AGE compounds and to their oligomeric content with the Rib-vH BSA having the most significant effect. Higher mitogenic effect of the Rib-vH BSA was observed in the PANC-1 cells when compared to the MIA PaCa-2 cells. Rib-vH BSA triggered cellular proliferation was identified to be RAGE dependent in both cell lines. To obtain a better understanding of the role of glycation induced oligomers in pancreatic cell proliferation, the isolated Rib-vH BSA oligomers were used to treat the PANC-1 and MIA PaCa-2 cells. An increase in cell proliferation was observed in both the cell lines when the cells were treated with the oligomers. This emphasizes the importance of glycation induced protein cross linking of the Rib-vH BSA for its mitogenic effects in pancreatic cancer cells. Rib-vH BSA treatment also induced increased colony formation in both the cell lines. The effect of Rib-vH BSA on cellular migration was also determined. On Rib-vH BSA treatment the migratory ability of PANC-1 and MIA PaCa-2 cells also increased. This indicates that the Rib-vH BSA not only influences cellular proliferation but also migration which could initiate metastasis. However, the signaling mechanisms involved in the Rib-vH BSA induced cellular effects could not be elucidated and require further studies. Our results suggest that Rib-vH BSA triggers diverse signaling pathways in the PANC-1 and MIA PaCa-2 cells even though they are RAGE dependent. We suspect other kinases such as p65 and JAK which has been reported to play a role in the RAGE induced autophagy [311] might play a role in the Rib-vH BSA triggered signaling. In the MIA PaCa-2 cells we suspect other transcription factors such as STAT-3 could play an important role. RAGE induced STAT-3 activation has been described in the Pan2.03 cells [235, 311].

The proliferative and migratory effect of Rib-vH BSA was also determined in the low RAGE expressing BxPC-3 cells. We observe that the AGE compounds induced cellular proliferation and the increase in cell proliferation could be correlated to their oligomeric content. The Rib-vH BSA induced cell proliferation was RAGE dependent as observed in the PANC-1 and MIA PaCa-2 cells. The isolated Rib-vH BSA oligomers also had a proliferative effect on the BxPC-3 cells. Rib-vH BSA also induced BxPC-3 migration as described in the other two cell lines.

Taken together our results suggest a novel role of AGE compounds in the pancreatic cancer cell proliferation and migration. Our results also emphasize the importance of glycation induced protein cross-linking in the toxicity of the AGE compounds. The role of RAGE in the AGE mediated effects can also be highlighted. Building on these results in future the intra cellular signaling of Rib-vH BSA can be evaluated. The receptors involved in AGE uptake also have to be determined.

The effect of extracellular matrix (ECM) glycation on cell adhesion was also determined. We observe decreased cell adhesion in the PANC-1 and the BxPC-3 cells. No change the cellular adhesion as observed in the MIA PaCa-2 cells on the glycated ECM. These results form the basis for future evaluations into the mechanisms of ECM glycation in pancreatic cancer as the ECM glycation has not been described and studied in pancreatic cancer.

CHAPTER 4: THE ROLE OF RIBOSE DERIVED ADVANCED GLYCATION END PRODUCTS (AGES) IN MACROPHAGE ACTIVATION AND PRO-INFLAMMATORY CYTOKINE RELEASE

Introduction

Advanced glycation end products (AGEs) and diabetes

Diabetes mellitus is characterized by long standing hyper glycemic conditions which promote the formation of AGEs by non-enzymatic glycation. AGE compound formation and deposition has been described in several microvascular and macrovascular complications of diabetes [312]. The cellular interaction of AGEs is believed to induce several biological responses, which are responsible for the development of diabetic vascular complications [313]. The AGE compounds interact with cell surface receptors such as RAGE [127], "AGE-receptor complex" and consists of three proteins AGE-R1 (OST-48), AGE-R2 (80-K-H) and AGE-R3. AGE-R3 is also known as galectin-3 (LGALS3) and is responsible for AGE binding [130], type I (SR-AI) and type II (SCARA2) macrophage scavenger receptors [122], CD-36 [123], FEEL-1 and FEEL -2 [124], scavenger receptor proteins SR-BI and SR-BII [125] and the lectin-like oxidized low-density lipoprotein receptor 1 (Lox-1) [126] and mediate their cellular effects. *In-Vitro* studies provide evidence that on AGE stimulation the renal tubular cells secrete MCP-1 or express ICAM-1[314, 315] which can in-turn trigger the recruitment of macrophages. The interaction of AGE compounds and scavenger receptors expressed on macrophages (RAW 264.7 cells) has been reported to induce the production of several cytokines such as plasmogen activator [316]. The AGE compounds can also trigger pro-inflammatory cytokine release, the methyl glyoxal modified human serum albumin has been reported to upregulate TNF-α and IL-1β mRNA levels [317]. AGE compounds such as heavily modified glycolaldehyde-derived AGE-LDL induced macrophage foam cell formation contributing to the pathogenesis of atherosclerosis [318]. Taken together, all these reports indicate a definitive role of AGE compounds in macrophage activation and cytokine release. However, there are gaps in our understanding of the role of AGE compounds mediated cellular effects in macrophages. The uptake and intra-cellular internalization of AGE compounds is not fully understood. This study was initiated to fill these gaps in our understanding of AGE mediated macrophage uptake. Previously, we have characterized a panel of AGE compounds using chemically different glycation reagents [220, 318, 319]. The Ribose modified BSA (Rib-vH BSA) had the most significant cellular effect hence, we select Rib-vH BSA as the model AGE compound and its uptake, effect on the mRNA levels of inflammatory mediators was determined in a murine macrophage cell line; RAW 264.7. This cell line was selected as the role of AGE uptake and some of its cellular consequences have been studied previously in this cell line [313, 316, 320-323] and moreover, this cell line also closely mimics human bone marrow-derived macrophages in terms of cell surface receptors and response to microbial ligands [324]. The role of Rib-vH BSA to increase macrophage proliferation was also determined.

Inflammation and diabetic complications

Diabetes mellitus is a chronic disease characterized by long standing hyperglycemic conditions. The effect of diabetes on human vascular tree is the major source of morbidity and mortality in both type I and type II diabetes [325] and diabetes has grown into pandemic proportions worldwide. The diabetic vascular complications can be divided into microvascular complications such as diabetic retinopathy, nephropathy and macrovascular complications such as peripheral arterial disease, coronary arterial disease and cardiomyopathy. In recent years, our knowledge regarding the pathophysiology of diabetic vascular complications has improved considerably at the molecular level. These studies provided clear evidence that the traditional factors such as metabolic and hemodynamic altercations are only a partial aspect of a more complex picture [326]. More importantly, the importance of immune system mediated inflammatory processes in the pathophysiology of diabetic complications has come into light. [327,328]

Accumulating evidence suggests that inflammatory signals play a very important role in the progression and development of many of the diabetic complications such as diabetic nephropathy which was traditionally considered to be a non-immune disease [329,330]. The role of proinflammatory cytokines, chemokines and other inflammatory molecules contributing to persistent low grade inflammation, leading to retinal vascular damage and neovascularization, has been supported by a large body of literature [87, 331-333]. Highly complex and diverse immune signaling are involved in the pathogenesis of diabetic complications. The role of several pro-inflammatory molecules such as chemokines (monocyte chemoattractant protein-1), [334, 335]enzymes like cyclooxygenase-2 and nitric oxide synthase [336-339], adhesion molecules (intercellular adhesion molecule-1 (ICAM-1) [315, 340], nuclear factors like NfkB [341, 342], growth factors such as vascular endothelial growth factor, insulin like growth factor (IGF) and tumor growth factor beta (TGF-β) [343-346] has been implicated in diabetic complications. The role of inflammatory cytokines in diabetic complications has considerable attention in the recent past. Pro-inflammatory cytokines such as IL-1, IL-6, IL-18, TNF-α have been implicated in the pathogenesis of diabetic complications. These cytokines can also active a wide range of immune cells including macrophages, leukocytes and monocytes [347-349].

Macrophages and diabetic complications

Macrophage literally means “big eaters” and is a leukocyte that identifies and engulfs several pathogenic particles, cell debris and also cancer cells by phagocytosis and plays a very important role in antigen presentation, in innate and adaptive immune responses. All tissues contain resident macrophages. Depending on stimulation with external stimuli the macrophages are activated into distinct cells [350, 351]. Inflammatory stimuli such as lipopolysaccharide (LPS), IFN-γ and TNF-α lead to classical activation which generates M1 macrophages with high antigen-presenting capacity which leads to the production of pro-inflammatory cytokines such as IL-1β, TNF-α, IL-6 and subsequent induction of Th1 response. On the other hand, cytokines such as IL-4 and IL-13 which are Th2 cytokines and lead to alternative activation of macrophages to M2 macrophages. The M2 macrophages play a role in tissue remodeling and immunoregulation. There are three main groups of M2 macrophages: M2a activated by IL-4 and IL-13, M2b induced by immune complexes or TLRs, and M2c activated by IL-10 [352]. Furthermore, the macrophages express general markers, such as F4/80, CD68, CD11b, and Ly6c, in a heterogeneous fashion, dependent on tissue of origin, maturation, and activation degree [353-355].

Several recent findings report a substantial increase in tissue macrophages as a common feature in diabetic complications including nephropathy, atherosclerosis, neuropathy and retinopathy [356-359]. Recent findings have helped to provide an understanding of the potential importance of macrophages in promoting these complications [360]. Macrophage accumulation has been described in human and experimental Type 2 diabetic nephropathy and its role has been reported to promote renal injury[349, 357]. Studies performed in genetically modified *db/db* mice, have demonstrated that macrophage-mediated injury plays a central role in the development of Type 2 diabetic nephropathy[314, 315].

In peripheral neuropathy, macrophage accumulation has been reported in perivascular lesions and their presence has been associated with nerve demyelination, suggesting that they may be involved in the nerve damage[359, 361, 362]. The presence of macrophages has been reported in the epiretinal membrane[356] and macrophage-derived cytokines are frequently detected in vitreous samples,[358, 363] among patients suffering from proliferative retinopathy which is another microvascular complication of Type 2 diabetes and it has been suggested that macrophages play a role in cell apoptosis, neovascularization and fibrosis. Macrophage accumulation has also been described in atherosclerotic lesions among patients suffering from acute myocardial infraction [42]. Animal studies have also demonstrated that macrophage depletion provides resistance to atherosclerosis [364, 365] emphasizing the role of macrophages in pathogenesis of atherosclerosis. It has also been reported that the development of Type 2 diabetes induces macrophage recruitment by upregulating the tissue expression of molecules including several macrophage-attracting chemokines, such as monocyte chemoattractant protein-1 (MCP-1), osteopontin, macrophage migration inhibitory factor (MIF) and macrophage colony stimulating factor and intercellular adhesion molecule-1 (ICAM-1)[315, 349, 366]. The infiltrated macrophages have been suggested to contribute to diabetic tissue injury through the production of reactive oxygen species (ROS) and metalloproteinases[367, 368].

We hypothesized that the AGE-RAGE interaction triggers cellular signaling leading to macrophage activation and pro-inflammatory cytokine release.

Materials and Methods

Reagents were of molecular biology or ACS purity grade and purchased through Fischer Scientific or VWR. Bovine serum albumin (BSA), fraction V, was purchased from Amresco. Antibodies and SiRNA were purchased from R&D Systems and SantaCruz Biotechnology. Molecular biology reagents and enzymes were purchased from New England Biolabs, Life Technologies, OriGene and Fermentas. Chromatography media for protein purification were purchased from GE Healthcare. Reagents and media for cell culture were from ATCC. The RAW blue cells were purchased from Invivogen.

AGE compound preparation

Described in chapter 2.

Cell culture conditions

RAW 264.7 cell line, a mouse macrophage cell line was purchased from ATCC and were cultured in DMEM media (ATCC) with 10% FBS (ATCC) as described by ATCC. RAW blue cells were purchased from Invivogen (San Diego, CA). The RAW blue cells were cultured in the presence of Zeocin (200ug/mL) and Normocin (100ug/mL) as described by the manufacturer. The cells were maintained in a sterile incubator at 37 °C with 5% CO_2.

RNA extraction and cDNA synthesis

The whole cell RNA was extracted from the RAW 264.7 cells using the Ambion's Protein and RNA Isolation System, PARIS™ (Life Technologies). Briefly, 50000 cells were seeded in each well of a 6 well plate. The cells were allowed to adhere and reach a confluency of 60% by incubating at 37 °C for 24 hours. After the cells reached the required confluency, the cells were stimulated with 1 mg/mL of Rib-vH BSA. The cells were then incubated at 37 °C. Cells were harvested at 30 min, 3 hrs, 6 hrs, 12 hrs and 24 hrs after stimulation and the RNA was extracted. The concentration of the RNA was measured by UV absorbance at 260 nm and the ratio of the absorbance at 260 nm/280 nm was calculated to estimate the purity of RNA. The RNA was immediately reverse transcribed using the Moloney Murine Leukemia Virus (M-MuLV) Reverse Transcriptase (NEB labs) using an oligo dT primer.

Quantitative real time PCR (q RT-PCR)

AGE induced upregulation of several pro-inflammatory genes were analyzed by real time PCR using Eva green (Solis BioDyne). We differentiated genes based on their function as oxidative stress genes, genes responsible for inflammation and we also determined the AGE mediated upregulation of AGE-receptors at the RNA level. In order to determine the accurate housekeeping gene we carried out a house keeping gene analysis using the Normfinder, Bestkeeper and GeNorm algorithms on a set of 14 housekeeping genes (Table 4.1). Normfinder program calculates the geometric mean of all the reference genes and takes into account systematic differences between sample subgroups to find the most appropriate housekeeping gene [369]. Bestkeeper program uses pair wise correlations to determine the most appropriate housekeeping gene [370]. Genorm calculates a gene expression normalization factor for each sample based on the geometric mean of the reference genes [371]. Rib-vH BSA induced changes in the house keeping gene expression was measured at 30 min, 3 hrs, 6 hrs, 12 hrs and 24 hrs. Based on the Ct values of the house keeping genes in the different treatment groups, RPL4 was determined to be the most stable housekeeping gene by all the three programs. No improvement was observed in theRPL4 gene stability in the presence of a second housekeeping gene. Hence we decided to use RPL4 alone as the house keeping gene. The fold change with respect to untreated control was calculated using the following equations

$$\Delta ct = \text{ct value of gene-ct value of housekeeping gene} \quad (4.1)$$

$$\Delta\Delta ct = \Delta ct \text{ value of the gene before treatment- } \Delta ct \text{ value of gene after treatment} \quad (4.2)$$

$$\text{Fold Increase} = 2^{\Delta\Delta ct} \quad (4.3)$$

Table 4.1. Housekeeping genes used in the study to determine the most stable housing keeping gene.

Gene (Gene ID)	**Function**	**Primers (5'→3')**
GAPDH (NM_008085)	Glyceraldehyde Dehydrogenase	Forward: CAAGGCTGTAGGCAAAGTCA Reverse: GAGACCACCTGGTCCTCTGT
PPIB (NM_011149)	Peptidyl-prolyl cis-trans isomerase B	Forward: TCGTCTTTGGACTCTTTGGA Reverse: TCTTTCCTCCTGTGCCATCT
TBP (NM_013684)	TATA box binding protein	Forward: CAGTGCCCAGCATCACTATT Reverse: AGCATAAGGTGGAAGGCTGT
ACTBG (NM_009609)	Actin beta and gamma	Forward: CATTGCTGACAGGATGCAGAAGG Reverse: TGCTGGAAGGTGGACAGTGAGG
ACTB (NM_007393)	Actin beta	Forward: AGTGTGACGTTGACATCCGT Reverse: TGCTAGGAGCCAGAGCAGTA
Casc3 (NM_138660)	Cancer susceptibility candidate 3	Forward: AGGAGATGCTGTTCTTTCCG Reverse: GCAGCATCGTTAGCTTCTGA
YWHAZ (NM_011740)	Tyrosine 3-monooxygenase/tryptophan 5-monooxygenase activation protein	Forward: GTCTGTCACCGTCTCCCTTT Reverse: GTAGGGTGTGAGCTTTGGGT
HMBS (NM_013551)	Hydroxymethylbilane synthase	Forward: ATCTTGGACCTAGTGAGTGTGT Reverse: GTACAGTTGCCCATCTTTCATCA
RPL37A (NM_009084)	Ribosomal protein L37A	Forward: GCTAAACGCACCAAGAAGGTC Reverse: GCCACTGTTTTCATGCAGGAA
EIF2B2 (NM_145445)	Eukaryotic translation initiation factor 2B, subunit 2 beta	Forward: TAGGACAGTTGAGGCCTTCC Reverse: GTGCCAATGATCACCTTGTT
RPL4 (NM_024212)	Ribosomal protein L4	Forward: CGCAACATCCCTGGTATTACT Reverse: AAAGCACTCTCCGTCCAGAT
SDHA (NM_023281)	Succinate dehydrogenase complex, subunit A	Forward: CTACAAGGGACAGGTGCTGA Reverse: GAGAGAATTTGCTCCAAGCC
HPRT1 (NM_013556)	Hypoxanthine phosphoribosyltransferase 1	Forward: AGGACCTCTCGAAGTGTTGG Reverse: CGTGATTCAAATCCCTGAAG
RPL13A (NM_009438)	Ribosomal protein L13A	Forward: AGCAGATCTTGAGGTTACGGA Reverse: TTATTGGGTTCACACCAGGA

Fluorescent labelling of Rib-vH BSA

The cysteine residues of the Rib-vH BSA were fluorescently labelled by a malemide derivative of a near infra-red cyanine dye called cyanine5.5 (Cy5.5® malemide, Lumiprobe). It has an excitation wavelength of 675 nm and an emission maximum at 695 nm. Cy5.5 ® malemide was dissolved in methanol aliquoted and dried by vacuum centrifugation and stored at -80 °C. Rib-vH BSA was diluted in PBS to a final concentration of 10 mg/mL and was then mixed with 2 molar excess of Cy5.5 and incubated for 30 min at RT by stirring. The free dye was removed by dialyzing the protein against 500 volumes of PBS. The presence of free dye was visualized by running the labelled protein on a SDS-PAGE gel and then visualizing the bands on infra-red fluorescence (NIRF) imaging using a Kodak FX Pro Imager (Carestream Health Incorporation, Rochester, NY) . Absorbance was measured at 280 nm and 675 nm and the moles of dye bound to the mole of protein was determined to be 0.3.

Rib-vH BSA uptake assay

The kinetics of Rib-vH BSA uptake was determined by measuring the fluorescence of Cy5.5 of the Rib-vH BSA_Cy5.5 at different time points. Briefly, 50,000 cells per well were seeded in a cell culture 24 well plate and incubated at 37 °C overnight for the cells to adhere. 50 µg/mL (25 µg per well) of the labelled Rib-vH BSA was added to each well and incubated at 37 °C. The media was aspirated and the cells were washed twice with PBS. The cells were lysed using TBS with 0.1% triton X-100 at different time points. For 0 hrs time point the cells were lysed immediately as soon as the compound was added. Fluorescence of the cell lysate was measured in a 40 µL quartz cuvette with an excitation of 675 nm and an emission of 691 nm with a slit setting of 5 nm on the Horiba Jobin Yvon Spectramax-4 fluorimeter. The exact protein content taken up was determined by a calibration curve of the labelled Rib-vH BSA.

Internalization of Rib-vH BSA by live cell confocal imaging

Rib-vH BSA tagged with Cy5.5 was used to determine the uptake in RAW 264.7 cells. The lysosomes of the RAW 264.7 cells were labelled using the CellLight® Lysosomes-GFP, BacMam 2.0 (Life Technologies). This system uses Bacmam 2.0 technology to transfect a construct expressing GFP fused to lamp1 (lysosomal associated membrane protein 1). 50,000 cells were seeded in an Ibidi µ-dish designed for live cell imaging and the cells were allowed to adhere overnight. 25µL of the CellLight® Lysosomes-GFP construct was added to the dish and incubated at 37 °C for 24 hrs. The dish was then placed in the environmental control chamber for time-lapse cell culture related experiments. The temperature of the chamber was set to 37 °C, with 5 % CO_2 and 95% humidity. 20 µL of the Rib-vH BSA_Cy5.5 (Final concentration of 1 mg/mL) was added and the cells were imaged at different time points. The imaging was carried out using the Zeiss AxioObserver Z1, fully motorized inverted scope with LSM700 laser scanning head attachment. Images were taken at different time points using Zeiss Zen Black software and analyzed using the Zeiss AxioVision Rev. 4.8.1.

Estimation of endotoxin content and endotoxin removal

The endotoxin content of the AGE samples was quantified using the Pierce™ *Limulus* Amebocyte Lysate (LAL) Chromogenic Endotoxin Quantitation Kit (Life Technologies) according to manufacturer's protocol. Briefly, 500 ng (50 µL) of AGE protein was pipetted in each well of a 96 well plate and incubated at 37 °C for 5 min. 50 µL of LAL was added and incubated at 37 °C for 10 min. After the incubation 100 µL of the substrate was added into each well and incubated at 37 °C for 6 min. The absorbance was then measured at 405 nm using the SpectraMax M5 plate reader.

Endotoxin was removed using the removed by phase separation using nonionic polyoxyethylene surfactant Triton X-114. Briefly, the Rib-vH BSA was diluted to a concentration of 5 mg/mL using phosphate buffered saline, pH 7.5. 1% v/v of Triton X-114[372] was added and this solution was vigorously stirred for 10 min. The solution was then heated to 55 °C for 15 min and immediately placed on ice for 10 min. The samples were then centrifuged at 10,000 rpm for 5 min. The supernatant was collected and the process was repeated 3 times. After the final purification the endotoxin content was determined as described above.

Estimation of reactive oxygen species (ROS)

AGE induced ROS formation was determined by a cell-permeable non-fluorescent ROS probe 2, 7-dichlorofluorescein diacetate. This compound is de-esterified intracellularly and on oxidation by ROS turns in to 2, 7- dichlorofluorescein which is highly fluorescent. 25,000 cells per well were seeded in a 96 well plate and incubated at 37 °C overnight. The media was aspirated and the cells were washed twice with PBS and were loaded with 5 µM per well of 2, 7-dichlorofluorescein diacetate and incubated at 37 °C for 30 min. The cells were then treated with the AGE compound (1 mg/mL) and incubated at 37 °C. Fluorescence emission was measured at 535 nm with an excitation wavelength of 500 nm using the SpectraMax M5 plate reader.

Estimation of nitric oxide formation

The effect of AGE compounds on nitric oxide production was evaluated by Griess reaction. Griess reaction measures the formation of the nitric oxide by measuring the nitrite ion which is a stable breakdown product of nitric oxide. 25,000 cells per well were seeded in a 96 well plate and were incubated at 37 °C overnight for the cells to adhere. The media was then aspirated and replenished with serum free media. The cells were then treated with 1 mg/mL Rib-vH BSA and incubated at 37 °C for 24 hrs. from each well 50 µL of the cell supernatant was collected and transferred to a fresh 96 well plate, 50 µL of sulfanilamide solution (solution 1) was added in each well and incubated at RT in dark for 10 minutes and finally 50 µl of N-1-napthylethylenediamine dihydrochloride (NED) solution was added and incubated I dark for 10 minutes at RT. The absorbance of the azo compound formed was measured at 570 nm. Serial dilutions of sodium nitrite were made and the nitrite content was determined and a calibration curve was obtained. The exact nitrate content of the cells was measured using this standard curve.

Estimation of NF-κB activity

The Nf-κB activity was determined by a commercially engineered cell line called RAW-blue ™ (Invivogen). RAW blue cells contain secreted embryonic alkaline phosphatase (SEAP) reporter construct inducible by NF-κB and AP-1. 100,000 cells were seeded in each well of 96 well plate as per supplier's protocol and the cells were immediately treated with the required concentration of AGE compounds and then incubated for 24 hrs at 37 °C. After the incubation 50 uL of the cell supernatant was collected and added to 150 µL of the supplied QUANTI-blue ™ media and then incubated at 37 °C for 1 hr. The absorbance was measured at 630nm using the SpectraMax® M5 plate reader.

RNA silencing

Small Interfering RNA (siRNA) were used to knockdown galectin-3, scavenging receptor; SR-A and MyD88 which is an adaptor protein of the toll like receptors (TLRs). The siRNAs were purchased from Santa Cruz Biotechnology (galectin-3: sc-35443, MyD88: sc-35987 and SR-A: sc-40188). The cells were transfected with the siRNA using lipofectamine® 2000 (Life Technologies). Briefly, the cells were seeded and allowed to adhere and reach about 50% confluency. The media was replaced with serum free media and the siRNA-lipofectamine®

2000 complex was added. The cells were then incubated at 37 °C for 24 hrs. After the incubation the cells were washed and the media was then replaced by normal serum containing media. The efficiency of knockdown was estimated by western blotting or by q RT-PCR.

Western Blot analysis

The siRNA knockdown was estimated using the western blotting. Briefly, 25 µg of the total cell protein was loaded on a 12% SDS-PAGE gel and run at 150 V. The bands were transferred on to a nitrocellulose membrane at 250 mA for 1 hr. The blot was then blocked using 5% milk powder in TBS-T. Primary antibody dilutions (1:1000) were made in 2% milk powder in TBS-T. The primary antibodies were purchased from Santa Cruz biotechnology (MyD88: sc-11356, galectin-3: sc-20157, SR-A: sc-20660). The blot was incubated with the primary antibody overnight at 4 °C. The blots were washed with TBS-T for 5 times (2 minutes each) and the HRP conjugated secondary antibody was added (Jackson: 711-035-152, 1:10000 dilution). The blots were incubated for 2 hrs at RT then washed and developed on the X-ray film using the ECL substrate.

Cell proliferation

To determine the mitogenic effect of Rib-vH BSA we measured cell proliferation by a fluorogenic oxidation-reduction indicator “Resazurin”. The non-fluorescent resazurin under goes reduction in the reducing environment of the cells to form resorufin which exhibits absorption/emission maxima at around 575 nm and 585 nm respectively. Briefly, 5000 cells were seeded in a cell culture 96 well plate and allowed to adhere overnight at 37 °C. The media was then replaced with fresh DMEM media with reduced serum of 2%. The cells were then treated with Rib-vH BSA (1mg/ml) for 24 hrs at 37 °C. After the required time period, 10% of the total well volume was added with resazurin (0.1 mg/ml in D.I water and sterile filtered) and the plate was incubated at 37 °C the emission maxima was measured at 585 nm using the SpectraMax M5 plate reader. For RAGE inhibition 25 µg/mL anti-RAGE antibody (2A11) or 1 µM small molecule inhibitor of RAGE (FPS-ZM1) were added with the Rib-vH BSA.

Results and discussion

AGE BSA uptake by the macrophages

Historically, AGE uptake (glucose modified AGEs) has been studied using radioactive isotopes [320, 321]. This method is highly sensitive but radioactive isotopes are hazardous to work and can have long lasting health issues. We develop a fluorescence based assay to study the uptake ribose modified BSA and this method can detect nano-gram quantities of the protein. Rib-vH BSA was labelled with a near infrared dye cyanine dye called Cy5.5 to determine the kinetics of AGE uptake by the macrophages. The cells were lysed and the fluorescence of the lysate was determined at different time points to quantify the AGE compound uptake. The total protein content was determined using the BCA assay and fluorescence was normalized based on the total protein content in the cells. A very rapid increase in the AGE compound fluorescence was observed. This is in agreement with previous reports of glucose modified AGE uptake [320, 321]. Our data indicates an 18 fold increase in the fluorescence emission after 10 min of incubation with AGE BSA. We observe 30 fold, 55 fold, and 81 fold increase in the fluorescence after 1, 3 and 6 hrs of incubation at 37 °C respectively. After 24 hrs we observe a 137 fold increase in the Rib-vH BSA fluorescence. This data demonstrate a rapid and continuous uptake of the Rib-vH BSA by the macrophages.

The amount of AGE compound accumulated in the macrophages was then determined using these fluorescence values. A standard curve was obtained by measuring the fluorescence of known amount of AGE compound under the exact same conditions. The results are presented as the amount of AGE compound internalized in the macrophages adhered in a well of a 24 well plate. After 24 hours of incubation about 25 µg of the AGE compound was internalized (Figure 4.1). Hence, the macrophages internalized the entire AGE compound added in the well over a period of 24 hrs. On the contrary, the uptake of non-glycated BSA has been reported to be very slow and very little amount of non-glycated BSA was taken up by the macrophages [320, 321, 373]. The RAW cells are cultured in the presence of 10% FBS and the FBS contains very high amounts of non-glycated serum albumin. Taken together these results suggest rapid uptake of the glycated serum albumin.

The kinetics of AGE uptake in macrophages is not very well understood, it is not clear whether the macrophages internalize the AGE compounds continuously or not. Glucose modified BSA has been used to study the uptake over a relatively short duration of time [320, 321, 373]. This study provides useful insights of the AGE compound uptake by macrophages. Macrophages are believed to play very important roles in AGE compound uptake and degradation. The role of tissue macrophages in AGE compound degradation has been proposed [374]. As described earlier the AGE compounds are believed to activate the macrophages and trigger the release of pro-inflammatory cytokines. However, it is not clear if the AGE compounds need to be internalized for them to activate the macrophage or if they initiate signaling by their interaction through pattern recognition receptors on the macrophages. To get a better understanding on AGE compound inter cellular compartmentalization we performed live cell imaging and is described later in this chapter.

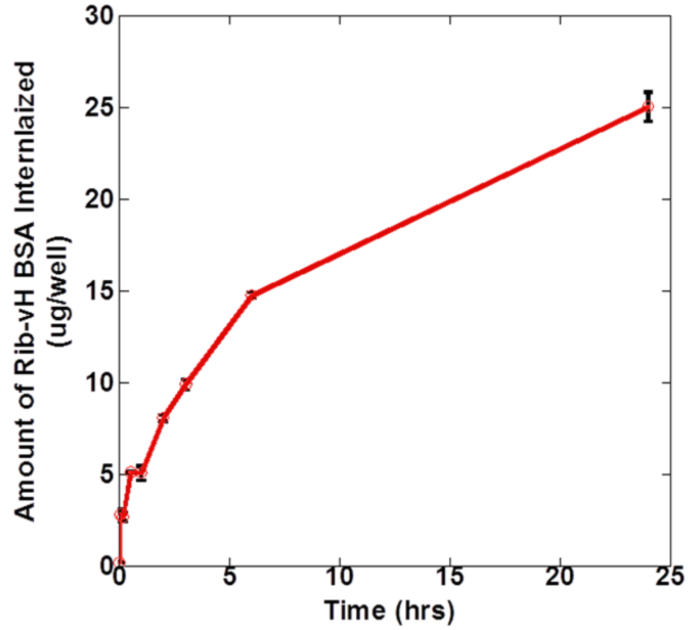

Figure 4.1. Internalization of Rib-vH BSA tagged with Cy5.5 into RAW 264.7 cells. Rapid uptake of the Rib-vH BSA was observed. (Representation of two independent experiments n=6 for each experiment).

To assess the specificity of the AGE BSA uptake of the cells a competition assay was performed using Cy5.5 labeled Rib-vH BSA and various concentrations of unlabeled Rib-vH BSA. The macrophages were treated with 50ug/mL of Cy5.5 labeled Rib-vH BSA and different concentrations of unlabeled Rib-vH BSA, the cells were incubated at 37 °C for 2 hours and then the cells were lysed and the fluorescence of the lysate was measured as described earlier. The unlabeled AGE compound efficiently competed with labeled AGE compound and reduced the uptake to < 5% of the control value (7µg) (Figure 4.2).

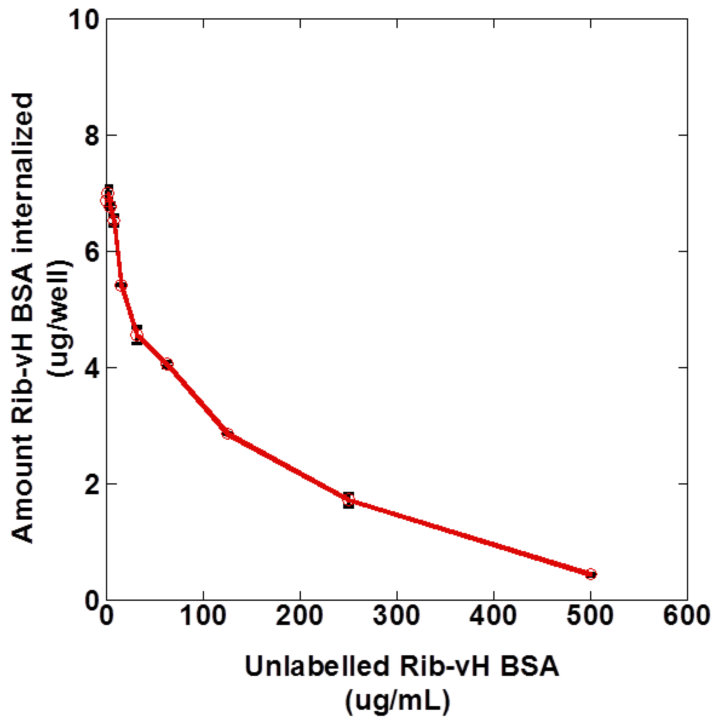

Figure 4.2. Competition assay was performed with increasing concentrations of unlabeled Rib-vH BSA.
The RAW 264.7 cells were incubated at 37 °C for 2 hours. (Representation of two independent experiments n=6 for each experiment).

AGE internalization in the macrophages

There is little information about the intracellular fate of endocytosed AGEs and their influence on proteolytic systems. A recent report suggested that in RAW 264.7 cells the AGE compounds increase the number of lysosomes and the increased the lysosomal activity, mRNA and protein expression of cathepsins D and L [322]. We performed live cell confocal fluorescence imaging to understand the internalization of Rib-vH BSA. The Cy5.5 labeled Rib-vH BSA was used to study the AGE internalization and the lysosomes were labeled using the CellLight® Lysosomes-GFP ®as described earlier. In agreement with the uptake assay, rapid internalization of the Rib-vH BSA_Cy 5.5 was observed in RAW 264.7 cells. Figure 4.3 shows the uptake of Rib-vH BSA at different time points; the green fluorescence represents lysosomes and Rib-vH BSA is represented by red fluorescence. Due to photo-bleaching images from same cell could not be presented. Figure 3.3A represents time 0; Rib-vH BSA did not enter the macrophage. The arrows represent the lysosomes inside the macrophages. Figure 4.3B and 4.3C shows the uptake at 1 hour and 2 hours respectively. We observe that Rib-vH BSA internalized into the lysosomes after 1 hour. Interestingly, we observe continuous internalization of Rib-vH BSA into the lysosome was observed even after 2 hours. The arrow in Figure 3.3C shows a new Rib-vH BSA particle being taken up the lysosome. These images confirm the lysosomal uptake of Rib-vH BSA. Hence, we conclude that the Rib-vH BSA is taken up by the lysosomes and there is continuous uptake and internalization of the Rib-vH BSA by the macrophages.

Macrophages can internalize particles by three major strategies, i.e. by pinocytosis, receptor-mediated endocytosis and phagocytosis[375]. Phagocytosis is an actin-dependent mechanism and clathrin independent mechanism which is responsible for the uptake of large particles (>0.5 µm). The Rib-vH BSA particles are the in the order of few nano meters hence it is unlikely that the Rib-vH BSA is internalized by phagocytosis. Pinocytosis and receptor mediated endocytosis are closely related they share a clathrin-mediated mechanism and do not involve actin polymerization. However, pinocytosis is a process by which fluid and solutes are taken up by the cell and cannot be involved in Rib-vH BSA uptake. Hence, most likely the Rib-vH BSA is internalized by receptor mediated endocytosis.

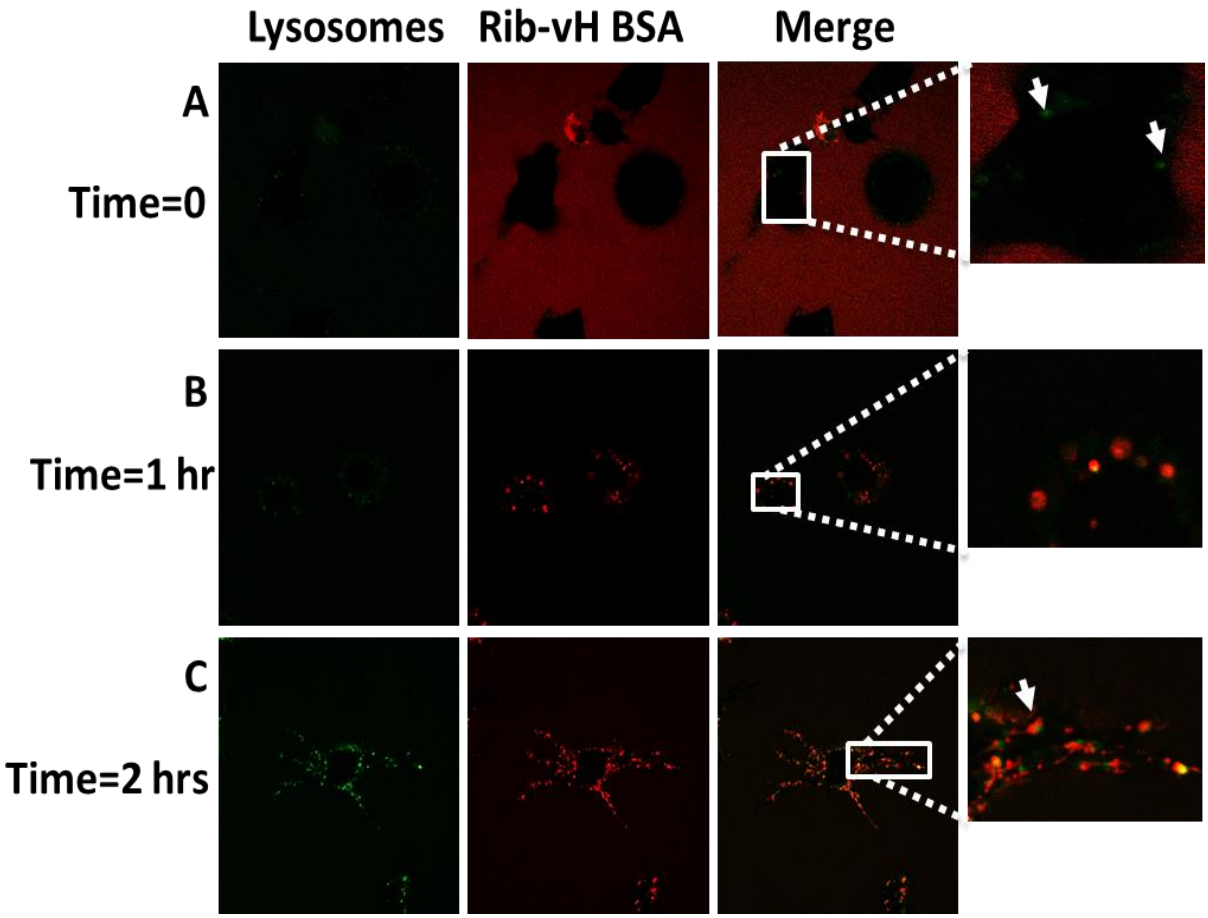

Figure 4.3. Rib-vH BSA uptake in the macrophages by live cell imaging.
Green: Lysosomes, Red: Rib-vH BSA. A), B), C) Time 0, 1hr and 2hrs after the addition of Rib-vH BSA respectively. (The experiment was performed 2 times independently).

Role of receptors in AGE uptake

Several AGE receptors have been identified and can be classified as clearance receptors which are responsible the clearance of AGEs or inflammatory receptors that are responsible for AGE induced signaling. Clearance of AGE proteins involves scavenger receptors CD36 [123, 376], FEEL-1 (STAB1), FEEL-2 (STAB2), SR-BI (SCARB1), SR-BII (SCARB2)[121, 124, 376-379], and the macrophage scavenger receptors type I (SR-AI, MSR1) and type II (SCARA2, MARCO)[122, 380]. Receptors that are not primarily involved in clearance, but have signaling functions are the AGE-receptor complex and the receptor for advanced glycation end products. The AGE-receptor complex consists of three proteins AGE-R1 (OST-48, DDOST), AGE-R2 (80 K-H, PRKCSH), and AGE-R3 (galectin-3, LGALS3) [130, 381-383]. The receptor for advanced glycation endproducts RAGE (AGER) belongs to the immunoglobulin-like protein family and mediates many of the physiological effects AGE products [28, 194, 384, 385]. Recently, in the macrophages the nucleolin receptor was reported to recognize the glycolaldehyde and glyceraldehyde AGEs [386].

In order to elucidate the role of AGE receptors expressed on the surface of macrophages in AGE uptake we perform real time quantitative PCR. We select 18 potential AGE binding cell surface receptors (Table 4.2) which include RAGE, galectin-3, scavenging receptors and pattern recognition receptors such as toll like receptors. Based on our housekeeping gene analysis the ribosomal protein L4 was selected as the house keeping gene and the ΔΔct values with respect to untreated control are reported in (Figure 4.4). On 24 hour Rib-vH BSA treatment we observe a significant upregulation in the genes of the AGE-receptor complex more specifically in the gal-3 (7.2±2.6 ct units) and the PRKCSH (5.3±3.1 ct units) genes. However, we do not see any upregulation of RAGE. We also observe an upregulation of the toll like receptors 2, 4, 6 and 9. TLR2 was upregulated by 5.8±0.45 ct units. The role of TLRs in AGE uptake and signaling has not been described and their upregulation suggests a possible role of pattern recognition receptors such as TLRs in Ribose modified AGE signaling. Further investigation is necessary in this direction to determine the role of TLRs in AGE uptake and signaling.

Table 4.2. Receptors genes studied using q RT PCR to determine their AGE induced expression.

Gene (Gene ID)	**Function**	**Primers 5’→3’**
RAGE (NM_007425)	Receptor for advanced glycation end products	Forward: AGAAGCTTGGAAGGTCCTGA Reverse: TTGGACTTGGTCTCCTTTCC
DDOST (NM_005216)	Advanced glycation endproduct receptor 1	Forward: TGCACATGAAGGAGAAGGAG Reverse: GAGGTAAGGCTGTGCCATTT
PRKCSH (NM_002743)	Advanced glycation endproduct receptor 2	Forward: GGAACTTGACGACAACATGG Reverse: CGGTCATAGAAGGAGGTGGT
LGAL3 (NM_005567)	Galectin-3; Advanced glycation endproduct receptor 3	Forward: AGACAGCTTTTCGCTTAACGA Reverse: GGGTAGGCACTAGGAGGAGC
TLR2 (NM_011905)	Toll like receptor 2	Forward: TTCTGATGGTGAAGGTTGGA Reverse: TTGACGCTTTGTCTGAGGTT
TLR4 (NM_021397)	Toll like receptor 4	Forward: ACACCAGGAAGCTTGAATCC Reverse: GAGGTGGTGTAAGCCATGC
TLR6 (AF314636)	Toll like receptor 6	Forward: TTGCTGGAACCCATTCTACA Reverse: CCTTCTCAGTAGGCCATTCC
TLR9 (NM_031178)	Toll like receptor 9	Forward: ATCTCCCAACATGGTTCTCC Reverse: CAGACTTCAGGAACAGCCAA
SCARB1 (CT010222)	Scavenging receptor	Forward: CCCGTCCCTTTCTACTTGTC Reverse: GGTGTCGTTGTCATTGAAGG
SCARB2 (NM_007644)	Scavenging receptor	Forward: TTCATCCGCTGATAAGCAAG Reverse: GGGTATACAGAAGCCAGCGT
STAB1 (NM_0151436)	Scavenging receptor	Forward: TTCTGCTCTGTGTCCTGGTC Reverse: AGGGACATAGTTGCCTCCTG
STAB2 (NM_017564)	Scavenging receptor	Forward: CGGAAGAGACTGTGTGGAGA Reverse: CAATTCCGTTTCCTCGAAAT
CD 36 (BC010262)	Scavenging receptor	Forward: GCCTTCACTGTCTGTTGGAA Reverse: GGAACCAAACTGAGGAATGG
MSR1 (BC003814)	Macrophage scavenger receptors Class A	Forward: GGATGCAATCTCCAAGTCCT Reverse: TGCGCTTGTTCTTCTTTCAC
MARCO (NM_010766)	Macrophage scavenging receptor type II	Forward: ACAGAGCCGATTTTGACCAAG Reverse: CAGCAGTGCAGTACCTGCC

Table 4.2. Receptors genes studied using q RT PCR to determine their AGE induced expression (Continued).

Gene (Gene ID)	Function	Primers 5'→3'
OLR1 (NM_138648)	Oxidized low-density lipoprotein receptor 1	Forward: CAGATGTTAGCCCAGCAGAA Reverse: GAGTTTGCAGCTCTTTGCAG
Ncl (BC005460)	Nucleolin	Forward: TCGAGAAGTCAACCATCCAA Reverse: GAACCAGTTTCCCGATCAGT

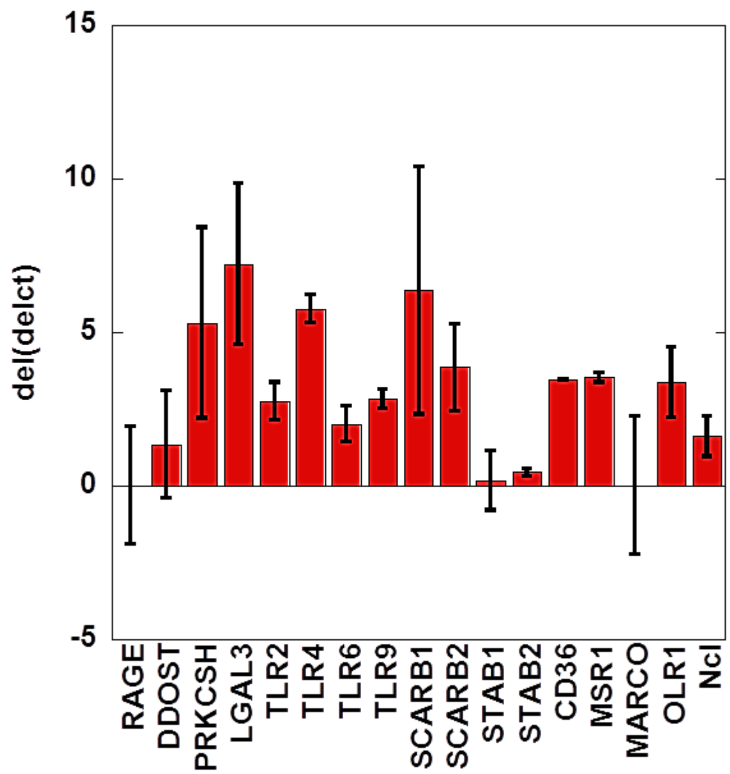

Figure 4.4. Rib-vH BSA induced receptor mRNA upregulation after 24 hours of treatment. Ribosomal protein L4 (RPL4) was used as the house keeping gene and the ΔΔct values are calculated with respect to the gene expression at time 0. (Representation of two independent experiments).

Macrophages also express several scavenging receptors [387-389]. These receptors play a very important role in the in the removal of many foreign substances and waste materials in the living body and hence contribute to the scavenging (cleaning) activity of the macrophages. We investigated the upregulation of known AGE binding scavenging receptors on Rib-vH BSA treatment. We observe a significant upregulation in the SCARB1 (6.38±4.03 ct units), SCARB2

(3.8±1.4 ct units) and CD 36 (3.46±0.01 ct units). No upregulation was observed in the STAB1 and STAB2 expression. A significant upregulation was observed in the MSR1 gene. This gene encodes the class A macrophage scavenger receptors, which include three different types (1, 2, 3) generated by alternative splicing of this gene. These results suggest a role for the class A macrophages scavenger receptors in the Rib-vH BSA uptake. The class A scavenger receptors are involved in the endocytosis of modified low density lipoproteins (LDLs) [390]. We also determined the upregulation of low density lipoprotein receptor (OLR1). The role of OLR1 has also been described to bind to sugar modified AGEs [391]. AGEs have been described to induce foam cell formation as well [392]. On Rib-vH BSA treatment the OLR1 was upregulated by around 3.4±1.15 ct units.

In order to elucidate the role of specific AGE receptors in Rib-vH BSA uptake we performed siRNA knock down of the receptors and also used receptor specific inhibitors. RAGE is the most well characterized receptor for AGEs; however our q RT-PCR data suggested very low expression of RAGE (31.25±1.73 ct units) in the RAW 264.7 cell line and no upregulation was observed in RAGE expression on Rib-vH BSA treatment (Figure 4.4). Hence we do not suspect the role of RAGE in Rib-vH BSA mediated uptake. Our q RT-PCR data suggest that galectin-3 was upregulated significantly, therefore the role of gal-3 in Rib-vH BSA uptake was determined. 500uM of N-acetyllactosamine, a potent inhibitor of gal-3 [393] was used to the role of gal-3 Rib-vH BSA uptake in RAW 264.7 cells. In the presence of N-acetyllactosamine we do not observe any difference in the Rib-vH BSA uptake kinetics (Figure 4.6). The rapid uptake of the Rib-vH BSA also suggests a scavenging receptor mechanism. SR-A, which is a type I macrophage scavenging receptor was upregulated on Rib-vH BSA treatment, hence we elucidate the role of SR-A in the Rib-vH BSA recognition and uptake. SR-A knocked down using siRNA.

The knock down was estimated by western blotting. A knockdown of 52.8±1.3% was observed (Figure 4.5). However, SR-A knockdown also did not influence the AGE uptake (Figure 4.6). These results do not conclusively point at any receptor involved in Rib-vH BSA uptake and needs further investigation. AGE biology is very complex and several different receptors have been reported in the uptake of AGE as described above. We observe a simultaneous upregulation of multiple receptors on AGE treatment hence a possibility of multi receptor complexes in AGE uptake cannot be ruled out. The role of phagocytosis in Rib-vH BSA is unlikely as reports suggest that AGE compounds reduce the phagocytic potential in macrophages [394].

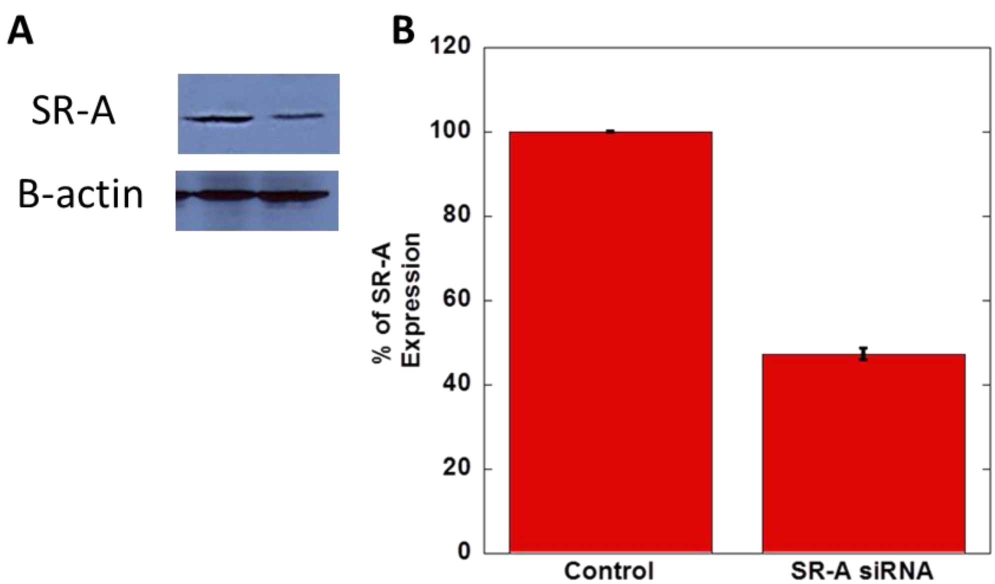

Figure 4.5. SR-A knockdown in RAW 264.7 cells by SR-A siRNA.
(Representation of two independent experiments).

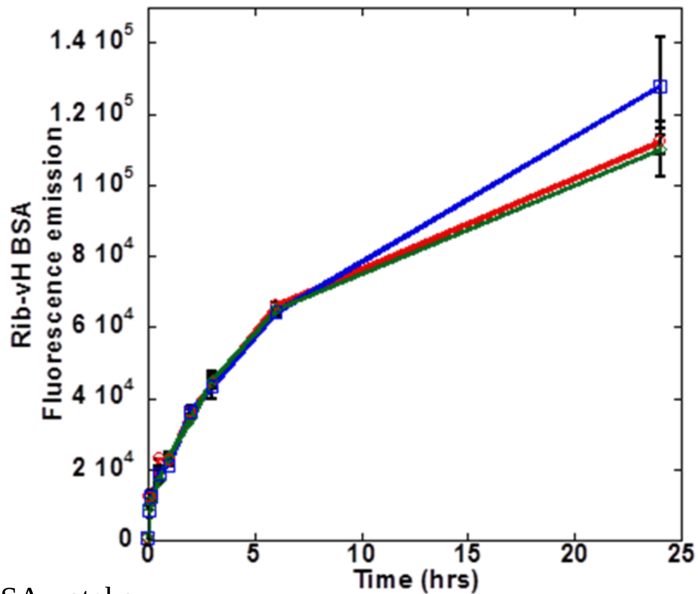

Figure 4.6. Rib-vH BSA uptake.
Red; Control cells, Blue; N-acetyllactosamine (galectin-3 inhibitor) and Green (SR-A) knockdown (Representation of two independent experiments, n=6 for each experiment).

Rib-vH BSA induced oxidative and nitrogen stress in RAW 264.7 cells

On stimulation with DAMPS macrophages are potent producer of reactive oxygen species (ROS) such as super oxide anion, singlet oxygen, hydroxyl radicle and hydrogen peroxide [395, 396]. The production of reactive nitrogen species such as nitric oxide has been described to play a key role in the pathological process observe in diabetes and has also been associated with the diabetic complications [397, 398]. Under diabetic conditions, there are several sources of ROS described, among them AGEs are one of the most potent sources[399]. A large volume of literature implicates the role of AGEs in oxidative stress formation and contribution to the chronic stress in diabetes [399-401]. Certain reports suggest the role of AGE induced oxidative stress in the macrophages[402]. However, the role of AGE induced oxidative stress in macrophages is not well understood. The role of AGE compounds in the upregulation of genes associated with oxidative stress has not been described.

We select a panel of a 10 genes which have been reported to be responsible for nitrogen and oxidative stress in macrophages (Table 4.3). The highest upregulation was observed in the inducible isoform of nitric oxide synthase (iNOS) gene; 12.4±0.25 ct units. The upregulation for iNOS was followed at different time points and a rapid upregulation was observed (Figure 4.7), a significant upregulation was observed after 30 min of AGE treatment and the upregulation increased over a 24 hrs. The iNOS upregulation and nitric oxide synthesis has been described extensively in the literature as an inflammatory response in macrophages [403]. The upregulation of iNOS suggests a pro-inflammatory role of the Rib-vH BSA. Rib-vH BSA induced nitric oxide production was quantified by the Griess assay. We quantify the nitric oxide produced after 24 hours of treatment with Rib-vH BSA and 1281.5±55.9 pmol of nitric oxide was produced (Figure 4.8).

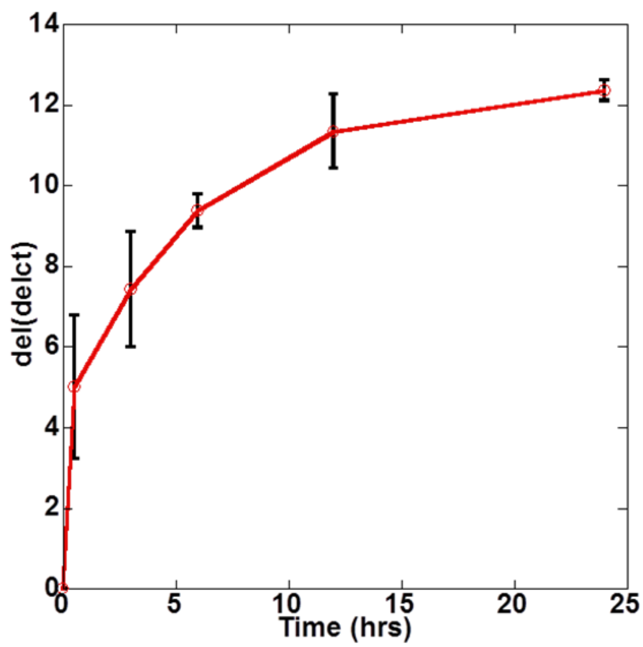

Figure 4.7. Time course of the iNOS mRNA upregulation on Rib-vH BSA treatment. Ribosomal protein L4 (RPL4) was used as the house keeping gene and the ΔΔct values are calculated with respect to the iNOS expression at time 0. (Representation of two independent experiments).

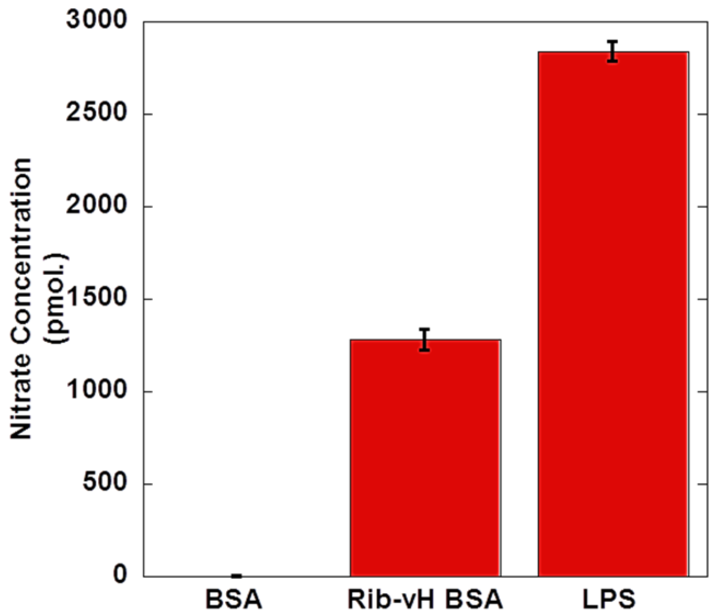

Figure 4.8. Nitric oxide produced after 24 hours on Rib-vH BSA treatment.
1ug/mL of LPS and 1mg/mL BSA was used as the positive and negative control respectively.
(Representation of two independent experiments).

Significant upregulation was also observed in the genes associated with oxidative stress such as COX-2 and NOX-2 (Figure 4.9). COX-2 is an inflammatory mediator that catalyzes the formation of prostaglandins from arachidonic acid and can in-turn cause the production of oxidative stress [404]. COX-2 is upregulated in several pathological processes involving inflammation, such as infectious diseases, cancer, arthritis and atherosclerosis [405-408]. The role of DAMPS such as LPS in the upregulation of COX-2 has been well elucidated [409]. However, the role of AGEs in COX-2 upregulation has not been described in the literature. The upregulation of COX-2 by Rib-vH BSA suggests the pro-inflammatory role of AGEs in activating the macrophages. The NOX2 was upregulated NOX or NADPH oxidase family transfer electrons across biological membranes and contributes significantly to the production of reactive oxygen species [410]. NOX-2 isoform is the most well characterized and abundantly reviewed in the recent past and its role in macrophage oxidative stress is very described and understood [411-413]. On Rib-vH BSA treatment upregulation of NOX-2 was observed (Figure 4.8) emphasizing the role of

AGEs in ROS generation in macrophages. We also observe upregulation of NOX-1 and NOX-4. The Rib-vH BSA mediated upregulation of COX-2 and NOX2 was determined at different time points (Figure 4.10 and 4.11). The expression levels of both the genes peaked at the 6 hour time point and then the expression flattened out till 24 hours of the treatment.

Table 4.3. Genes associated with oxidative stress studied using q RT PCR to determine their AGE induced expression.

Gene (Gene ID)	**Function**	**Primer 5'→3'**
iNOS (NM_010927)	Inducible nitric oxide synthase	Forward: GTTCTCAGCCCAACAATACAAGA Reverse: GTGGACGGGTCGATGTCAC
COX-2 (NM_011198)	Cyclooxygenase-2	Forward: TTCAACACACTCTATCACTGGC Reverse: AGAAGCGTTTGCGGTACTCAT
NOX1 (NM_172203)	NADPH oxidase 1	Forward: GTTTCTGGTTTCCTGGTTGG Reverse: AGCAGATTTCGACACACAGG
NOX2 (NM_007807)	NADPH oxidase 2	Forward: GTGAGAGGTTGGTTCGGTTT Reverse: GGAGCAGAGGTCAGTGTGAA
NOX4 (AF276957)	NADPH oxidase 4	Forward: GTTGGGCCTAGGATTGTGTT Reverse: CTCCTGCTAGGGACCTTCTG
HIF1a (AF003695)	Hypoxia-inducible factor 1-alpha	Forward: CGACACCATCATCTCTCTGG Reverse: AAAGGAGACATTGCCAGGTT

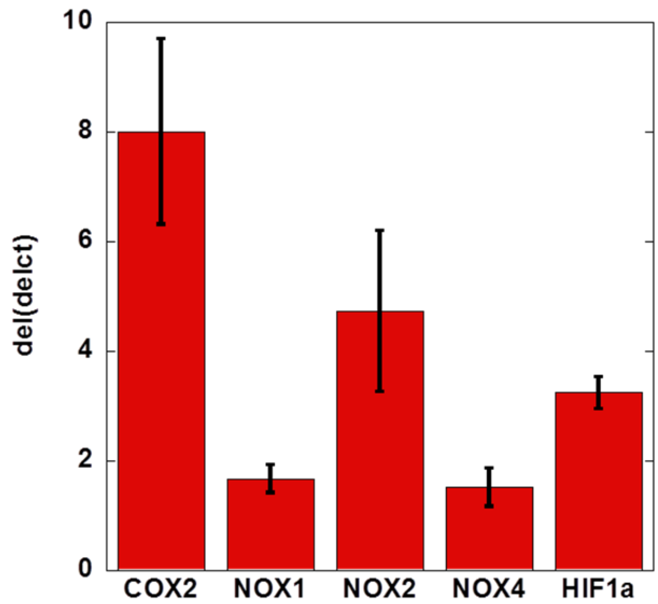

Figure 4.9. Upregulation of genes associated with oxidative stress after 24 hrs of Rib-vH BSA treatment.
Ribosomal protein L4 (RPL4) was used as the house keeping gene and the ΔΔct values are calculated with respect to the gene expression at time 0. (Representation of two independent experiments).

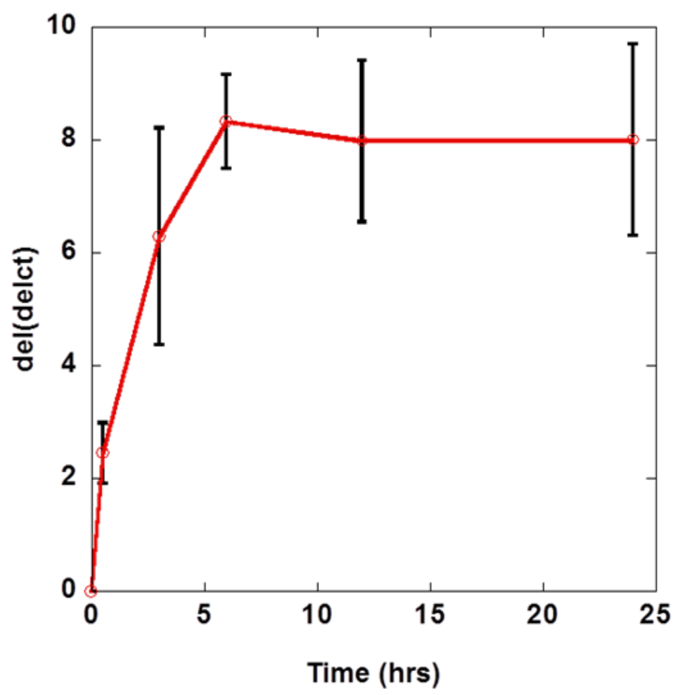

Figure 4.10. Time course of the COX-2 mRNA upregulation on Rib-vH BSA treatment.
Ribosomal protein L4 (RPL4) was used as the house keeping gene and the ΔΔct values are calculated with respect to the COX-2 expression at time 0. (Representation of two independent experiments).

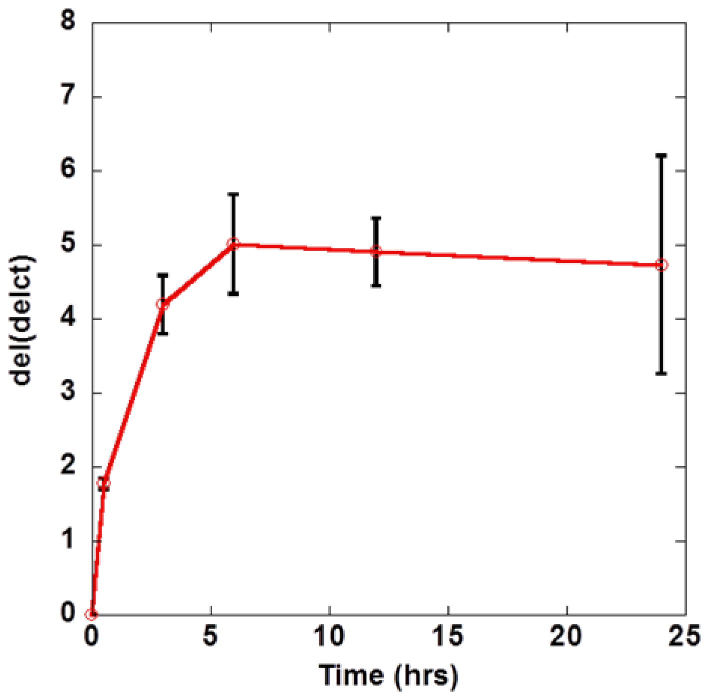

Figure 4.11. Time course of the NOX-2 mRNA upregulation on Rib-vH BSA treatment. Ribosomal protein L4 (RPL4) was used as the house keeping gene and the ΔΔct values are calculated with respect to the NOX-2 expression at time 0. (Representation of two independent experiments).

Building up on these studies we determined the AGE induced ROS production by determining the fluorescence of 2, 7- dichlorofluorescein (DCF). DCF is de-esterified intracellularly and undergoes oxidation by ROS to form the highly fluorescent 2, 7-dichlorofluorescein. DCF measures hydrogen peroxide, hydroxyl radicles, peroxyl radicles, peroxynitrite anion and super oxide anions. A basal fluorescence in control cells was measured to be 1008.7±58 counts on Rib-vH BSA treatment for 24 hours the fluorescence emission increased about 2.5 times to 2529.1±165.5 counts indicating significant increase in the ROS production. The Rib-vH BSA induced ROS production was followed at different time points and we observe a linear correlation of the ROS production and time. When we used an ROS inhibitor 500 µM N-acetyl cysteine (NAC), the Rib-vH BSA induced ROS attenuated (Figure 4.13). AGE induced ROS production was also determined for the other AGE compounds (Figure 4.12). The highly modified AGE compounds were used and a detailed characterization of all the AGE compounds is described in chapter 1. The MG-H BSA treatment also induced significant ROS production (Figure 4.12). The MG-H BSA induced ROS levels were similar to the Rib-vH BSA induced ROS levels. The role of methyl glyoxal derived AGE compounds in macrophage activation and ROS production has been described previously described[414] and our data validates the same. Increased ROS levels were also observed with the But-H BSA and Gly-H BSA and all other AGE compounds including the glucose derived AGE compounds did not show any ROS production. These differences among different AGE compounds could be a result from the heterogeneity of these AGE compounds and this emphasizes the fact that each AGE compound is unique and has certain structural features which are responsible for their recognition and uptake. For this work we concentrate only on the Rib-vH BSA however, this data suggest that other AGE compounds can also trigger ROS production in macrophages.

ROS production upregulates several ROS responsive genes one such gene is the Hypoxia inducing factor (HIF-α). HIF-α is undetectable or present at very low levels under normal oxygen supply however, in the inflammatory response under normoxic conditions HIF-α is upregulated by reactive oxygen and reactive nitrogen species (ROS and RNS)[415-418]. Rib-vH BSA also induced a significant upregulation of the Hypoxia inducing factor-alpha (HIF-α) and the upregulation increased in a time dependent manner. Upregulation of HIF-α is crucial for differentiation, survival and functionality of immune cells, and HIF-1α seems to be a potent cellular survival factor [419] and Rib-vH BSA plays an important role in survival of macrophages.

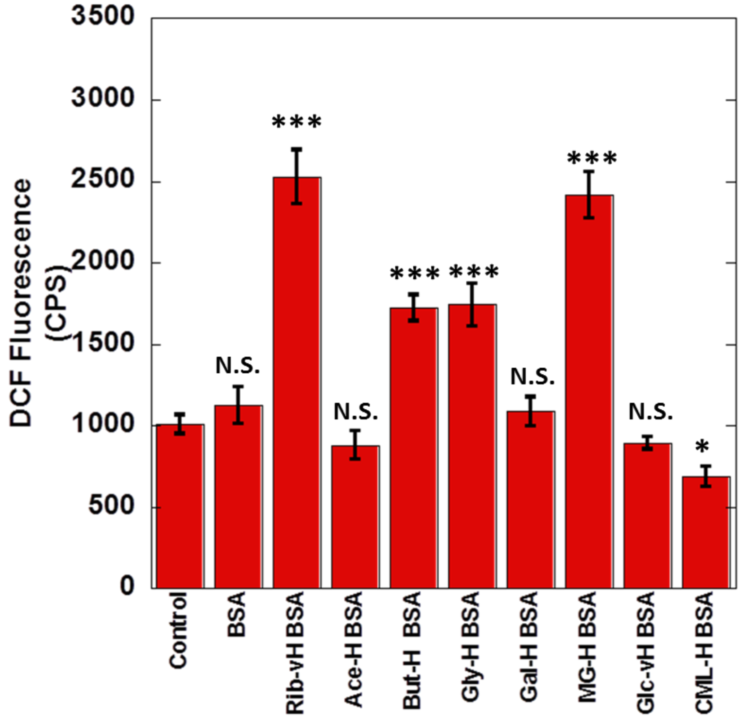

Figure 4.12. ROS production in RAW 264.7 cells after 24 hrs of AGE compound treatment. (Representation of two independent experiments, n=6, ***P<0.0005, *P<0.01, N.S.: not significant).

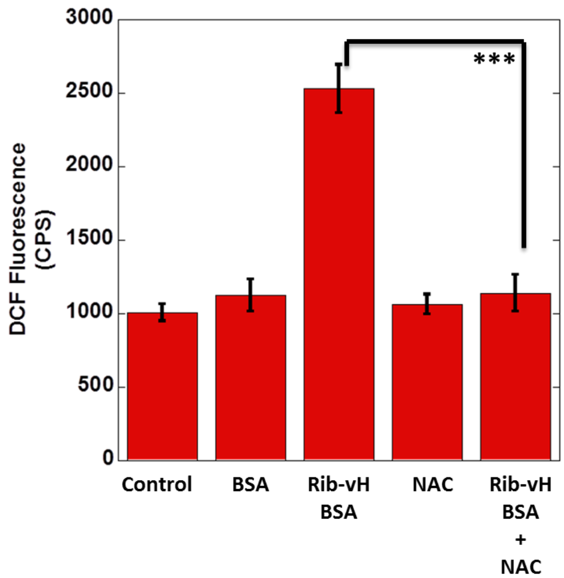

Figure 4.13. 500uM N-acetyl cysteine (NAC) quenched the Rib-vH BSA induced oxidative stress.
(Representation of two independent experiments, n=6).

AGE induced NF-κB activation

Following the ROS production, the NF-κB signaling is one of the most important pathways described to be activated. NF-κB is a nuclear transcription factor and its activation in the macrophages mainly leads to the expression of several genes involved in inflammation[420]. Several reports emphasize the role of AGE-RAGE interaction and NF-κB activation in-vitro which is mediated via the oxidative stress generated in cell types such as endothelial cells, vascular cells and pulmonary smooth muscle cells [32, 271, 421]. The role of AGE compounds and NF-κB activation has been described in different disease states such diabetes [280] and also in age related macular degeneration [279]. AGE induced ROS production and NF-κB activation has been suggested in the macrophages however, the role of AGE induced ROS production in NF-κB activation in macrophages has not been described. We study the AGE induced NF-κB activation in the commercially engineered cell line called RAW-blue ™ (InvivoGen). RAW blue cells are engineered RAW cells with chromosomal integration of secreted alkaline phosphatase (SEAP) reporter construct which is inducible by NF-κB. The cells were treated with 1mg/mL AGE compound for 24 hours. A significant increase ($P<0.0005$) was observed the NF-kB activity when the cells were treated with the Rib-vH BSA, MG-H BSA, Glc-vH BSA, But-H BSA and Gly-H BSA. Increase in the NF-κB activity was also observed with the Ace-H BSA and Gal-H BSA ($P<0.001$). No increase was observed when the cells were treated with H-CML BSA (Figure 4.14). The Rib-vH BSA showed the most pronounced activity. In order to confirm the role of ROS in NF-κB activity we used N-acetyl cysteine to quench the Rib-vH BSA induced ROS. On the addition of N-acetyl cysteine the Rib-vH BSA induced NF-κB activity disappeared (Figure 4.15). This confirms the role of Rib-vH BSA induced ROS in the NF-κB activation in macrophages.

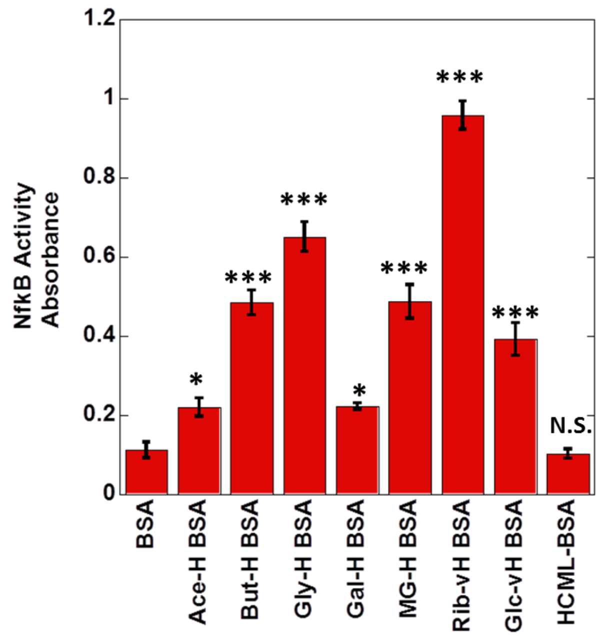

Figure 4.14. AGE induced NFκB activation after 24 hrs of treatment.
(Representation of two independent experiments, n=6 in each experiment, ***P<0.0005,*P<0.001, N.S.: Not significant).

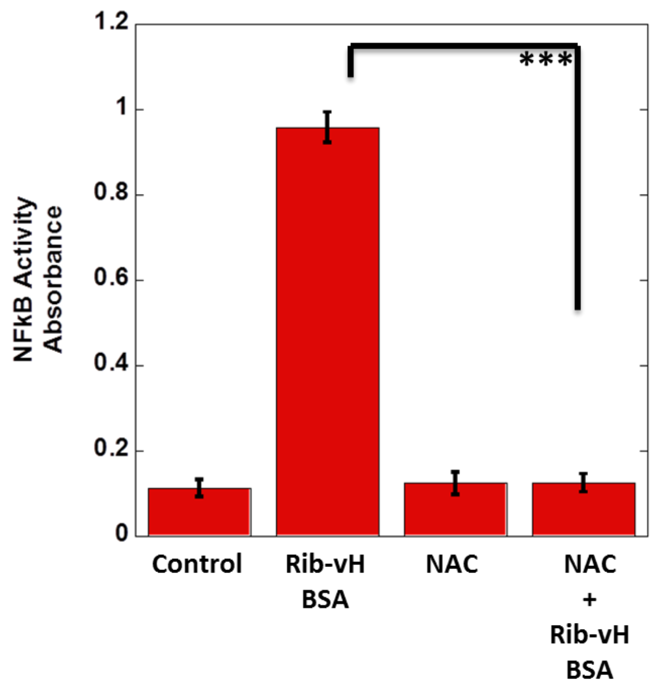

Figure 4.15. 500uM N-acetyl cysteine (NAC) inhibited the Rib-vH BSA induced NFκB activation.
(Representation of two independent experiments, n=6 for each experiment, ***P<0.0005).

Inflammatory cytokines

The activation of NF-κB leads to the activation of several pro-inflammatory cytokines such as IL-1β, IL-6 and TNF-α [420]. A huge body of literature also suggests that activated macrophages can also secrete several other cytokines and inflammatory factors such as MCP-1, MIP-2, GMCSF-1. We select a panel of cytokines and inflammatory mediators (Table 4.4) and their Rib-vH BSA induced expression was followed at different time points by real time quantitative PCR.

Table 4.4. Inflammatory cytokine and mediator genes used in the study to determine the effect of Rib-vH BSA treatment.

Gene	**Function**	**Primers 5'→3'**	**Basal expression levels (Ct)**
IL-1β (NM_000576)	Interleukin-1β	Forward: GAAATGCCACCTTTTGACAGTG Reverse: TGGATGCTCTCATCAGGACAG	28.38±0.82
IL-6 (NM_031168)	Interleukin-6	Forward: AGTCCGGAGAGGAGACTTCA Reverse: TTGCCATTGCACAACTCTTT	32.02±1.51
TNF-α (NM_013693)	Tumor necrosis factor-alpha	Forward: CAGACCCTCACACTCAGATCA Reverse: TTGTCTTTGAGATCCATGCC	24.62±1.48
MCP-1 (BC145869)	Monocyte chemoattractant protein-1	Forward: GCTCTCTCTTCCTCCACCAC Reverse: CAGCCTACTCATTGGGATCA	29.74±0.28
MIP-2 (BC119511)	Macrophage inflammatory protein-2	Forward: CTGTCCCTCAACGGAAGAAC Reverse: TAACAACATCTGGGCAATGG	26.06±0.26

Table 4.4. Inflammatory cytokine and mediator genes used in the study to determine the effect of Rib-vH BSA treatment (continued).

Gene	**Function**	**Primers 5'→3'**	**Basal expression levels (Ct)**
GM-CSF (X03019)	Granulocyte macrophage colony-stimulating factor	Forward: GAAGCATGTAGAGGCCATCA Reverse: TTGAGTTTGGTGAAATTGCC	28.66±1.41
CSF-2α (NM_009970)	GM-CSF receptor-alpha	Forward: CTGCTCTTCTCCACGCTACTG Reverse: GAGACTCGCCGGTGTATCC	33.04±0.23
MKI-67 (BC053453)	Ki-67; Marker of proliferation	Forward: TTCCAAACATCAGGCCATAA Reverse: CGTGAACTTTCCTCAGACCA	24.87±1.48

Rib-vH BSA induced pro-inflammatory gene upregulation is shown in Figure 4.16. Our PCR data suggests a significant increase in the expression of pro-inflammatory genes such as IL-1β, IL-6 and TNF-α. IL-1β is a pro-inflammatory cytokine which is a part of the IL-1 family of cytokines. IL-1β expression has been reported to be induced by NFκB in macrophages after their exposure with DAMPS [422]. We observe an upregulation of IL-1β of 6.32±0.7 ct units when compared to the control. The upregulation of IL-1β increased over time and peaked at 6 hrs, the upregulation was constant at 12 hrs and then a slight decrease in the upregulation was observed at 24hrs (Figure 4.17). The secreted IL-1β has been described to be involved in a wide range of immune responses, the ability of IL-1β in the upregulation of COX-2 and iNOS which account for increased prostaglandin-E2 and nitric oxide (NO) production has been described [423]. The ability of IL-1β to increase the expression of cell adhesion molecules on mesenchymal cells and endothelial cells has also been described [424]. These properties lead to the infiltration of inflammatory and immunocompetent cells from the circulation into the extravascular space and then into tissues where tissue remodeling is the end result of chronic IL-1-induced inflammation[425]. The production of IL-1β has also been implicated to upregulate the production of certain other cytokines such as IL-6 [426]. The qRT-PCR data indicates a huge upregulation of IL-6 (8.61±0.11 ct units). The IL-6 upregulation was also observed to be time dependent (Figure 4.18) and the upregulation peaked around 6 hours and the expression was constant till about 24 hrs. IL-6 has been reported to have important role in both innate and adaptive immunity[427]. It also plays a very important role in attracting monocytes, IL-6 *trans-signaling* has been shown to promote macrophage differentiation from monocytes by upregulating GM-CSF receptor expression[428]. On Rib-vH BSA treatment the upregulation of TNF-α was also observed. The expression levels of TNF-α gene was upregulated after 30 min of treatment and the expression levels remained same till 24 hours (Figure 4.19). TNF-α plays vital roles in macrophage activation and leads to NFκB activation through autocrine signaling [429]. TNF-α is also termed as the master cytokine regulator and plays a very important role in orchestrating the production of pro-inflammatory cytokine cascade[430]. The role of TNF-α in macrophage survival and proliferation has also been described [431]. These results emphasize the role of AGE compounds in pro-inflammatory cytokine release. The expression of pro-inflammatory cytokines such as IL-1β, IL-6 and TNF-α induces the upregulation of chemokines such as macrophage inflammatory proteins (MIP) and macrophage chemoattractant protein (MCP) [432]. We determine the upregulation of MIP- 2α and MCP-1. Rib-vH BSA also induced a significant upregulation of the MIP-2α and MCP-1(Figure 4.16). MIP-2α, MCP-1 and other chemokines play an important role in guiding immune cell traffic such as neutrophils and hematopoietic stem cells to site of inflammation [433, 434].

The granulocyte monocyte-colony stimulating factor (GM-CSF) is a haemopoietic growth factor which is identified to production and differentiation of haemopoietic cells from precursors[435]. In macrophages it is responsible for macrophage polarization into "M1-like" inflammatory macrophages in combination with other inflammatory stimuli [436]. GM-CSF binds to the GM-CSF receptor (CSF2R) which is a heterodimer, composed of a specific ligand-binding α-chain (CSF2Rα), which binds GM-CSF with low affinity and a signal-transducing β-chain (CSF2Rβ) [437, 438]. The binding of GM-CSF to CSF2Rα triggers pro-inflammatory signaling in macrophages. AGE induced upregulation of the GM-CSF and CSF2Rα was determined using the q RT-PCR. Rib-vH BSA treatment induced upregulation of GM-CSF by 2.59±0.5 ct units and CSF2Rα by 8.46±0.5 ct units. Finally, we determine the AGE upregulation of marker of proliferation Ki-67 (MKI67). Rib-vH BSA treatment induced an upregulation of MKI67 4.47±0.1 ct units. This suggests the mitogenic ability of the Rib-vH BSA. Taken together our q RT-PCR data suggests the Rib-vH BSA activates pro-inflammatory signaling.

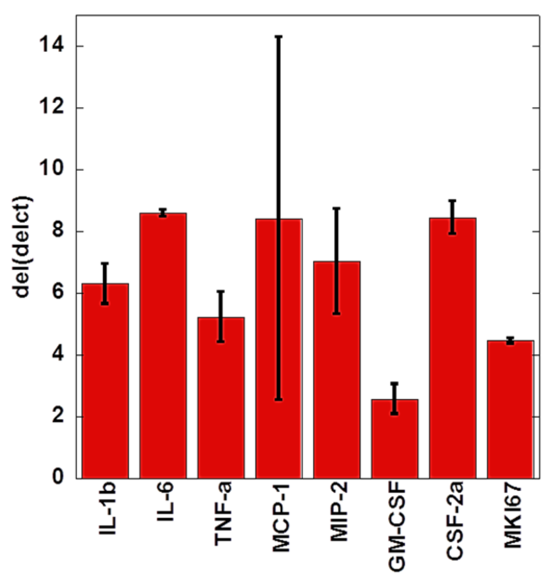

Figure 4.16. Pro-inflammatory gene upregulation on 24 hrs of Rib-vH BSA treatment. Ribosomal protein L4 (RPL4) was used as the house keeping gene and the ΔΔct values are calculated with respect to the gene expression at time 0. (Representation of two independent experiments).

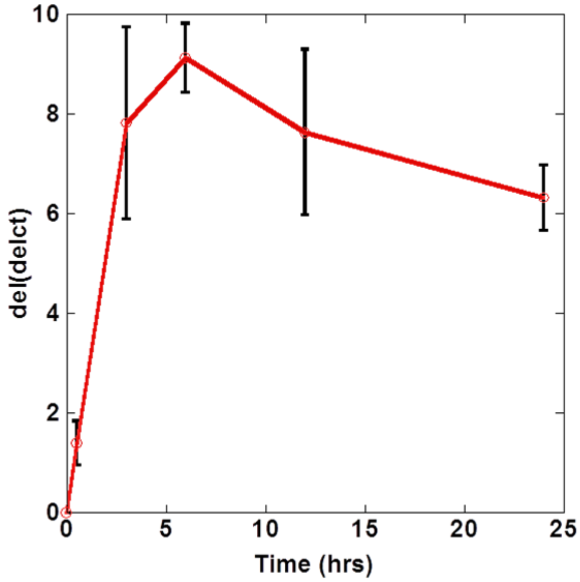

Figure 4.17. Time course of Rib-vH BSA induced IL-1β upregulation.
Ribosomal protein L4 (RPL4) was used as the house keeping gene and the ΔΔct values are calculated with respect to the gene expression at time 0. (Representation of two independent experiments).

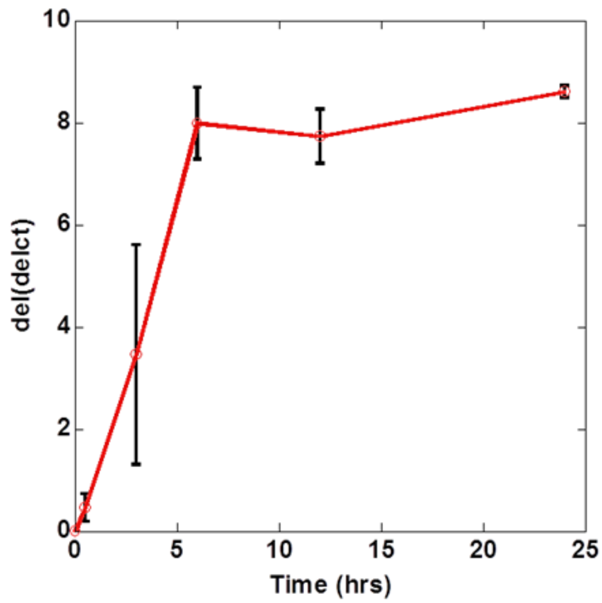

Figure 4.18. Time course of Rib-vH BSA induced IL-6 upregulation.
Ribosomal protein L4 (RPL4) was used as the house keeping gene and the ΔΔct values are calculated with respect to the gene expression at time 0. (Representation of two independent experiments).

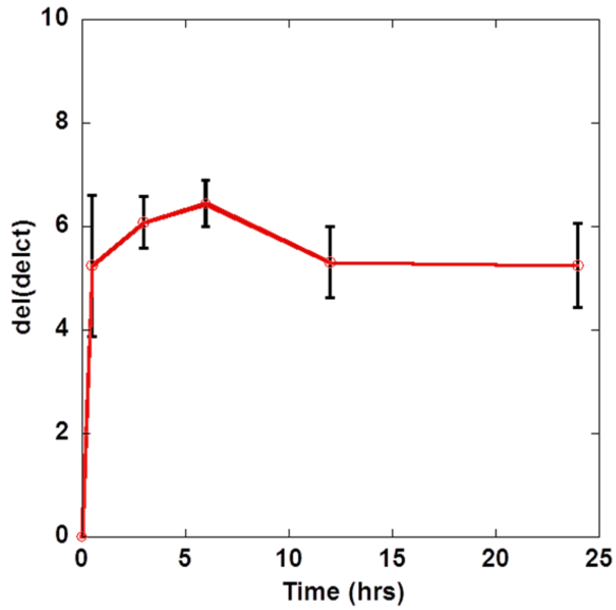

Figure 4.19. Time course of Rib-vH BSA induced TNF-α upregulation.
Ribosomal protein L4 (RPL4) was used as the house keeping gene and the ΔΔct values are calculated with respect to the gene expression at time 0. (Representation of two independent experiments).

Rib-vH BSA induced macrophage proliferation

Classically, the concept that monocyte recruitment dictates macrophage buildup is well accepted. However, recent studies also reveal that macrophage accumulation does not depend on monocyte recruitment in some inflammatory contexts and involves the proliferation of macrophages. The proliferation of macrophages has been described in disease states such as atherosclerosis [439-441] and in certain inflammatory conditions involving the T_H2 cells [442]. The mitogenic effect of Rib-vH BSA on macrophages was determined using the redox active dye, Resazurin. On Rib-vH BSA after 24 hours we observe a 1.46±0.06 fold increase in the rate of proliferation (Figure 4.20). Figure 4.21 shows the dose response curve of the Rib-vH BSA induced proliferation. To emphasize the role of RAGE signaling, we use 25ug/mL of anti-RAGE antibody (2A11) or 1 µM of a small molecule inhibitor of RAGE (FPS-ZM1) to inhibit the AGE-RAGE interaction and no difference was observed in the Rib-vH BSA induced macrophage proliferation. This suggests a RAGE independent pathway of the Rib-vH BSA in macrophages.

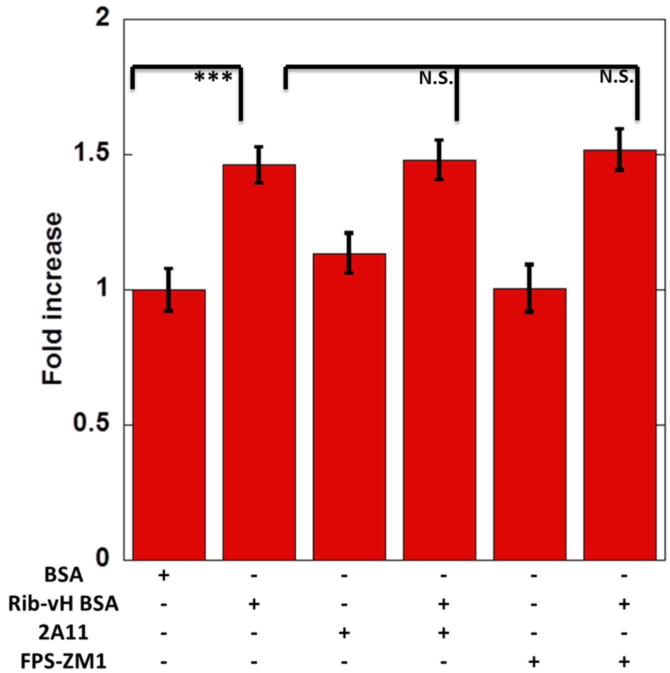

Figure 4.20. Rib-vH BSA induced macrophage proliferation is RAGE independent. (Representation of two independent experiments, n=6 for each experiment).

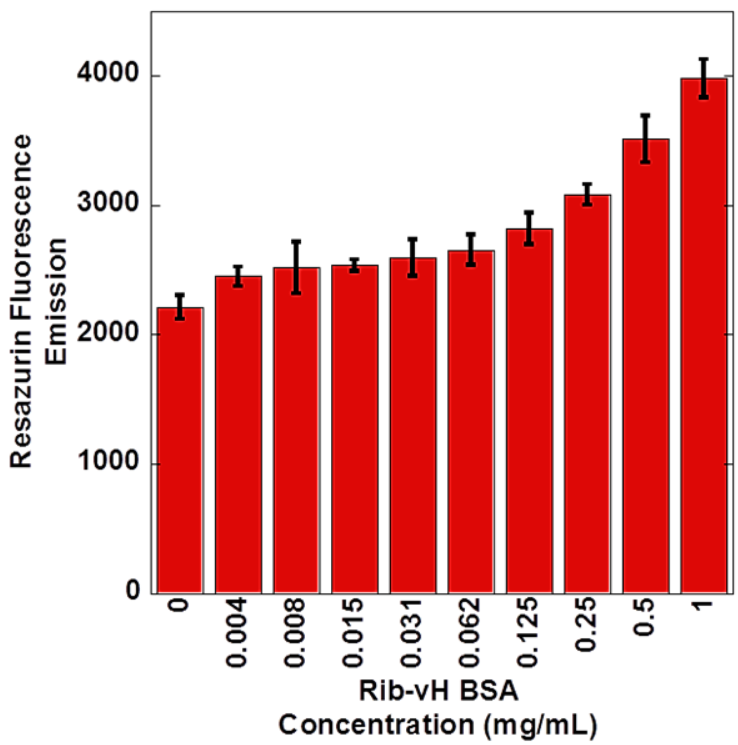

Figure 4.21. Dose response curve of Rib-vH BSA induced macrophage proliferation. (Representation of two independent experiments, n=6 for each experiment).

Role of TLR signaling in Rib-vH BSA mediated cellular effects

The Rib-vH BSA induced activation of macrophages and proinflammatory-cytokine release observed is typical to TLR signaling in macrophages when activated by DAMPS. A clear role of RAGE, galectin-3 or the scavenger receptor SR-A could not be established. The macrophages express several pattern recognition receptors such as the toll like receptors (TLRs) and we hypothesize that the TLRs play an important role in AGE induced macrophage activation and cytokine release. The upregulation of TLR2, 4, 6 and 9 genes was determined after 24 hours of Rib-vH BSA treatment. We observe the most significant upregulation in the expression of TLR4, 5.8±0.45 ct units (Figure 4.23). The upregulation of TLR2, TLR6 and TLR9 was also observed. The role of TLR signaling on the AGE induced inflammation in macrophages was further elucidated by siRNA knockdown of myeloid differentiation primary response 88 (MyD88). MyD88 is an adaptor protein which is necessary for the activation of TLR signaling[443]. Evidence from the literature suggests of a MyD88 dependent signaling which is common to all TLRs a MyD88-independent pathway that is peculiar to the TLR3- and TLR4 signaling pathways[444]. MyD88 was knocked down using the MyD88 siRNA and the knockdown was confirmed by western blotting using the MyD88 antibody (sc-11356) and a knockdown of 82.24±2.9% was achieved (Figure 4.22). After 24 hours of knockdown the cells were treated Rib-vH BSA and the q-RT PCR was performed after 24 hours of the treatment. Firstly, our RT-PCR data also confirms the knockdown of MyD88 we observe a 27.8±1.74 fold (4.8±0.8 ct units) knockdown of MyD88. Interestingly; we also observe the knockdown of TIRAP which is another important adaptor molecule which plays an important role in TLR-mediated MyD88-dependent signaling. The expression of 12 pro-inflammatory genes which were upregulated previously on Rib-vH BSA treatment was determined. As shown in the Figure 4.23, we observe partial down regulation of the upregulated pro-inflammatory cytokines such as IL-1β and a complete down regulation of TNF-α were observed. The down regulation of IL-6 and COX-2 was not significant. Down regulation was also observed in the expression of iNOS and CSF-2a genes. These observations are very interesting and are different from the MyD88 knockdown studies by Björkbacka et al., [445] where the authors use LPS for stimulation. On LPS stimulation in MyD88 knockdown mice bone marrow macrophages the expression of IL- β, IL-6 and COX-2 completely disappeared and the expression of TNF-α did not completely subside [445]. These results suggest a role for the TLRs in the observed Rib-vH BSA induced inflammation. However, we do not observe any significant down regulation of MIP-2 and MCP-1 genes on MyD88 knock down. This suggests a MyD88 independent pathway for the upregulation of MIP-2 and MCP-1 genes. The MyD88 independent upregulation of MIP-2 and MCP-1 has been reported in the literature using LPS stimulation in bone marrow macrophages [445]. Taken together, these results suggest the role of TLRs in Rib-vH BSA induced inflammation; however, this needs further investigation. We suspect TLRs in conjunction with other AGE receptors could play a major role in AGE compound induced macrophage activation and inflammation. Figure 4.24 summarizes TLR dependent AGE signaling.

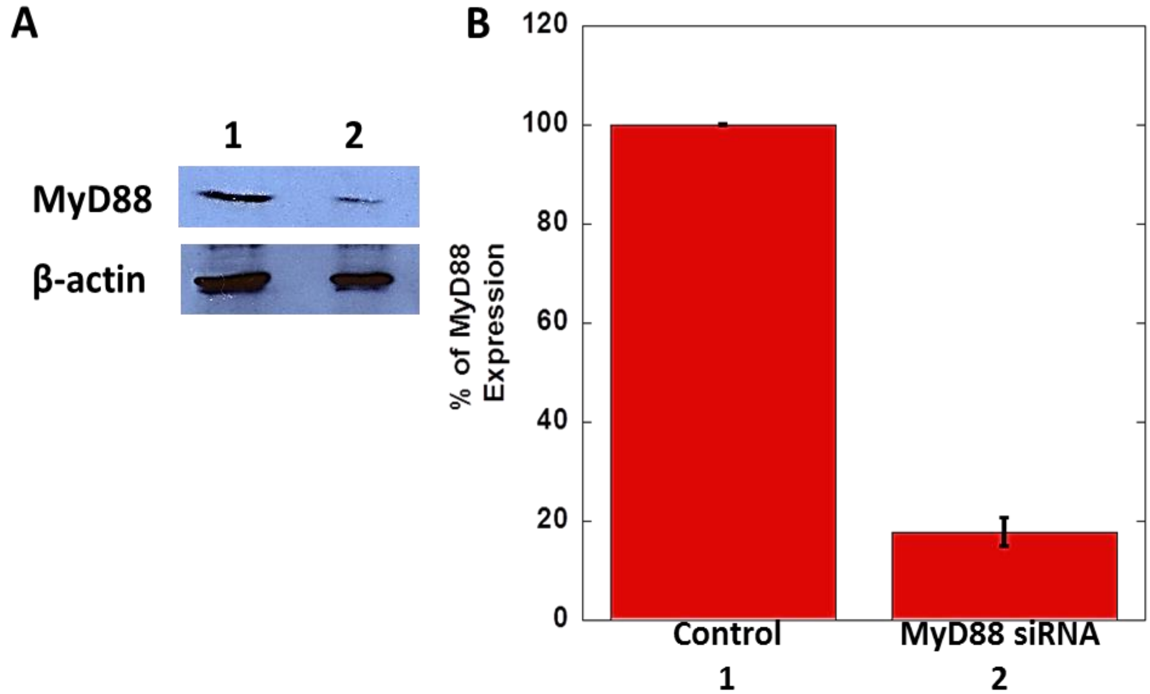

Figure 4.22. siRNA mediated knockdown of MyD88 in RAW 264.7 cells. (Representation of two independent experiments).

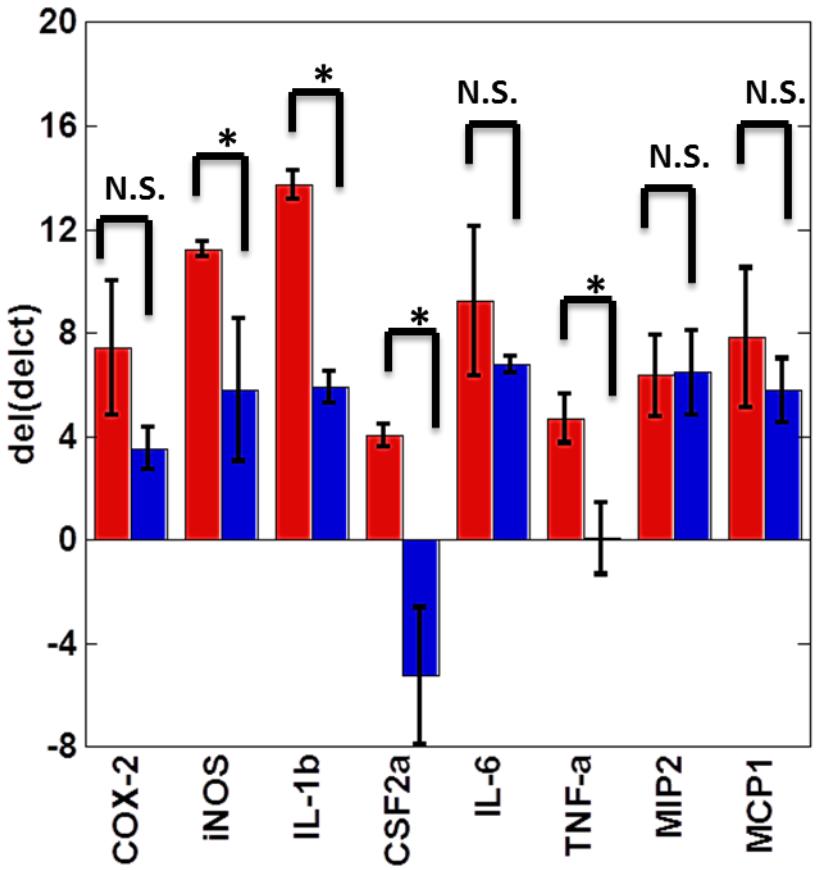

Figure 4.23. Effect of MyD88 knockdown on pro-inflammatory genes upregulation. Ribosomal protein L4 (RPL4) was used as the house keeping gene and the ΔΔct values are calculated with respect to the gene expression at time 0. (Representation of two independent experiments, *P<0.01, N.S.: Not significant).

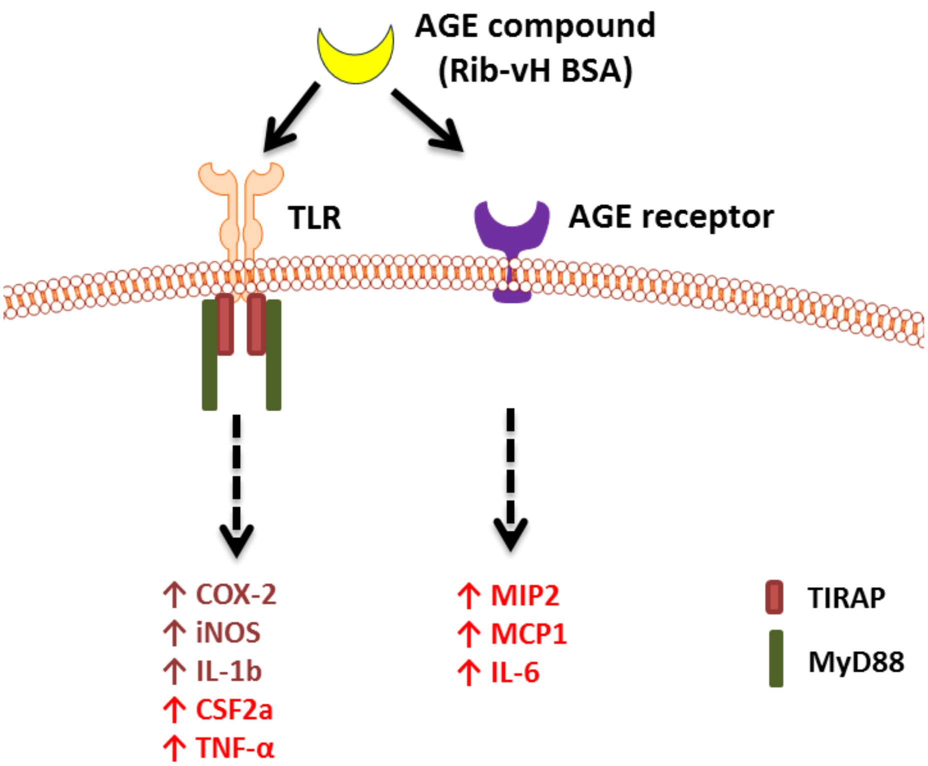

Figure 4.24. TLR dependent AGE signaling in RAW 264.7 cells.
AGE dependent TLR signaling was determined by MyD88 knockdown. On knockdown the expression of TNF-α and CSF2a completely decreased (red). A decrease was also observed in the expression of COX-2, iNOS and IL-1b. No decrease was observed in the expression of MIP2, MCP1 and IL-6 suggesting a TLR independent pathway.

Endotoxin contamination of AGE compounds

Endotoxins interfere with the signaling as they are recognized by pattern recognition receptors and can trigger inflammation. The level of endotoxins in the AGE compounds was determined using the Pierce LAL Chromogenic Endotoxin Quantitation Kit (Life Technologies ®). We observe a significant contamination of the AGE compounds with endotoxins. The Rib-vH BSA has an endotoxin content of around 709.08±16.3 EU/mg and the endotoxin content of unmodified BSA was 719±52.4 EU/mg (Figure 4.25). This means that the endotoxin contamination of the Rib-vH BSA comes from the BSA used for glycation.

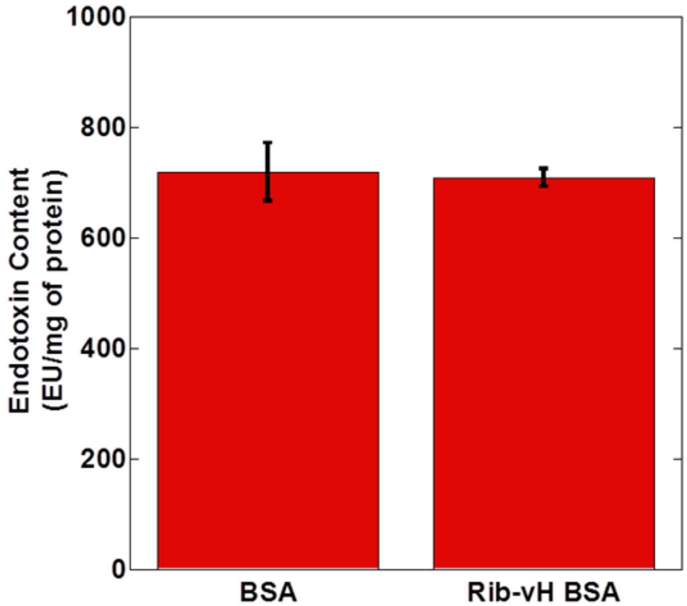

Figure 4.25. Endotoxin content in the unmodified BSA and Rib-vH BSA. (Representation of two independent experiments).

The endotoxin was removed by phase separation using nonionic polyoxyethylene surfactant Triton X-114. On treatment with Triton X-114 Rib-vH BSA was >98% endotoxin free after two steps of purification. However, when the RAW 264.7 cells were treated with 1mg/mL of detoxified Rib-vH BSA the mitogenic affects disappeared (Figure 4.27, represented as Rib-vH BSA E.F). This result is in agreement with a previously reported paper, where the detoxification of glycolaldehyde modified β-lactoglobulin with Triton X-114 led to the loss of activity in human lung epithelial cell line, Beas2b[446]. The authors concluded that the glycolaldehyde modified β-lactoglobulin is benign and the cellular effects are due to the LPS. We wanted to get a better insight into the loss of activity of the Rib-vH BSA detoxified with Triton X-114 and confirm if the possible endotoxin contamination is what which leads to the cellular activity or if the Triton X-114 modified the protein structure which led to the loss of activity. Dynamic light scattering experiments were performed to determine the particle size distribution of the Rib-vH BSA. The hydrodynamic radius of Rib-vH BSA is 8.72±0.10 with a polydispersity index of 0.31±0.008 and on treatment with Triton X-114 the hydrodynamic radius increased two fold to

17.6±0.52 with a polydispersity index of 0.27±0.003. The size versus percentage intensity plots reveal that Rib-vH BSA has two peaks and whereas on treatment with the Triton X-114 only one peak was observed (Figure 4.26). This suggests that Triton X-114 treatment induced a biophysical change in the protein. We suspect this could be the reason for the loss of activity. In order to obtain further insights, Rib-vH BSA was detoxified by chromatographic methods. We use the Detoxi-Gel endotoxin removing columns ™ (Thermo- Scientific) which uses Polymixin B ligand immobilized on beaded affinity resin to bind and extract endotoxins from antibody or protein samples as this is milder method when compared to the Triton X-114 extraction. When the Rib-vH BSA was passed through the column the entire colored i.e. glycated fraction of the AGE compound bound to the column and we could not elute this fraction even under extremely basic conditions. This also led to a considerable loss of the protein. We could not determine the reason why the AGE compound could not be eluted out of the column.

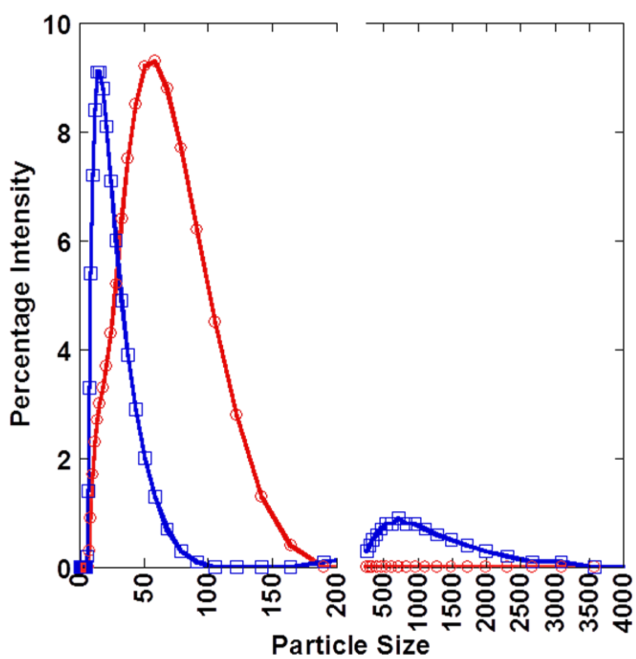

Figure 4.26. Effect of Triton X-114 on the particle size of Rib-vH BSA.
Blue: Rib-vH BSA and Red: Rib-vH BSA treated with Triton X-114 (Representation of 10 independent experiments).

In order to further address the role of possible endotoxin contamination in AGE-induced cellular effects. We performed the proliferation assay by treating the cells with equal amounts of LPS (72 ng) and no effect was observed with LPS alone. We also pre-mixed 1mg/mL detoxified Rib-vH BSA (Rib-vH BSA E.F.) with LPS (72 ng) and the cell were treated with this material for 24 hours. No increase in cellular proliferation was observed. And finally, we treated the Rib-vH BSA for 5 minutes at 100 °C before adding to RAW 264.7 cells as described earlier[447]. As shown in Figure 4.23, heated Rib-vH BSA also failed to induce any proliferation suggesting that the endotoxin contamination does not play a role in the mitogenic effect of Rib-vH BSA. And all the experiments were performed with BSA as the control to rule out any possible effect from the endotoxin. The MyD88 knockdown also suggests that pro-inflammatory effect of Rib-vH BSA is independent of the endotoxin contamination.

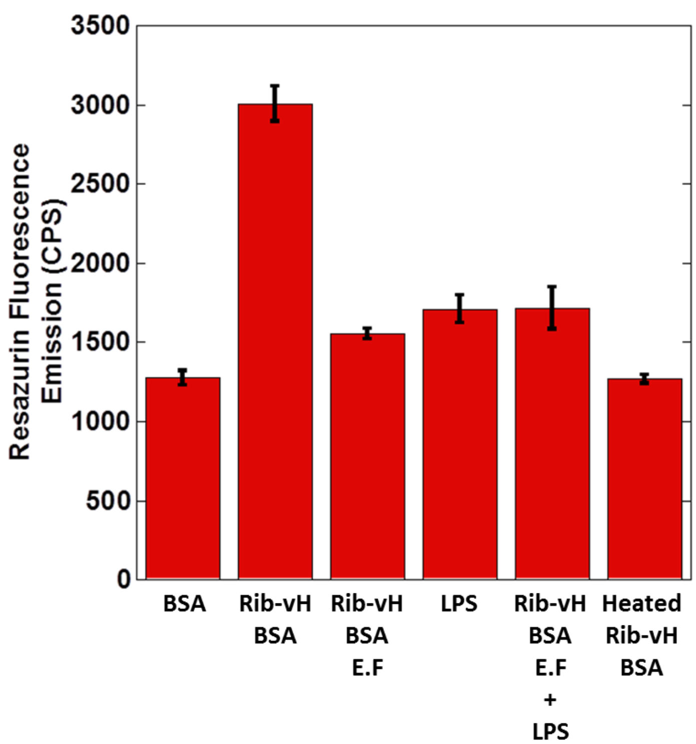

Figure 4.27. Rib-vH BSA induced macrophage cell proliferation is LPS independent. (Representation of two independent experiments, n=6 for each experiment).

Conclusions

The goal of this study was understand the uptake and internalization of AGE compounds and their role in pro-inflammatory cytokine release and macrophage proliferation. Based on our previous studies we used Rib-vH BSA as a model for diabetic AGE compounds to study the effects of AGE compounds in a murine macrophage cell line RAW 264.7.

A rapid uptake of the Rib-vH BSA was observed by the fluorescence based uptake assay and the Rib-vH BSA internalized into the lysosomes after an hour of incubation. We tested the role of AGE receptors RAGE, galectin-3 and SR-A in AGE uptake however, the receptor responsible for Rib-vH BSA uptake could not be established by knockdown studies such as the SR-A knockdown or by using specific receptor inhibitors to inhibit the binding of AGE to RAGE and galectin-3 and requires further investigation. The internalization of Rib-vH BSA led to an upregulation of genes associated with increased oxidative stress such as the NADPH oxidase 2 and hypoxia inducing factor-α and also led to the increased ROS production. The oxidative stress triggered NFκB activity in the RAW 264.7 cells. The Rib-vH BSA treatment also triggered the upregulation of pro-inflammatory cytokines such as IL-1β, IL-6 and TNF-α mRNA. The upregulation of inflammatory genes such as MIP-2, MCP-1, COX-2, CSF2R and iNOS was also observed indicating that the Rib-vH BSA internalization led to the activation of the macrophages and polarized them into "M1-like" inflammatory macrophages.

The Rib-vH BSA also had a mitogenic effect on the macrophages, a 1.46±0.06 fold increase in the macrophage proliferation was observed on Rib-vH BSA treatment after 24 hours. Upregulation of the proliferation marker KI67 was also observed.

The upregulation of several cell surface receptors such as AGE receptor complex, class A scavenging receptors and TLRs was observed on Rib-vH BSA treatment. The role of RAGE could not be established in the Rib-vH BSA induced cellular effects in macrophages. Our q RT-PCR data suggest a role of the TLRs in Rib-vH BSA induced effects. Figure 4.28 summarizes the AGE compound signaling in RAW 264.7 cells.

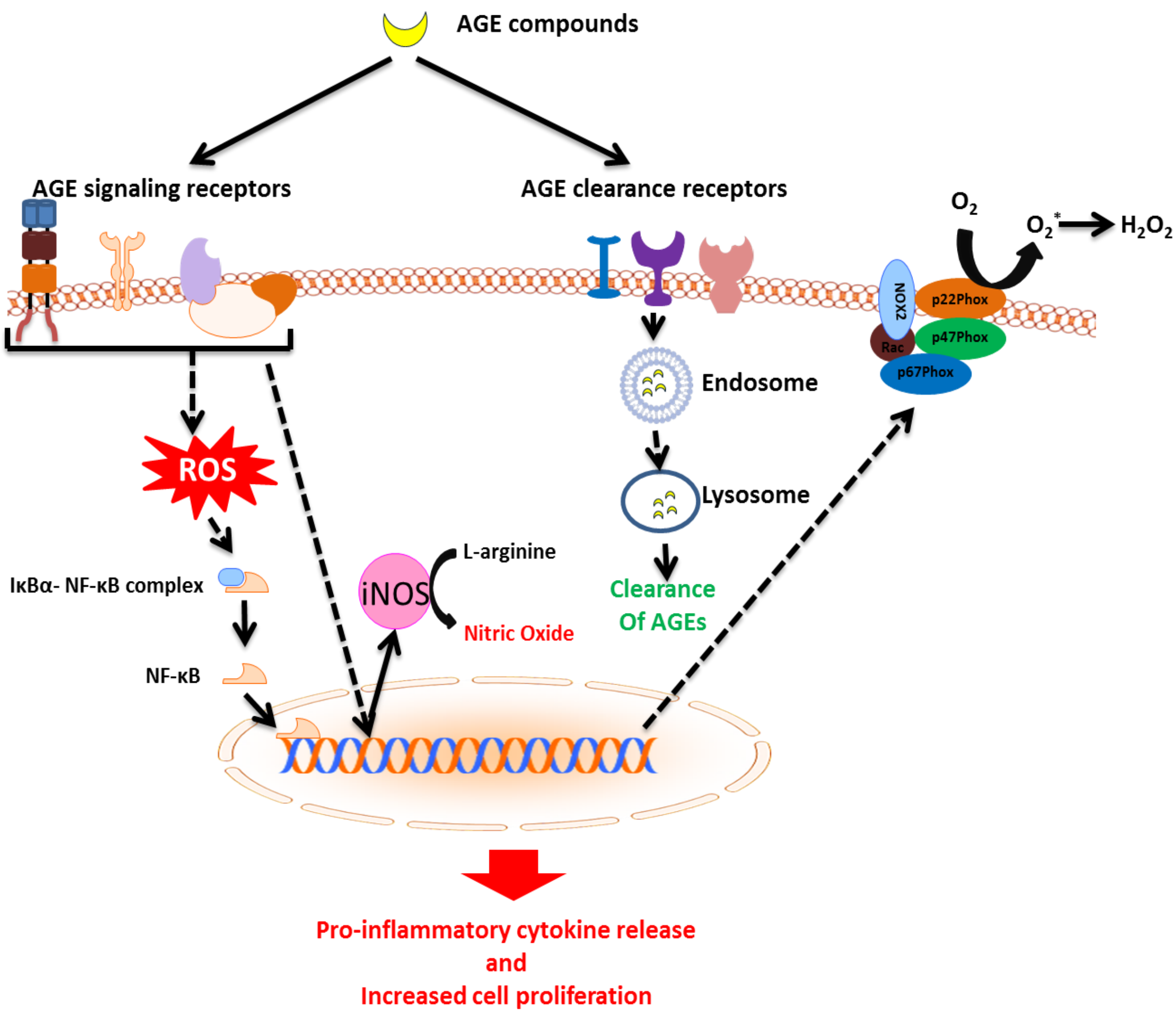

Figure 4.28. AGE dependent signaling in RAW 264.7 cells.
AGE compounds interact with AGE signaling receptors such as RAGE and AGE-receptor complex to trigger ROS formation which can in-turn trigger NF-κB activation. NF-κB is translocated into the nucleus where it binds to specific DNA sequence to trigger the upregulation of various pro-inflammatory cytokines. The upregulation of NOX2 has also been observed on AGE activation (dashed arrow) which can trigger ROS formation in the intra cellular space. RAGE activation also upregulates the iNOS expression leading the generation of nitric oxide. AGE compounds are cleared by the AGE clearance receptors such as the scavenging receptors. AGE compounds are internalized and degraded by the endosomes and lysosomes respectively.

Endotoxin contamination of the AGE compounds was observed and the endotoxin removal by Triton X-114 modified the biophysical properties of the protein which led to the loss of activity and the endotoxin could not by purified using the polymyxin-B column. Several control experiments were performed with LPS which suggest that the Rib-vH BSA induced effects observed are independent of the endotoxin contamination.

In summary, these results provide us a better understanding on the AGE compound uptake and macrophage activation. Our findings should accelerate our understanding of the biological role of AGE compounds in the pathogenesis of diabetic complications.

CHAPTER 5: THE ROLE OF TRYPTOPHAN RESIDUES OF RAGE FOR V-DOMAIN STABILITY AND S100B BINDING

Introduction

RAGE, RAGE-ligand interaction and disease

The receptor for advanced glycation end products (RAGE) is an immunoglobulin type cell surface receptor sensing damage associated molecular patterns (DAMPs) in stressed and damaged tissues [21, 22]. As described earlier, the ligands of RAGE are structurally diverse and include advanced glycation end products (AGE), for which the receptor is named, members of the S100 protein family, high mobility group box protein (HMGB1), nucleic acids, phospholipids, negatively charged polysaccharides, as well as amyloid peptides [1-3, 15, 16 17-20]. A significant body of cell biological and preclinical animal studies have identified RAGE activation as an important contributing factor to diabetic vascular complications [52, 53], neurodegeneration [50, 51], chronic inflammatory diseases [46, 47] and certain cancers [54]. Animal studies provide strong support for the hypothesis that RAGE inhibition could be beneficial to the treatment of these diseases (Described in detail in Chapter 1).

Despite the recognition of RAGE as a disease relevant receptor protein and as a potential pharmacological target, fundamental mechanistic questions regarding ligand recognition and induction of ligand specific signaling by RAGE remain unanswered. In particular, it remains unknown how RAGE can on the one side recognize structurally unrelated ligands, such as S100 proteins, AGE compounds and amyloid beta peptide, and on the other side demonstrate exquisite ligand specificity. RAGE cannot only distinguish between individual members of the S100 protein family [448], but also activate distinct cellular signaling pathways as a function of ligand concentration.

The extracellular portion of RAGE consists of three Ig-like domains, a single pass transmembrane helix and a C-terminal intracellular tail [1-3] . The majority of RAGE ligands have been shown to interact with the V-domain, but some appear to also be able to bind to the C1 and C2 domains. The mechanism(s) by which ligand binding leads to intracellular signaling via RAGE are generally believed to involve the multimerization of the receptor, followed by rearrangement of the C-terminal tail and subsequent exchange or recruitment of intracellular signaling proteins [449].

The observation that most RAGE ligands bind to the V-domain raises the question if structural adaptation by either the RAGE V-domain or the bound ligand facilitates RAGE: ligand complex formation.

S100 proteins and RAGE

The S100 protein type RAGE ligands are small, single domain, calcium-binding proteins that form conformationally rigid homo- and hetero-dimers [198]. The calcium concentration in the extracellular milieu is sufficiently high to saturate the calcium-binding sites of S100B, thus locking the protein into a stable conformation. Higher order oligomers (tetramers [450], hexamers [451] and octamers [452] can also be formed by the calcium-loaded forms of S100 proteins. Binding of zinc, copper and manganese to additional metal binding site in some S100 proteins may allow additional conformations [198, 453, 454].

In contrast to the stable folding of the S100 proteins, the V-domain of RAGE is less stable and displays more structural flexibility. This is reflected in multiple NMR and X-ray structures of the V-domain, that show significant differences on local secondary structure, domain organization and loop arrangements [197, 455, 456].

It has also been pointed out that many RAGE ligands, including the S100 protein ligands, are negatively charged, while the VC1-domain of RAGE contains a positively charged surface [449]. Thus, electrostatic interactions have been suggested as a major driving force for RAGE-ligand interactions[449]. However, simple charge complementarity may be not sufficient to explain the low micromolar binding affinity of different S100 proteins to the RAGE V-domain and suggests that structural changes within the V-domain facilitate multi-modal S100 protein binding to RAGE.

These observations suggest that structural changes in the V-domain are enabling the multi-ligand binding properties of RAGE. Understanding those structural changes in the RAGE V-domain should be useful for understanding mechanistic aspects of RAGE biology, as well for the development of ligand specific RAGE inhibitors.

Tryptophan residues and RAGE

Tryptophan (Trp) is the largest of the naturally occurring amino acids, which has an indole ring that accounts for its hydrophobicity. The high electron density of the aromatic ring results in the energetically favorable cation-[pi] interactions [457, 458]. It can also form hydrogen bonds due to the dipole moment of the nitrogen atom in the indole ring [459]. Trp is fluorescent with high a quantum yield and more importantly its fluorescence properties like emission, quantum yield and quenching depends on its position in the protein and its surrounding environment, which makes it a good probe of the protein conformation [460, 461]. The environmental sensitivity of Trp fluorescence intensity is due to non-radioactive processes like inter system crossing, solvent quenching, excited-state proton transfer and excited-state electron transfer, which compete with emission for deactivation of excited state [460] . Lastly, it has also been reported that the Trp residues are enriched in the binding hotspots of protein interfaces than any other amino acid indicating that Trp plays an important role in the stability of protein complexes [462]. Trp is the least abundant amino acid in proteins [463]. However, the V-domain contains three Trp residues and these residues occur within a stretch of 21 amino acids (Trp51, Trp61 and Trp72). These residues could function as hydrophobic anchor residues for the binding of S100B and other S100 proteins.

We hypothesized that the Trp residues in the V domain of RAGE are necessary of domain stability and S100B binding.

To investigate these possibilities, we have generated three single, three double and one triple Trp→Ala mutant of the RAGE V-domain and characterized folding and stability of the recombinant domains. Our spectroscopic studies identify the relative location of each Trp residues within the V-domain and V-domain: S100B complex and its contribution to V-domain folding and stability. To gain further insights at the atomic level in the RAGE:S100B interaction, we solved the crystal structures of S100B in complex with peptide Trp61[464] and in complex with Trp72, which were derived from the RAGE V-domain and contain Trp61 and Trp72 respectively as a central residue.

Materials and Methods

The crystallization of the S100B and the Trp containing RAGE peptides and their structure solutions were performed by Jaime Jensen and Dr. Christopher Colbert.

Protein mutagenesis, expression and purification

The V-domain of RAGE (residues 23 – 132) was cloned into the pET15b expression vector using the NcoI and XhoI restriction sites. Site-specific mutation of tryptophan to alanine was achieved using the quick change site specific mutagenesis kit (Stratagene, La Jolla). The plasmids' regions encoding the RAGE domain genes were sequenced to confirm correct mutagenesis and sequence integrity.

Proteins were expressed in the disulfide isomerase (DsbC) expressing *E.coli* strain Shuffle T7 Express (New England Biolabs) in LB medium. The plasmid (1 µL) was inserted into electro-competent Shuffle T7 Express cells (100 µL) by electroporation at 1600 V. The cells were expanded in Luria-Bertani (L.B.) media containing the selection antibiotic ampicillin. The cells were grown in 400 mL media in 2 L culture flasks at 37 °C with continuous shaking at 220 rpm. The cells were induced with 100mM IPTG after they have reached an OD_{600} of 0.6. After induction the temperature was reduced to 30 °C, the cells were grown for 4 hours and harvested by centrifugation at 4000rpm. The cells from 4 liter culture were suspended in a buffer containing 50mM Tris, 20mM Imidazole, 300mM NaCl, pH-8.0 and frozen at -20 °C.

For purification, the cells expressing V domain were thawed on ice and sonicated with a power of 15 (Misonix XL-2000). The cell debris was separated by centrifugation at 16000 RCF at 4 °C and the supernatant was collected. The protein was purified from the supernatant by a two-step process. First, using a pre-packed 1mL HisTrap HP column (GE Lifesciences) the His-tagged RAGE VC1 was purified. The bound RAGE-VC1 was eluted using 50mM Tris, 200mM Imidazole, 300mM NaCl, pH-8.0. Protein elution was detected by 280 nm UV absorbance at 1 second intervals. The eluted protein was collected and diluted (1:1) using 10mM Na-acetate buffer, pH 5.5. We then used the pre packed HiTrap SP FF column (GE Lifesciences) which contains the cation sulfopropyl to separate out the DNA bound to the protein. The bound protein was eluted from the column using a linear gradient of NaCl from 0 M to 1 M in the 10 mM Na-acatate buffer, pH 5.5. The eluted protein was collected, concentrated by ultra-filtration using regenerated cellulose 3 KDa MWCO membrane (Millipore), aliquoted and stored at -80 °C. The purity of the protein was estimated by sodium dodecyl sulfate polyacrylamide gel electrophoresis (SDS-PAGE).

Recombinant human S100B was expressed in the plasmid pGEMEX and was purified as described by Smith et al. [465]. Briefly, S100B was expressed in the BL-21 E. Coli cells and were grown at 37 °C overnight. The cells were harvested as described above and resuspended in 50 mM Tris, 5 mM $MgCl_2$, pH 8.0 and frozen. The cells were sonicated on ice and centrifuged at 10,000 g to remove the cell debris. Ammonium sulfate was added to a final saturation of 90% and the pH was adjusted to 8 and was stirred on ice for 30 min. The sample was then centrifuged at 10,000 g. The supernatant was collected and the pH was reduced to 4 with 10% H_3PO_4. The sample was then centrifuged at 10000 g and the pellet was collected and dissolved in 50mM Tris 1 mM EDTA and again centrifuged at 10,000 g to remove any insoluble materials. The sample was then dialyzed against 25 mM Tris, 1 mM EDTA and 5 mM BME. pH 7.6. The sample was then loaded on a Q-Sepharose column and eluted with a linear gradient of buffer B containing 1M NaCl. The fraction which contain protein was pooled and then loaded on the phenyl Sepharose column. S100B was eluted with a step gradient of buffer B containing 50 mM Tris 2 mM EDTA, pH 7.7.

Peptide synthesis

(Peptides were synthesized by Kevin P. Cunningham and titration experiments were performed by Timothy Logue at Florida Atlantic University University)

Peptides (Table 5.1) were synthesized using standard solid phase peptide synthesis with Fmoc-protection and HBTU/HOBt activation chemistry. The dansyl fluorophore was coupled to a C-terminal gamma-amino butyric acid (γAbu) spacer by reaction with dansyl-chloride in dichloromethane / methanol and triethylamine as base. Peptide were cleaved off the resin and side chains deprotected with 95% trifluoroacetic acid, 2.5% triisopropyl silane and 2.5% water. The crude peptides were further purified by preparative HPLC to single peak purity on an analytical HPLC column. MALDI-TOF mass spectrometry was used to confirm the expected molecular of the peptides.

Table 5.1. RAGE peptides in the study.

Peptide	Sequence
51 Trp	KPPQRLE**W**KLNTGRT
61 Trp	NTGRTEA**W**KVLSPQG
72 Trp	SPQGGGP**W**DSVARVL
51 Ala	KPPQRLE**A**KLNTGRT
61 Ala	NTGRTEA**A**KVLSPQG
72 Ala	SPQGGGP**A**DSVARVL

Steady state fluorescence measurements

Steady state excitation and emission spectra were recorded on a FluoroMax® (Horiba Jvon Yvon) spectrofluorometer using quartz cuvettes of either 5 mm or 10 mm path length. Tryptophan was excited at 295 nm to eliminate the tyrosine excitation. Three scans were recorded and averaged.

Fluorescence life-time measurements

Time resolved tryptophan fluorescence lifetime measurements of the V domain of RAGE and its mutants were determined using the photon counting fluorohub® (Horiba Jobin Yvon) connected to Fluoromax®. The samples were excited at 280nm with a nano LED. The emission was recorded at 350 nm and 375 nm to reduce the tyrosine influence. Peak saturation was set to 1000 counts and 4 nm slit width was used for the measurements. For fluorescence decay experiments 1μM of the protein was used in a quartz cuvette with reduced path length of 5 nm to record the tryptophan lifetime. The effect of S100B binding on fluorescence lifetimes of the mutants was also studied. S100B was mixed with V domains in the presence of 2 mM calcium and the lifetimes were measured after an equilibration period of 2 min. To study the affect the Guanidinium chloride (GudCl) unfolding on the decay times, the protein samples were unfolded with 5 M GudCl overnight and the lifetimes of the samples were measured. The lifetimes of the samples were analyzed by the DAS6 software (Horiba Jvon Yvon). A two exponential model was used to determine the lifetimes of the WT, single mutants and double mutants.

Fluorescence quenching

Acrylamide quenching of tryptophan fluorescence measurements were performed with a protein concentration of 1 µM and increasing acrylamide concentrations up to 0.25 M. A quartz cuvette with 5mm path length was used. A correction factor of ε_{295}=0.25 $M^{-1}cm^{-1}$ was applied to account for the inner filter effect of acrylamide [466]. The samples were excited at 295nm and the emission spectra were recorded.

Fluorescence based S100B: V-domain binding measurements

S100B was labelled with fluorescein isothiocyanate (FITC) and the binding affinity between S100B and the wild type and all the mutants of the RAGE V-domain was determined by measuring the change in fluorescence polarization as a function of V-domain concentration. The V-domain was titrated into a solution of fluorescein-labeled S100B (1 mM) in 30mM Tris pH 7.1, 300 mM NaCl, 2 mM $CaCl_2$ and fluorescence polarization was calculated with an excitation wavelength of 494nm and an emission wavelength of 518 nm. Titrations were repeated in triplicates and the best fit for the titration curves was obtained using a 1:1 RAGE:S100B stoichiometry model as described by Andersen et al. [172] and Vetter et al. [467].

The binding of RAGE V-domain derived peptides to S100B was measured by fluorescence titration using a dansyl labeled peptide, similar to as described above.

Secondary structure analysis by circular dichroism (CD) spectroscopy

The role of tryptophan residues in the structural stability of the V domain was evaluated by CD spectroscopy. The spectra were recorded on a Jasco J815 spectropolarimeter equipped with a PFD-425S Peltier cell holder in a 1 mm path length cuvette. 25 µM of protein was used to record the spectra. The samples were scanned from 180 nm to 260 nm with a scanning rate of 10 nm per minute and an integration time of 8 sec. CD-spectra were deconvoluted using spectral data ranging from 180 to 260 nm using the CONTIN algorithm in the DichroWeb software[170].

Crystallization of S100B with the W61 and W72 peptides

(Experiment performed by Jaime Jensen)

S100B in 25 mM Tris HCl pH 7.8, 150 mM NaCl, 4mM $CaCl_2$ was concentrated by centrifugation to 50 mg/mL. For co-crystallization of S100B and W61, 2 mM S100B was combined with 2 mM W61 peptide and stored on ice for 30 min prior to crystallization-tray setup. Crystallization trials were performed via the sitting-drop vapor-diffusion method by mixing 0.75 µl drops of S100B–W61 peptide with 0.75 µl reservoir solution consisting of 0.1 M sodium cacodylate pH 6.8, 25%(w/v) PEG 3350, 9 mM CaCl2 and incubating at 20C against 500 ml reservoir solution. Crystals were observed within one week, and were harvested and flash cooled in liquid nitrogen using reservoir solution plus 20 %(v/v) glycerol as a cryoprotectant prior to diffraction experiments.

For S100B-W72 Lyophilized peptide W72 was resuspended in water to 8 mM, respectively. For co-crystallization of S100B and W72, 2 mM S100B was combined with 3 mM peptide and stored on ice for ~ 30 min prior to crystallization tray set-up. Crystallization trials were performed by the sitting drop diffusion method by mixing 0.75 µL drops of protein-peptide with 0.75 µL of the 500 µL reservoir. Diffracting crystals were obtained with 0.1 M cacodylate pH 6.8, 22% w/v PEG 3350, 5 mM $CaCl_2$ for W72 (3 mM) and 0.1 M cacodylate pH 6.8, 25% w/v PEG 3350, 9 mM $CaCl_2$ for W61 (2 mM). Crystals were observed within 1 week at 20°C, and were immersed in cryo-protectant solution and flash-frozen in liquid nitrogen prior to data collection. The cryo-protectant solution contained reservoir solution of the respective crystals plus 20% v/v glycerol.

Crystal structure determination of S100B-W61 RAGE peptide and S100B-W72 RAGE peptide complexes

(Structures were solved by Jaime Jensen and Dr. Christopher Colbert)

Diffraction data were collected under cryogenic conditions (100 K). The high-resolution diffraction data used for refinement were collected at a wavelength of 0.9792 Å on NE-CAT beamline 24-ID-C of the Advanced Photon Source (APS), Argonne, Illinois, USA. The S100B structures were determined using the molecular replacement method and the peptides were built into the electron density

Atomic models and structure factors have been deposited in the Protein Data Bank as PDB entry 4XYN for S100B-W61 RAGE peptide complex and PDB entry 5D7F for S100B-W72 RAGE peptide complex.

Sensitivity of V-domain mutants to trypsin digestion

The V-domains were prepared to a final concentration of 500 µg/mL in 100 mM Tris buffer pH-7.5. Sequencing grade, modified trypsin (Promega) was dissolved in 20 µL of resuspension buffer provided at a concentration of 1 mg/ml and further diluted in 100 mM Tris buffer pH-7.5. The V-domain and the trypsin solutions were mixed 1:1 to reach a final V-domain: trypsin ration of 50,000:1. The reaction was incubated at 37 °C and 20 µL samples were collected at time points 0, 10, 20, 30, 45, 60, 120 and 240 minutes. Samples were immediately mixed with SDS-PAGE sample buffer with β-mercaptoethanol, dipped into boiling water for 3-5 min and then stored on ice. Samples from a single digestion experiments were separated on a single 18% SDS-PAGE gel and stained with Coomassie blue. The final developed gels were scanned and the band intensity of the non-digested material was quantified with the ImageJ software package [468].

Thermofluor assay to determine protein stability

The thermal stability of the V domain Trp mutants was determined using a fluorescent dye called SYPRO orange which binds to the hydrophobic regions of the protein. Briefly, the 5000X stock solution of SYPRO orange (Sigma Aldrich #S5692) was diluted in water to obtain a final concentration of 100X. This 100X solution was further diluted down to 10X in phosphate buffered saline. 5 µM stock solutions of the V domain mutants in 1M ammonium sulfate were prepared. 25 µL of the V domain stock was mixed with 25 µL of the Sypro orange stock. The assay was carried out in the Stratagene Mx3000P ™ qPCR machine. The molecular beacon melting curve program was used and FRROX filter setting were selected. The first segment of the program was set to 25 °C for 3 minutes and in the second segment; starting at 25 °C the sample was heated in 1 °C increments for 30 seconds for 74 cycles. Hence, the protein sample was heated from 25 °C to 99 °C with a rate of 2 °C/min and the fluorescence was measured after 30 sec. The assay was performed as two independent experiments and a new stock of protein was used for each experiment. In each experiment, the sample was run 5 times.

1M ammonium sulfate buffer was selected based on our initial screening. We used the HR2-110 crystal screen (Hampton Research) to screen different buffer conditions to determine the stability of the wild type V domain. We observed that the V domain was not stable in low salt containing buffers. Our data indicate two buffer conditions in which the V domain was the most stable. The V domain was highly stable in 1 M ammonium sulfate and in 0.1M HEPES, pH 7.5 containing 1.4 M sodium citrate tribasic dehydrate. We select 2M ammonium sulfate to perform the assay.

Results

Trp residues are not required for folding of the RAGE V-domain

The mutation of Trp to Ala replaces the large hydrophobic indole ring system of Trp with a single hydrogen in Ala. Depending of the position of the replaced side chain within the folded protein, this can create voids in the packing of protein side chains and may prevent folding of the polypeptide [461, 469-471]. We found that all seven V-domain mutants not only expressed well in *E.coli*, but also folded spontaneously and were recovered from the soluble fraction from NEB T7 SHuffle express cells. This engineered E.coli strain constitutively expresses the disulfide isomerase DsbC and supports the correct formation of a single disulfide bridge within the V-domain between residues Cys38 and Cys99.

Detailed characterization of the secondary structure composition of the purified V-domain and its mutants was done by circular dichroism spectrometry (Table 1). Our analysis of CD-spectra of wild type V-domain showed that approximately one third (32%) of all residues are in beta-sheet conformation, one third (36%) of residues are unordered, 22% are in turn conformation and 10% in a helical conformation. These values are comparable to a previous report of the CD secondary structure analysis of the V-domain, in which a beta-sheet content of 33 % and coil content of 35.2% was reported [472]. The secondary structure analysis of the published NMR structure of the V-domain (pdb: E2E5) using the program Stride [473] resulted in similar values as well (37% beta-sheet, 27% turn, 28% coil, and 8% helical). Substitution of any one of the three Trp residues had no major effect on the secondary structure composition. We found a slight increase in beta-sheet content, accompanied by a reduction of amino acids in helical, unordered or turn conformations. Statistical comparison between the wild-type V-domain and the single substitution mutants showed that these changes were statistically significant ($p<0.05$) only for alpha-helical and beta-sheet content for the Trp51Ala substitution. Similar trends were seen for the double mutants, which all had statistically significantly ($p<0.05$) decreased helical content, but only the W51A W61A double mutant also showed a significant increase in beta-sheet secondary structure (Table 5.2). The triple mutant, containing no Trp residues , showed the highest beta-sheet (40%) and lowest helical content (4%).

These data show that the Trp residues are not required for folding of the V-domain to occur and that the absence or presence of Trp residues has only a limited effect of the overall secondary structure of the V-domain.

In general, the dominant secondary structure elements of the V-domain and its Trp→Ala mutants, are beta-sheets and turns, with a minor alpha helical content and a significant number of residues in an unordered conformation. This is in agreement with the overall IgG fold and the known structure of the V-domain. The finding that the Trp residues are not required by the domain to adopt its fold, indicate that they are not critically involved on the folding process of the domain itself, nor are they required to maintain the overall fold. On the other side, about one third of all residues are in an unordered conformation, indicating a high degree of plasticity in the structure.

Table 5.2. Secondary structure analysis of the V domain mutants by circular dichroism.

V-domain Mutant	Helix %	β-Sheet %	Turn %	Unordered %
WT	10.1 ± 0.4	32.2 ± 1.2	22.1 ± 0.3	35.6 ± 0.6
W51A	6.6 ± 0.4	39.8 ± 0.6	21.4 ± 1.7	32.2 ± 1.8
W61A	9.6 ± 0.8	37.5 ± 1.3	21.3 ± 0.8	31.6 ± 1.2
W72A	9.3 ± 0.4	38.1 ± 0.3	20.1 ± 0.5	32.5 ± 0.4
W51A W61A	5.0 ± 0.3	39.3 ± 1.3	21.6 ± 0.8	34.1 ± 0.7
W51A W72A	5.4 ± 0.5	38.4 ± 1.6	22.3 ± 0.2	33.9 ± 0.8
W61A W72A	5.5 ± 0.6	37.0 ± 1.9	23.5 ± 0.9	34.0 ± 2.2
W51A W61A W72A	4.0 ± 0.4	40.8 ± 1.0	21.3 ± 0.9	33.9 ± 0.3

Trp→ Ala mutations enhance the stability of the V-domain to proteolytic degradation

We next compared the susceptibility of the mutants to proteolytic degradation by trypsin. Limited proteolytic digestion can be used to assess the folding rigidity and plasticity of proteins and protein complexes [474, 475]. A protein with a tightly packed protein fold and therefore little plasticity exposes fewer potential trypsin cleavage sites on its surface and thus shows slower proteolytic degradation compared to a protein with a loosely folded structure and a high degree of structural plasticity. Because the RAGE V-domain is folded in as a single domain, proteolytic susceptibility will correlate with structural plasticity.

The RAGE V-domain has 15 potential trypsin cleavage sites and we monitored the time-dependent degradation of the V-domains by trypsin by quantifying the disappearance of the full-length protein band by SDS-PAGE. The kinetics of the proteolytic degradation process is complex because of the sequential cleavage at multiple sites within the protein sequence and because cleavage of short peptide sequences close to the N-or C-terminus may not be detected by SDS-PAGE. Our experiment therefore monitored the cleavage of the V-domain in one or multiple position(s) that generated fragments, which could be clearly distinguished from the full-length V-domain by SDS-PAGE. The representation of the trypsin digestion of the wild type, W72A and W51AW61AW72A is shown in Figure 5.1

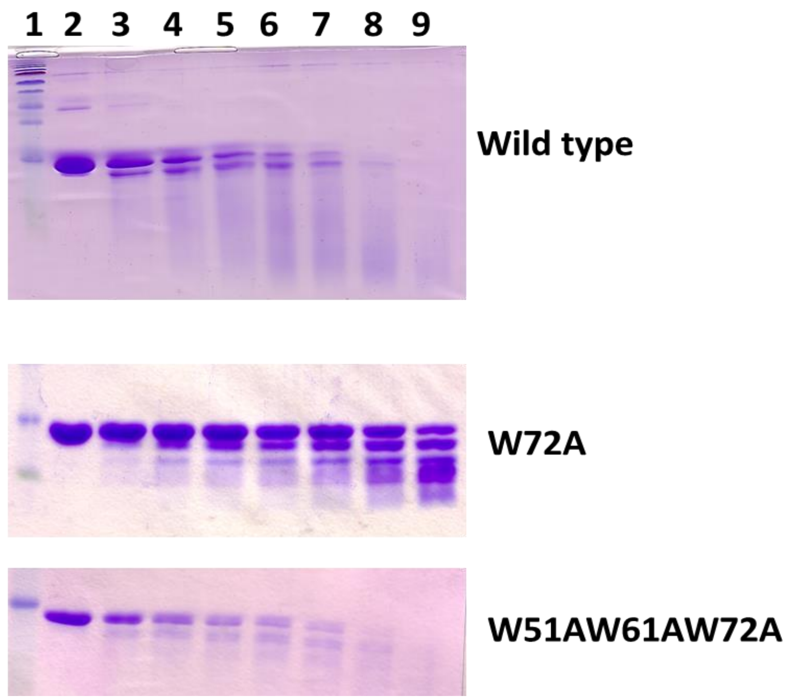

Figure 5.1. Representation of trypsin digestion of the V domain mutants.
1) Ladder 2) 0 min 3) 10 min 4) 20 min 5) 30 min 6) 45 min 7) 60 min 8) 120 min 9) 240 min of trypsin digestion.

The trypsin digestion of the V-domain mutants showed distinct kinetics (Figure 5.2). The wild type V-domain and the mutant domains with two or all three Trp residues substitute by Ala showed degradation kinetics that could be approximated with a first order reaction kinetics.

The wild type V-domain is readily degraded by trypsin with an estimated ($t_{1/2}$ ~ 14.3 min). Interestingly, substitution of one or two Trp residues for Ala decreased the susceptibility to typsin proteolysis of the mutant V-domains. Mutant domain with two Trp→Ala substitution showed similar domain stability with $t_{1/2}$ ranging from about $t_{1/2}$ ~18 to $t_{1/2}$ ~20 min (Table 5.3). The triple Trp mutant in contrast showed the least resistance to trypsin degradation ($t_{1/2}$ ~8 min), suggesting that the removal of all three Trp residues greatly destabilized the domain.

The single Trp mutants showed more complex multi-phasic degradation kinetics. All three mutants appear to be more stable than the wild-type. Enhanced stability was particular evident for the Trp72Ala mutant compared to the wild type domain ($t_{1/2}$ ~31 vs. $t_{1/2}$ ~14 min). The Trp51Ala mutant showed pronounced biphasic proteolysis kinetics, possibly indicating the presence two alternate conformations with distinct proteolytic resistance.

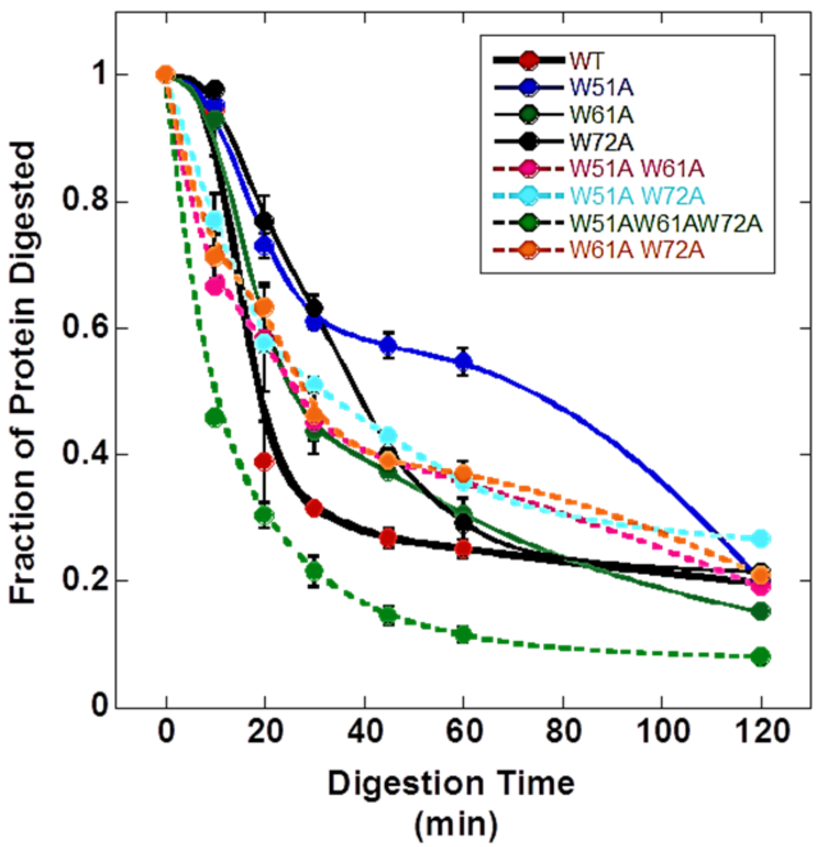

Figure 5.2. The trypsin digestion kinetics of the V domain mutants.

Table 5.3. Trypsin digestion kinetics of the V domain mutants.

Sample	**Rate Constant**	**T ½ (min)**
WT	0.048537	14.3
W51A	0.03303	21.0
W61A	0.030517	22.7
W72A	0.022260	31.1
W51A W61A	0.038225	18.1
W51A W72A	0.038008	18.2
W61A W72A	0.034400	20.2
W51A W61A W72A	0.088396	7.8

The V-domain stability (measured as $t_{1/2}$) could be correlated with the content of helical secondary structure. We found that the individual mutants clustered into defined groups (Figure 5.3). The least stable mutant was found to be the mutant with all three Trp residues replaced by alanine. This mutant was also the mutant with the least helical content (4%). The three mutants, in which two Trp had been replaced showed very similar domain stability among each other and at the same time a significant reduction in helicity by about 50 % compared to the wild-type V-domain (5.0 to 5.5% compared to 10%, $p < 0.03$).

The data suggest that residues Trp 61 and Trp 72 contribute relatively little to the folding of the V-domain, while at the same time increasing the plasticity of the domain. In contrast Trp51, clearly stabilizes the helical component of the folded domain and its mutation to alanine causes shift to a domain fold with increased beta-sheet content.

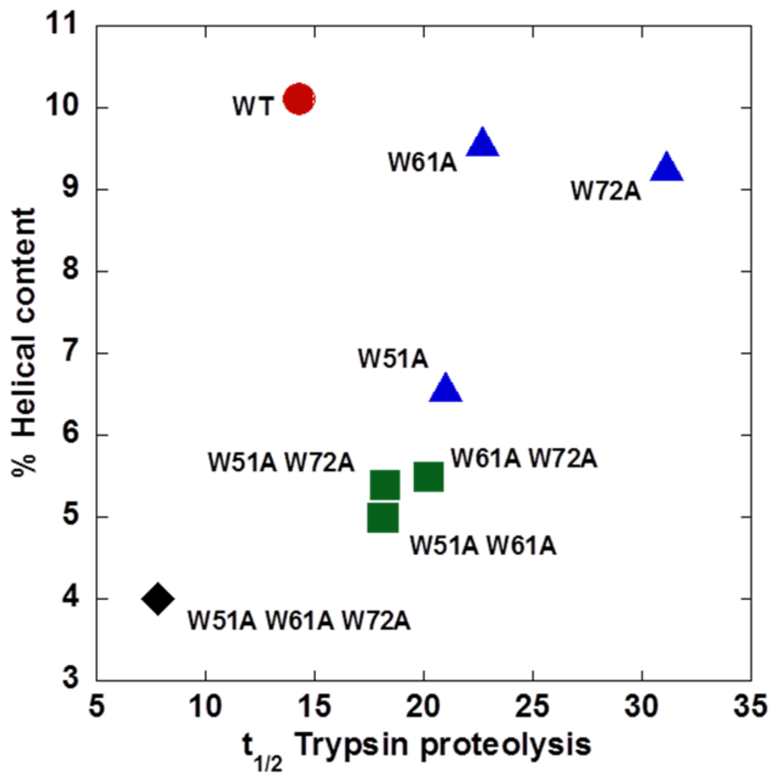

Figure 5.3. Correlation of V domain mutant stability to the α-helical content.

To further rationalize these differences is was important to determine the relative positions of the three Trp residues within the folded V-domain. We used a classical spectroscopic approach exploiting the environmental sensitivity of Trp fluorescence.

Steady state fluorescence data

The fluorescence properties of the tryptophan indole side chain, such as quantum yield, emission spectrum and lifetime are sensitive to its environment [460]. Trp emission maxima can vary from 308 nm to 353 nm in proteins and reflect the interaction of the local environment with the excited state of the indole ring system. In general, hydrophobic environments lead to emission maxima at shorter wavelength, whereas tryptophan residues in a more polar environment have emission maxima at longer wavelengths [476 477]. The observed florescence spectra are the sum of the combined contributions of each of the three Trp residue fluorescence emission and fluorescence quenching. Substitution of individual Trp residues reduces the total number of Trp residues, thus eliminating the contribution of these residues to the observed overall fluorescence spectra. Comparative analysis of the wild-type V-domain and its single and double Trp→Ala substitution mutants allows identifying the relative position of each Trp residue within the folded V-domain.

The steady state fluorescence emission spectra of wild-type V-domain at four different excitation wavelengths (280 nm, 285 nm, 290 nm, 295 nm) show a single peak and no shoulders or other features. The emission scans of the V domain mutants when excited at 295 nm are shown in Figure 5.4 and 5.5. The emission maxima (343 to 344 nm) did not shift with changing excitation wavelengths, showing that the contribution of two Phe and two Tyr residues to the overall fluorescence of the protein is negligible. The WT V-domain has an emission maximum of 344 nm with a half-peak width of 58 nm (Figure 5.4), which is about 8 nm blue shifted compared to free tryptophan in water. This indicates that the Trp residues are partially exposed to water molecules with long dipole relaxation times, typical for water molecules within the hydration shell of the protein.

Similarly, the fluorescence spectra of all Trp→Ala mutants are very similar in terms of emission maxima (342-345 nm) and overall peak shape (Table 5.4). The wavelength of the emission maxima suggest that the three Trp residues of the RAGE V-domain are all in a polarizable environment, but it does not preclude the possibility that the tryptophan rings are partially or completely in the interior of the protein.

Changes in fluorescence intensity under different salt conditions can be associated with changes in fluorescence quenching, either by solvent molecules or by internal Trp fluorescence quenching within the folded protein domain. Comparing the steady state fluorescence properties under low salt (50 mM NaCl) and high salt (300 mM NaCl) did not reveal significant changes in spectral properties, but did show a reduction in reduced fluorescence intensities. The single Trp→Ala mutants clearly show that Trp51 is distinct from Trp 61 and Trp72 (Figure 5.4 and 5.5). Substitution of Trp51 by Ala leads to a much more pronounced decrease in fluorescence intensity than substitution of residues Trp61 or Trp72 and suggests that Trp51 is the least quenched Trp residue of the V-domain. This would agree with the hypothesis that Trp51 is located in the interior of the folded domain and shielded from solvent molecules

The single Trp61Ala mutation has only a minor effect on the overall fluorescence intensity of the V-domain and this can be interpreted as either, demonstrating that Trp61 fluorescence is largely quenched in the wild-type V-domain, or that the Trp61Ala mutation leads to an “unquenching” of the Trp 51 and/or Trp 72 fluorescence and thus compensates for the loss of fluorescence emission by Trp61.

The double Trp→Ala mutants show lower than expected fluorescence intensities, which can be explained by increased fluorescence quenching, compared to the wild-type and the single-Trp mutants. Increased quenching is probably the results of increased solvent exposure of the Trp residues, which in turn indicates increased plasticity of these domain mutants. Data for the double mutants suggest that Trp61 and Trp72 are both equally solvent exposed, whereas Trp51 is in a more solvent shielded, interior, position.

Important additional information can be gained from changes in quantum yield upon mutation of individual residues. Quantum yields of Trp in proteins can vary between 0.4 to close to 0 and several mechanisms can contribute to the quenching of the excited state and lead to low quantum yields. Prominent mechanisms of Trp fluorescence quenching in proteins include radiation less energy transfer to other Trp or His residues, proton transfer from nearby protonated acidic groups or electron transfer to disulfides, amides or the protein backbone. The exact contribution of each of these mechanisms to Trp fluorescence quenching is difficult to assess, but changes in quantum yield are clear indications of changes in the environment of the fluorophore.

Figure 5.4 shows the fluorescence emission spectra for the WT V-domain and the mutants in which a single Trp residue has been replaced. The areas under the spectral curve are directly proportional to the fluorescence intensity and therefore representative of the quantum yields of the individual mutants.

The Trp61Ala mutant has nearly the same fluorescence intensity as the wild type protein, despite the fact that the mutant has only two instead of three Trp residues. Thus, residue Trp61 does not appear to contribute to the overall fluorescence of the WT V-domain. In contrast, mutants Trp51Ala and Trp72Ala show a clearly reduced fluorescence intensity compared to the wild type. Removal of Trp51 does in fact reduce the fluorescence intensity by more than 50% compared to the WT V-domain, which indicates that Trp51 contributes disproportionately to the fluorescence of the WT V-domain. The double mutants, in which only one of three Trp residues is retained, lead to the same conclusion, showing about twice the fluorescence intensity for the mutant containing Trp51 compared to the two mutants lacking Trp51.

As mentioned above, Trp fluorescence can be quenched by multiple mechanisms, one of which is radiation less resonance energy transfer to nearby Trp residues. The RAGE V-domain is small (100 residues) and contains three Trp residues in close proximity. The Forster distances for Trp-Trp resonance energy transfer are between 4 to 16 nm and our analysis of the available NMR and X-ray structures of the RAGE V-domain showed that the three Trp residues are within a distances suitable for quenching. We interpret the observed changes in fluorescence intensities for the V-domain mutants in two different ways: i) either Trp51 and Trp 72 quench each other effectively, or ii) they are only weakly fluorescent due to other quenching mechanisms.

The Trp double mutants contain only a single Trp residue and allow us to further dissect the contribution of the individual residues to the overall fluorescence. As can be seen in Figure 5.5, the mutant that contains only Trp 51 (mutants W61A W72A) shows strong fluorescence exceeding 50% of the intensity of the wild type domain with three Trp residues. In contrast, the mutants with either only Trp 61 (mutant W51A W72A) or Trp 72 (W51A, W61A) have nearly identical fluorescence intensities, but these are about 50% weaker than the fluorescence associated with Trp51. These results suggest the Trp 61 and Trp 72 are weak fluorophores for reasons other than Trp-Trp resonance energy transfer.

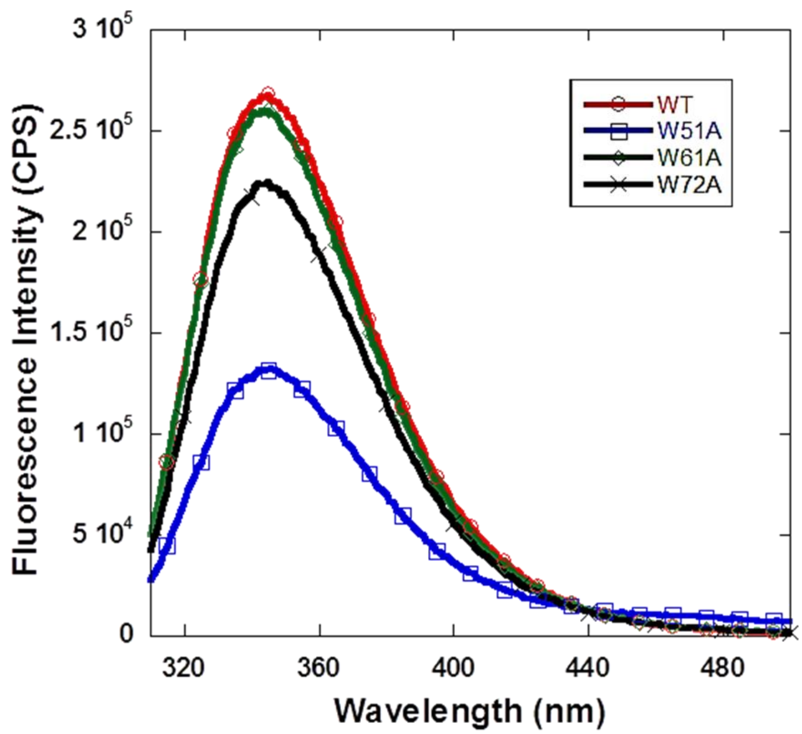

Figure 5.4. Fluorescence emission scans of the V-domain single mutants and the wild type.

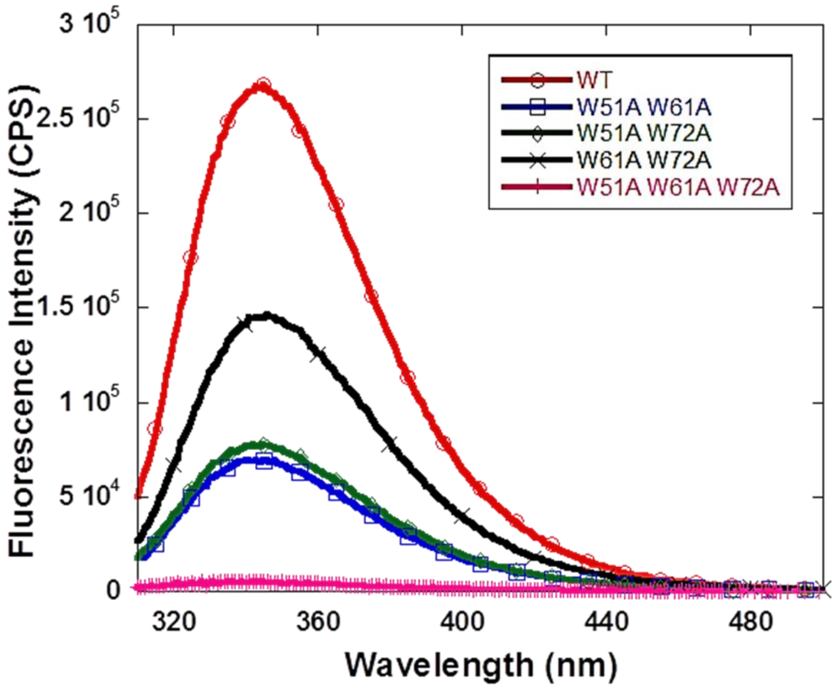

Figure 5.5. Fluorescence emission scans of the V-domain double and triple mutants.

Table 5.4. Fluorescence properties of the V-domain mutants and the V-domain S100B complexes.

V-domain mutant	λmax (Vdom)	λmax (Vdom:S100B)	Δλ (nm)	Ratio FL Intensity (Vdom)/(Vdom:S100B)
WT	344	336	8	1.45
W51A	346	337	9	1.54
W61A	345	334	11	1.11
W72A	345	336	9	1.1
W51A W61A	346	337	9	0.99
W51A W72A	342	336	6	1.30
W61A W72A	346	332	14	2.14

Fluorescence quenching

To directly investigate the solvent exposure of the individual Trp residues we used collision quenching. In this technique, the excited state of the fluorophore is quenched without radiation by direct collision with a quencher. We used acrylamide, as a commonly used quencher. Acrylamide does not readily penetrate into compact folded proteins and consequently Trp residues on the protein surface are more susceptible to quenching then Trp residues in the protein interior [478 479].

Stern-Volmer plots of the quench experiment are shown in Figure 5.6 and we used a modified Stern-Volmer equation to calculate fractional quenching for the individual mutants Figure 5.7. Fractional quenching identifies the fraction of fluorescence that is not quenched and thus can identify residues that are better shielded from quenching within a protein with two or more Trp residues. The interpretation of increased shielding from quenching suggests that these Trp residues are protected from the quencher and thus embedded in the protein's interior. As can be seen from Figure 5.8 only a minor fraction (20-25%) of the total fluorescence is protected from quenching. In the single Trp mutants, the fluorescence originating in residue Trp61is more accessible to the quencher then residues Trp51 and Trp72. This is also seen in the double mutants. The quenchability of fluorescence associated with residues Trp51 and Trp72 appears to be similar in the single mutants, whereas in the double mutant residue Trp51 appears more sensitive to quenching than Trp72. However, it is important to consider that the absolute fluorescence intensity originating from Trp51 is higher than from the other two Trp residues, thus increased sensitivity to the quencher is not unexpected.

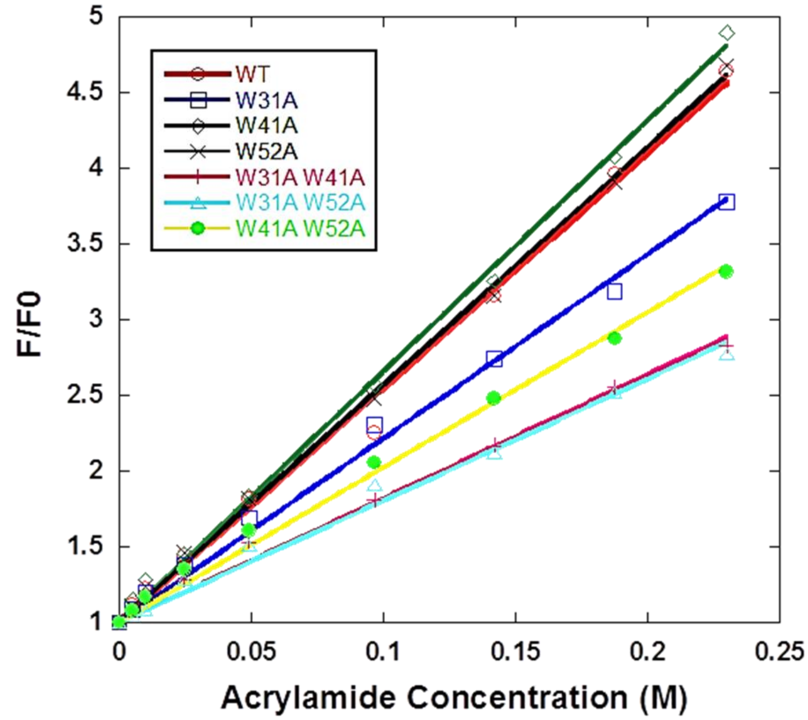

Figure 5.6. Acrylamide quenching of the V-domain mutants.

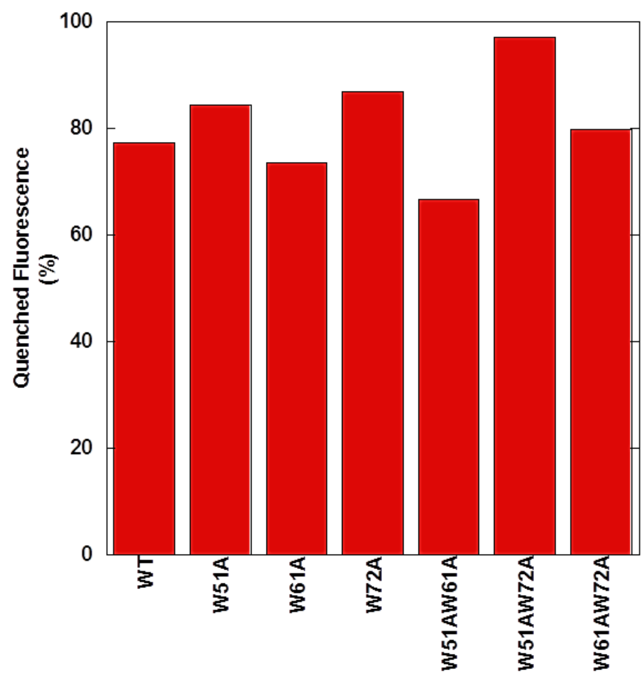

Figure 5.7. Percentage of quenched fluorescence in the V-domain mutants.

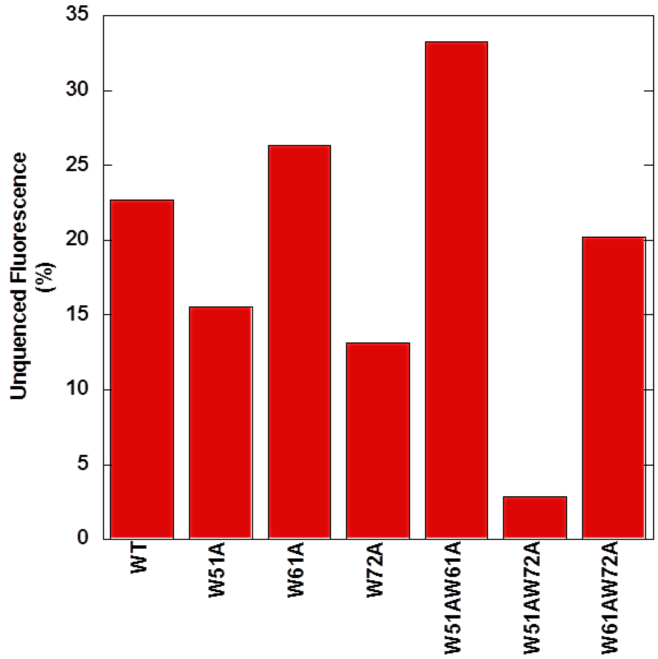

Figure 5.8. Percentage of unquenched fluorescence in the V-domain mutants.

Fluorescence lifetime

The lifetime of tryptophan fluorescence is two exponential in water at pH 7.0, it has lifetimes of 0.5 ns and 3.1ns [480]. The reason for the short and long lifetime components is due to structural heterogeneity in the ground state of tryptophan which exposes the indole ring to different environments. However, the fluorescence decay of tryptophan in proteins is multi exponential and the lifetimes vary widely from 0.014 ns to 9.8 ns even though only one tryptophan is present [480].

The tryptophan lifetime depends on several factors like the environment surrounding the tryptophan residues, its neighboring residues and also the multiple microstates of the protein can add to the heterogeneity of the Trp lifetimes [481]. Thus by studying the Trp lifetimes of the different mutants we aim to understand the microenvironment surrounding these Trp and also their effect on overall structure of the protein.

We measured Trp fluorescence life times for all mutants generated and the wild type under folded conditions and after complete denaturation in 6M guanidinium chloride. The deconvolution and interpretation of Trp fluorescence lifetimes with multiple Trp residues is complex. The time dependent emission intensity traces were analyzed by double-exponential fitting, which yielded the best fitting results among several fitting models evaluated. The double-exponential models yielded a short lifetime component of 2.3 ns and a long life-time component of 6.4 ns in the wild type V-domain. The corresponding amplitudes were 0.33 and 0.67, respectively. These numbers should be interpreted as fitting parameters that reflect the overall combined fluorescence properties of the fluorescent systems. To further simplify the interpretation of the fluorescence lifetime data we used the mean lifetime τ_m for each system. The mean lifetime is the weighted average of the two life times and amplitudes obtained by double exponential fitting [481]. Figure 5.9 shows the mean life times at 350 nm emission wavelength for the wild type V-domain and the six Trp mutants. It is clear that the double mutants, with only a single Trp residue, have short τ_m values of around 3.5 ns. In contrast, the wild type domains with all three tryptophans have a significantly longer τ_m of about 5 ns. For the single Trp mutants, which still have two Trp residues a dependence of τ_m on site of Trp mutation is observed. The Trp51Ala mutant has a significantly shorter τ_m, suggesting that Trp51 contributed a long lived fluorescence component to the system in the wild type domain. The Trp72Ala mutant had an increased τ_m compared to the wild type, suggesting that Trp 72 contributes predominately a short lived component to the wild type system. The lifetime of an excited state depends on many factors and changes in lifetimes reflect changes in the physico-chemical environment of the fluorophore. However, it is often not possible to predict what specific changes in the environment of a fluorophore have caused changes in lifetime. This complicates the interpretation of changes in lifetimes as the results of induced structural changes in a protein as results of mutations or protein-ligand interactions.

We also measured the lifetimes of the domains after denaturation in 6M guanidinium chloride. This was done as a control to show by fluorescence life-time that the Trp residues in the individual domains are indeed in a particular folded state. Under denaturing conditions, the V-domains assume a random coil conformation and the Trp residues are thus all exposed to an identical random environment. Correspondingly, fluorescence τ_m values are nearly identical for all mutants and they were clearly shorter than the τ_m observed in folded domains. Lifetimes of τ_1 <1 ns, and τ_2 ~ 4 to 5 ns were obtained by double exponential fitting of the decay data. These values are very typical for GudCl denatured Trp containing proteins [481].

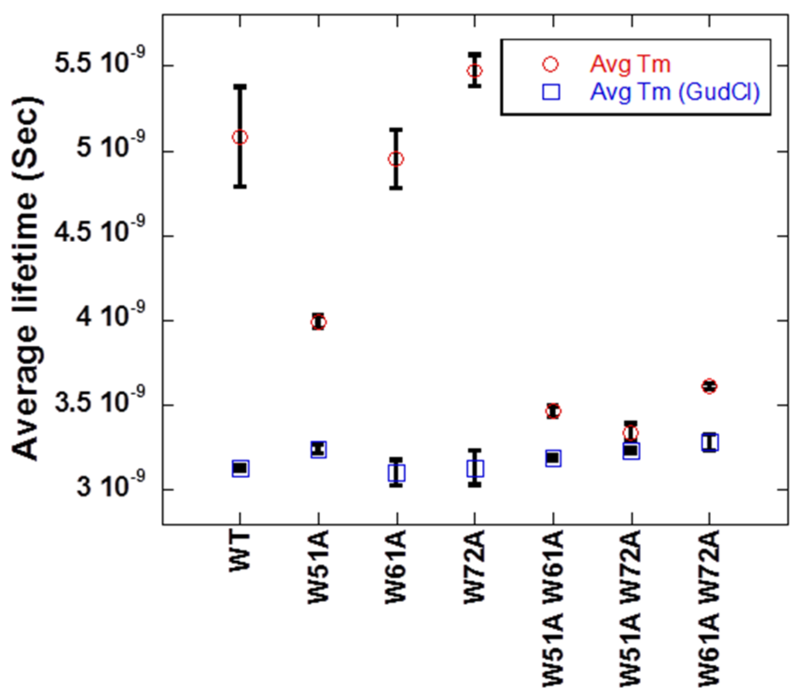

Figure 5.9. Average Trp lifetime of the of the V-domain mutants.
Red: Average τ_m of V-domain mutants, Blue: Average τ_m of the V-domain mutants in the presence of guanidinium chloride.

Figure 5.10 and Table 5.5 also contains lifetimes for the V-domains in the presence of S100B. The binding of S100B will be discussed in more detail below. S100B does not contain a

Trp residue and the observed changes in Trp life-time are exclusively the results of the interaction between the V-domains and S100B. The interpretation of the observed changes in lifetime is not unambiguous. However, the measured lifetimes upon addition of S100B reflect changes in the physico-chemical environment of the Trp fluorophores. A decrease in lifetime does not necessarily mean that a residue becomes more solvent exposed, it can also be the result of repositioning of amino acid that can quench the excited state. Quenching of Trp fluorescence can occur by proton transfer from nearby acid groups, through electron acceptors such as protonated acidic groups, electron transfer to disulfides, amides or the protein backbone, or quenching by other side chains such as Trp (indole side chain), Phe (phenyl side chain), or His (imidazole side chain).

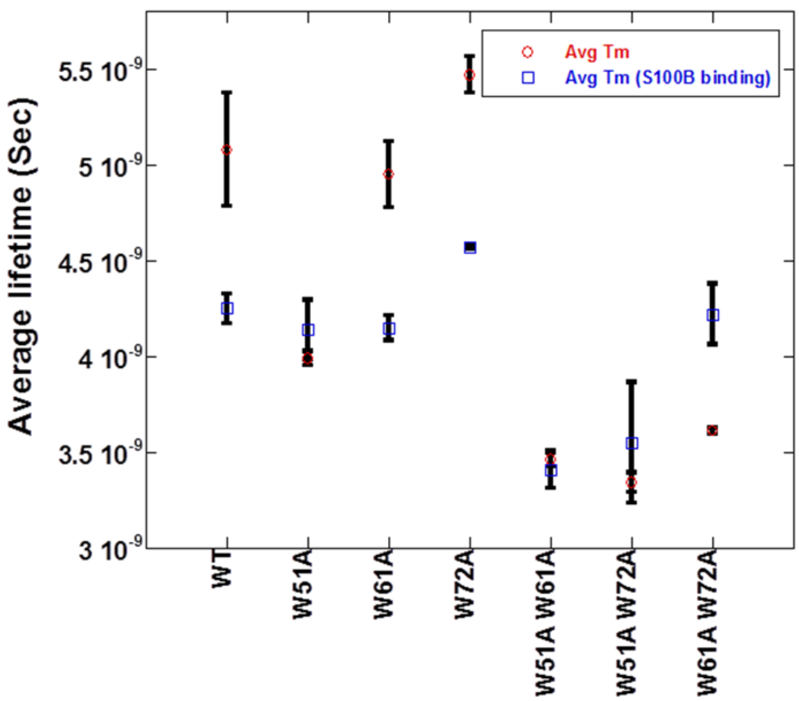

Figure 5.10. Average Trp lifetime of the of the V-domain mutants on S100B binding. Red: Average τ_m of V-domain mutants, Blue: Average τ_m of the V-domain mutants in the presence of S100B.

Table 5.5. Average Trp lifetime of the V-domain mutants.

Sample	K_d (μM)
WT	2.7±0.3
W51A	0.5±0.06
W61A	1.3±0.2
W72A	0.6±0.03
W51A W61A	0.5±0.07
W51A W72A	0.5±0.04
W61A W72A	0.4±0.01
W51AW61A W72A	0.07±0.005

S100B-peptide binding

To further explore the possibility of multiple binding modes between RAGE and S100B, we have measured the binding between S100B and three short V-domain peptides that could be directly involved in the protein: protein interaction. These three peptides containTrp51, Trp61 and Trp72 as central residues and we speculated that the Trp residues could function as hydrophobic anchor residues to S100B. The calcium loaded form of S100B exposes a hydrophobic surface area, which has previously shown to be involved in the binding of S100B binding peptides [492].

We performed binding titrations between dansylated-V domain peptides and S100B. Table 5.6 summarizes calculated binding affinities. From these studies it became apparent that all three peptides did bind to S100B with comparable binding affinities and that the replacement of the Trp residues within the peptides by Ala did not abolish binding affinity. The binding interaction was also sensitive to the ionic strength of the solvent, suggesting a significant contribution of ionic and H-bond interactions to the binding.

Table 5.6. Binding affinities of Trp containing RAGE peptides to S100B.

Peptide	**Low Ionic Condition (20mM NaCl)**	**High Ionic Condition (150mM NaCl)**	**Ca-dependent**
Dns-51Trp	0.6 μM	8 μM	Yes
Dns-51Ala	1 μM	5 μM	Yes
Dns-61Trp	3 μM	14 μM	Yes
Dns-61Ala	4 μM	25 μM	Yes
Dns-72Trp	20 μM	80 μM	Yes
Dns-72Ala	20 μM	65 μM	Yes

Interaction of W61 and W72 RAGE peptides with S100B

(The structures were solved by Jaime Jensen and Dr. Christopher Colbert. Only a brief summary is provided here)

To investigate the atomic details of S100B ability to accommodate different modes of interaction with the RAGE V-domain we determined the structure of the two RAGE derived peptides (W61 and W72) in complex with S100B and compared the binding of these peptides to the TRTK-12:S100B model (PDB: 3IQQ) [492]. Figure 5.17 shows the structure of S100B in complex with all the three peptides. Interestingly, the W72 peptide binds in the same S100B surface groove as the TRTK-12 peptide, but runs in the opposite direction, which results in the Trp being buried in a completely different pocket on the surface of S100B. Additionally, our S100B structures clearly extend beyond the edge of the binding groove where the TRTK12 structure tucks its C-terminus into the binding groove of S100B [464]

Structures of S100B: peptide complexes determined by nuclear magnetic resonance- S100B:p53 C-terminal regulatory domain (1DT7; [486]) and S100B: NDR kinase N-terminal regulatory domain (1PSB; [493])- indicate selective binding of the partially-helical peptide to binding site 1 of the “three persistent binding sites” of the S100B dimer [487]. Thus far, no data are available for proteins, peptides, or small molecules that join all three binding sites, although development of inhibitors to target all sites is of particular interest [487].

Structures of S100B:peptide complexes determined by nuclear magnetic resonance- S100B:p53 C-terminal regulatory domain (1DT7; [494]) and S100B:NDR kinase N-terminal regulatory domain (1PSB;[493])- indicate selective binding of the partially-helical peptide to binding site 1 of the "three persistent binding sites" of the S100B dimer [487]. Small molecule inhibitors typically bind either sites 1, 2, or 3 of the S100B [487, 488 489-491]. Thus far, no data are available for proteins, peptides, or small molecules that join all three binding sites, although development of inhibitors to target all sites is of particular interest.

Unlike the S100B:W61 and S100B:TRTK12 complexes, the S100B:W72 structure exhibits a significant 4 residue extension beyond binding site 2. Notably, the orientation of the N- and C-termini varies between the S100B:W72 structure, and the S100B:W61 and S100B:TRTK12 structures. In the S100B:W72 model, the C-terminus extends beyond the hinge region, with the N-terminus positioned for extension beyond helix 3. Both the S100B:W61 and S100B:TRTK12 structures orient the C-termini near helix 3, with the N-termini extending near the hinge region.

Although available S100B: peptide complexes solved by X-ray crystallography all incorporate a tryptophan-containing peptide, the S100B: peptide complexes display variability in the positioning of the tryptophan within the S100B hydrophobic groove, and in binding site 1, in particular. Each tryptophan indole occupies a different cavity within binding site 1. For the S100B:TRTK12 complex, the site occupied by Trp7 for TRTK12 is populated by Ala60 of W61 [464]. Similarly, the hydrophobic pocket that positions Trp72 of the W72 peptide is equivalently occupied by Ile10 in the TRTK12 peptide, and Val63 in the W61 peptide. Compared to the

S100B:W61 and S100B:TRTK12 structures, the S100B:W72 Trp exhibits the greatest buried surface area at 164.4 Å^2, compared to 65.9 Å^2 and 141.2 Å^2 for the Trp residues in the S100B:W61 and S100B:TRTK12 structures, respectively. The total ligand surface area is also the greatest for the W72 peptide, and the W72 peptide reveals the most interface polar contacts, with 5 hydrogen bonds and one bidentate salt bridge. Neither the W61 peptide nor the TRTK12 peptide are stabilized by a salt bridge. Differences in peptide conformations are summarized in Table 5.7.

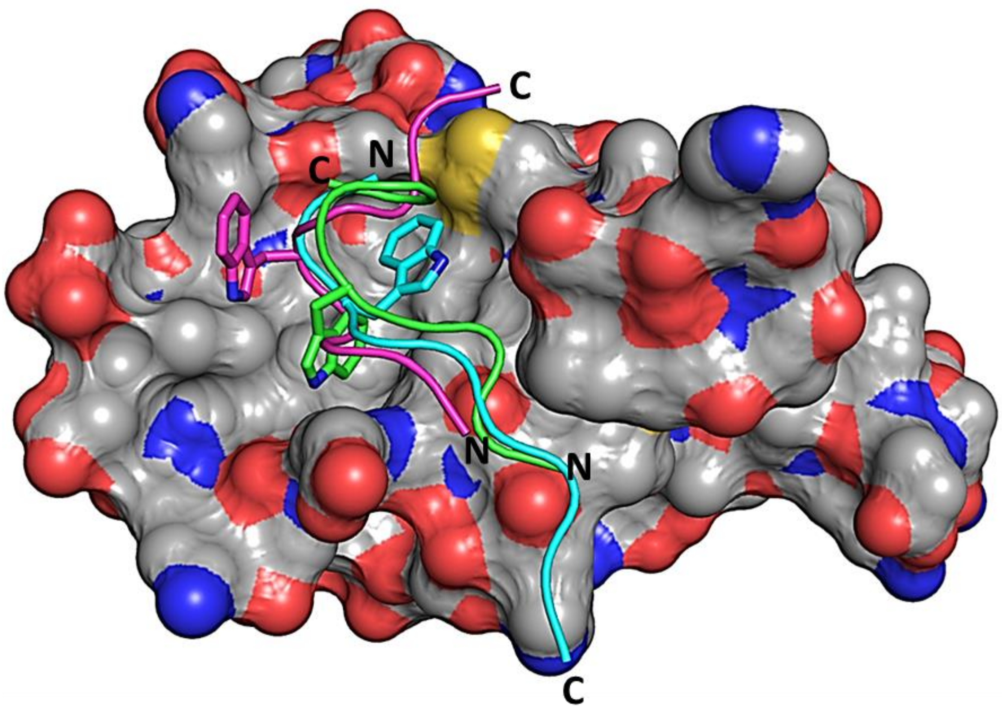

Figure 5.11. Surface representation of S100B with W61, W71 and TRTK-12 peptides.
Pink: W61 RAGE peptide; Cyan: W72 RAGE peptide; Green: TRTK-12 peptide.

Table 5.7. Differences in peptide conformations of the W61, W71 and the TRTK-12 binding to S100B.

Peptide	Total ligand surface area (Å^2)	Ligand interface area (Å^2)	Ligand interface area (%)	Interface polar contacts	Buried surface area of Trp (Å^2)
W72	1565.3	537.8	34.4	5 H-bonds, 1 salt bridge	164.4
W61	1334.3	485.6	36.4	3 H-bonds	65.9
TRTK12	1219.3	586.7	48.1	6 H-bonds	141.2

Conclusions

This study was initiated to understand the role of tryptophan residues in stability and ligand binding of V-domain of RAGE. RAGE-ligand interactions are not well understood. The exact binding region on the V domain of RAGE has not been identified. Role of tryptophan residues in the stability of proteins has been well elucidated [461, 495, 496]. Tryptophan residues have also been described to be enriched in binding hotspots for their stabilization of protein-protein interactions. However, the role of tryptophan residues has not been extensively studied in the context of V-domain even though it has three tryptophan residues in its 94 amino acid long sequence which is unique as tryptophan is one of the least abundant amino acids in proteins [462].

We have utilized the fluorescence properties of tryptophan to probe the environment surrounding the tryptophan residues. The results from our fluorescence experiments indicate that the positions of the three tryptophan residues in the V-domain are in agreement with known structures of tryptophan (PDB ID: 2L7U, 3CJJ, 3S58, 3S59, 3O3U, 2E5E, 2M1K, 4LP4, 4LP5, 4OI7, 4OI8, 2MJW, 4OF5, 4OFV, 4P2Y, 2MOV) [455 197, 456, 497-500]. The position of Trp51 is on the interior of the protein and Trp61is on the exterior, but the position of Trp72 is ambiguous indicating that this residue can shuttle between the interior and the exterior regions of the protein. We expect RAGE to have a certain degree of flexibility that enables it to bind to several different ligands. The flexibility of Trp72 adds to the plasticity of the V-domain. Our CD data show that the Trp residues are not required for folding of the V-domain and that the absence or presence of Trp residues has only a limited effect on the overall secondary structure of the V-domain. This finding , indicate that the Trp residues are not critically involved in the folding process of the domain itself, nor are they required to maintain the overall fold. On the other hand, about one third of the V-domain residues are in an unordered conformation, indicating a high degree of plasticity in the structure.

Our fluorescence emission scans suggest that the Trp51 is the strongest fluorophor followed by Trp72 and Trp61. From the fluorescence lifetime results of the single mutants we could conclude that the Trp61 contributed a long lived fluorescence component to the system in the wild type domain. The Trp72Ala mutant had an increased τ_m compared to the wild type, suggesting that Trp 72 contributes predominately a short lived component to the wild type system. The measured lifetimes upon addition of S100B reflect changes in the physico-chemical environment of the Trp fluorophores.

Thermofluor data provide insights in the function of individual Trp residues for domain stability and show that Trp51 stabilizes the RAGE V-domain, whereas Trp61 has a limited contribution to domain stability and Trp72 appears to destabilize the domain. Our fluorescence polarization results indicate tighter binding of the S100B to the Trp mutants. This suggests that RAGE V-domain mutants are able to refold to effect S100B binding and RAGE being a multiligand receptor capable of binding many different protein ligands and structural changes in the V-domain are probably necessary to bind different ligands. Our S100B-Trp containing RAGE peptide structures indicate that S100B can accommodate different modes of interaction of the RAGE V-domain.

The results described in this study improve our understanding about the V domain of RAGE and its domain stability. Understanding the structural basis behind RAGE: S100B interaction would assist in the discovery of new and efficient RAGE inhibitors.

CHAPTER 6. SUMMARY AND FUTURE DIRECTIONS

This thesis provides novel insights into the understanding of the RAGE-ligand interactions; more specifically the interaction RAGE with AGEs and S100B has been elucidated.

AGEs are highly heterogeneous in nature and multiple glycation reagents lead to the formation of diverse and distinct AGEs. AGE modifications are not equally significant from a patho-physiological stand point. Only certain glycation reactions yield AGE compounds which are toxic (glycotoxins) while the others are benign [118, 220, 501, 502]. AGEs derived under a wide variety of conditions have been used by various researchers which have not been characterized (reviewed in [118, 220]) hence; it is very difficult to compare results as the nature of modification responsible for their toxicity has not been elucidated. To obtain further insights into the process of glycation and to co-relate the glycation induced changes to activity we prepared a panel of AGEs by using different glycation reagents under near physiological conditions by using serum albumin as the model protein. Our biochemical and biophysical characterization of the AGEs reveal that each of the glycation reagents modified the protein differently. The chemical reactivity and concentration of the glycation reagent determined the extent of side chain modification. For example, ribose and the aldehydic intermediates such as glycolaldehyde or methylglyoxal were more potent glycation reagent when compared to glucose. Fluorescence spectroscopic analysis also shows the formation of unique AGE compounds with distinct fluorescence properties. These results suggest the possibility of using spectroscopic analysis for the characterization of the AGE compounds. Spectroscopic analysis has been previously used to estimate the levels of glycated albumin [162, 503]. Differences were also observed in the thermal stability and secondary structure of the glycated albumin and were dependent on the glycation reagent used. However, we observe that even high levels of glycation did not unfold the protein completely but lead to heterogeneous population of molten globulin like conformations. Glycation also induced protein multimerization with ribose having the most significant effect and no aggregation was observed. The fact that BSA remains soluble even in a highly glycated state may not be a general feature of glycation. Few reports in the literature suggest that high levels of glycation induced protein aggregation [223, 224]. This suggests that the highly glycated AGE compounds can exist in a soluble form and bind to AGE signaling receptors such as RAGE and galectin-3 to trigger signaling. *In vitro* binding studies between AGE-BSA and RAGE or galectin-3 revealed that binding of most compounds to the AGE-receptors is weaker than our detection limit (K_d ~ 50 μM). However, ribose glycated protein bound tightly to RAGE (2.0 μM), as well as to galectin-3 (2.0 μM). Interestingly, the binding affinity (K_d) increased with the extent of glycation, which suggests a qualitative difference between the samples. It may be possible that higher glycation generates more potential binding sites for RAGE or galectin-3 in the protein surface, or that oligomerization clusters more binding epitopes. In both scenarios, avidity effectively increases the apparent macroscopic binding affinity.

The biological effect of the AGE compounds was elucidated by determining the mitogenic effect of AGEs on cancer cell proliferation. A melanoma cell line (WM115) over expressing RAGE was used to determine the mitogenic effect of the AGE compounds. The observed increase in cell proliferation could be correlated with the extent of lysine residue modification, β-sheet content and oligomerization state of the glycated protein. However, other factors, most probably the chemical structure of the formed AGE modifications on the protein surface are important too. It is conceivable that RAGE or galectin-3 receptors form larger clusters on the cell surface, thus effectively increasing binding affinity by avidity. In fact, RAGE has been shown to form dimers in the plasma membrane [225]. Alternatively, RAGE or galectin-3 may associate with additional co-receptors on the cell surface, which could increase binding affinity for glycated proteins.

Building on these results we then determined the role of AGE-RAGE interaction in pancreatic cancer cell proliferation and migration. Recent studies have shown that there is an upregulation of RAGE significantly during PDAC progression and could be a potential therapeutic target [237]. It has been reported that on interaction with its ligands such as S100 proteins and HMGB1, RAGE can trigger cell survival and proliferation [235, 236, 239, 240, 311]. However, the role of AGE compounds has not been described in pancreatic cancer. We hypothesized that AGE-RAGE interaction can trigger pro-inflammatory cellular signaling which leads to cancer cell proliferation. Two pancreatic cancer cell lines with high RAGE expression; PANC-1 and MIA PaCa-2 were selected to understand the role of AGE compounds. Our results show the AGE-RAGE interaction triggered inflammation in the pancreatic cancer cells by inducing ROS production and eventually leading to cellular proliferation. To obtain a better understanding of the role of glycation induced oligomers in pancreatic cell proliferation, the isolated Rib-vH BSA oligomers were used to treat the PANC-1 and MIA PaCa-2 cells. An increase in cell proliferation was observed in both the cell lines when the cells were treated with the oligomers. This emphasizes the importance of glycation induced protein cross linking of the Rib-vH BSA for its mitogenic effects in pancreatic cancer cells. Treatment with anti-RAGE antibody inhibited the AGE induced cellular proliferation emphasizing the role for anti-RAGE treatment strategies in combinational anti-pancreatic cancer therapies. Interestingly, we observe diverse intracellular signaling in both the cell lines. The upregulation of NF-κB was observed only in the PANC-1 cells and not in the MIA PaCa-2 cells. However, the intracellular signaling pathways including the activation of kinases could not be elucidated and is a matter of future investigation by the lab. Building on the *in-vitro* data, the *in-vivo* efficacy of anti-RAGE antibodies in tumor xenograft mice models can be determined in the near future. I also propose the identification of the chemical nature of the AGE induced cross-linkages which lead to the cellular effects and finally to identify these AGE-cross linkages in human pancreatic cancer tissue arrays by immunofluorescence in the future.

To further elucidate the pro-inflammatory role of the AGEs, the role of AGEs in macrophage activation and pro-inflammatory cytokine release was determined in the macrophage cell line; RAW 264.7 cells. The cellular interaction of AGEs is believed to induce several biological responses, which are responsible for the development of various pro-inflammatory diabetic vascular complications [313]. Several recent findings report a substantial increase in tissue macrophages as a common feature in diabetic complications including nephropathy, atherosclerosis, neuropathy and retinopathy [356-359]. Recent findings have helped to provide an understanding of the potential importance of macrophages in promoting these complications [360]. The AGE compounds can also trigger pro-inflammatory cytokine release, the methyl glyoxal modified human serum albumin has been reported to upregulate TNF-α and IL-1β mRNA levels [317]. AGE compounds such as heavily modified glycolaldehyde-derived AGE-LDL induced macrophage foam cell formation contributing to the pathogenesis of atherosclerosis [318]. Taken together, all these reports indicate a definitive role of AGE compounds in macrophage activation and cytokine release. However, there are gaps in our understanding of the role of AGE compounds mediated cellular effects in macrophages. The uptake and intra-cellular internalization of AGE compounds is not fully understood. The role of AGE-RAGE interaction in macrophage activation has not been described. This study was initiated to fill these gaps in our understanding of the role of AGEs in macrophage activation.

We hypothesized that AGE-RAGE interaction triggers cellular signaling leading macrophage activation and pro-inflammatory cytokine release.

The uptake of the AGE compounds by macrophages was determined by fluorescence based uptake assay. A rapid uptake of the Rib-vH BSA was observed and the Rib-vH BSA internalized into the lysosomes after an hour of incubation. We tested the role of AGE receptors RAGE, galectin-3 and SR-A in AGE uptake however, the receptor responsible for Rib-vH BSA uptake could not be established by knockdown studies such as the SR-A knockdown or by using specific receptor inhibitors to inhibit the binding of AGE to RAGE and galectin-3 and requires further investigation. AGE treatment lead to the increase in pro-inflammatory gene expression, ROS production and NF-κB upregulation indicating that the Rib-vH BSA internalization led to the activation of the macrophages and polarized them into "M1-like" inflammatory macrophages. The role of RAGE in AGE mediated cellular effects could not elucidated and our results suggest a RAGE independent pathway for the AGE activity. Our results for the first time indicate the role of TLRs in certain AGE mediated cellular effects in the macrophages. These results provide a novel understanding of the role of AGE mediated macrophage activation and also emphasize the importance of targeting the AGE compounds to prevent the inflammation in diabetic complications. However, further studies are required to understand the AGE-receptor interactions leading to the AGE induced cellular effects which include the identification of the receptor responsible for the AGE mediated macrophage activation.

Finally, the structural basis behind the RAGE-S100B interaction was determined. RAGE is an immunoglobulin type cell surface receptor sensing damage associated molecular patterns (DAMPs) in stressed and damaged tissues [21, 22]. Despite the recognition of RAGE as a disease relevant receptor protein and as a potential pharmacological target, fundamental mechanistic questions regarding ligand recognition and induction of ligand specific signaling by RAGE remain unanswered. In particular, it remains unknown how RAGE can on the one side recognize structurally unrelated ligands, such as S100 proteins, AGE compounds and amyloid beta peptide, and on the other side demonstrate exquisite ligand specificity. RAGE cannot only distinguish between individual members of the S100 protein family [448], but also activate distinct cellular signaling pathways as a function of ligand concentration. S100B is an alarmin detected in wide range of clinical conditions including inflammatory and neurodegenerative diseases [198, 504] and is also a well-established prognostic marker for melanoma [505]. RAGE-S100B interaction has been reported to trigger inflammatory responses including the generation of oxidative stress and the upregulation of NF-κB in monocytes [33]and human peripheral blood mononuclear cells [506]. RAGE-S100B interaction can also trigger the release of pro-inflammatory cytokine and chemokine release [507]. In order to develop more robust inhibitors to prevent RAGE-S100B interaction it is important to understand the structural basis behind the RAGE-S100B interaction. We hypothesize that the Trp residues in the V-domain of RAGE are necessary for ligand stability and S100B binding. It has been reported that the Trp residues are enriched in the binding hotspots of protein interfaces than any other amino acid indicating that Trp plays an important role in the stability of protein complexes [462]. Trp is the largest of the naturally occurring amino acids, which has an indole ring that accounts for its hydrophobicity. Trp is fluorescent with high a quantum yield and more importantly its fluorescence properties like emission, quantum yield and quenching depends on its position in the protein and its surrounding environment, which makes it a good probe of the protein conformation [460, 461]. Trp is the least abundant amino acid in proteins [462]. However, the V-domain contains three Trp residues and these residues occur within a stretch of 21 amino acids (Trp51, Trp61 and Trp72). These residues could function as hydrophobic anchor residues for the binding of S100B and other S100 proteins.

Our fluorescence data show that the position of Trp51 is on the interior of the protein and Trp61is on the exterior, but the position of Trp72 is ambiguous indicating that this residue can shuttle between the interior and the exterior regions of the protein. These results are in agreement with known structures of the V-domain (PDB ID: 2L7U, 3CJJ, 3S58, 3S59, 3O3U, 2E5E, 2M1K, 4LP4, 4LP5, 4OI7, 4OI8, 2MJW, 4OF5, 4OFV, 4P2Y, 2MOV) [455 197, 456, 497-500 508, 509]. We expect RAGE to have a certain degree of flexibility that enables it to bind to several different ligands and the flexibility of Trp72 could add to the plasticity of the V-domain. Thermofluor data provide insights in the function of individual Trp residues for domain stability and show that Trp72 appears to destabilize the domain suggesting its role in plasticity. The different NMR and crystal structures also show that the region containing the W72 can adopt multiple confirmations, few of the structures report a short helix (PDB ID: 3O3U, 2E5E, 2M1K, 4LP4, 4LP5, 4OI7, 4OI8, 2MOV)[455, 456, 498-500] and others report random coils (PDB ID: 2L7U, 3CJJ, 2MJW, 4OF5, 4OFV, 4P2Y) [197, 497, 508, 509].

Interestingly, our fluorescence polarization results indicate tighter binding of the S100B to the Trp mutants than the wild type and the tightest binding was observed with the triple mutant. We suspect this mean that the RAGE V-domain mutants are able to refold owing to the smaller alanine side chains allowing them to more easily adopt a confirmation that would be complimentary to S100B hydrophobic groove and RAGE being a multiligand receptor capable of binding many different protein ligands and structural changes in the V-domain are probably necessary to bind different ligands. However, the presence of additional sites on the V-domain that might further stabilize or even provide alternate binding sequences to interact with S100B cannot be ruled out.

To obtain further insights into the role of Trp residues in S100B binding we studied the binding of Trp containing RAGE peptides to S100B. The mutation of the W51, 61 and 72 to alanine did not affect their binding to S100B. The W72 peptide has the least binding affinity when compared to the other two peptides. To investigate the atomic details of S100B ability to accommodate different modes of interaction with the RAGE V-domain we determined the structure of the two RAGE derived peptides (W61 and W72) in complex with S100B and compared the binding of these peptides to the TRTK-12:S100B model (PDB: 3IQQ) [492]. The presence of either the W61 or the W72 peptides did not alter the structure of S100B. Interestingly, the W72 peptide binds in the same S100B surface groove as the TRTK-12 peptide and the W61, but runs in the opposite direction, which results in the Trp being buried in a completely different pocket on the surface of S100B as opposed to the W61 where the Trp is solvent exposed partially [464] . This provides an interesting model whereby the structural stability of S100B may force flexible regions, such as those found on the RAGE V-domain, to adopt conformations that favor the interaction in this hydrophobic groove. These results provide novel understanding of the structural basis for RAGE:S100B interaction. However, to fully understand the RAGE:S100B interaction and to determine how different ligands mediate RAGE signaling further structural and biophysical investigation are necessary.

Taken together, my thesis provides a better understanding of RAGE-ligand interactions and would assist in the discovery of new and efficient RAGE inhibitors in the near future.

REFERENCES

[1] Neeper, M., Schmidt, A. M., Brett, J., Yan, S. D., Wang, F., Pan, Y. C., Elliston, K., Stern, D., and Shaw, A. (1992). Cloning and Expression of a Cell Surface Receptor for Advanced Glycosylation End Products of Proteins. *The Journal of Biological Chemistry 267*, 14998-15004.

[2] Schmidt, A. M., Vianna, M., Gerlach, M., Brett, J., Ryan, J., Kao, J., Esposito, C., Hegarty, H., Hurley, W., Clauss, M., and et al. (1992). Isolation and Characterization of Two Binding Proteins for Advanced Glycosylation End Products from Bovine Lung Which Are Present on the Endothelial Cell Surface. *The Journal of Biological Chemistry 267*, 14987-14997.

[3] Schmidt, A. M., Mora, R., Cao, R., Yan, S. D., Brett, J., Ramakrishnan, R., Tsang, T. C., Simionescu, M., and Stern, D. (1994). The Endothelial Cell Binding Site for Advanced Glycation End Products Consists of a Complex: An Integral Membrane Protein and a Lactoferrin-Like Polypeptide. *The Journal of Biological Chemistry269*, 9882-9888.

[4] Malherbe, P., Richards, J. G., Gaillard, H., Thompson, A., Diener, C., Schuler, A., and Huber, G. (1999). Cdna Cloning of a Novel Secreted Isoform of the Human Receptor for Advanced Glycation End Products and Characterization of Cells Co-Expressing Cell-Surface Scavenger Receptors and Swedish Mutant Amyloid Precursor Protein. *Brain Research Molecular Brain Research 71*, 159-170.

[5] Yonekura, H., Yamamoto, Y., Sakurai, S., Petrova, R. G., Abedin, M. J., Li, H., Yasui, K., Takeuchi, M., Makita, Z., Takasawa, S., Okamoto, H., Watanabe, T., and Yamamoto, H. (2003). Novel Splice Variants of the Receptor for Advanced Glycation End-Products Expressed in Human Vascular Endothelial Cells and Pericytes, and Their Putative Roles in Diabetes-Induced Vascular Injury. *The Biochemical Journal 370*, 1097-1109.

[6] Yang, B., Millward, A., and Demaine, A. (2003). Functional Differences between the Susceptibility Z-2/C-106 and Protective Z+2/T-106 Promoter Region Polymorphisms of the Aldose Reductase Gene May Account for the Association with Diabetic Microvascular Complications. *Biochimica et Biophysica Acta 1639*, 1-7.

[7] Ding, Q., and Keller, J. N. (2005). Evaluation of Rage Isoforms, Ligands, and Signaling in the Brain. *Biochimica et Biophysica Acta 1746*, 18-27.

[8] Koyama, H., Yamamoto, H., and Nishizawa, Y. (2007). Rage and Soluble Rage: Potential Therapeutic Targets for Cardiovascular Diseases. *Molecular Medicine 13*, 625-635.

[9] Hanford, L. E., Enghild, J. J., Valnickova, Z., Petersen, S. V., Schaefer, L. M., Schaefer, T. M., Reinhart, T. A., and Oury, T. D. (2004). Purification and Characterization of Mouse Soluble Receptor for Advanced Glycation End Products (Srage). *The Journal of Biological Chemistry279*, 50019-50024.

[10] Kosaka, T., Fukui, R., Matsui, M., Kurosaka, Y., Nishimura, H., Tanabe, M., Takakura, Y., Iwai, K., Waki, T., and Fujita, T. (2014). Rage, Receptor of Advanced Glycation Endoproducts. Negatively Regulates Chondrocytes Differentiation, *PloS One 9*, e108819.

[11] Yan, S. D., Chen, X., Fu, J., Chen, M., Zhu, H., Roher, A., Slattery, T., Zhao, L., Nagashima, M., Morser, J., Migheli, A., Nawroth, P., Stern, D., and Schmidt, A. M. (1996). Rage and Amyloid-Beta Peptide Neurotoxicity in Alzheimer's Disease. *Nature 382*, 685-691.

[12] Du Yan, S., Zhu, H., Fu, J., Yan, S. F., Roher, A., Tourtellotte, W. W., Rajavashisth, T., Chen, X., Godman, G. C., Stern, D., and Schmidt, A. M. (1997). Amyloid-Beta Peptide-Receptor for Advanced Glycation Endproduct Interaction Elicits Neuronal Expression of Macrophage-Colony Stimulating Factor: A Proinflammatory Pathway in Alzheimer Disease. *Proceedings of the National Academy of Sciences of the United States of America 94*, 5296-5301.

[13] Ding, Q., and Keller, J. N. (2005). Splice Variants of the Receptor for Advanced Glycosylation End Products (Rage) in Human Brain. *Neuroscience Letters 373*, 67-72.

[14] Schmidt, A. M., Yan, S. D., Yan, S. F., and Stern, D. M. (2000). The Biology of the Receptor for Advanced Glycation End Products and Its Ligands. *Biochimica et Biophysica Acta 1498*, 99-111.

[15] Hofmann, M. A., Drury, S., Fu, C., Qu, W., Taguchi, A., Lu, Y., Avila, C., Kambham, N., Bierhaus, A., Nawroth, P., Neurath, M. F., Slattery, T., Beach, D., McClary, J., Nagashima, M., Morser, J., Stern, D., and Schmidt, A. M. (1999). Rage Mediates a Novel Proinflammatory Axis: A Central Cell Surface Receptor for S100/Calgranulin Polypeptides. *Cell 97*, 889-901.

[16] Marenholz, I., Heizmann, C. W., and Fritz, G. (2004). S100 Proteins in Mouse and Man: From Evolution to Function and Pathology (Including an Update of the Nomenclature). *Biochemical and Biophysical Research Communications 322*, 1111-1122.

[17] Hori, O., Brett, J., Slattery, T., Cao, R., Zhang, J., Chen, J. X., Nagashima, M., Lundh, E. R., Vijay, S., Nitecki, D., and et al. (1995). The Receptor for Advanced Glycation End Products (Rage) Is a Cellular Binding Site for Amphoterin. Mediation of Neurite Outgrowth and Co-Expression of Rage and Amphoterin in the Developing Nervous System. *The Journal of Biological Chemistry270*, 25752-25761.

[18] Wang, H., Bloom, O., Zhang, M., Vishnubhakat, J. M., Ombrellino, M., Che, J., Frazier, A., Yang, H., Ivanova, S., Borovikova, L., Manogue, K. R., Faist, E., Abraham, E., Andersson, J., Andersson, U., Molina, P. E., Abumrad, N. N., Sama, A., and Tracey, K. J. (1999). Hmg-1 as a Late Mediator of Endotoxin Lethality in Mice. *Science 285*, 248-251.

[19] Andersson, U., and Tracey, K. J. (2003). Hmgb1 in Sepsis. *Scandinavian Journal of Infectious Diseases 35*, 577-584.

[20] Treutiger, C. J., Mullins, G. E., Johansson, A. S., Rouhiainen, A., Rauvala, H. M., Erlandsson-Harris, H., Andersson, U., Yang, H., Tracey, K. J., Andersson, J., and Palmblad, J. E. (2003). High Mobility Group 1 B-Box Mediates Activation of Human Endothelium. *Journal of Internal Medicine 254*, 375-385.

[21] Bucciarelli, L. G., Wendt, T., Rong, L., Lalla, E., Hofmann, M. A., Goova, M. T., Taguchi, A., Yan, S. F., Yan, S. D., Stern, D. M., and Schmidt, A. M. (2002). Rage Is a Multiligand Receptor of the Immunoglobulin Superfamily: Implications for Homeostasis and Chronic Disease. *Cell and Molecular Life Sciences 59*, 1117-1128.

[22] Schmidt, A. M., Yan, S. D., Yan, S. F., and Stern, D. M. (2001). The Multiligand Receptor Rage as a Progression Factor Amplifying Immune and Inflammatory Responses. *The Journal of Clinical Investigation 108*, 949-955.

[23] Yan, S. D., Zhu, H., Zhu, A., Golabek, A., Du, H., Roher, A., Yu, J., Soto, C., Schmidt, A. M., Stern, D., and Kindy, M. (2000). Receptor-Dependent Cell Stress and Amyloid Accumulation in Systemic Amyloidosis. *Nature Medicine 6*, 643-651.

[24] Sasaki, N., Takeuchi, M., Chowei, H., Kikuchi, S., Hayashi, Y., Nakano, N., Ikeda, H., Yamagishi, S., Kitamoto, T., Saito, T., and Makita, Z. (2002). Advanced Glycation End

Products (Age) and Their Receptor (Rage) in the Brain of Patients with Creutzfeldt-Jakob Disease with Prion Plaques. *Neuroscience Letters 326*, 117-120.

[25] Chavakis, T., Bierhaus, A., Al-Fakhri, N., Schneider, D., Witte, S., Linn, T., Nagashima, M., Morser, J., Arnold, B., Preissner, K. T., and Nawroth, P. P. (2003). The Pattern Recognition Receptor (Rage) Is a Counterreceptor for Leukocyte Integrins: A Novel Pathway for Inflammatory Cell Recruitment. *The Journal of Experimental Medicine 198*, 1507-1515.

[26] Bierhaus, A., Schiekofer, S., Schwaninger, M., Andrassy, M., Humpert, P. M., Chen, J., Hong, M., Luther, T., Henle, T., Kloting, I., Morcos, M., Hofmann, M., Tritschler, H., Weigle, B., Kasper, M., Smith, M., Perry, G., Schmidt, A. M., Stern, D. M., Haring, H. U., Schleicher, E., and Nawroth, P. P. (2001). Diabetes-Associated Sustained Activation of the Transcription Factor Nuclear Factor-Kappab. *Diabetes 50*, 2792-2808.

[27] Li, J., and Schmidt, A. M. (1997). Characterization and Functional Analysis of the Promoter of Rage, the Receptor for Advanced Glycation End Products. *The Journal of Biological Chemistry272*, 16498-16506.

[28] Bierhaus, A., Humpert, P. M., Morcos, M., Wendt, T., Chavakis, T., Arnold, B., Stern, D. M., and Nawroth, P. P. (2005). Understanding Rage, the Receptor for Advanced Glycation End Products. *Journal of Molecular Medicine 83*, 876-886.

[29] Cortizo, A. M., Lettieri, M. G., Barrio, D. A., Mercer, N., Etcheverry, S. B., and McCarthy, A. D. (2003). Advanced Glycation End-Products (Ages) Induce Concerted Changes in the Osteoblastic Expression of Their Receptor Rage and in the Activation of Extracellular Signal-Regulated Kinases (Erk). *Molecular and Cellular Biochemistry 250*, 1-10.

[30] Sorci, G., Riuzzi, F., Agneletti, A. L., Marchetti, C., and Donato, R. (2004). S100b Causes Apoptosis in a Myoblast Cell Line in a Rage-Independent Manner. *Journal of Cellular Physiology 199*, 274-283.

[31] Li, J. H., Wang, W., Huang, X. R., Oldfield, M., Schmidt, A. M., Cooper, M. E., and Lan, H. Y. (2004). Advanced Glycation End Products Induce Tubular Epithelial-Myofibroblast Transition through the Rage-Erk1/2 Map Kinase Signaling Pathway. *The American Journal of Pathology 164*, 1389-1397.

[32] Lander, H. M., Tauras, J. M., Ogiste, J. S., Hori, O., Moss, R. A., and Schmidt, A. M. (1997). Activation of the Receptor for Advanced Glycation End Products Triggers a P21(Ras)-Dependent Mitogen-Activated Protein Kinase Pathway Regulated by Oxidant Stress. *The Journal of Biological Chemistry272*, 17810-17814.

[33] Shanmugam, N., Kim, Y. S., Lanting, L., and Natarajan, R. (2003). Regulation of Cyclooxygenase-2 Expression in Monocytes by Ligation of the Receptor for Advanced Glycation End Products. *The Journal of Biological Chemistry278*, 34834-34844.

[34] Yeh, C. H., Sturgis, L., Haidacher, J., Zhang, X. N., Sherwood, S. J., Bjercke, R. J., Juhasz, O., Crow, M. T., Tilton, R. G., and Denner, L. (2001). Requirement for P38 and P44/P42 Mitogen-Activated Protein Kinases in Rage-Mediated Nuclear Factor-Kappab Transcriptional Activation and Cytokine Secretion. *Diabetes 50*, 1495-1504.

[35] Sorci, G., Riuzzi, F., Arcuri, C., Giambanco, I., and Donato, R. (2004). Amphoterin Stimulates Myogenesis and Counteracts the Antimyogenic Factors Basic Fibroblast Growth Factor and S100b Via Rage Binding. *Molecular and Cellular Biology 24*, 4880-4894.

[36] Taguchi, A., Blood, D. C., del Toro, G., Canet, A., Lee, D. C., Qu, W., Tanji, N., Lu, Y., Lalla, E., Fu, C., Hofmann, M. A., Kislinger, T., Ingram, M., Lu, A., Tanaka, H., Hori, O., Ogawa, S., Stern, D. M., and Schmidt, A. M. (2000). Blockade of Rage-Amphoterin Signalling Suppresses Tumour Growth and Metastases. *Nature 405*, 354-360.

[37] Huttunen, H. J., Fages, C., and Rauvala, H. (1999). Receptor for Advanced Glycation End Products (Rage)-Mediated Neurite Outgrowth and Activation of Nf-Kappab Require the Cytoplasmic Domain of the Receptor but Different Downstream Signaling Pathways. *The Journal of Biological Chemistry274*, 19919-19924.

[38] Huang, J. S., Guh, J. Y., Chen, H. C., Hung, W. C., Lai, Y. H., and Chuang, L. Y. (2001). Role of Receptor for Advanced Glycation End-Product (Rage) and the Jak/Stat-Signaling Pathway in Age-Induced Collagen Production in Nrk-49f Cells. *Journal of Cellular Biochemistry 81*, 102-113.

[39] Brett, J., Schmidt, A. M., Yan, S. D., Zou, Y. S., Weidman, E., Pinsky, D., Nowygrod, R., Neeper, M., Przysiecki, C., Shaw, A., and et al. (1993). Survey of the Distribution of a Newly Characterized Receptor for Advanced Glycation End Products in Tissues. *The American Journal of Pathology 143*, 1699-1712.

[40] Wilhelm, M., Schlegl, J., Hahne, H., Moghaddas Gholami, A., Lieberenz, M., Savitski, M. M., Ziegler, E., Butzmann, L., Gessulat, S., Marx, H., Mathieson, T., Lemeer, S., Schnatbaum, K., Reimer, U., Wenschuh, H., Mollenhauer, M., Slotta-Huspenina, J., Boese, J. H., Bantscheff, M., Gerstmair, A., Faerber, F., and Kuster, B. (2014) Mass-Spectrometry-Based Draft of the Human Proteome. *Nature 509*, 582-587.

[41] Kokkola, R., Andersson, A., Mullins, G., Ostberg, T., Treutiger, C. J., Arnold, B., Nawroth, P., Andersson, U., Harris, R. A., and Harris, H. E. (2005). Rage Is the Major Receptor for the Proinflammatory Activity of Hmgb1 in Rodent Macrophages. *Scandinavian Journal of Immunology 61*, 1-9.

[42] Sakatani, S., Yamada, K., Homma, C., Munesue, S., Yamamoto, Y., Yamamoto, H., and Hirase, H. (2009). Deletion of Rage Causes Hyperactivity and Increased Sensitivity to Auditory Stimuli in Mice. *PloS One 4*, e8309.

[43] Huttunen, H. J., Kuja-Panula, J., Sorci, G., Agneletti, A. L., Donato, R., and Rauvala, H. (2000). Coregulation of Neurite Outgrowth and Cell Survival by Amphoterin and S100 Proteins through Receptor for Advanced Glycation End Products (Rage) Activation. *The Journal of Biological Chemistry*275, 40096-40105.

[44] Donato, R. (2001). S100: A Multigenic Family of Calcium-Modulated Proteins of the Ef-Hand Type with Intracellular and Extracellular Functional Roles. *International Journal of Biochemistry and Cell Biology 33*, 637-668.

[45] Buckley, S. T., and Ehrhardt, C. (2010). The Receptor for Advanced Glycation End Products (Rage) and the Lung. *Journal of Biomedicine and Biotechnology 2010*, 917108.

[46] Bierhaus, A., Stern, D. M., and Nawroth, P. P. (2006). Rage in Inflammation: A New Therapeutic Target?. *Current Opinion in Investigational Drugs 7*, 985-991.

[47] Clynes, R., Moser, B., Yan, S. F., Ramasamy, R., Herold, K., and Schmidt, A. M. (2007). Receptor for Age (Rage): Weaving Tangled Webs within the Inflammatory Response. *Current Molocular Medicine 7*, 743-751.

[48] Yan, S. F., Ramasamy, R., Bucciarelli, L. G., Wendt, T., Lee, L. K., Hudson, B. I., Stern, D. M., Lalla, E., S, D. U. Y., Rong, L. L., Naka, Y., and Schmidt, A. M. (2004). Rage and Its Ligands: A Lasting Memory in Diabetic Complications?. *Diabetes and Vascular Disease Research 1*, 10-20.

[49] Hudson, B. I., Wendt, T., Bucciarelli, L. G., Rong, L. L., Naka, Y., Yan, S. F., and Schmidt, A. M. (2005). Diabetic Vascular Disease: It's All the Rage. *Antioxidants & Redox Signaling 7*, 1588-1600.
[50] Ramasamy, R., Vannucci, S. J., Yan, S. S., Herold, K., Yan, S. F., and Schmidt, A. M. (2005). Advanced Glycation End Products and Rage: A Common Thread in Aging, Diabetes, Neurodegeneration, and Inflammation. *Glycobiology 15*, 16R-28R.
[51] Srikanth, V., Maczurek, A., Phan, T., Steele, M., Westcott, B., Juskiw, D., and Munch, G. (2011). Advanced Glycation Endproducts and Their Receptor Rage in Alzheimer's Disease. *Neurobiology and Aging 32*, 763-777.
[52] Kalea, A. Z., Schmidt, A. M., and Hudson, B. I. (2009). Rage: A Novel Biological and Genetic Marker for Vascular Disease. *Clinical Science 116*, 621-637.
[53] Farmer, D. G., and Kennedy, S. (2009). Rage, Vascular Tone and Vascular Disease. *Pharmacology and Therapeutics 124*, 185-194.
[54] Malik, P., Chaudhry, N., Mittal, R., and Mukherjee, T. K. (2015). Role of Receptor for Advanced Glycation End Products in the Complication and Progression of Various Types of Cancers. *Biochimica et Biophysica Acta 1850*, 1898-1904.
[55] Liliensiek, B., Weigand, M. A., Bierhaus, A., Nicklas, W., Kasper, M., Hofer, S., Plachky, J., Grone, H. J., Kurschus, F. C., Schmidt, A. M., Yan, S. D., Martin, E., Schleicher, E., Stern, D. M., Hammerling, G. G., Nawroth, P. P., and Arnold, B. (2004). Receptor for Advanced Glycation End Products (Rage) Regulates Sepsis but Not the Adaptive Immune Response. *The Journal of Clinical Investigation 113*, 1641-1650.
[56] Gold, J. A., Parsey, M., Hoshino, Y., Hoshino, S., Nolan, A., Yee, H., Tse, D. B., and Weiden, M. D. (2003). Cd40 Contributes to Lethality in Acute Sepsis: In Vivo Role for Cd40 in Innate Immunity. *Infection and Immunity 71*, 3521-3528.
[57] Wendt, T. M., Tanji, N., Guo, J., Kislinger, T. R., Qu, W., Lu, Y., Bucciarelli, L. G., Rong, L. L., Moser, B., Markowitz, G. S., Stein, G., Bierhaus, A., Liliensiek, B., Arnold, B., Nawroth, P. P., Stern, D. M., D'Agati, V. D., and Schmidt, A. M. (2003). Rage Drives the Development of Glomerulosclerosis and Implicates Podocyte Activation in the Pathogenesis of Diabetic Nephropathy. *The American Journal of Pathology 162*, 1123-1137.
[58] Bierhaus, A., Haslbeck, K. M., Humpert, P. M., Liliensiek, B., Dehmer, T., Morcos, M., Sayed, A. A., Andrassy, M., Schiekofer, S., Schneider, J. G., Schulz, J. B., Heuss, D., Neundorfer, B., Dierl, S., Huber, J., Tritschler, H., Schmidt, A. M., Schwaninger, M., Haering, H. U., Schleicher, E., Kasper, M., Stern, D. M., Arnold, B., and Nawroth, P. P. (2004). Loss of Pain Perception in Diabetes Is Dependent on a Receptor of the Immunoglobulin Superfamily. *The Journal of Clinical Investigation 114*, 1741-1751.
[59] Sakaguchi, T., Yan, S. F., Yan, S. D., Belov, D., Rong, L. L., Sousa, M., Andrassy, M., Marso, S. P., Duda, S., Arnold, B., Liliensiek, B., Nawroth, P. P., Stern, D. M., Schmidt, A. M., and Naka, Y. (2003). Central Role of Rage-Dependent Neointimal Expansion in Arterial Restenosis. *The Journal of Clinical Investigation 111*, 959-972.
[60] Schmidt, A. M., Yan, S. D., Wautier, J. L., and Stern, D. (1999). Activation of Receptor for Advanced Glycation End Products: A Mechanism for Chronic Vascular Dysfunction in Diabetic Vasculopathy and Atherosclerosis. *Circulation Research 84*, 489-497.
[61] Jandeleit-Dahm, K., and Cooper, M. E. (2008). The Role of Ages in Cardiovascular Disease. *Current Pharmaceutical Design 14*, 979-986.

[62] Bouma, G., Lam-Tse, W. K., Wierenga-Wolf, A. F., Drexhage, H. A., and Versnel, M. A. (2004). Increased Serum Levels of Mrp-8/14 in Type 1 Diabetes Induce an Increased Expression of Cd11b and an Enhanced Adhesion of Circulating Monocytes to Fibronectin. *Diabetes 53*, 1979-1986.

[63] Kosaki, A., Hasegawa, T., Kimura, T., Iida, K., Hitomi, J., Matsubara, H., Mori, Y., Okigaki, M., Toyoda, N., Masaki, H., Inoue-Shibata, M., Nishikawa, M., and Iwasaka, T. (2004). Increased Plasma S100a12 (En-Rage) Levels in Patients with Type 2 Diabetes. *Journal of Clinical Endocrinology & Metabolism 89*, 5423-5428.

[64] Yan, X. X., Lu, L., Peng, W. H., Wang, L. J., Zhang, Q., Zhang, R. Y., Chen, Q. J., and Shen, W. F. (2009). Increased Serum Hmgb1 Level Is Associated with Coronary Artery Disease in Nondiabetic and Type 2 Diabetic Patients. *Atherosclerosis 205*, 544-548.

[65] Skrha, J., Jr., Kalousova, M., Svarcova, J., Muravska, A., Kvasnicka, J., Landova, L., Zima, T., and Skrha, J. (2012). Relationship of Soluble Rage and Rage Ligands Hmgb1 and En-Rage to Endothelial Dysfunction in Type 1 and Type 2 Diabetes Mellitus. *Experiment and Clinical Endocrinology & Diabetes120*, 277-281.

[66] Mackic, J. B., Stins, M., McComb, J. G., Calero, M., Ghiso, J., Kim, K. S., Yan, S. D., Stern, D., Schmidt, A. M., Frangione, B., and Zlokovic, B. V. (1998). Human Blood-Brain Barrier Receptors for Alzheimer's Amyloid-Beta 1- 40. Asymmetrical Binding, Endocytosis, and Transcytosis at the Apical Side of Brain Microvascular Endothelial Cell Monolayer. *The Journal of Clinical Investigation 102*, 734-743.

[67] Lue, L. F., Walker, D. G., Brachova, L., Beach, T. G., Rogers, J., Schmidt, A. M., Stern, D. M., and Yan, S. D. (2001). Involvement of Microglial Receptor for Advanced Glycation Endproducts (Rage) in Alzheimer's Disease: Identification of a Cellular Activation Mechanism. *Experimental Neurology171*, 29-45.

[68] Arancio, O., Zhang, H. P., Chen, X., Lin, C., Trinchese, F., Puzzo, D., Liu, S., Hegde, A., Yan, S. F., Stern, A., Luddy, J. S., Lue, L. F., Walker, D. G., Roher, A., Buttini, M., Mucke, L., Li, W., Schmidt, A. M., Kindy, M., Hyslop, P. A., Stern, D. M., and Du Yan, S. S. (2004). Rage Potentiates Abeta-Induced Perturbation of Neuronal Function in Transgenic Mice. *The EMBO Journal 23*, 4096-4105.

[69] Deane, R., Singh, I., Sagare, A. P., Bell, R. D., Ross, N. T., LaRue, B., Love, R., Perry, S., Paquette, N., Deane, R. J., Thiyagarajan, M., Zarcone, T., Fritz, G., Friedman, A. E., Miller, B. L., and Zlokovic, B. V. (2012). A Multimodal Rage-Specific Inhibitor Reduces Amyloid Beta-Mediated Brain Disorder in a Mouse Model of Alzheimer Disease. *The Journal of Clinical Investigation 122*, 1377-1392.

[70] Miki, S., Kasayama, S., Miki, Y., Nakamura, Y., Yamamoto, M., Sato, B., and Kishimoto, T. (1993). Expression of Receptors for Advanced Glycosylation End Products on Renal Cell Carcinoma Cells in Vitro. *Biochemical and Biophysical Research Communications 196*, 984-989.

[71] Mercado-Pimentel, M. E., Onyeagucha, B. C., Li, Q., Pimentel, A. C., Jandova, J., and Nelson, M. A. (2015). The S100p/Rage Signaling Pathway Regulates Expression of Microrna-21 in Colon Cancer Cells. *FEBS letters 589*, 2388-2393.

[72] Bao, J. M., He, M. Y., Liu, Y. W., Lu, Y. J., Hong, Y. Q., Luo, H. H., Ren, Z. L., Zhao, S. C., and Jiang, Y. (2015). Age/Rage/Akt Pathway Contributes to Prostate Cancer Cell Proliferation by Promoting Rb Phosphorylation and Degradation. *American Journal of Cancer Research 5*, 1741-1750.

[73] Bhawal, U. K., Ozaki, Y., Nishimura, M., Sugiyama, M., Sasahira, T., Nomura, Y., Sato, F., Fujimoto, K., Sasaki, N., Ikeda, M. A., Tsuji, K., Kuniyasu, H., and Kato, Y. (2005). Association of Expression of Receptor for Advanced Glycation End Products and Invasive Activity of Oral Squamous Cell Carcinoma. *Oncology 69*, 246-255.
[74] Lata, K., and Mukherjee, T. K. (2014). Knockdown of Receptor for Advanced Glycation End Products Attenuate 17alpha-Ethinyl-Estradiol Dependent Proliferation and Survival of Mcf-7 Breast Cancer Cells. *Biochimica et Biophysica Acta 1840*, 1083-1091.
[75] Liang, H., Zhong, Y., Zhou, S., and Peng, L. (2011) Knockdown of Rage Expression Inhibits Colorectal Cancer Cell Invasion and Suppresses Angiogenesis in Vitro and in Vivo. *Cancer Lett 313*, 91-98.
[76] Kuniyasu, H., Oue, N., Wakikawa, A., Shigeishi, H., Matsutani, N., Kuraoka, K., Ito, R., Yokozaki, H., and Yasui, W. (2002). Expression of Receptors for Advanced Glycation End-Products (Rage) Is Closely Associated with the Invasive and Metastatic Activity of Gastric Cancer.*Journal of Pathology 196*, 163-170.
[77] Logsdon, C. D., Fuentes, M. K., Huang, E. H., and Arumugam, T. (2007). Rage and Rage Ligands in Cancer. *Current Molecular Medicine7*, 777-789.
[78] Onyeagucha, B. C., Mercado-Pimentel, M. E., Hutchison, J., Flemington, E. K., and Nelson, M. A. (2013). S100p/Rage Signaling Regulates Microrna-155 Expression Via Ap-1 Activation in Colon Cancer. *Experiment Cell Research319*, 2081-2090.
[79] Shimomoto, T., Luo, Y., Ohmori, H., Chihara, Y., Fujii, K., Sasahira, T., Denda, A., and Kuniyasu, H. (2012) Advanced Glycation End Products (Age) Induce the Receptor for Age in the Colonic Mucosa of Azoxymethane-Injected Fischer 344 Rats Fed with a High-Linoleic Acid and High-Glucose Diet. *J Gastroenterol 47*, 1073-1083.
[80] Meghnani, V., Wagh, A., Indurthi, V. S., Koladia, M., Vetter, S. W., Law, B., and Leclerc, E. (2014) The Receptor for Advanced Glycation End Products Influences the Expression of Its S100 Protein Ligands in Melanoma Tumors. *Int J Biochem Cell Biol 57*, 54-62.
[81] Arumugam, T., Ramachandran, V., Gomez, S. B., Schmidt, A. M., and Logsdon, C. D. (2012). S100p-Derived Rage Antagonistic Peptide Reduces Tumor Growth and Metastasis. *Clinical Cancer Research 18*, 4356-4364.
[82] Horvat, S., and Jakas, A. (2004). Peptide and Amino Acid Glycation: New Insights into the Maillard Reaction. *Journal of Peptide Science 10*, 119-137.
[83] Adams, S., Green, P., Claxton, R., Simcox, S., Williams, M. V., Walsh, K., and Leeuwenburgh, C. (2001). Reactive Carbonyl Formation by Oxidative and Non-Oxidative Pathways. *Frontiers in Biosciences 6*, A17-24.
[84] Ahmed, N., and Thornalley, P. J. (2002). Chromatographic Assay of Glycation Adducts in Human Serum Albumin Glycated in Vitro by Derivatization with 6-Aminoquinolyl-N-Hydroxysuccinimidyl-Carbamate and Intrinsic Fluorescence. *Biochemical Journal364*, 15-24.
[85] Barnaby, O. S., Cerny, R. L., Clarke, W., and Hage, D. S. (2011). Quantitative Analysis of Glycation Patterns in Human Serum Albumin Using (16)O/(18)O-Labeling and Maldi-Tof Ms. *Clinica Chemica Acta 412*, 1606-1615.
[86] Munch, G., Schicktanz, D., Behme, A., Gerlach, M., Riederer, P., Palm, D., and Schinzel, R. (1999). Amino Acid Specificity of Glycation and Protein-Age Crosslinking Reactivities Determined with a Dipeptide Spot Library. *Nature Biotechnology 17*, 1006-1010.

[87] Basta, G., Schmidt, A. M., and De Caterina, R. (2004). Advanced Glycation End Products and Vascular Inflammation: Implications for Accelerated Atherosclerosis in Diabetes. *Cardiovascular Research 63*, 582-592.

[88] Pu, L. J., Lu, L., Shen, W. F., Zhang, Q., Zhang, R. Y., Zhang, J. S., Hu, J., Yang, Z. K., Ding, F. H., Chen, Q. J., Shen, J., Fang, D. H., and Lou, S. (2007). Increased Serum Glycated Albumin Level Is Associated with the Presence and Severity of Coronary Artery Disease in Type 2 Diabetic Patients. *Circulation Journal 71*, 1067-1073.

[89] Peacock, T. P., Shihabi, Z. K., Bleyer, A. J., Dolbare, E. L., Byers, J. R., Knovich, M. A., Calles-Escandon, J., Russell, G. B., and Freedman, B. I. (2008). Comparison of Glycated Albumin and Hemoglobin a(1c) Levels in Diabetic Subjects on Hemodialysis. *Kidney International 73*, 1062-1068.

[90] Inaba, M., Okuno, S., Kumeda, Y., Yamada, S., Imanishi, Y., Tabata, T., Okamura, M., Okada, S., Yamakawa, T., Ishimura, E., and Nishizawa, Y. (2007). Glycated Albumin Is a Better Glycemic Indicator Than Glycated Hemoglobin Values in Hemodialysis Patients with Diabetes: Effect of Anemia and Erythropoietin Injection. *Journal of American Society of Nephrology18*, 896-903.

[91] De Groot, L., Hinkema, H., Westra, J., Smit, A. J., Kallenberg, C. G., Bijl, M., and Posthumus, M. D. (2011). Advanced Glycation Endproducts Are Increased in Rheumatoid Arthritis Patients with Controlled Disease. *Arthritis Research and Therapy 13*, R205.

[92] Vytasek, R., Sedova, L., and Vilim, V. (2010). Increased Concentration of Two Different Advanced Glycation End-Products Detected by Enzyme Immunoassays with New Monoclonal Antibodies in Sera of Patients with Rheumatoid Arthritis. *BMC Musculoskeletal Disorders 11*, 83.

[93] Mostafa, A. A., Randell, E. W., Vasdev, S. C., Gill, V. D., Han, Y., Gadag, V., Raouf, A. A., and El Said, H. (2007). Plasma Protein Advanced Glycation End Products, Carboxymethyl Cysteine, and Carboxyethyl Cysteine, Are Elevated and Related to Nephropathy in Patients with Diabetes. *Molecular and Cellular Biochemistry 302*, 35-42.

[94] Sebekova, K., Kupcova, V., Schinzel, R., and Heidland, A. (2002). Markedly Elevated Levels of Plasma Advanced Glycation End Products in Patients with Liver Cirrhosis - Amelioration by Liver Transplantation. *Journal of Hepatology 36*, 66-71.

[95] Halushka, M. K., Selvin, E., Lu, J., Macgregor, A. M., and Cornish, T. C. (2009). Use of Human Vascular Tissue Microarrays for Measurement of Advanced Glycation Endproducts. *Journal of Histochemistry and Cytochemistry 57*, 559-566.

[96] Jono, T., Kimura, T., Takamatsu, J., Nagai, R., Miyazaki, K., Yuzuriha, T., Kitamura, T., and Horiuchi, S. (2002). Accumulation of Imidazolone, Pentosidine and N(Epsilon)-(Carboxymethyl)Lysine in Hippocampal Ca4 Pyramidal Neurons of Aged Human Brain. *Pathology International 52*, 563-571.

[97] Van Heijst, J. W., Niessen, H. W., Hoekman, K., and Schalkwijk, C. G. (2005). Advanced Glycation End Products in Human Cancer Tissues: Detection of Nepsilon-(Carboxymethyl)Lysine and Argpyrimidine. *Annals of the New York Academy of Sciences 1043*, 725-733.

[98] Avery, N. C., and Bailey, A. J. (2006). The Effects of the Maillard Reaction on the Physical Properties and Cell Interactions of Collagen, *Pathologie-Biologie 54*, 387-395.

[99] Tessier, F., Obrenovich, M., and Monnier, V. M. (1999). Structure and Mechanism of Formation of Human Lens Fluorophore Lm-1. Relationship to Vesperlysine a and the

Advanced Maillard Reaction in Aging. Diabetes, and Cataractogenesis, *The Journal of Biological Chemistry274*, 20796-20804.

[100] Hudson, B. I., Hofmann, M. A., Bucciarelli, L., Wendt, T., Moser, B., Lu, Y., Qu, W., Stern, D. M., D'Agati, V., Du Yan, S., Yan, S. F., Grant, P. J., and Schmidt, A. M. (2002). Glycation and Diabetes: The Rage Connection. *Current Science India 83*, 1515-1521.

[101] Goldstein, D. E., Little, R. R., Lorenz, R. A., Malone, J. I., Nathan, D., Peterson, C. M., and Sacks, D. B. (2004). Tests of Glycemia in Diabetes. *Diabetes Care 27*, 1761-1773.

[102] (1995). The Relationship of Glycemic Exposure (Hba1c) to the Risk of Development and Progression of Retinopathy in the Diabetes Control and Complications Trial. *Diabetes 44*, 968-983.

[103] Hudson, B. I., and Schmidt, A. M. (2004). Rage: A Novel Target for Drug Intervention in Diabetic Vascular Disease. *Pharmaceutical Research 21*, 1079-1086.

[104] Rong, L. L., Gooch, C., Szabolcs, M., Herold, K. C., Lalla, E., Hays, A. P., Yan, S. F., Yan, S. S., and Schmidt, A. M. (2005). Rage: A Journey from the Complications of Diabetes to Disorders of the Nervous System - Striking a Fine Balance between Injury and Repair. *Restorative Neurology and Neuroscience 23*, 355-365.

[105] Barile, G. R., and Schmidt, A. M. (2007). Rage and Its Ligands in Retinal Disease. *Current Molecular Medicine 7*, 758-765.

[106] Thomas, M. C., Forbes, J. M., MacIsaac, R., Jerums, G., and Cooper, M. E. (2005). Low-Molecular Weight Advanced Glycation End Products: Markers of Tissue Age Accumulation and More?. *Annals of New York Academy of Sciences 1043*, 644-654.

[107] Lo, T. W., Westwood, M. E., McLellan, A. C., Selwood, T., and Thornalley, P. J. (1994). Binding and Modification of Proteins by Methylglyoxal under Physiological Conditions. A Kinetic and Mechanistic Study with N Alpha-Acetylarginine, N Alpha-Acetylcysteine, and N Alpha-Acetyllysine, and Bovine Serum Albumin. *The Journal of Biological Chemistry269*, 32299-32305.

[108] Dhar, A., Desai, K., Liu, J., and Wu, L. (2009). Methylglyoxal, Protein Binding and Biological Samples: Are We Getting the True Measure?. *Journal of chromatography 877*, 1093-1100.

[109] Thornalley, P. J., Langborg, A., and Minhas, H. S. (1999). Formation of Glyoxal, Methylglyoxal and 3-Deoxyglucosone in the Glycation of Proteins by Glucose. *Biochemical Journal 344 Pt 1*, 109-116.

[110] Westwood, M. E., and Thornalley, P. J. (1996). Induction of Synthesis and Secretion of Interleukin 1 Beta in the Human Monocytic Thp-1 Cells by Human Serum Albumins Modified with Methylglyoxal and Advanced Glycation Endproducts. *Immunology Letters 50*, 17-21.

[111] Turk, Z., Nemet, I., Varga-Defteardarovic, L., and Car, N. (2006). Elevated Level of Methylglyoxal During Diabetic Ketoacidosis and Its Recovery Phase. *Diabetes & Metabolism 32*, 176-180.

[112] Ahmed, N., Battah, S., Karachalias, N., Babaei-Jadidi, R., Horanyi, M., Baroti, K., Hollan, S., and Thornalley, P. J. (2003). Increased Formation of Methylglyoxal and Protein Glycation, Oxidation and Nitrosation in Triosephosphate Isomerase Deficiency. *Biochimica et Biophysica Acta 1639*, 121-132.

[113] Krautwald, M., and Munch, G. (2010). Advanced Glycation End Products as Biomarkers and Gerontotoxins - a Basis to Explore Methylglyoxal-Lowering Agents for Alzheimer's Disease?. *Exp Gerontol 45*, 744-751.
[114] Rabbani, N., Sebekova, K., Sebekova, K., Jr., Heidland, A., and Thornalley, P. J. (2007). Accumulation of Free Adduct Glycation, Oxidation, and Nitration Products Follows Acute Loss of Renal Function. *Kidney International 72*, 1113-1121.
[115] Andrassy, M., Igwe, J., Autschbach, F., Volz, C., Remppis, A., Neurath Markus, F., Schleicher, E., Humpert Per, M., Wendt, T., Liliensiek, B., Morcos, M., Schiekofer, S., Thiele, K., Chen, J., Kientsch-Engel, R., Schmidt, A.-M., Stremmel, W., Stern David, M., Katus Hugo, A., Nawroth Peter, P., and Bierhaus, A. (2006). Posttranslationally Modified Proteins as Mediators of Sustained Intestinal Inflammation. *American Journal of Pathology 169*, 1223-1237.
[116] Abe, R., Shimizu, T., Sugawara, H., Watanabe, H., Nakamura, H., Choei, H., Sasaki, N., Yamagishi, S.-i., Takeuchi, M., and Shimizu, H. (2004). Regulation of Human Melanoma Growth and Metastasis by Age-Age Receptor Interactions. *Journal of Investigational Dermatology 122*, 461-467.
[117] Takeuchi, M., and Yamagishi, S. (2004). Tage (Toxic Ages) Hypothesis in Various Chronic Diseases. *Medical Hypotheses 63*, 449-452.
[118] Vetter, S. W., and Indurthi, V. S. (2011). Moderate Glycation of Serum Albumin Affects Folding, Stability, and Ligand Binding. *Clinica Chimica Acta 412*, 2105-2116.
[119] Mera, K., Takeo, K., Izumi, M., Maruyama, T., Nagai, R., and Otagiri, M. (2010). Effect of Reactive-Aldehydes on the Modification and Dysfunction of Human Serum Albumin. *Journal of Pharmaceutical Sciences 99*, 1614-1625.
[120] Thornalley, P. J. (1998). Cell Activation by Glycated Proteins. Age Receptors, Receptor Recognition Factors and Functional Classification of Ages. *Cell and Molecular Biology 44*, 1013-1023.
[121] Horiuchi, S., Sakamoto, Y., and Sakai, M. (2003). Scavenger Receptors for Oxidized and Glycated Proteins. *Amino Acids 25*, 283-292.
[122] Araki, N., Higashi, T., Mori, T., Shibayama, R., Kawabe, Y., Kodama, T., Takahashi, K., Shichiri, M., and Horiuchi, S. (1995). Macrophage Scavenger Receptor Mediates the Endocytic Uptake and Degradation of Advanced Glycation End Products of the Maillard Reaction. *European Journal of Biochemistry 230*, 408-415.
[123] Ohgami, N., Nagai, R., Ikemoto, M., Arai, H., Miyazaki, A., Hakamata, H., Horiuchi, S., and Nakayama, H. (2002). Cd36, Serves as a Receptor for Advanced Glycation Endproducts (Age). *Journal of Diabetes and its Complications 16*, 56-59.
[124] Tamura, Y., Adachi, H., Osuga, J., Ohashi, K., Yahagi, N., Sekiya, M., Okazaki, H., Tomita, S., Iizuka, Y., Shimano, H., Nagai, R., Kimura, S., Tsujimoto, M., and Ishibashi, S. (2003). Feel-1 and Feel-2 Are Endocytic Receptors for Advanced Glycation End Products. *The Journal of Biological Chemistry 278*, 12613-12617.
[125] Ohgami, N., Nagai, R., Miyazaki, A., Ikemoto, M., Arai, H., Horiuchi, S., and Nakayama, H. (2001). Scavenger Receptor Class B Type I-Mediated Reverse Cholesterol Transport Is Inhibited by Advanced Glycation End Products. *The Journal of Biological Chemistry 276*, 13348-13355.
[126] Yoshimoto, R., Fujita, Y., Kakino, A., Iwamoto, S., Takaya, T., and Sawamura, T. (2011). The Discovery of Lox-1, Its Ligands and Clinical Significance. *Cardiovascular Drugs and Therapeutics 25*, 379-391.

[127] Ramasamy, R., Yan, S. F., and Schmidt, A. M. (2007). Arguing for the Motion: Yes, Rage Is a Receptor for Advanced Glycation Endproducts. *Molecular Nutrition and Food Research . 51*, 1111-1115.

[128] Bierhaus, A., Chevion, S., Chevion, M., Hofmann, M., Quehenberger, P., Illmer, T., Luther, T., Berentshtein, E., Tritschler, H., Muller, M., Wahl, P., Ziegler, R., and Nawroth, P. P. (1997). Advanced Glycation End Product-Induced Activation of Nf-Kappab Is Suppressed by Alpha-Lipoic Acid in Cultured Endothelial Cells. *Diabetes 46*, 1481-1490.

[129] Wu, C. H., Huang, C. M., Lin, C. H., Ho, Y. S., Chen, C. M., and Lee, H. M. (2002). Advanced Glycosylation End Products Induce Nf-Kappab Dependent Inos Expression in Raw 264.7 Cells. *Molecular and Cellular Endocrinology 194*, 9-17.

[130] Vlassara, H., Li, Y. M., Imani, F., Wojciechowicz, D., Yang, Z., Liu, F. T., and Cerami, A. (1995). Identification of Galectin-3 as a High-Affinity Binding Protein for Advanced Glycation End Products (Age): A New Member of the Age-Receptor Complex. *Molecular Medicine 1*, 634-646.

[131] McFarlane, S., Glenn, J. V., Lichanska, A. M., Simpson, D. A., and Stitt, A. W. (2005). Characterisation of the Advanced Glycation Endproduct Receptor Complex in the Retinal Pigment Epithelium. *British Journal of Ophthalmol 89*, 107-112.

[132] Stitt, A. W., He, C., and Vlassara, H. (1999). Characterization of the Advanced Glycation End-Product Receptor Complex in Human Vascular Endothelial Cells. *Biochemical and Biophysical Research Communications 256*, 549-556.

[133] Iacobini, C., Amadio, L., Oddi, G., Ricci, C., Barsotti, P., Missori, S., Sorcini, M., Di Mario, U., Pricci, F., and Pugliese, G. (2003). Role of Galectin-3 in Diabetic Nephropathy. *Journal of American Society of Nephrology14*, S264-S270.

[134] Butscheid, M., Hauptvogel, P., Fritz, P., Klotz, U., and Alscher, D. M. (2007). Hepatic Expression of Galectin-3 and Receptor for Advanced Glycation End Products in Patients with Liver Disease. *Journal of Clinical Pathology 60*, 415-418.

[135] Maruyama, K., Nishigori, H., and Iwatsuru, M. (1986). Location of Drug Binding Sites on Human Serum Albumin. *Chemical and Pharmaceutical Bulletin 34*, 2989-2993.

[136] Brunner, F., Zini, R., and Tillement, J. P. (1983). Dependence of Drug-Protein Binding Parameters on Human Serum and Albumin Concentration. *Journal of Pharmacy and Pharmacology 35*, 526-528.

[137] Vallianatou, T., Lambrinidis, G., and Tsantili-Kakoulidou, A. (2013). In Silico Prediction of Human Serum Albumin Binding for Drug Leads. *Expert Opinions on Drug Discovery 8*, 583-595.

[138] Sulkowska, A. (2013), Interaction of Drugs with Bovine and Human Serum Albumin. *Journal of Molecular Structure 614*, 227-232.

[139] Han, X. L., Tian, F. F., Ge, Y. S., Jiang, F. L., Lai, L., Li, D. W., Yu, Q. L., Wang, J., Lin, C., and Liu, Y. (2012). Spectroscopic, Structural and Thermodynamic Properties of Chlorpyrifos Bound to Serum Albumin: A Comparative Study between Bsa and Has. *Journal of Photochemistry and Photobiology B 109*, 1-11.

[140] Ghuman, J., Zunszain, P. A., Petitpas, I., Bhattacharya, A. A., Otagiri, M., and Curry, S. (2005). Structural Basis of the Drug-Binding Specificity of Human Serum Albumin. *Journal of Molecular Biology 353*, 38-52.

[141] Sollenne, N. P., and Means, G. E. (1979). Characterization of a Specific Drug Binding Site of Human Serum Albumin. *Molecular Pharmacology 15*, 754-757.

[142] Ascenzi, P., Bocedi, A., Notari, S., Fanali, G., Fesce, R., and Fasano, M. (2006). Allosteric Modulation of Drug Binding to Human Serum Albumin. *Mini Review in Medicinal Chemistry 6*, 483-489.
[143] Zhu, L., Yang, F., Chen, L., Meehan, E. J., and Huang, M. (2008). A New Drug Binding Subsite on Human Serum Albumin and Drug-Drug Interaction Studied by X-Ray Crystallography. *Journal of Structural Biology 162*, 40-49.
[144] Zsila, F., Bikadi, Z., Malik, D., Hari, P., Pechan, I., Berces, A., and Hazai, E. (2011). Evaluation of Drug-Human Serum Albumin Binding Interactions with Support Vector Machine Aided Online Automated Docking. *Bioinformatics 27*, 1806-1813.
[145] Zsila, F. (2013). Subdomain Ib Is the Third Major Drug Binding Region of Human Serum Albumin: Toward the Three-Sites Model. *Molecular Pharmacology 10*, 1668-1682.
[146] Oettl, K., and Stauber, R. E. (2007). Physiological and Pathological Changes in the Redox State of Human Serum Albumin Critically Influence Its Binding Properties. *British Journal of Pharmacology 151*, 580-590.
[147] Baraka-Vidot, J., Guerin-Dubourg, A., Bourdon, E., and Rondeau, P. (2012). Impaired Drug-Binding Capacities of in Vitro and in Vivo Glycated Albumin. *Biochimie 94*, 1960-1967.
[148] Joseph, K. S., Anguizola, J., and Hage, D. S. (2011). Binding of Tolbutamide to Glycated Human Serum Albumin. *Journal of Pharmaceutical and Biomedical Analysis 54*, 426-432.
[149] Joseph, K. S., Anguizola, J., Jackson, A. J., and Hage, D. S. (2010). Chromatographic Analysis of Acetohexamide Binding to Glycated Human Serum Albumin. *Journal Chromatography B 878*, 2775-2781.
[150] Chamouard, J. M., Barre, J., Urien, S., Houin, G., and Tillement, J. P. (1985). Diclofenac Binding to Albumin and Lipoproteins in Human Serum. *Biochemical Pharmacology 34*, 1695-1700.
[151] Wang, D., Y., Z., Y.-N., L., and Wang, J. (2008). Estimation of Binding Constants for Diclofenac Sodium and Bovine Serum Albumin by Affinity Capillary Electrophoresis and Fluorescence Spectroscopy. *Journal of Liquid Chromatography & Related Technology 31*, 2077-2088.
[152] Dutta, S. K., Basu, S. K., and Sen, K. K. (2006). Binding of Diclofenac Sodium with Bovine Serum Albumin at Different Temperatures, Ph and Ionic Strengths. *Indian Journal of Experimental Biology 44*, 123-127.
[153] Sharma, R., Choudhary, S., and Kishore, N. (2012). Insights into the Binding of the Drugs Diclofenac Sodium and Cefotaxime Sodium to Serum Albumin: Calorimetry and Spectroscopy. *European Journal of Pharmaceutical Sciences 46*, 435-445.
[154] Ji, Z. S., Li, C. G., Mao, X. A., Liu, M. L., and Hu, J. M. (2002). Nmr Study on the Low-Affinity Interaction of Human Serum Albumin with Diclofenac Sodium. *Chemical and Pharmaceutical Bulletin 50*, 1017-1021.
[155] Russeva, V., and Mihailova, D. (1996). Modelling of Indometacin and Diclofenac Sodium Binding to the Molecule of Human Serum Albumin. *Arzneimittelforschung 46*, 288-292.
[156] Valencia, J. V., Mone, M., Koehne, C., Rediske, J., and Hughes, T. E. (2004). Binding of Receptor for Advanced Glycation End Products (Rage) Ligands Is Not Sufficient to

Induce Inflammatory Signals: Lack of Activity of Endotoxin-Free Albumin-Derived Advanced Glycation End Products (Ages). *Diabetologia 47*, 844-852.
[157] Bouma, B., Kroon-Batenburg, L. M., Wu, Y. P., Brunjes, B., Posthuma, G., Kranenburg, O., de Groot, P. G., Voest, E. E., and Gebbink, M. F. (2003). Glycation Induces Formation of Amyloid Cross-Beta Structure in Albumin. *The Journal of Biological Chemistry278*, 41810-41819.
[158] Ahlsson, F., Gedeborg, R., Hesselager, G., Tuvemo, T., and Enblad, P. (2004). Treatment of Extreme Hyperglycemia Monitored with Intracerebral Microdialysis. *Pediatric Critical Care Medicine 5*, 89-92.
[159] Dhar, A., Desai, K., Liu, J., and Wu, L. (2009). Methylglyoxal, Protein Binding and Biological Samples: Are We Getting the True Measure?. *Journal of Chromatography B 877*, 1093-1100.
[160] Schmitt, A., Gasic-Milenkovic, J., and Schmitt, J. (2005). Characterization of Advanced Glycation End Products: Mass Changes in Correlation to Side Chain Modifications. *Analytical Biochemistry 346*, 101-106.
[161] Schmitt, A., Meiners, I., Schmitt, J., Noeller, J., Ihling, C., Muench, G., Sinz, A., and Nieber, K. (2005). Two Analytical Methods to Study the Interaction of Ages with Cell Surface Proteins. *Journal of Biochemical and Biophysical Methods 65*, 121-136.
[162] Schmitt, A., Schmitt, J., Munch, G., and Gasic-Milencovic, J. (2005). Characterization of Advanced Glycation End Products for Biochemical Studies: Side Chain Modifications and Fluorescence Characteristics. *Analytical Biochemistry 338*, 201-215.
[163] Ahmed, N., Argirov, O. K., Minhas, H. S., Cordeiro, C. A., and Thornalley, P. J. (2002). Assay of Advanced Glycation Endproducts (Ages): Surveying Ages by Chromatographic Assay with Derivatization by 6-Aminoquinolyl-N-Hydroxysuccinimidyl-Carbamate and Application to Nepsilon-Carboxymethyl-Lysine- and Nepsilon-(1-Carboxyethyl)Lysine-Modified Albumin. *Biochemical Journal364*, 1-14.
[164] Udenfriend, S., Stein, S., Bohlen, P., Dairman, W., Leimgruber, W., and Weigele, M. (1972). Fluorescamine: A Reagent for Assay of Amino Acids, Peptides, Proteins, and Primary Amines in the Picomole Range. *Science 178*, 871-872.
[165] Lorenzen, A., and Kennedy, S. W. (1993). A Fluorescence-Based Protein Assay for Use with a Microplate Reader. *Analytical Biochemistry 214*, 346-348.
[166] Smith, R. E., and MacQuarrie, R. (1978). A Sensitive Fluorometric Method for the Determination of Arginine Using 9,10-Phenanthrenequinone. *Analytical biochemistry 90*, 246-255.
[167] Itano, H. A., and Yamada, S. (1972). 2-Aminophenanthroimidazole, Fluorescent Product of the Reaction of Phenanthrenequinone with Arginine. *Analytical biochemistry 48*, 483-490.
[168] Fields, R., and Dixon, H. B. (1971). Micro Method for Determination of Reactive Carbonyl Groups in Proteins and Peptides, Using 2,4-Dinitrophenylhydrazine. *Biochemical Journal121*, 587-589.
[169] Whitmore, L., and Wallace, B. A. (2004). Dichroweb, an Online Server for Protein Secondary Structure Analyses from Circular Dichroism Spectroscopic Data. *Nucleic Acids Research 32*, W668-673.
[170] Whitmore, L., and Wallace, B. A. (2008). Protein Secondary Structure Analyses from Circular Dichroism Spectroscopy: Methods and Reference Databases. *Biopolymers 89*, 392-400.

[171] Sreerama, N., Venyaminov, S. Y., and Woody, R. W. (2001). Analysis of Protein Circular Dichroism Spectra Based on the Tertiary Structure Classification. *Analytical Biochemistry 299*, 271-274.
[172] Anderson, K. S., Sikorski, J. A., and Johnson, K. A. (1988). Evaluation of 5-Enolpyruvoylshikimate-3-Phosphate Synthase Substrate and Inhibitor Binding by Stopped-Flow and Equilibrium Fluorescence Measurements. *Biochemistry 27*, 1604-1610.
[173] Otsuka, M., Mine, T., Ohuchi, K., and Ohmori, S. (1996). A Detoxication Route for Acetaldehyde: Metabolism of Diacetyl, Acetoin, and 2,3-Butanediol in Liver Homogenate and Perfused Liver of Rats. *Journal of Biochemistry 119*, 246-251.
[174] Suomalainen, H., and Ronkainen, P. (1968). Mechanism of Diacetyl Formation in Yeast Fermentation. *Nature 220*, 792-793.
[175] Harber, P., Saechao, K., and Boomus, C. (2006). Diacetyl-Induced Lung Disease. *Toxicology Review 25*, 261-272.
[176] Conway, B., Edmundowicz, D., Matter, N., Maynard, J., and Orchard, T. (2010). Skin Fluorescence Correlates Strongly with Coronary Artery Calcification Severity in Type 1 Diabetes. *Diabetes Technology and Therapeutics 12*, 339-345.
[177] Handl, M., Filova, E., Kubala, M., Lansky, Z., Kolacna, L., Vorlicek, J., Trc, T., Pach, M., and Amler, E. (2007). Fluorescent Advanced Glycation End Products in the Detection of Factual Stages of Cartilage Degeneration. *Physiology Research 56*, 235-242.
[178] Kessel, L., Kalinin, S., Nagaraj, R. H., Larsen, M., and Johansson, L. B. (2002). Time-Resolved and Steady-State Fluorescence Spectroscopic Studies of the Human Lens with Comparison to Argpyrimidine, Pentosidine and 3-Oh-Kynurenine. *Photochemistry and Photobiology 76*, 549-554.
[179] Degenhardt, T. P., Thorpe, S. R., and Baynes, J. W. (1998). Chemical Modification of Proteins by Methylglyoxal. *Cellular and Molecular Biology 44*, 1139-1145.
[180] Oya, T., Hattori, N., Mizuno, Y., Miyata, S., Maeda, S., Osawa, T., and Uchida, K. (1999). Methylglyoxal Modification of Protein. Chemical and Immunochemical Characterization of Methylglyoxal-Arginine Adducts. *The Journal of Biological Chemistry 274*, 18492-18502.
[181] Barnaby, O. S., Cerny, R. L., Clarke, W., and Hage, D. S. (2011). Comparison of Modification Sites Formed on Human Serum Albumin at Various Stages of Glycation. *Clinica Chemica Acta 412*, 277-285.
[182] Barnaby, O. S., Wa, C., Cerny, R. L., Clarke, W., and Hage, D. S. (2010). Quantitative Analysis of Glycation Sites on Human Serum Albumin Using (16)O/(18)O-Labeling and Matrix-Assisted Laser Desorption/Ionization Time-of-Flight Mass Spectrometry. *Clinica Chemica Acta 411*, 1102-1110.
[183] Bunn, H. F., and Higgins, P. J. (1981). Reaction of Monosaccharides with Proteins: Possible Evolutionary Significance. *Science 213*, 222-224.
[184] Westwood, M. E., and Thornalley, P. J. (1995). Molecular Characteristics of Methylglyoxal-Modified Bovine and Human Serum Albumins. Comparison with Glucose-Derived Advanced Glycation Endproduct-Modified Serum Albumins. *Journal of Protein Chemistry 14*, 359-372.
[185] Takeda, K., Wada, A., Yamamoto, K., Moriyama, Y., and Aoki, K. (1989). Conformational Change of Bovine Serum Albumin by Heat Treatment. *Journal of Protein Chemistry 8*, 653-659.

[186] Rondeau, P., Navarra, G., Cacciabaudo, F., Leone, M., Bourdon, E., and Militello, V. (2010). Thermal Aggregation of Glycated Bovine Serum Albumin. *Biochimica et Biophysica Acta 1804*, 789-798.
[187] Povey, J. F., Howard, M. J., Williamson, R. A., and Smales, C. M. (2008). The Effect of Peptide Glycation on Local Secondary Structure. *Journal of Structural Biology 161*, 151-161.
[188] Cleary, J. P., Walsh, D. M., Hofmeister, J. J., Shankar, G. M., Kuskowski, M. A., Selkoe, D. J., and Ashe, K. H. (2005). Natural Oligomers of the Amyloid-Beta Protein Specifically Disrupt Cognitive Function. *Nature Neuroscience 8*, 79-84.
[189] Hardy, J., and Selkoe, D. J. (2002). The Amyloid Hypothesis of Alzheimer's Disease: Progress and Problems on the Road to Therapeutics. *Science 297*, 353-356.
[190] Leclerc, E., Sturchler, E., Vetter, S. W., and Heizmann, C. W. (2009). Crosstalk between Calcium, Amyloid Beta and the Receptor for Advanced Glycation Endproducts in Alzheimer's Disease. *Reviews in the Neuroscience 20*, 95-110.
[191] Michnik, A. (2003). Thermal Stability of Bovine Serum Albumin Dsc Study. *Journal of Thermal Analysis and Calorimetry 71*, 509-519.
[192] Oakes, J. (1976). Thermally Denatured Proteins. Nuclear Magnetic Resonance, Binding Isotherm and Chemical Modification Studies of Thermally Denatured Bovine Serum Albumin. *Jornal of the Chemical Society 1 72*, 228-237.
[193] Pico, G. A. (1997). Thermodynamic Features of the Thermal Unfolding of Human Serum Albumin. *International Journal of Biological Macromolecules 20*, 63-73.
[194] Schmidt, A. M., Hori, O., Cao, R., Yan, S. D., Brett, J., Wautier, J. L., Ogawa, S., Kuwabara, K., Matsumoto, M., and Stern, D. (1996). Rage: A Novel Cellular Receptor for Advanced Glycation End Products. *Diabetes 45 Suppl 3*, S77-80.
[195] Yan, S. D., Stern, D., and Schmidt, A. M. (1997). What's the Rage? The Receptor for Advanced Glycation End Products (Rage) and the Dark Side of Glucose. *European Journal of Clinical Investigation 27*, 179-181.
[196] Pricci, F., Leto, G., Amadio, L., Iacobini, C., Romeo, G., Cordone, S., Gradini, R., Barsotti, P., Liu, F. T., Di Mario, U., and Pugliese, G. (2000). Role of Galectin-3 as a Receptor for Advanced Glycosylation End Products. *Kidney International Supplements 77*, S31-39.
[197] Koch, M., Chitayat, S., Dattilo, B. M., Schiefner, A., Diez, J., Chazin, W. J., and Fritz, G. (2010). Structural Basis for Ligand Recognition and Activation of Rage. *Structure 18*, 1342-1352.
[198] Leclerc, E., Fritz, G., Vetter, S. W., and Heizmann, C. W. (2009). Binding of S100 Proteins to Rage: An Update. *Biochimica et Biophysica Acta 1793*, 993-1007.
[199] Deane, R., Du Yan, S., Submamaryan, R. K., LaRue, B., Jovanovic, S., Hogg, E., Welch, D., Manness, L., Lin, C., Yu, J., Zhu, H., Ghiso, J., Frangione, B., Stern, A., Schmidt, A. M., Armstrong, D. L., Arnold, B., Liliensiek, B., Nawroth, P., Hofman, F., Kindy, M., Stern, D., and Zlokovic, B. (2003). Rage Mediates Amyloid-Beta Peptide Transport across the Blood-Brain Barrier and Accumulation in Brain. *Nature Medicine 9*, 907-913.
[200] Park, H., and Boyington, J. C. (2010). The 1.5 a Crystal Structure of Human Receptor for Advanced Glycation Endproducts (Rage) Ectodomains Reveals Unique Features Determining Ligand Binding. *The Journal of Biological Chemistry285*, 40762-40770.
[201] Dumic, J., Dabelic, S., and Flogel, M. (2006). Galectin-3: An Open-Ended Story. *Biochimica et Biophysica Acta 1760*, 616-635.

[202] Pugliese, G., Pricci, F., Iacobini, C., Leto, G., Amadio, L., Barsotti, P., Frigeri, L., Hsu, D. K., Vlassara, H., Liu, F. T., and Di Mario, U. (2001). Accelerated Diabetic Glomerulopathy in Galectin-3/Age Receptor 3 Knockout Mice. *Faseb Journal 15*, 2471-2479.
[203] Leclerc, E., Fritz, G., Weibel, M., Heizmann, C. W., and Galichet, A. (2007). S100b and S100a6 Differentially Modulate Cell Survival by Interacting with Distinct Rage (Receptor for Advanced Glycation End Products) Immunoglobulin Domains. *Journal of Biological Chemistry 282*, 31317-31331.
[204] Ostendorp, T., Leclerc, E., Galichet, A., Koch, M., Demling, N., Weigle, B., Heizmann, C. W., Kroneck, P. M. H., and Fritz, G. (2007). Structural and Functional Insights into Rage Activation by Multimeric S100b. *EMBO Journal 26*, 3868-3878.
[205] Buetler, T. M., Leclerc, E., Baumeyer, A., Latado, H., Newell, J., Adolfsson, O., Parisod, V., Richoz, J., Maurer, S., Foata, F., Piguet, D., Junod, S., Heizmann Claus, W., and Delatour, T. (2008). N(Epsilon)-Carboxymethyllysine-Modified Proteins Are Unable to Bind to Rage and Activate an Inflammatory Response. *Molecular Nutrition and Food Research 52*, 370-378.
[206] Valencia, J. V., Weldon, S. C., Quinn, D., Kiers, G. H., DeGroot, J., TeKoppele, J. M., and Hughes, T. E. (2004). Advanced Glycation End Product Ligands for the Receptor for Advanced Glycation End Products: Biochemical Characterization and Formation Kinetics. *Analytical Biochemistry 324*, 68-78.
[207] Ballinger, M. L., Thomas, M. C., Nigro, J., Ivey, M. E., Dilley, R. J., and Little, P. J. (2005). Glycated and Carboxy-Methylated Proteins Do Not Directly Activate Human Vascular Smooth Muscle Cells. *Kidney International 68*, 2756-2765.
[208] Lieuw-a-Fa, M. L. M., Schalkwijk, C. G., Engelse, M., and van Hinsbergh, V. W. M. (2006). Interaction of Ne(Carboxymethyl)Lysine- and Methylglyoxal-Modified Albumin with Endothelial Cells and Macrophages. Splice Variants of Rage May Limit the Responsiveness of Human Endothelial Cells to Ages. *Thrombosis and Haemostasis 95*, 320-328.
[209] Kislinger, T., Fu, C., Huber, B., Qu, W., Taguchi, A., Du Yan, S., Hofmann, M., Yan, S. F., Pischetsrieder, M., Stern, D., and Schmidt, A. M. (1999). N(Epsilon)-(Carboxymethyl)Lysine Adducts of Proteins Are Ligands for Receptor for Advanced Glycation End Products That Activate Cell Signaling Pathways and Modulate Gene Expression. *The Journal of Biological Chemistry274*, 31740-31749.
[210] Hudson, B. I., Bucciarelli, L. G., Wendt, T., Sakaguchi, T., Lalla, E., Qu, W., Lu, Y., Lee, L., Stern David, M., Naka, Y., Ramasamy, R., Yan Shi, D., Yan Shi, F., D'Agati, V., and Schmidt, A. M. (2003). Blockade of Receptor for Advanced Glycation Endproducts: A New Target for Therapeutic Intervention in Diabetic Complications and Inflammatory Disorders. *Archives of Biochemistry and Biophysics 419*, 80-88.
[211] Leclerc, E., Heizmann, C. W., and Vetter, S. W. (2009). Rage and S100 Protein Transcription Levels Are Highly Variable in Human Melanoma Tumors and Cells. *General Physiology and Biophysics 28*, F65-75.
[212] Meghnani, V., Vetter, S. W., and Leclerc, E. (2014). Rage Overexpression Confers a Metastatic Phenotype to the Wm115 Human Primary Melanoma Cell Line. *Biochimica et Biophysica Acta 1842*, 1017-1027.

[213] Freyer, M. W., and Lewis, E. A. (2008). Isothermal Titration Calorimetry: Experimental Design, Data Analysis, and Probing Macromolecule/Ligand Binding and Kinetic Interactions. *Methods Cell Biology 84*, 79-113.
[214] Willis, J. V., Kendall, M. J., Flinn, R. M., Thornhill, D. P., and Welling, P. G. (1979). The Pharmacokinetics of Diclofenac Sodium Following Intravenous and Oral Administration. *European Journal of Clinical Pharmacology 16*, 405-410.
[215] Miyatake, S., Ichiyama, H., Kondo, E., and Yasuda, K. (2009). Randomized Clinical Comparisons of Diclofenac Concentration in the Soft Tissues and Blood Plasma between Topical and Oral Applications. *British Journal of Clinical Pharmacology 67*, 125-129.
[216] Gill, P., Moghadam, T. T., and Ranjbar, B. (2010). Differential Scanning Calorimetry Techniques: Applications in Biology and Nanoscience. *Journal of Biomolecular Technology 21*, 167-193.
[217] Bruylants, G., Wouters, J., and Michaux, C. (2005). Differential Scanning Calorimetry in Life Science: Thermodynamics, Stability, Molecular Recognition and Application in Drug Design. *Curr Med Chem 12*, 2011-2020.
[218] Relkin, P. (1996). Thermal Unfolding of Beta-Lactoglobulin, Alpha-Lactalbumin, and Bovine Serum Albumin. A Thermodynamic Approach. *Critical Reviews in Food Science and Nutrition 36*, 565-601.
[219] Farruggia, B., Rodriguez, F., Rigatuso, R., Fidelio, G., and Pico, G. (2001). The Participation of Human Serum Albumin Domains in Chemical and Thermal Unfolding. *Journal of Protein Chemistry 20*, 81-89.
[220] Indurthi, V. S., Leclerc, E., and Vetter, S. W. (2012). Interaction between Glycated Serum Albumin and Age-Receptors Depends on Structural Changes and the Glycation Reagent. *Archives of Biochemistry and Biophysics 528*, 185-196.
[221] Brownsey, G. J., Noel, T. R., Parker, R., and Ring, S. G. (2003). The Glass Transition Behavior of the Globular Protein Bovine Serum Albumin. *Biophysics Journal 85*, 3943-3950.
[222] Jachimska, B., Wasilewska, M., and Adamczyk, Z. (2008). Characterization of Globular Protein Solutions by Dynamic Light Scattering, Electrophoretic Mobility, and Viscosity Measurements. *Langmuir 24*, 6866-6872.
[223] Wei, Y., Chen, L., Chen, J., Ge, L., and He, R. Q. (2009). Rapid Glycation with D-Ribose Induces Globular Amyloid-Like Aggregations of Bsa with High Cytotoxicity to Sh-Sy5y Cells. *BMC Cell Biology 10*, 10.
[224] Wei, Y., Han, C. S., Zhou, J., Liu, Y., Chen, L., and He, R. Q. (2012). D-Ribose in Glycation and Protein Aggregation. *Biochimica et Biophysica Acta 1820*, 488-494.
[225] Zong, H., Madden, A., Ward, M., Mooney, M. H., Elliott, C. T., and Stitt, A. W. (2010). Homodimerization Is Essential for the Receptor for Advanced Glycation End Products (Rage)-Mediated Signal Transduction. *The Journal of Biological Chemistry285*, 23137-23146.
[226] Parkin, D. M., Bray, F., Ferlay, J., and Pisani, P. (2005). Global Cancer Statistics. 2002, *CA Cancer Journal for Clinicians 55*, 74-108.
[227] Jemal, A., Siegel, R., Xu, J., and Ward, E. (2010) Cancer Statistics, 2010. *CA Cancer Journal for Clinicians 60*, 277-300.
[228] Edwards, B. K., Brown, M. L., Wingo, P. A., Howe, H. L., Ward, E., Ries, L. A., Schrag, D., Jamison, P. M., Jemal, A., Wu, X. C., Friedman, C., Harlan, L., Warren, J., Anderson, R. N., and Pickle, L. W. (2005). Annual Report to the Nation on the Status of Cancer,

1975-2002, Featuring Population-Based Trends in Cancer Treatment. *Journal of National Cancer Institute 97*, 1407-1427.

[229] Arslan, A. A., Helzlsouer, K. J., Kooperberg, C., Shu, X. O., Steplowski, E., Bueno-de-Mesquita, H. B., Fuchs, C. S., Gross, M. D., Jacobs, E. J., Lacroix, A. Z., Petersen, G. M., Stolzenberg-Solomon, R. Z., Zheng, W., Albanes, D., Amundadottir, L., Bamlet, W. R., Barricarte, A., Bingham, S. A., Boeing, H., Boutron-Ruault, M. C., Buring, J. E., Chanock, S. J., Clipp, S., Gaziano, J. M., Giovannucci, E. L., Hankinson, S. E., Hartge, P., Hoover, R. N., Hunter, D. J., Hutchinson, A., Jacobs, K. B., Kraft, P., Lynch, S. M., Manjer, J., Manson, J. E., McTiernan, A., McWilliams, R. R., Mendelsohn, J. B., Michaud, D. S., Palli, D., Rohan, T. E., Slimani, N., Thomas, G., Tjonneland, A., Tobias, G. S., Trichopoulos, D., Virtamo, J., Wolpin, B. M., Yu, K., Zeleniuch-Jacquotte, A., Patel, A. V., and Pancreatic Cancer Cohort, C. (2010). Anthropometric Measures, Body Mass Index, and Pancreatic Cancer: A Pooled Analysis from the Pancreatic Cancer Cohort Consortium (Panscan). *Archives of Internal Medicine 170*, 791-802.

[230] Lohr, M. (2006). Is It Possible to Survive Pancreatic Cancer?. *Nature Clinical Practice. Gastroenterology & Hepatology 3*, 236-237.

[231] Jones, S., Zhang, X., Parsons, D. W., Lin, J. C., Leary, R. J., Angenendt, P., Mankoo, P., Carter, H., Kamiyama, H., Jimeno, A., Hong, S. M., Fu, B., Lin, M. T., Calhoun, E. S., Kamiyama, M., Walter, K., Nikolskaya, T., Nikolsky, Y., Hartigan, J., Smith, D. R., Hidalgo, M., Leach, S. D., Klein, A. P., Jaffee, E. M., Goggins, M., Maitra, A., Iacobuzio-Donahue, C., Eshleman, J. R., Kern, S. E., Hruban, R. H., Karchin, R., Papadopoulos, N., Parmigiani, G., Vogelstein, B., Velculescu, V. E., and Kinzler, K. W. (2008). Core Signaling Pathways in Human Pancreatic Cancers Revealed by Global Genomic Analyses. *Science 321*, 1801-1806.

[232] Biankin, A. V., and Waddell, N., and Kassahn, K. S., and Gingras, M. C., and Muthuswamy, L. B., and Johns, A. L., and Miller, D. K., and Wilson, P. J., and Patch, A. M., and Wu, J., and Chang, D. K., and Cowley, M. J., and Gardiner, B. B., and Song, S., and Harliwong, I., and Idrisoglu, S., and Nourse, C., and Nourbakhsh, E., and Manning, S., and Wani, S., and Gongora, M., and Pajic, M., and Scarlett, C. J., and Gill, A. J., and Pinho, A. V., and Rooman, I., and Anderson, M., and Holmes, O., and Leonard, C., and Taylor, D., and Wood, S., and Xu, Q., and Nones, K., and Fink, J. L., and Christ, A., and Bruxner, T., and Cloonan, N., and Kolle, G., and Newell, F., and Pinese, M., and Mead, R. S., and Humphris, J. L., and Kaplan, W., and Jones, M. D., and Colvin, E. K., and Nagrial, A. M., and Humphrey, E. S., and Chou, A., and Chin, V. T., and Chantrill, L. A., and Mawson, A., and Samra, J. S., and Kench, J. G., and Lovell, J. A., and Daly, R. J., and Merrett, N. D., and Toon, C., and Epari, K., and Nguyen, N. Q., and Barbour, A., and Zeps, N., and Australian Pancreatic Cancer Genome, I., and Kakkar, N., and Zhao, F., and Wu, Y. Q., and Wang, M., and Muzny, D. M., and Fisher, W. E., and Brunicardi, F. C., and Hodges, S. E., and Reid, J. G., and Drummond, J., and Chang, K., and Han, Y., and Lewis, L. R., and Dinh, H., and Buhay, C. J., and Beck, T., and Timms, L., and Sam, M., and Begley, K., and Brown, A., and Pai, D., and Panchal, A., and Buchner, N., and De Borja, R., and Denroche, R. E., and Yung, C. K., and Serra, S., and Onetto, N., and Mukhopadhyay, D., and Tsao, M. S., and Shaw, P. A., and Petersen, G. M., and Gallinger, S., and Hruban, R. H., and Maitra, A., and Iacobuzio-Donahue, C. A., and Schulick, R. D., and Wolfgang, C. L., and Morgan, R. A., and Lawlor, R. T., and Capelli, P., and Corbo, V., and Scardoni, M., and Tortora, G., and Tempero, M. A., and Mann, K.

M., and Jenkins, N. A., and Perez-Mancera, P. A., and Adams, D. J., and Largaespada, D. A., and Wessels, L. F., and Rust, A. G., and Stein, L. D., and Tuveson, D. A., and Copeland, N. G., and Musgrove, E. A., and Scarpa, A., and Eshleman, J. R., and Hudson, T. J., and Sutherland, R. L., and Wheeler, D. A., and Pearson, J. V., and McPherson, J. D., and Gibbs, R. A., and Grimmond, S. M. (2012). Pancreatic Cancer Genomes Reveal Aberrations in Axon Guidance Pathway Genes. *Nature 491*, 399-405.

[233] Hidalgo, M., Cascinu, S., Kleeff, J., Labianca, R., Lohr, J. M., Neoptolemos, J., Real, F. X., Van Laethem, J. L., and Heinemann, V. (2015). Addressing the Challenges of Pancreatic Cancer: Future Directions for Improving Outcomes. *Pancreatology : official journal of the International Association of Pancreatology 15*, 8-18.

[234] Gebhardt, C., Riehl, A., Durchdewald, M., Nemeth, J., Furstenberger, G., Muller-Decker, K., Enk, A., Arnold, B., Bierhaus, A., Nawroth, P. P., Hess, J., and Angel, P. (2008). Rage Signaling Sustains Inflammation and Promotes Tumor Development. *The Journal of Experimental Medicine 205*, 275-285.

[235] Kang, R., Tang, D., Livesey, K. M., Schapiro, N. E., Lotze, M. T., and Zeh, H. J., 3rd. (2011). The Receptor for Advanced Glycation End-Products (Rage) Protects Pancreatic Tumor Cells against Oxidative Injury. *Antioxidants & Redox Signaling 15*, 2175-2184.

[236] Kang, R., Tang, D., Schapiro, N. E., Livesey, K. M., Farkas, A., Loughran, P., Bierhaus, A., Lotze, M. T., and Zeh, H. J. (2010). The Receptor for Advanced Glycation End Products (Rage) Sustains Autophagy and Limits Apoptosis, Promoting Pancreatic Tumor Cell Survival. *Cell Death and Differentiation 17*, 666-676.

[237] DiNorcia, J., Lee, M. K., Moroziewicz, D. N., Winner, M., Suman, P., Bao, F., Remotti, H. E., Zou, Y. S., Yan, S. F., Qiu, W., Su, G. H., Schmidt, A. M., and Allendorf, J. D. (2012). Rage Gene Deletion Inhibits the Development and Progression of Ductal Neoplasia and Prolongs Survival in a Murine Model of Pancreatic Cancer. *Journal of Gastrointestinal Surgery : official journal of the Society for Surgery of the Alimentary Tract 16*, 104-112; discussion 112.

[238] Boone, B. A., Orlichenko, L., Schapiro, N. E., Loughran, P., Gianfrate, G. C., Ellis, J. T., Singhi, A. D., Kang, R., Tang, D., Lotze, M. T., and Zeh, H. J. (2015). The Receptor for Advanced Glycation End Products (Rage) Enhances Autophagy and Neutrophil Extracellular Traps in Pancreatic Cancer. *Cancer Gene Therapy 22*, 326-334.

[239] Arumugam, T., Simeone, D. M., Van Golen, K., and Logsdon, C. D. (2005). S100p Promotes Pancreatic Cancer Growth, Survival, and Invasion. *Clinical Cancer Research 11*, 5356-5364.

[240] Arumugam, T., and Logsdon, C. D. (2011). S100p: A Novel Therapeutic Target for Cancer. *Amino Acids 41*, 893-899.

[241] Abe, R., Shimizu, T., Sugawara, H., Watanabe, H., Nakamura, H., Choei, H., Sasaki, N., Yamagishi, S., Takeuchi, M., and Shimizu, H. (2004). Regulation of Human Melanoma Growth and Metastasis by Age-Age Receptor Interactions. *The Journal of Investigative Dermatology 122*, 461-467.

[242] Huttunen, H. J., Fages, C., Kuja-Panula, J., Ridley, A. J., and Rauvala, H. (2002). Receptor for Advanced Glycation End Products-Binding Cooh-Terminal Motif of Amphoterin Inhibits Invasive Migration and Metastasis. *Cancer Research 62*, 4805-4811.

[243] Han, Y. T., Choi, G. I., Son, D., Kim, N. J., Yun, H., Lee, S., Chang, D. J., Hong, H. S., Kim, H., Ha, H. J., Kim, Y. H., Park, H. J., Lee, J., and Suh, Y. G. (2012). Ligand-Based Design, Synthesis, and Biological Evaluation of 2-Aminopyrimidines, a Novel Series of

Receptor for Advanced Glycation End Products (Rage) Inhibitors. *Journal of Medicinal Chemistry 55*, 9120-9135.

[244] Palsson-McDermott, E. M., and O'Neill, L. A. (2013). The Warburg Effect Then and Now: From Cancer to Inflammatory Diseases. *BioEssays 35*, 965-973.

[245] Vander Heiden, M. G., Cantley, L. C., and Thompson, C. B. (2009). Understanding the Warburg Effect: The Metabolic Requirements of Cell Proliferation. *Science 324*, 1029-1033.

[246] Sharaf, H., Matou-Nasri, S., Wang, Q., Rabhan, Z., Al-Eidi, H., Al Abdulrahman, A., and Ahmed, N. (2015). Advanced Glycation Endproducts Increase Proliferation, Migration and Invasion of the Breast Cancer Cell Line Mda-Mb-231. *Biochimica et Biophysica Acta 1852*, 429-441.

[247] Takino, J., Yamagishi, S., and Takeuchi, M. (2010). Cancer Malignancy Is Enhanced by Glyceraldehyde-Derived Advanced Glycation End-Products. *Journal of Oncology 2010*, 739852.

[248] Ko, S. Y., Ko, H. A., Shieh, T. M., Chang, W. C., Chen, H. I., Chang, S. S., and Lin, I. H. (2014). Cell Migration Is Regulated by Age-Rage Interaction in Human Oral Cancer Cells in Vitro. *PloS One 9*, e110542.

[249] Yamamoto, Y., Yamagishi, S., Hsu, C. C., and Yamamoto, H. (1996). Advanced Glycation Endproducts-Receptor Interactions Stimulate the Growth of Human Pancreatic Cancer Cells through the Induction of Platelet-Derived Growth Factor-B. *Biochemical and Biophysical Research Communications 222*, 700-705.

[250] Cui, Y., and Andersen, D. K. (2012). Diabetes and Pancreatic Cancer. *Endocrine-Related Cancer 19*, F9-F26.

[251] Pannala, R., Leirness, J. B., Bamlet, W. R., Basu, A., Petersen, G. M., and Chari, S. T. (2008). Prevalence and Clinical Profile of Pancreatic Cancer-Associated Diabetes Mellitus. *Gastroenterology 134*, 981-987.

[252] Li, D., Tang, H., Hassan, M. M., Holly, E. A., Bracci, P. M., and Silverman, D. T. (2011). Diabetes and Risk of Pancreatic Cancer: A Pooled Analysis of Three Large Case-Control Studies. *Cancer Causes Control 22*, 189-197.

[253] Liu, Z., Jia, X., Duan, Y., Xiao, H., Sundqvist, K. G., Permert, J., and Wang, F. (2013). Excess Glucose Induces Hypoxia-Inducible Factor-1alpha in Pancreatic Cancer Cells and Stimulates Glucose Metabolism and Cell Migration. *Cancer Biology & Therapy 14*.

[254] Takada, M., Koizumi, T., Toyama, H., Suzuki, Y., and Kuroda, Y. (2001). Differential Expression of Rage in Human Pancreatic Carcinoma Cells. *Hepato-gastroenterology 48*, 1577-1578.

[255] Deer, E. L., Gonzalez-Hernandez, J., Coursen, J. D., Shea, J. E., Ngatia, J., Scaife, C. L., Firpo, M. A., and Mulvihill, S. J. (2010). Phenotype and Genotype of Pancreatic Cancer Cell Lines. *Pancreas 39*, 425-435.

[256] Unoki, H., and Yamagishi, S. (2008). Advanced Glycation End Products and Insulin Resistance. *Current Pharmaceutical Design 14*, 987-989.

[257] Yamagishi, S. (2009). Advanced Glycation End Products and Receptor-Oxidative Stress System in Diabetic Vascular Complications. *Therapeutic Apheresis and Dialysis 13*, 534-539.

[258] Yamagishi, S., Maeda, S., Matsui, T., Ueda, S., Fukami, K., and Okuda, S. (2012). Role of Advanced Glycation End Products (Ages) and Oxidative Stress in Vascular Complications in Diabetes. *Biochimica et Biophysica Acta 1820*, 663-671.

[259] Lal, M. A., Brismar, H., Eklof, A. C., and Aperia, A. (2002). Role of Oxidative Stress in Advanced Glycation End Product-Induced Mesangial Cell Activation. *Kidney International 61*, 2006-2014.

[260] Yu, J. H., and Kim, H. (2014). Oxidative Stress and Cytokines in the Pathogenesis of Pancreatic Cancer. *Journal of Cancer Prevention 19*, 97-102.

[261] Farrow, B., and Evers, B. M. (2002). Inflammation and the Development of Pancreatic Cancer. *Surgical Oncology 10*, 153-169.

[262] Ju, K. D., Lim, J. W., Kim, K. H., and Kim, H. (2011). Potential Role of Nadph Oxidase-Mediated Activation of Jak2/Stat3 and Mitogen-Activated Protein Kinases and Expression of Tgf-Beta1 in the Pathophysiology of Acute Pancreatitis. *Inflammation Research 60*, 791-800.

[263] Green, D. R. (2003). Death and Nf-Kappab in T Cell Activation: Life at the Edge. *Molecular Cell 11*, 551-552.

[264] Lee, J. K., Edderkaoui, M., Truong, P., Ohno, I., Jang, K. T., Berti, A., Pandol, S. J., and Gukovskaya, A. S. (2007). Nadph Oxidase Promotes Pancreatic Cancer Cell Survival Via Inhibiting Jak2 Dephosphorylation by Tyrosine Phosphatases. *Gastroenterology 133,* 1637-1648.

[265] Fukuda, A., Wang, S. C., Morris, J. P. t., Folias, A. E., Liou, A., Kim, G. E., Akira, S., Boucher, K. M., Firpo, M. A., Mulvihill, S. J., and Hebrok, M. (2011). Stat3 and Mmp7 Contribute to Pancreatic Ductal Adenocarcinoma Initiation and Progression. *Cancer Cell 19*, 441-455.

[266] Huang, P., Feng, L., Oldham, E. A., Keating, M. J., and Plunkett, W. (2000). Superoxide Dismutase as a Target for the Selective Killing of Cancer Cells. *Nature 407,* 390-395.

[267] Du, J., Nelson, E. S., Simons, A. L., Olney, K. E., Moser, J. C., Schrock, H. E., Wagner, B. A., Buettner, G. R., Smith, B. J., Teoh, M. L., Tsao, M. S., and Cullen, J. J. (2013). Regulation of Pancreatic Cancer Growth by Superoxide. *Molecular Carcinogenesis 52,* 555-567.

[268] Du, J., Liu, J., Smith, B. J., Tsao, M. S., and Cullen, J. J. (2011). Role of Rac1-Dependent Nadph Oxidase in the Growth of Pancreatic Cancer. *Cancer Gene Therapy 18*, 135-143.

[269] O'Leary, B. R., Fath, M. A., Bellizzi, A. M., Hrabe, J. E., Button, A. M., Allen, B. G., Case, A. J., Altekruse, S., Wagner, B. A., Buettner, G. R., Lynch, C. F., Hernandez, B. Y., Cozen, W., Beardsley, R. A., Keene, J., Henry, M. D., Domann, F. E., Spitz, D. R., and Mezhir, J. J. (2015). Loss of Sod3 (Ecsod) Expression Promotes an Aggressive Phenotype in Human Pancreatic Ductal Adenocarcinoma. *Clinical Cancer Research 21,* 1741-1751.

[270] Coughlan, M. T., Thorburn, D. R., Penfold, S. A., Laskowski, A., Harcourt, B. E., Sourris, K. C., Tan, A. L., Fukami, K., Thallas-Bonke, V., Nawroth, P. P., Brownlee, M., Bierhaus, A., Cooper, M. E., and Forbes, J. M. (2009). Rage-Induced Cytosolic Ros Promote Mitochondrial Superoxide Generation in Diabetes. *Journal of the American Society of Nephrology : JASN 20,* 742-752.

[271] Schmidt, A. M., Hori, O., Brett, J., Yan, S. D., Wautier, J. L., and Stern, D. (1994). Cellular Receptors for Advanced Glycation End Products. Implications for Induction of Oxidant Stress and Cellular Dysfunction in the Pathogenesis of Vascular Lesions. *Arteriosclerosis and Thrombosis 14,* 1521-1528.

[272] Yao, D., and Brownlee, M. (2010). Hyperglycemia-Induced Reactive Oxygen Species Increase Expression of the Receptor for Advanced Glycation End Products (Rage) and Rage Ligands. *Diabetes 59*, 249-255.
[273] Fink, B., Laude, K., McCann, L., Doughan, A., Harrison, D. G., and Dikalov, S. (2004). Detection of Intracellular Superoxide Formation in Endothelial Cells and Intact Tissues Using Dihydroethidium and an Hplc-Based Assay. *American Journal of Physiology. Cell physiology 287*, C895-902.
[274] Soro-Paavonen, A., Zhang, W. Z., Venardos, K., Coughlan, M. T., Harris, E., Tong, D. C., Brasacchio, D., Paavonen, K., Chin-Dusting, J., Cooper, M. E., Kaye, D., Thomas, M. C., and Forbes, J. M. (2010). Advanced Glycation End-Products Induce Vascular Dysfunction Via Resistance to Nitric Oxide and Suppression of Endothelial Nitric Oxide Synthase. *Journal of Hypertension 28*, 780-788.
[275] Goldin, A., Beckman, J. A., Schmidt, A. M., and Creager, M. A. (2006). Advanced Glycation End Products: Sparking the Development of Diabetic Vascular Injury. *Circulation 114*, 597-605.
[276] Sugita, H., Kaneki, M., Furuhashi, S., Hirota, M., Takamori, H., and Baba, H. (2010). Nitric Oxide Inhibits the Proliferation and Invasion of Pancreatic Cancer Cells through Degradation of Insulin Receptor Substrate-1 Protein. *Molecular Cancer Research 8*, 1152-1163.
[277] Fujita, M., Imadome, K., Endo, S., Shoji, Y., Yamada, S., and Imai, T. (2014). Nitric Oxide Increases the Invasion of Pancreatic Cancer Cells Via Activation of the Pi3k-Akt and Rhoa Pathways after Carbon Ion Irradiation. *FEBS Letters 588*, 3240-3250.
[278] Karin, M., and Greten, F. R. (2005). Nf-Kappab: Linking Inflammation and Immunity to Cancer Development and Progression. *Nature Reviews Immunology 5*, 749-759.
[279] Hammes, H. P., Hoerauf, H., Alt, A., Schleicher, E., Clausen, J. T., Bretzel, R. G., and Laqua, H. (1999). N(Epsilon)(Carboxymethyl)Lysin and the Age Receptor Rage Colocalize in Age-Related Macular Degeneration. *Investigative Ophthalmology & Visual Science 40*, 1855-1859.
[280] Alves, M., Calegari, V. C., Cunha, D. A., Saad, M. J., Velloso, L. A., and Rocha, E. M. (2005). Increased Expression of Advanced Glycation End-Products and Their Receptor, and Activation of Nuclear Factor Kappa-B in Lacrimal Glands of Diabetic Rats. *Diabetologia 48*, 2675-2681.
[281] Tothova, V., and Gibadulinova, A. (2013). S100p, a Peculiar Member of S100 Family of Calcium-Binding Proteins Implicated in Cancer *Acta Virologica 57*, 238-246.
[282] Sasahira, T., Kirita, T., Oue, N., Bhawal, U. K., Yamamoto, K., Fujii, K., Ohmori, H., Luo, Y., Yasui, W., Bosserhoff, A. K., and Kuniyasu, H. (2008). High Mobility Group Box-1-Inducible Melanoma Inhibitory Activity Is Associated with Nodal Metastasis and Lymphangiogenesis in Oral Squamous Cell Carcinoma. *Cancer Science 99*, 1806-1812.
[283] Arumugam, T., Ramachandran, V., and Logsdon, C. D. (2006). Effect of Cromolyn on S100p Interactions with Rage and Pancreatic Cancer Growth and Invasion in Mouse Models. *Journal of the National Cancer Institute 98*, 1806-1818.
[284] Hanahan, D., and Weinberg, R. A. (2011). Hallmarks of Cancer: The Next Generation. *Cell 144*, 646-674.
[285] Cohen, M. P., and Ziyadeh, F. N. (1994). Amadori Glucose Adducts Modulate Mesangial Cell Growth and Collagen Gene Expression. *Kidney International 45*, 475-484.

[286] Yui, S., Sasaki, T., Araki, N., Horiuchi, S., and Yamazaki, M. (1994). Induction of Macrophage Growth by Advanced Glycation End Products of the Maillard Reaction. *Journal of Immunology 152*, 1943-1949.
[287] Mikhailov, A. A., Danil'chenko, M. A., and Zakharova, A. V. (1973). Experience in the Treatment of Hypertensive States with Beta-Blockaders. *Kardiologiia 13*, 70-75.
[288] Ojima, A., Oda, E., Higashimoto, Y., Matsui, T., and Yamagishi, S. (2014). DNA Aptamer Raised against Advanced Glycation End Products Inhibits Neointimal Hyperplasia in Balloon-Injured Rat Carotid Arteries. *International Journal of Cardiology 171*, 443-446.
[289] Kim, J. Y., Park, H. K., Yoon, J. S., Kim, S. J., Kim, E. S., Ahn, K. S., Kim, D. S., Yoon, S. S., Kim, B. K., and Lee, Y. Y. (2008). Advanced Glycation End Product (Age)-Induced Proliferation of Hel Cells Via Receptor for Age-Related Signal Pathways. *International Journal of Oncology 33*, 493-501.
[290] Ishibashi, Y., Matsui, T., Takeuchi, M., and Yamagishi, S. (2013). Metformin Inhibits Advanced Glycation End Products (Ages)-Induced Growth and Vegf Expression in Mcf-7 Breast Cancer Cells by Suppressing Ages Receptor Expression Via Amp-Activated Protein Kinase. *Hormone and Metabolic Research 45*, 387-390.
[291] Ojima, A., Matsui, T., Maeda, S., Takeuchi, M., Inoue, H., Higashimoto, Y., and Yamagishi, S. (2014). DNA Aptamer Raised against Advanced Glycation End Products Inhibits Melanoma Growth in Nude Mice. *Laboratory Investigation 94*, 422-429.
[292] Scholzen, T., and Gerdes, J. (2000). The Ki-67 Protein: From the Known and the Unknown. *Journal of Cellular Physiology 182*, 311-322.
[293] Chue, B. M. (2009). Five-Year Survival of Metastatic Pancreatic Carcinoma: A Study of Courage and Hope. *Gastrointestinal Cancer Research 3*, 208-211.
[294] Garcia, M. N., Grasso, D., Lopez-Millan, M. B., Hamidi, T., Loncle, C., Tomasini, R., Lomberk, G., Porteu, F., Urrutia, R., and Iovanna, J. L. (2014). Ier3 Supports Krasg12d-Dependent Pancreatic Cancer Development by Sustaining Erk1/2 Phosphorylation. *The Journal of Clinical Investigation 124*, 4709-4722.
[295] Wang, M., Lu, X., Dong, X., Hao, F., Liu, Z., Ni, G., and Chen, D. (2015). Perk1/2 Silencing Sensitizes Pancreatic Cancer Bxpc-3 Cell to Gemcitabine-Induced Apoptosis Via Regulating Bax and Bcl-2 Expression. *World journal of surgical oncology 13*, 66.
[296] Tafani, M., Schito, L., Pellegrini, L., Villanova, L., Marfe, G., Anwar, T., Rosa, R., Indelicato, M., Fini, M., Pucci, B., and Russo, M. A. (2011). Hypoxia-Increased Rage and P2x7r Expression Regulates Tumor Cell Invasion through Phosphorylation of Erk1/2 and Akt and Nuclear Translocation of Nf-{Kappa}B. *Carcinogenesis 32*, 1167-1175.
[297] Hill, R., Li, Y., Tran, L. M., Dry, S., Calvopina, J. H., Garcia, A., Kim, C., Wang, Y., Donahue, T. R., Herschman, H. R., and Wu, H. (2012). Cell Intrinsic Role of Cox-2 in Pancreatic Cancer Development. *Molecular Cancer Therapeutics 11*, 2127-2137.
[298] Fiorini, C., Menegazzi, M., Padroni, C., Dando, I., Dalla Pozza, E., Gregorelli, A., Costanzo, C., Palmieri, M., and Donadelli, M. (2013). Autophagy Induced by P53-Reactivating Molecules Protects Pancreatic Cancer Cells from Apoptosis. *Apoptosis 18*, 337-346.
[299] Chen, S. H., Hung, W. C., Wang, P., Paul, C., and Konstantopoulos, K. (2013). Mesothelin Binding to Ca125/Muc16 Promotes Pancreatic Cancer Cell Motility and Invasion Via Mmp-7 Activation. *Scientific Reports 3*, 1870.

[300] Takahashi, R., Hirata, Y., Sakitani, K., Nakata, W., Kinoshita, H., Hayakawa, Y., Nakagawa, H., Sakamoto, K., Hikiba, Y., Ijichi, H., Moses, H. L., Maeda, S., and Koike, K. (2013). Therapeutic Effect of C-Jun N-Terminal Kinase Inhibition on Pancreatic Cancer. *Cancer Science 104*, 337-344.
[301] Lu, P., Weaver, V. M., and Werb, Z. (2012). The Extracellular Matrix: A Dynamic Niche in Cancer Progression. *The Journal of Cell Biology 196*, 395-406.
[302] Schnider, S. L., and Kohn, R. R. (1980). Glucosylation of Human Collagen in Aging and Diabetes Mellitus. *The Journal of Clinical Investigation 66*, 1179-1181.
[303] Verzijl, N., DeGroot, J., Thorpe, S. R., Bank, R. A., Shaw, J. N., Lyons, T. J., Bijlsma, J. W., Lafeber, F. P., Baynes, J. W., and TeKoppele, J. M. (2000). Effect of Collagen Turnover on the Accumulation of Advanced Glycation End Products. *The Journal of Biological Chemistry275*, 39027-39031.
[304] Sivan, S. S., Wachtel, E., Tsitron, E., Sakkee, N., van der Ham, F., Degroot, J., Roberts, S., and Maroudas, A. (2008). Collagen Turnover in Normal and Degenerate Human Intervertebral Discs as Determined by the Racemization of Aspartic Acid. *The Journal of Biological Chemistry 283*, 8796-8801.
[305] Bunn, H. F., Gabbay, K. H., and Gallop, P. M. (1978). The Glycosylation of Hemoglobin: Relevance to Diabetes Mellitus. *Science 200*, 21-27.
[306] Frank, R. N. (1991). On the Pathogenesis of Diabetic Retinopathy. A 1990 Update. *Ophthalmology 98*, 586-593.
[307] Vitek, M. P., Bhattacharya, K., Glendening, J. M., Stopa, E., Vlassara, H., Bucala, R., Manogue, K., and Cerami, A. (1994). Advanced Glycation End Products Contribute to Amyloidosis in Alzheimer Disease. *Proceedings of the National Academy of Sciences of the United States of America 91*, 4766-4770.
[308] Sasaki, N., Fukatsu, R., Tsuzuki, K., Hayashi, Y., Yoshida, T., Fujii, N., Koike, T., Wakayama, I., Yanagihara, R., Garruto, R., Amano, N., and Makita, Z. (1998). Advanced Glycation End Products in Alzheimer's Disease and Other Neurodegenerative Diseases. *The American Journal of Pathology 153*, 1149-1155.
[309] Glenn, J. V., and Stitt, A. W. (2009). The Role of Advanced Glycation End Products in Retinal Ageing and Disease. *Biochimica et Biophysica Acta 1790*, 1109-1116.
[310] Bartling, B., Desole, M., Rohrbach, S., Silber, R. E., and Simm, A. (2009). Age-Associated Changes of Extracellular Matrix Collagen Impair Lung Cancer Cell Migration. *FASEB Journal 23*, 1510-1520.
[311] Kang, R., Loux, T., Tang, D., Schapiro, N. E., Vernon, P., Livesey, K. M., Krasinskas, A., Lotze, M. T., and Zeh, H. J., 3rd. (2012). The Expression of the Receptor for Advanced Glycation Endproducts (Rage) Is Permissive for Early Pancreatic Neoplasia. *Proceedings of the National Academy of Sciences of the United States of America 109*, 7031-7036.
[312] Peppa, M., and Vlassara, H. (2005). Advanced Glycation End Products and Diabetic Complications: A General Overview. *Hormones 4*, 28-37.
[313] Nagai, R., Fujiwara, Y., Mera, K., and Otagiri, M. (2007). Investigation of Pathways of Advanced Glycation End-Products Accumulation in Macrophages. *Molecular Nutrition & Food Research 51*, 462-467.
[314] Chow, F. Y., Nikolic-Paterson, D. J., Ma, F. Y., Ozols, E., Rollins, B. J., and Tesch, G. H. (2007). Monocyte Chemoattractant Protein-1-Induced Tissue Inflammation Is Critical

for the Development of Renal Injury but Not Type 2 Diabetes in Obese Db/Db Mice. *Diabetologia 50*, 471-480.
[315] Chow, F. Y., Nikolic-Paterson, D. J., Ozols, E., Atkins, R. C., and Tesch, G. H. (2005). Intercellular Adhesion Molecule-1 Deficiency Is Protective against Nephropathy in Type 2 Diabetic Db/Db Mice. *Journal of the American Society of Nephrology 16*, 1711-1722.
[316] Saishoji, T., Higashi, T., Ikeda, K., Sano, H., Jinnouchi, Y., Ogawa, M., and Horiuchi, S. (1995). Advanced Glycation End Products Stimulate Plasminogen Activator Activity Via Gm-Csf in Raw 264.7 Cells. *Biochemical and Biophysical Research Communications 217*, 278-285.
[317] Webster, L., Abordo, E. A., Thornalley, P. J., and Limb, G. A. (1997). Induction of Tnf Alpha and Il-1 Beta Mrna in Monocytes by Methylglyoxal- and Advanced Glycated Endproduct-Modified Human Serum Albumin. *Biochemical Society Transactions 25*, 250S.
[318] Jinnouchi, Y., Sano, H., Nagai, R., Hakamata, H., Kodama, T., Suzuki, H., Yoshida, M., Ueda, S., and Horiuchi, S. (1998). Glycolaldehyde-Modified Low Density Lipoprotein Leads Macrophages to Foam Cells Via the Macrophage Scavenger Receptor. *Journal of Biochemistry 123*, 1208-1217.
[319] Indurthi, V. S., Leclerc, E., and Vetter, S. W. (2014). Calorimetric Investigation of Diclofenac Drug Binding to a Panel of Moderately Glycated Serum Albumins. *European Journal of Pharmaceutical Sciences 59*, 58-68.
[320] Vlassara, H., Brownlee, M., and Cerami, A. (1985). High-Affinity-Receptor-Mediated Uptake and Degradation of Glucose-Modified Proteins: A Potential Mechanism for the Removal of Senescent Macromolecules. *Proceedings of the National Academy of Sciences of the United States of America 82*, 5588-5592.
[321] Vlassara, H., Brownlee, M., and Cerami, A. (1984). Accumulation of Diabetic Rat Peripheral Nerve Myelin by Macrophages Increases with the Presence of Advanced Glycosylation Endproducts. *The Journal of Experimental Medicine 160*, 197-207.
[322] Grimm, S., Horlacher, M., Catalgol, B., Hoehn, A., Reinheckel, T., and Grune, T. (2012). Cathepsins D and L Reduce the Toxicity of Advanced Glycation End Products. *Free Radical Biology & Medicine 52*, 1011-1023.
[323] Neyen, C., Pluddemann, A., Roversi, P., Thomas, B., Cai, L., van der Westhuyzen, D. R., Sim, R. B., and Gordon, S. (2009). Macrophage Scavenger Receptor a Mediates Adhesion to Apolipoproteins a-I and E. *Biochemistry 48*, 11858-11871.
[324] Berghaus, L. J., Moore, J. N., Hurley, D. J., Vandenplas, M. L., Fortes, B. P., Wolfert, M. A., and Boons, G. J. (2010). Innate Immune Responses of Primary Murine Macrophage-Lineage Cells and Raw 264.7 Cells to Ligands of Toll-Like Receptors 2, 3, and 4. *Comparative Immunology, Microbiology and Infectious Diseases 33*, 443-454.
[325] Karu, T. I., Pyatibrat, L. V., Moskvin, S. V., Andreev, S., and Letokhov, V. S. (2008). Elementary Processes in Cells after Light Absorption Do Not Depend on the Degree of Polarization: Implications for the Mechanisms of Laser Phototherapy. *Photomedicine and Laser Surgery 26*, 77-82.
[326] Navarro-Gonzalez, J. F., and Mora-Fernandez, C. (2008). The Role of Inflammatory Cytokines in Diabetic Nephropathy. *Journal of the American Society of Nephrology : JASN 19*, 433-442.
[327] Williams, M. D., and Nadler, J. L. (2007). Inflammatory Mechanisms of Diabetic Complications. *Current Diabetes Reports 7*, 242-248.

[328] Navarro, J. F., and Mora, C. (2005). Role of Inflammation in Diabetic Complications. *Nephrology, Dialysis, Transplantation 20*, 2601-2604.
[329] Tuttle, K. R. (2005). Linking Metabolism and Immunology: Diabetic Nephropathy Is an Inflammatory Disease., *Journal of the American Society of Nephrology : JASN 16*, 1537-1538.
[330] Mora, C., and Navarro, J. F. (2006). Inflammation and Diabetic Nephropathy. *Current Diabetes Reports 6*, 463-468.
[331] Joussen, A. M., Poulaki, V., Le, M. L., Koizumi, K., Esser, C., Janicki, H., Schraermeyer, U., Kociok, N., Fauser, S., Kirchhof, B., Kern, T. S., and Adamis, A. P. (2004). A Central Role for Inflammation in the Pathogenesis of Diabetic Retinopathy. *FASEB Journal 18*, 1450-1452.
[332] Savoia, C., and Schiffrin, E. L. (2007). Vascular Inflammation in Hypertension and Diabetes: Molecular Mechanisms and Therapeutic Interventions. *Clinical Science 112*, 375-384.
[333] Van Beijnum, J. R., Buurman, W. A., and Griffioen, A. W. (2008). Convergence and Amplification of Toll-Like Receptor (Tlr) and Receptor for Advanced Glycation End Products (Rage) Signaling Pathways Via High Mobility Group B1 (Hmgb1). *Angiogenesis 11*, 91-99.
[334] Ihm, C. G. (1997). Monocyte Chemotactic Peptide-1 in Diabetic Nephropathy. *Kidney International 60*, S20-22.
[335] Chow, F. Y., Nikolic-Paterson, D. J., Ozols, E., Atkins, R. C., Rollin, B. J., and Tesch, G. H. (2006). Monocyte Chemoattractant Protein-1 Promotes the Development of Diabetic Renal Injury in Streptozotocin-Treated Mice. *Kidney International 69*, 73-80.
[336] Cheng, H. F., Wang, C. J., Moeckel, G. W., Zhang, M. Z., McKanna, J. A., and Harris, R. C. (2002). Cyclooxygenase-2 Inhibitor Blocks Expression of Mediators of Renal Injury in a Model of Diabetes and Hypertension. *Kidney International 62*, 929-939.
[337] Komers, R., Lindsley, J. N., Oyama, T. T., and Anderson, S. (2007). Cyclo-Oxygenase-2 Inhibition Attenuates the Progression of Nephropathy in Uninephrectomized Diabetic Rats. *Clinical and Experimental Pharmacology & Physiology 34*, 36-41.
[338] Levine, D. Z. (2006). Hyperfiltration, Nitric Oxide, and Diabetic Nephropathy. *Current Hypertension Reports 8*, 153-157.
[339] Quaggin, S. E., and Coffman, T. M. (2007). Toward a Mouse Model of Diabetic Nephropathy: Is Endothelial Nitric Oxide Synthase the Missing Link?. *Journal of the American Society of Nephrology : JASN 18*, 364-366.
[340] Okada, S., Shikata, K., Matsuda, M., Ogawa, D., Usui, H., Kido, Y., Nagase, R., Wada, J., Shikata, Y., and Makino, H. (2003). Intercellular Adhesion Molecule-1-Deficient Mice Are Resistant against Renal Injury after Induction of Diabetes. *Diabetes 52*, 2586-2593.
[341] Mezzano, S., Aros, C., Droguett, A., Burgos, M. E., Ardiles, L., Flores, C., Schneider, H., Ruiz-Ortega, M., and Egido, J. (2004). Nf-Kappab Activation and Overexpression of Regulated Genes in Human Diabetic Nephropathy. *Nephrology, Dialysis, Transplantation 19*, 2505-2512.
[342] Schmid, H., Boucherot, A., Yasuda, Y., Henger, A., Brunner, B., Eichinger, F., Nitsche, A., Kiss, E., Bleich, M., Grone, H. J., Nelson, P. J., Schlondorff, D., Cohen, C. D., Kretzler, M., and European Renal c, D. N. A. B. C. (2006). Modular Activation of Nuclear Factor-Kappab Transcriptional Programs in Human Diabetic Nephropathy. *Diabetes 55*, 2993-3003.

[343] Nakagawa, T. (2007). Uncoupling of the Vegf-Endothelial Nitric Oxide Axis in Diabetic Nephropathy: An Explanation for the Paradoxical Effects of Vegf in Renal Disease. *American journal of Physiology. Renal Physiology 292*, F1665-1672.
[344] Flyvbjerg, A., Khatir, D. S., Jensen, L. J., Dagnaes-Hansen, F., Gronbaek, H., and Rasch, R. (2004). The Involvement of Growth Hormone (Gh), Insulin-Like Growth Factors (Igfs) and Vascular Endothelial Growth Factor (Vegf) in Diabetic Kidney Disease. *Current Pharmaceutical Design 10*, 3385-3394.
[345] Pantsulaia, T. (2006). Role of Tgf-Beta in Pathogenesis of Diabetic Nephropathy. *Georgian Medical News*, 13-18.
[346] Schena, F. P., and Gesualdo, L. (2005). Pathogenetic Mechanisms of Diabetic Nephropathy. *Journal of the American Society of Nephrology : JASN 16 Suppl 1*, S30-33.
[347] Shikata, K., and Makino, H. (2001). Role of Macrophages in the Pathogenesis of Diabetic Nephropathy. *Contributions to Nephrology*, 46-54.
[348] Galkina, E., and Ley, K. (2006). Leukocyte Recruitment and Vascular Injury in Diabetic Nephropathy. *Journal of the American Society of Nephrology : JASN 17*, 368-377.
[349] Chow, F., Ozols, E., Nikolic-Paterson, D. J., Atkins, R. C., and Tesch, G. H. (2004). Macrophages in Mouse Type 2 Diabetic Nephropathy: Correlation with Diabetic State and Progressive Renal Injury. *Kidney International 65*, 116-128.
[350] Gordon, S. (2003). Alternative Activation of Macrophages. *Nature Reviews Immunology 3*, 23-35.
[351] Stout, R. D., Jiang, C., Matta, B., Tietzel, I., Watkins, S. K., and Suttles, J. (2005). Macrophages Sequentially Change Their Functional Phenotype in Response to Changes in Microenvironmental Influences. *Journal of Immunology 175*, 342-349.
[352] Mantovani, A., Sica, A., Sozzani, S., Allavena, P., Vecchi, A., and Locati, M. (2004). The Chemokine System in Diverse Forms of Macrophage Activation and Polarization. *Trends in Immunology 25*, 677-686.
[353] Pillai, M. M., Hayes, B., and Torok-Storb, B. (2009). Inducible Transgenes under the Control of the Hcd68 Promoter Identifies Mouse Macrophages with a Distribution That Differs from the F4/80 - and Csf-1r-Expressing Populations. *Experimental Hematology 37*, 1387-1392.
[354] Gordon, S., and Mantovani, A. (2011). Diversity and Plasticity of Mononuclear Phagocytes. *European Journal of Immunology 41*, 2470-2472.
[355] Balbo, P., Silvestri, M., Rossi, G. A., Crimi, E., and Burastero, S. E. (2001). Differential Role of Cd80 and Cd86 on Alveolar Macrophages in the Presentation of Allergen to T Lymphocytes in Asthma. *Clinical and Experimental Allergy 31*, 625-636.
[356] Tang, S., Scheiffarth, O. F., Thurau, S. R., and Wildner, G. (1993). Cells of the Immune System and Their Cytokines in Epiretinal Membranes and in the Vitreous of Patients with Proliferative Diabetic Retinopathy. *Ophthalmic Research 25*, 177-185.
[357] Nguyen, D., Ping, F., Mu, W., Hill, P., Atkins, R. C., and Chadban, S. J. (2006). Macrophage Accumulation in Human Progressive Diabetic Nephropathy. *Nephrology 11*, 226-231.
[358] Fukumoto, H., Naito, Z., Asano, G., and Aramaki, T. (1998). Immunohistochemical and Morphometric Evaluations of Coronary Atherosclerotic Plaques Associated with Myocardial Infarction and Diabetes Mellitus. *Journal of Atherosclerosis and Thrombosis 5*, 29-35.

[359] Said, G., Lacroix, C., Lozeron, P., Ropert, A., Plante, V., and Adams, D. (2003). Inflammatory Vasculopathy in Multifocal Diabetic Neuropathy. *Brain 126*, 376-385.
[360] Tesch, G. H. (2007). Role of Macrophages in Complications of Type 2 Diabetes. *Clinical and Experimental Pharmacology & Physiology 34*, 1016-1019.
[361] Pascoe, M. K., Low, P. A., Windebank, A. J., and Litchy, W. J. (1997). Subacute Diabetic Proximal Neuropathy. *Mayo Clinic proceedings 72*, 1123-1132.
[362] Dyck, P. J., and Windebank, A. J. (2002). Diabetic and Nondiabetic Lumbosacral Radiculoplexus Neuropathies: New Insights into Pathophysiology and Treatment. *Muscle & Nerve 25*, 477-491.
[363] Demircan, N., Safran, B. G., Soylu, M., Ozcan, A. A., and Sizmaz, S. (2006). Determination of Vitreous Interleukin-1 (Il-1) and Tumour Necrosis Factor (Tnf) Levels in Proliferative Diabetic Retinopathy. *Eye 20*, 1366-1369.
[364] Collins, R. G., Velji, R., Guevara, N. V., Hicks, M. J., Chan, L., and Beaudet, A. L. (2000). P-Selectin or Intercellular Adhesion Molecule (Icam)-1 Deficiency Substantially Protects against Atherosclerosis in Apolipoprotein E-Deficient Mice. *The Journal of Experimental Medicine 191*, 189-194.
[365] Gu, L., Okada, Y., Clinton, S. K., Gerard, C., Sukhova, G. K., Libby, P., and Rollins, B. J. (1998). Absence of Monocyte Chemoattractant Protein-1 Reduces Atherosclerosis in Low Density Lipoprotein Receptor-Deficient Mice. *Molecular Cell 2*, 275-281.
[366] Tashimo, A., Mitamura, Y., Nagai, S., Nakamura, Y., Ohtsuka, K., Mizue, Y., and Nishihira, J. (2004). Aqueous Levels of Macrophage Migration Inhibitory Factor and Monocyte Chemotactic Protein-1 in Patients with Diabetic Retinopathy. *Diabetic Medicine 21*, 1292-1297.
[367] Kimura, H., Minakami, H., Kimura, S., Sakurai, T., Nakamura, T., Kurashige, S., Nakano, M., and Shoji, A. (1995). Release of Superoxide Radicals by Mouse Macrophages Stimulated by Oxidative Modification of Glycated Low Density Lipoproteins. *Atherosclerosis 118*, 1-8.
[368] Cipollone, F., Iezzi, A., Fazia, M., Zucchelli, M., Pini, B., Cuccurullo, C., De Cesare, D., De Blasis, G., Muraro, R., Bei, R., Chiarelli, F., Schmidt, A. M., Cuccurullo, F., and Mezzetti, A. (2003). The Receptor Rage as a Progression Factor Amplifying Arachidonate-Dependent Inflammatory and Proteolytic Response in Human Atherosclerotic Plaques: Role of Glycemic Control. *Circulation 108*, 1070-1077.
[369] Andersen, C. L., Jensen, J. L., and Orntoft, T. F. (2004). Normalization of Real-Time Quantitative Reverse Transcription-Pcr Data: A Model-Based Variance Estimation Approach to Identify Genes Suited for Normalization. Applied to Bladder and Colon Cancer Data Sets, *Cancer Research 64*, 5245-5250.
[370] Pfaffl, M. W., Tichopad, A., Prgomet, C., and Neuvians, T. P. (2004). Determination of Stable Housekeeping Genes, Differentially Regulated Target Genes and Sample Integrity: Bestkeeper--Excel-Based Tool Using Pair-Wise Correlations. *Biotechnology Letters 26*, 509-515.
[371] Vandesompele, J., De Preter, K., Pattyn, F., Poppe, B., Van Roy, N., De Paepe, A., and Speleman, F. (2002). Accurate Normalization of Real-Time Quantitative Rt-Pcr Data by Geometric Averaging of Multiple Internal Control Genes. *Genome Biology 3*, RESEARCH0034.
[372] Liu, S., Tobias, R., McClure, S., Styba, G., Shi, Q., and Jackowski, G. (1997). Removal of Endotoxin from Recombinant Protein Preparations. *Clinical Biochemistry 30*, 455-463.

[373] Sano, H., Higashi, T., Matsumoto, K., Melkko, J., Jinnouchi, Y., Ikeda, K., Ebina, Y., Makino, H., Smedsrod, B., and Horiuchi, S. (1998). Insulin Enhances Macrophage Scavenger Receptor-Mediated Endocytic Uptake of Advanced Glycation End Products. *The Journal of Biological Chemistry 273*, 8630-8637.
[374] Makita, Z., Radoff, S., Rayfield, E. J., Yang, Z., Skolnik, E., Delaney, V., Friedman, E. A., Cerami, A., and Vlassara, H. (1991). Advanced Glycosylation End Products in Patients with Diabetic Nephropathy. *The New England Journal of Medicine 325*, 836-842.
[375] Aderem, A., and Underhill, D. M. (1999). Mechanisms of Phagocytosis in Macrophages. *Annual Review of Immunology 17*, 593-623.
[376] Sourris, K. C., and Forbes, J. M. (2009). Interactions between Advanced Glycation End-Products (Age) and Their Receptors in the Development and Progression of Diabetic Nephropathy - Are These Receptors Valid Therapeutic Targets. *Current Drug Targets 10*, 42-50.
[377] Prevo, R., Banerji, S., Ni, J., and Jackson, D. G. (2004). Rapid Plasma Membrane-Endosomal Trafficking of the Lymph Node Sinus and High Endothelial Venule Scavenger Receptor/Homing Receptor Stabilin-1 (Feel-1/Clever-1). *The Journal of Biological Chemistry 279*, 52580-52592.
[378] Miyazaki, A., Nakayama, H., and Horiuchi, S. (2002). Scavenger Receptors That Recognize Advanced Glycation End Products. *Trends in Cardiovascular Medicine 12*, 258-262.
[379] Marsche, G., Weigle, B., Sattler, W., and Malle, E. (2007). Soluble Rage Blocks Scavenger Receptor Cd36-Mediated Uptake of Hypochlorite-Modified Low-Density Lipoprotein. *FASEB Journal 21*, 3075-3082.
[380] Greaves, D. R., and Gordon, S. (2009). The Macrophage Scavenger Receptor at 30 Years of Age: Current Knowledge and Future Challenges. *Journal of Lipid Research 50 Suppl*, S282-286.
[381] Li, Y. M., Mitsuhashi, T., Wojciechowicz, D., Shimizu, N., Li, J., Stitt, A., He, C., Banerjee, D., and Vlassara, H. (1996). Molecular Identity and Cellular Distribution of Advanced Glycation Endproduct Receptors: Relationship of P60 to Ost-48 and P90 to 80k-H Membrane Proteins. *Proceedings of the National Academy of Sciences of the United States of America 93*, 11047-11052.
[382] Stitt, A. W., Burke, G. A., Chen, F., McMullen, C. B., and Vlassara, H. (2000). Advanced Glycation End-Product Receptor Interactions on Microvascular Cells Occur within Caveolin-Rich Membrane Domains. *FASEB Journal 14*, 2390-2392.
[383] Stitt, A. W., McGoldrick, C., Rice-McCaldin, A., McCance, D. R., Glenn, J. V., Hsu, D. K., Liu, F. T., Thorpe, S. R., and Gardiner, T. A. (2005). Impaired Retinal Angiogenesis in Diabetes: Role of Advanced Glycation End Products and Galectin-3. *Diabetes 54*, 785-794.
[384] Miyata, T., Hori, O., Zhang, J., Yan, S. D., Ferran, L., Iida, Y., and Schmidt, A. M. (1996). The Receptor for Advanced Glycation End Products (Rage) Is a Central Mediator of the Interaction of Age-Beta2microglobulin with Human Mononuclear Phagocytes Via an Oxidant-Sensitive Pathway. Implications for the Pathogenesis of Dialysis-Related Amyloidosis. *The Journal of Clinical Investigation 98*, 1088-1094.

[385] Ramasamy, R., Yan, S. F., and Schmidt, A. M. (2007). Arguing for the Motion: Yes, Rage Is a Receptor for Advanced Glycation Endproducts. *Molecular Nutrition & Food Research 51*, 1111-1115.
[386] Miki, Y., Dambara, H., Tachibana, Y., Hirano, K., Konishi, M., and Beppu, M. (2014). Macrophage Recognition of Toxic Advanced Glycosylation End Products through the Macrophage Surface-Receptor Nucleolin. *Biological & Pharmaceutical Bulletin 37*, 588-596.
[387] Canton, J., Neculai, D., and Grinstein, S. (2013). Scavenger Receptors in Homeostasis and Immunity. *Nature reviews. Immunology 13*, 621-634.
[388] Langmann, T. (2013). Class a Scavenger Receptors Shed Light on Immune Cell Recruitment and Cnv. *Investigative Ophthalmology & Visual Science 54*, 5971.
[389] Park, Y. M. (2014). Cd36, a Scavenger Receptor Implicated in Atherosclerosis. *Experimental & Molecular Medicine 46*, e99.
[390] Holvoet, P., Perez, G., Bernar, H., Brouwers, E., Vanloo, B., Rosseneu, M., and Collen, D. (1994). Stimulation with a Monoclonal Antibody (Mab4e4) of Scavenger Receptor-Mediated Uptake of Chemically Modified Low Density Lipoproteins by Thp-1-Derived Macrophages Enhances Foam Cell Generation. *The Journal of Clinical Investigation 93*, 89-98.
[391] Chen, X., Zhang, T., and Du, G. (2008). Advanced Glycation End Products Serve as Ligands for Lectin-Like Oxidized Low-Density Lipoprotein Receptor-1(Lox-1): Biochemical and Binding Characterizations Assay. *Cell Biochemistry and Function 26*, 760-770.
[392] Yuan, Y., Zhao, L., Chen, Y., Moorhead, J. F., Varghese, Z., Powis, S. H., Minogue, S., Sun, Z., and Ruan, X. Z. (2011). Advanced Glycation End Products (Ages) Increase Human Mesangial Foam Cell Formation by Increasing Golgi Scap Glycosylation in Vitro. *American Journal of Physiology. Renal Physiology 301*, F236-243.
[393] Sorme, P., Qian, Y., Nyholm, P. G., Leffler, H., and Nilsson, U. J. (2002). Low Micromolar Inhibitors of Galectin-3 Based on 3'-Derivatization of N-Acetyllactosamine. *Chembiochem 3*, 183-189.
[394] Liu, B. F., Miyata, S., Kojima, H., Uriuhara, A., Kusunoki, H., Suzuki, K., and Kasuga, M. (1999). Low Phagocytic Activity of Resident Peritoneal Macrophages in Diabetic Mice: Relevance to the Formation of Advanced Glycation End Products. *Diabetes 48*, 2074-2082.
[395] Chung, T., and Kim, Y. B. (1988). Two Distinct Cytolytic Mechanisms of Macrophages and Monocytes Activated by Phorbol Myristate Acetate. *Journal of Leukocyte Biology 44*, 329-336.
[396] Flescher, E., Gonen, P., and Keisari, Y. (1984). Oxidative Burst-Dependent Tumoricidal and Tumorostatic Activities of Paraffin Oil-Elicited Mouse Macrophages. *Journal of the National Cancer Institute 72*, 1341-1347.
[397] Giacco, F., and Brownlee, M. (2010). Oxidative Stress and Diabetic Complications. *Circulation Research 107*, 1058-1070.
[398] Leahy, J. L. (2005). Pathogenesis of Type 2 Diabetes Mellitus. *Archives of Medical Research 36*, 197-209.
[399] Nowotny, K., Jung, T., Hohn, A., Weber, D., and Grune, T. (2015). Advanced Glycation End Products and Oxidative Stress in Type 2 Diabetes Mellitus. *Biomolecules 5*, 194-222.

[400] Moridi, H., Karimi, J., Sheikh, N., Goodarzi, M. T., Saidijam, M., Yadegarazari, R., Khazaei, M., Khodadadi, I., Tavilani, H., Piri, H., Asadi, S., Zarei, S., and Rezaei, A. (2015). Resveratrol-Dependent Down-Regulation of Receptor for Advanced Glycation End-Products and Oxidative Stress in Kidney of Rats with Diabetes. *International Journal of Endocrinology and Metabolism 13*, e23542.
[401] Whitman, R. (1963). The Reconstruction Operation for Arthritis Deformans of the Hip Joint. *Clinical Orthopaedics and Related Research 31*, 3-6.
[402] Machado, J. T., Iborra, R. T., Fusco, F. B., Castilho, G., Pinto, R. S., Machado-Lima, A., Nakandakare, E. R., Seguro, A. C., Shimizu, M. H., Catanozi, S., and Passarelli, M. (2014). N-Acetylcysteine Prevents Endoplasmic Reticulum Stress Elicited in Macrophages by Serum Albumin Drawn from Chronic Kidney Disease Rats and Selectively Affects Lipid Transporters, Abca-1 and Abcg-1. *Atherosclerosis 237*, 343-352.
[403] Bogdan, C. (2015). Nitric Oxide Synthase in Innate and Adaptive Immunity: An Update. *Trends in Immunology 36*, 161-178.
[404] Tsai, M. H., Lin, Z. C., Liang, C. J., Yen, F. L., Chiang, Y. C., and Lee, C. W. (2014). Eupafolin Inhibits Pge2 Production and Cox2 Expression in Lps-Stimulated Human Dermal Fibroblasts by Blocking Jnk/Ap-1 and Nox2/P47(Phox) Pathway. *Toxicology and Applied Pharmacology 279*, 240-251.
[405] Mitchell, J. A., and Evans, T. W. (1998). Cyclooxygenase-2 as a Therapeutic Target. *Inflammation Research 47 Suppl 2*, S88-92.
[406] Liao, Z., Mason, K. A., and Milas, L. (2007). Cyclo-Oxygenase-2 and Its Inhibition in Cancer: Is There a Role?. *Drugs 67*, 821-845.
[407] Funk, C. D., and FitzGerald, G. A. (2007). Cox-2 Inhibitors and Cardiovascular Risk. *Journal of Cardiovascular Pharmacology 50*, 470-479.
[408] Iniguez, M. A., Rodriguez, A., Volpert, O. V., Fresno, M., and Redondo, J. M. (2003). Cyclooxygenase-2: A Therapeutic Target in Angiogenesis. *Trends in Molecular Medicine 9*, 73-78.
[409] Diaz-Munoz, M. D., Osma-Garcia, I. C., Fresno, M., and Iniguez, M. A. (2012). Involvement of Pge2 and the Camp Signalling Pathway in the up-Regulation of Cox-2 and Mpges-1 Expression in Lps-Activated Macrophages. *The Biochemical Journal 443*, 451-461.
[410] Ellestad-Sayed, J. J., Haworth, J. C., Coodin, F. J., and Dilling, L. A. (1981). Growth and Nutrition of Preschool Indian Children in Manitoba: Ii. Nutrient Intakes. *Canadian Journal of Public Health 72*, 127-133.
[411] Babior, B. M., Lambeth, J. D., and Nauseef, W. (2002). The Neutrophil Nadph Oxidase. *Archives of Biochemistry and Biophysics 397*, 342-344.
[412] Cross, A. R., and Segal, A. W. (2004). The Nadph Oxidase of Professional Phagocytes--Prototype of the Nox Electron Transport Chain Systems. *Biochimica et Biophysica Acta 1657*, 1-22.
[413] Nauseef, W. M. (2004). Assembly of the Phagocyte Nadph Oxidase. *Histochemistry and Cell Biology 122*, 277-291.
[414] Cai, W., Ramdas, M., Zhu, L., Chen, X., Striker, G. E., and Vlassara, H. (2012). Oral Advanced Glycation Endproducts (Ages) Promote Insulin Resistance and Diabetes by Depleting the Antioxidant Defenses Age Receptor-1 and Sirtuin 1. *Proceedings of the National Academy of Sciences of the United States of America 109*, 15888-15893.

[415] Muellner, M. K., Schreier, S. M., Schmidbauer, B., Moser, M., Quehenberger, P., Kapiotis, S., Goldenberg, H., and Laggner, H. (2010). Vitamin C Inhibits No-Induced Stabilization of Hif-1alpha in Huvecs. *Free Radical Research 44*, 783-791.
[416] Sandau, K. B., Fandrey, J., and Brune, B. (2001). Accumulation of Hif-1alpha under the Influence of Nitric Oxide. *Blood 97*, 1009-1015.
[417] Palmer, L. A., Gaston, B., and Johns, R. A. (2000). Normoxic Stabilization of Hypoxia-Inducible Factor-1 Expression and Activity: Redox-Dependent Effect of Nitrogen Oxides. *Molecular Pharmacology 58*, 1197-1203.
[418] Shatrov, V. A., Sumbayev, V. V., Zhou, J., and Brune, B. (2003). Oxidized Low-Density Lipoprotein (Oxldl) Triggers Hypoxia-Inducible Factor-1alpha (Hif-1alpha) Accumulation Via Redox-Dependent Mechanisms. *Blood 101*, 4847-4849.
[419] Frede, S., Berchner-Pfannschmidt, U., and Fandrey, J. (2007). Regulation of Hypoxia-Inducible Factors During Inflammation. *Methods in Enzymology 435*, 405-419.
[420] Gwinn, M. R., and Vallyathan, V. (2006). Respiratory Burst: Role in Signal Transduction in Alveolar Macrophages. *Journal of Toxicology and Environmental Health. Part B, Critical reviews 9*, 27-39.
[421] Yan, S. D., Schmidt, A. M., Anderson, G. M., Zhang, J., Brett, J., Zou, Y. S., Pinsky, D., and Stern, D. (1994). Enhanced Cellular Oxidant Stress by the Interaction of Advanced Glycation End Products with Their Receptors/Binding Proteins. *The Journal of Biological Chemistry 269*, 9889-9897.
[422] Lee, J. Y., Sohn, K. H., Rhee, S. H., and Hwang, D. (2001). Saturated Fatty Acids, but Not Unsaturated Fatty Acids, Induce the Expression of Cyclooxygenase-2 Mediated through Toll-Like Receptor 4. *The Journal of Biological Chemistry 276*, 16683-16689.
[423] Dinarello, C. A. (2009) Immunological and Inflammatory Functions of the Interleukin-1 Family. *Annual review of immunology 27*, 519-550.
[424] Yu, Y. M., Wang, Z. H., Liu, C. H., and Chen, C. S. (2007). Ellagic Acid Inhibits Il-1beta-Induced Cell Adhesion Molecule Expression in Human Umbilical Vein Endothelial Cells. *British Journal of Nutrition 97*, 692-698.
[425] Dinarello, C. A. (1996) Biologic Basis for Interleukin-1 in Disease. *Blood 87*, 2095-2147.
[426] O'Hara, A., Lim, F. L., Mazzatti, D. J., and Trayhurn, P. (2012). Stimulation of Inflammatory Gene Expression in Human Preadipocytes by Macrophage-Conditioned Medium: Upregulation of Il-6 Production by Macrophage-Derived Il-1beta. *Molecular and Cellular Endocrinology 349*, 239-247.
[427] Scheller, J., Chalaris, A., Schmidt-Arras, D., and Rose-John, S. (2011). The Pro- and Anti-Inflammatory Properties of the Cytokine Interleukin-6. *Biochimica et Biophysica Acta 1813*, 878-888.
[428] Hughes-Jones, W. E. (1975). George Robin Adlington Syme. *The Australian and New Zealand Journal of Surgery 45*, 321-322.
[429] Riches, D. W., Chan, E. D., and Winston, B. W. (1996). Tnf-Alpha-Induced Regulation and Signalling in Macrophages. *Immunobiology 195*, 477-490.
[430] Maini, R. N., Elliott, M. J., Brennan, F. M., and Feldmann, M. (1995). Beneficial Effects of Tumour Necrosis Factor-Alpha (Tnf-Alpha) Blockade in Rheumatoid Arthritis (Ra). *Clinical and Experimental Immunology 101*, 207-212.
[431] Lombardo, E., Alvarez-Barrientos, A., Maroto, B., Bosca, L., and Knaus, U. G. (2007). Tlr4-Mediated Survival of Macrophages Is Myd88 Dependent and Requires Tnf-Alpha Autocrine Signalling. *Journal of Immunology 178*, 3731-3739.

[432] Arango Duque, G., and Descoteaux, A. (2014). Macrophage Cytokines: Involvement in Immunity and Infectious Diseases. *Frontiers in Immunology 5*, 491.
[433] Moser, B., Clark-Lewis, I., Zwahlen, R., and Baggiolini, M. (1990). Neutrophil-Activating Properties of the Melanoma Growth-Stimulatory Activity. *The Journal of Experimental Medicine 171*, 1797-1802.
[434] Pelus, L. M., and Fukuda, S. (2006). Peripheral Blood Stem Cell Mobilization: The Cxcr2 Ligand Grobeta Rapidly Mobilizes Hematopoietic Stem Cells with Enhanced Engraftment Properties. *Experimental Hematology 34*, 1010-1020.
[435] Van Nieuwenhuijze, A., Koenders, M., Roeleveld, D., Sleeman, M. A., van den Berg, W., and Wicks, I. P. (2013). Gm-Csf as a Therapeutic Target in Inflammatory Diseases. *Molecular Immunology 56*, 675-682.
[436] Fleetwood, A. J., Lawrence, T., Hamilton, J. A., and Cook, A. D. (2007). Granulocyte-Macrophage Colony-Stimulating Factor (Csf) and Macrophage Csf-Dependent Macrophage Phenotypes Display Differences in Cytokine Profiles and Transcription Factor Activities: Implications for Csf Blockade in Inflammation. *Journal of Immunology 178*, 5245-5252.
[437] Gearing, D. P., King, J. A., Gough, N. M., and Nicola, N. A. (1989). Expression Cloning of a Receptor for Human Granulocyte-Macrophage Colony-Stimulating Factor. *The EMBO Journal 8*, 3667-3676.
[438] Hayashida, K., Kitamura, T., Gorman, D. M., Arai, K., Yokota, T., and Miyajima, A. (1990). Molecular Cloning of a Second Subunit of the Receptor for Human Granulocyte-Macrophage Colony-Stimulating Factor (Gm-Csf): Reconstitution of a High-Affinity Gm-Csf Receptor. *Proceedings of the National Academy of Sciences of the United States of America 87*, 9655-9659.
[439] Robbins, C. S., Hilgendorf, I., Weber, G. F., Theurl, I., Iwamoto, Y., Figueiredo, J. L., Gorbatov, R., Sukhova, G. K., Gerhardt, L. M., Smyth, D., Zavitz, C. C., Shikatani, E. A., Parsons, M., van Rooijen, N., Lin, H. Y., Husain, M., Libby, P., Nahrendorf, M., Weissleder, R., and Swirski, F. K. (2013). Local Proliferation Dominates Lesional Macrophage Accumulation in Atherosclerosis. *Nature Medicine 19*, 1166-1172.
[440] Randolph, G. J. (2013). Proliferating Macrophages Prevail in Atherosclerosis. *Nature Medicine 19*, 1094-1095.
[441] Murphy, A. J., and Tall, A. R. (2014). Proliferating Macrophages Populate Established Atherosclerotic Lesions. *Circulation Research 114*, 236-238.
[442] Jenkins, S. J., Ruckerl, D., Cook, P. C., Jones, L. H., Finkelman, F. D., van Rooijen, N., MacDonald, A. S., and Allen, J. E. (2011). Local Macrophage Proliferation, Rather Than Recruitment from the Blood. Is a Signature of Th2 Inflammation, *Science 332*, 1284-1288.
[443] Takeda, K., and Akira, S. (2004). Tlr Signaling Pathways. *Seminars in Immunology 16*, 3-9.
[444] Akira, S., Takeda, K., and Kaisho, T. (2001). Toll-Like Receptors: Critical Proteins Linking Innate and Acquired Immunity. *Nature Immunology 2*, 675-680.
[445] Bjorkbacka, H., Fitzgerald, K. A., Huet, F., Li, X., Gregory, J. A., Lee, M. A., Ordija, C. M., Dowley, N. E., Golenbock, D. T., and Freeman, M. W. (2004). The Induction of Macrophage Gene Expression by Lps Predominantly Utilizes Myd88-Independent Signaling Cascades. *Physiological Genomics 19*, 319-330.

[446] Buetler, T. M., Latado, H., Leclerc, E., Weigle, B., Baumeyer, A., Heizmann, C. W., and Scholz, G. (2011). Glycolaldehyde-Modified Beta-Lactoglobulin Ages Are Unable to Stimulate Inflammatory Signaling Pathways in Rage-Expressing Human Cell Lines. *Molecular Nutrition & Food Research 55*, 291-299.
[447] Xu, J., Jiang, Y., Wang, J., Shi, X., Liu, Q., Liu, Z., Li, Y., Scott, M. J., Xiao, G., Li, S., Fan, L., Billiar, T. R., Wilson, M. A., and Fan, J. (2014). Macrophage Endocytosis of High-Mobility Group Box 1 Triggers Pyroptosis. *Cell Death and Differentiation 21*, 1229-1239.
[448] Leclerc, E., Fritz, G., Weibel, M., Heizmann, C. W., and Galichet, A. (2007). S100b and S100a6 Differentially Modulate Cell Survival by Interacting with Distinct Rage (Receptor for Advanced Glycation End Products) Immunoglobulin Domains. *The Journal of Biological Chemistry 282*, 31317-31331.
[449] Fritz, G. (2011). Rage: A Single Receptor Fits Multiple Ligands. *Trends in Biochemical Sciences 36*, 625-632.
[450] Korndorfer, I. P., Brueckner, F., and Skerra, A. (2007). The Crystal Structure of the Human (S100a8/S100a9)2 Heterotetramer, Calprotectin, Illustrates How Conformational Changes of Interacting Alpha-Helices Can Determine Specific Association of Two Ef-Hand Proteins. *Journal of Molecular Biology 370*, 887-898.
[451] Moroz, O. V., Antson, A. A., Dodson, E. J., Burrell, H. J., Grist, S. J., Lloyd, R. M., Maitland, N. J., Dodson, G. G., Wilson, K. S., Lukanidin, E., and Bronstein, I. B. (2002). The Structure of S100a12 in a Hexameric Form and Its Proposed Role in Receptor Signalling. *Acta Crystallography D Biological Crystallography 58*, 407-413.
[452] Ostendorp, T., Leclerc, E., Galichet, A., Koch, M., Demling, N., Weigle, B., Heizmann, C. W., Kroneck, P. M., and Fritz, G. (2007). Structural and Functional Insights into Rage Activation by Multimeric S100b. *The EMBO Journal 26*, 3868-3878.
[453] Moroz, O. V., Wilson, K. S., and Bronstein, I. B. (2011). The Role of Zinc in the S100 Proteins: Insights from the X-Ray Structures. *Amino Acids 41*, 761-772.
[454] Damo, S. M., Kehl-Fie, T. E., Sugitani, N., Holt, M. E., Rathi, S., Murphy, W. J., Zhang, Y., Betz, C., Hench, L., Fritz, G., Skaar, E. P., and Chazin, W. J. (2013). Molecular Basis for Manganese Sequestration by Calprotectin and Roles in the Innate Immune Response to Invading Bacterial Pathogens. *Proceedings of the National Academy of Sciences of the United States of America 110*, 3841-3846.
[455] Park, H., Adsit, F. G., and Boyington, J. C. (2010). The 1.5 a Crystal Structure of Human Receptor for Advanced Glycation Endproducts (Rage) Ectodomains Reveals Unique Features Determining Ligand Binding. *The Journal of Biological Chemistry 285*, 40762-40770.
[456] Xue, J., Ray, R., Singer, D., Bohme, D., Burz, D. S., Rai, V., Hoffmann, R., and Shekhtman, A. (2014). The Receptor for Advanced Glycation End Products (Rage) Specifically Recognizes Methylglyoxal-Derived Ages. *Biochemistry 53*, 3327-3335.
[457] Zacharias, N., and Dougherty, D. A. (2002). Cation-Pi Interactions in Ligand Recognition and Catalysis. *Trends in Pharmacology Sciences 23*, 281-287.
[458] Burley, S. K., and Petsko, G. A. (1986). Amino-Aromatic Interactions in Proteins. *FEBSs Letters 203*, 139-143.
[459] Andersen, O. S., Greathouse, D. V., Providence, L. L., Becker, M. D., and Koeppe, R. E. (1998). Importance of Tryptophan Dipoles for Protein Function: 5-Fluorination of

Tryptophans in Gramicidin a Channels. *Journal of American Chemical Society 120*, 5142-5146.
[460] Chen, Y., and Barkley, M. D. (1998). Toward Understanding Tryptophan Fluorescence in Proteins. *Biochemistry 37*, 9976-9982.
[461] Rasmussen, A., Rasmussen, T., Edwards, M. D., Schauer, D., Schumann, U., Miller, S., and Booth, I. R. (2007). The Role of Tryptophan Residues in the Function and Stability of the Mechanosensitive Channel Mscs from Escherichia Coli. *Biochemistry 46*, 10899-10908.
[462] Bogan, A. A., and Thorn, K. S. (1998). Anatomy of Hot Spots in Protein Interfaces. *Journal of Molecular Biology 280*, 1-9.
[463] Brooks, D. J., Fresco, J. R., Lesk, A. M., and Singh, M. (2002). Evolution of Amino Acid Frequencies in Proteins over Deep Time: Inferred Order of Introduction of Amino Acids into the Genetic Code. *Molecular Biology and Evolution 19*, 1645-1655.
[464] Jensen, J. L., Indurthi, V. S., Neau, D. B., Vetter, S. W., and Colbert, C. L. (2015). Structural Insights into the Binding of the Human Receptor for Advanced Glycation End Products (Rage) by S100b, as Revealed by an S100b-Rage-Derived Peptide Complex. *Acta Crystallography D Biological Crystallography 71*, 1176-1183.
[465] Smith, S. P., Barber, K. R., Dunn, S. D., and Shaw, G. S. (1996). Structural Influence of Cation Binding to Recombinant Human Brain S100b: Evidence for Calcium-Induced Exposure of a Hydrophobic Surface. *Biochemistry 35*, 8805-8814.
[466] Strambini, G. B., and Gonnelli, M. (2010). Fluorescence Quenching of Buried Trp Residues by Acrylamide Does Not Require Penetration of the Protein Fold. *The Journal of Physical Chemistry. B 114*, 1089-1093.
[467] Leclerc, E., and Vetter, S. (1998). Characterization of a Calcium-Dependent Calmodulin-Binding Domain in the 135-Kd Human Protein 4.1 Isoform. *European Journal of Biochemistry 258*, 567-571.
[468] Schneider, C. A., Rasband, W. S., and Eliceiri, K. W. (2012). Nih Image to Imagej: 25 Years of Image Analysis. *Natute Methods 9*, 671-675.
[469] Bottomley, S. P., Popplewell, A. G., Scawen, M., Wan, T., Sutton, B. J., and Gore, M. G. (1994). The Stability and Unfolding of an Igg Binding-Protein Based Upon the B-Domain of Protein-a from Staphylococcus-Aureus Probed by Tryptophan Substitution and Fluorescence Spectroscopy. *Protein Engineering 7*, 1463-1470.
[470] Aronsson, G., Martensson, L. G., Carlsson, U., and Jonsson, B. H. (1995). Folding and Stability of the N-Terminus of Human Carbonic-Anhydrase-Ii. *Biochemistry 34*, 2153-2162.
[471] Chang, Y., Zajicek, J., and Castellino, F. J. (1997). Role of Tryptophan-63 of the Kringle 2 Domain of Tissue-Type Plasminogen Activator in Its Thermal Stability, Folding, and Ligand Binding Properties. *Biochemistry 36*, 7652-7663.
[472] Dattilo, B. M., Fritz, G., Leclerc, E., Kooi, C. W., Heizmann, C. W., and Chazin, W. J. (2007). The Extracellular Region of the Receptor for Advanced Glycation End Products Is Composed of Two Independent Structural Units. *Biochemistry 46*, 6957-6970.
[473] Frishman, D., and Argos, P. (1995). Knowledge-Based Protein Secondary Structure Assignment. *Proteins 23*, 566-579.
[474] Ramzan, M. A., Cookson, E. J., and Beynon, R. J. (1991). Limited Proteolysis as a Probe for Protein Folding. *Biochemical Society Transactions 19*, 296S.

[475] Rudolph, R. (1985). The Use of Limited Proteolysis in Studies on Protein Folding and Association. *Biochemical Society Transactions 13*, 308-311.
[476] Vivian, J. T., and Callis, P. R. (2001). Mechanisms of Tryptophan Fluorescence Shifts in Proteins. *Biophysical Journal 80*, 2093-2109.
[477] Van Duffelen, M., Chrin, L. R., and Berger, C. L. (2004). Nucleotide Dependent Intrinsic Fluorescence Changes of W29 and W36 in Smooth Muscle Myosin. *Biophysical Journal 87*, 1767-1775.
[478] Eftink, M. R., and Ghiron, C. A. (1976). Exposure of Tryptophanyl Residues in Proteins - Quantitative-Determination by Fluorescence Quenching Studies. *Biochemistry 15*, 672-680.
[479] Eftink, M. R., and Ghiron, C. A. (1975). Dynamics of a Protein Matrix Revealed by Fluorescence Quenching. *Proceedings of the National Academy of Sciences of the United States of America 72*, 3290-3294.
[480] Beechem, J. M., and Brand, L. (1985). Time-Resolved Fluorescence of Proteins. *Annual Review of Biochemistry 54*, 43-71.
[481] Swaminathan, R., Krishnamoorthy, G., and Periasamy, N. (1994). Similarity of Fluorescence Lifetime Distributions for Single Tryptophan Proteins in the Random Coil State. *Biophysics Journal 67*, 2013-2023.
[482] Pantoliano, M. W., Petrella, E. C., Kwasnoski, J. D., Lobanov, V. S., Myslik, J., Graf, E., Carver, T., Asel, E., Springer, B. A., Lane, P., and Salemme, F. R. (2001). High-Density Miniaturized Thermal Shift Assays as a General Strategy for Drug Discovery. *Journal of Biomolecular Screening 6*, 429-440.
[483] Matulis, D., Kranz, J. K., Salemme, F. R., and Todd, M. J. (2005). Thermodynamic Stability of Carbonic Anhydrase: Measurements of Binding Affinity and Stoichiometry Using Thermofluor. *Biochemistry 44*, 5258-5266.
[484] Phillips, K., and de la Pena, A. H. (2011). The Combined Use of the Thermofluor Assay and Thermoq Analytical Software for the Determination of Protein Stability and Buffer Optimization as an Aid in Protein Crystallization. *Current Protocols in Molecular Biology Chapter 10*, Unit10 28.
[485] Leclerc, E. (2013). Measuring Binding of S100 Proteins to Rage by Surface Plasmon Resonance. *Methods Molecular Biology 963*, 201-213.
[486] Rustandi, R. R., Baldisseri, D. M., and Weber, D. J. (2000). Structure of the Negative Regulatory Domain of P53 Bound to S100b(Betabeta). *Nature Structural Biology 7*, 570-574.
[487] Cavalier, M. C., Pierce, A. D., Wilder, P. T., Alasady, M. J., Hartman, K. G., Neau, D. B., Foley, T. L., Jadhav, A., Maloney, D. J., Simeonov, A., Toth, E. A., and Weber, D. J. (2014). Covalent Small Molecule Inhibitors of Ca(2+)-Bound S100b. *Biochemistry 53*, 6628-6640.
[488] Charpentier, T. H., Wilder, P. T., Liriano, M. A., Varney, K. M., Pozharski, E., MacKerell, A. D., Jr., Coop, A., Toth, E. A., and Weber, D. J. (2008). Divalent Metal Ion Complexes of S100b in the Absence and Presence of Pentamidine. *Journal of Molecular Biology 382*, 56-73.
[489] Charpentier, T. H., Wilder, P. T., Liriano, M. A., Varney, K. M., Zhong, S., Coop, A., Pozharski, E., MacKerell, A. D., Jr., Toth, E. A., and Weber, D. J. (2009). Small Molecules Bound to Unique Sites in the Target Protein Binding Cleft of Calcium-Bound

S100b as Characterized by Nuclear Magnetic Resonance and X-Ray Crystallography. *Biochemistry 48*, 6202-6212.
[490] McKnight, L. E., Raman, E. P., Bezawada, P., Kudrimoti, S., Wilder, P. T., Hartman, K. G., Godoy-Ruiz, R., Toth, E. A., Coop, A., Mackerell, A. D., Jr., and Weber, D. J. (2012). Structure-Based Discovery of a Novel Pentamidine-Related Inhibitor of the Calcium-Binding Protein S100b. *ACS Medicinal Chemistry Letters 3*, 975-979.
[491] Wilder, P. T., Charpentier, T. H., Liriano, M. A., Gianni, K., Varney, K. M., Pozharski, E., Coop, A., Toth, E. A., Mackerell, A. D., and Weber, D. J. (2010). In Vitro Screening and Structural Characterization of Inhibitors of the S100b-P53 Interaction, *International Journal of High Throughput Screen 2010*, 109-126.
[492] Charpentier, T. H., Thompson, L. E., Liriano, M. A., Varney, K. M., Wilder, P. T., Pozharski, E., Toth, E. A., and Weber, D. J. (2010). The Effects of Capz Peptide (Trtk-12) Binding to S100b-Ca2+ as Examined by Nmr and X-Ray Crystallography. *Journal of Molecular Biology 396*, 1227-1243.
[493] Bhattacharya, S., Large, E., Heizmann, C. W., Hemmings, B., and Chazin, W. J. (2003). Structure of the Ca2+/S100b/Ndr Kinase Peptide Complex: Insights into S100 Target Specificity and Activation of the Kinase. *Biochemistry 42*, 14416-14426.
[494] Rustandi, R. R., Baldisseri, D. M., Dorhat, A. C., and Weber, D. J. (1999). Structural changes in the C-terminus of Ca2+-bound rat S100B (beta beta) upon binding to a peptide derived from the C-terminal regulatory domain of p53. *Protein Science* 8, 1743-1751.
[495] Yutani, K., Ogasahara, K., Tsujita, T., and Sugino, Y. (1987). Dependence of Conformational Stability on Hydrophobicity of the Amino Acid Residue in a Series of Variant Proteins Substituted at a Unique Position of Tryptophan Synthase Alpha Subunit. *Proceedings of the National Academy of Sciences of the United States of America 84*, 4441-4444.
[496] Shortle, D., Stites, W. E., and Meeker, A. K. (1990). Contributions of the Large Hydrophobic Amino Acids to the Stability of Staphylococcal Nuclease. *Biochemistry 29*, 8033-8041.
[497] Xue, J., Rai, V., Singer, D., Chabierski, S., Xie, J., Reverdatto, S., Burz, D. S., Schmidt, A. M., Hoffmann, R., and Shekhtman, A. (2011). Advanced Glycation End Product Recognition by the Receptor for Ages. *Structure 19*, 722-732.
[498] Mohan, S. K., Gupta, A. A., and Yu, C. (2013). Interaction of the S100a6 Mutant (C3s) with the V Domain of the Receptor for Advanced Glycation End Products (Rage). *Biochemical and Biophysical Research Communications 434*, 328-333.
[499] Yatime, L., and Andersen, G. R. (2013). Structural Insights into the Oligomerization Mode of the Human Receptor for Advanced Glycation End-Products. *FEBS J*ournal*280*, 6556-6568.
[500] Sirois, C. M., Jin, T., Miller, A. L., Bertheloot, D., Nakamura, H., Horvath, G. L., Mian, A., Jiang, J., Schrum, J., Bossaller, L., Pelka, K., Garbi, N., Brewah, Y., Tian, J., Chang, C., Chowdhury, P. S., Sims, G. P., Kolbeck, R., Coyle, A. J., Humbles, A. A., Xiao, T. S., and Latz, E. (2013). Rage Is a Nucleic Acid Receptor That Promotes Inflammatory Responses to DNA. *The Journal of Experimental Medicine 210*, 2447-2463.
[501] Kandarakis, S. A., Piperi, C., Moschonas, D. P., Korkolopoulou, P., Papalois, A., and Papavassiliou, A. G. (2015). Dietary Glycotoxins Induce Rage and Vegf up-Regulation in the Retina of Normal Rats. *Experimental Eye Research 137*, 1-10.

[502] Cai, W., Uribarri, J., Zhu, L., Chen, X., Swamy, S., Zhao, Z., Grosjean, F., Simonaro, C., Kuchel, G. A., Schnaider-Beeri, M., Woodward, M., Striker, G. E., and Vlassara, H. (2014). Oral Glycotoxins Are a Modifiable Cause of Dementia and the Metabolic Syndrome in Mice and Humans. *Proceedings of the National Academy of Sciences of the United States of America 111*, 4940-4945.
[503] Deyl, Z., Miksik, I., and Zicha, J. (1999). Multicomponent Analysis by Off-Line Combination of Synchronous Fluorescence Spectroscopy and Capillary Electrophoresis of Collagen Glycation Adducts. *Journal of Chromatography A 836*, 161-171.
[504] Rothermundt, M., Peters, M., Prehn, J. H., and Arolt, V. (2003). S100b in Brain Damage and Neurodegeneration. *Microscopy Research and Techiques 60*, 614-632.
[505] Kruijff, S., and Hoekstra, H. J. (2012). The Current Status of S-100b as a Biomarker in Melanoma. *European Jpurnal of Surgical Oncology 38*, 281-285.
[506] Valencia, J. V., Mone, M., Koehne, C., Rediske, J., and Hughes, T. E. (2004). Binding of Receptor for Advanced Glycation End Products (Rage) Ligands Is Not Sufficient to Induce Inflammatory Signals: Lack of Activity of Endotoxin-Free Albumin-Derived Advanced Glycation End Products. *Diabetologia 47*, 844-852.
[507] Reddy, M. A., Li, S. L., Sahar, S., Kim, Y. S., Xu, Z. G., Lanting, L., and Natarajan, R. (2006). Key Role of Src Kinase in S100b-Induced Activation of the Receptor for Advanced Glycation End Products in Vascular Smooth Muscle Cells. *The Journal of Biological Chemistry 281*, 13685-13693.
[508] Penumutchu, S. R., Chou, R. H., and Yu, C. (2014). Structural Insights into Calcium-Bound S100p and the V Domain of the Rage Complex. *PloS One 9*, e103947.
[509] Yatime, L., and Andersen, G. R. (2014). The Specificity of DNA Recognition by the Rage Receptor. *The Journal of Experimental Medicine 211*, 749-750.